

Hidden order behind cooperation in social systems

Edited by

Dun Han, Jianbo Wang and Jianrong Wang

Published in

Frontiers in Physics



FRONTIERS EBOOK COPYRIGHT STATEMENT

The copyright in the text of individual articles in this ebook is the property of their respective authors or their respective institutions or funders. The copyright in graphics and images within each article may be subject to copyright of other parties. In both cases this is subject to a license granted to Frontiers.

The compilation of articles constituting this ebook is the property of Frontiers.

Each article within this ebook, and the ebook itself, are published under the most recent version of the Creative Commons CC-BY licence. The version current at the date of publication of this ebook is CC-BY 4.0. If the CC-BY licence is updated, the licence granted by Frontiers is automatically updated to the new version.

When exercising any right under the CC-BY licence, Frontiers must be attributed as the original publisher of the article or ebook, as applicable.

Authors have the responsibility of ensuring that any graphics or other materials which are the property of others may be included in the CC-BY licence, but this should be checked before relying on the CC-BY licence to reproduce those materials. Any copyright notices relating to those materials must be complied with.

Copyright and source acknowledgement notices may not be removed and must be displayed in any copy, derivative work or partial copy which includes the elements in question.

All copyright, and all rights therein, are protected by national and international copyright laws. The above represents a summary only. For further information please read Frontiers' Conditions for Website Use and Copyright Statement, and the applicable CC-BY licence.

ISSN 1664-8714
ISBN 978-2-8325-2206-6
DOI 10.3389/978-2-8325-2206-6

About Frontiers

Frontiers is more than just an open access publisher of scholarly articles: it is a pioneering approach to the world of academia, radically improving the way scholarly research is managed. The grand vision of Frontiers is a world where all people have an equal opportunity to seek, share and generate knowledge. Frontiers provides immediate and permanent online open access to all its publications, but this alone is not enough to realize our grand goals.

Frontiers journal series

The Frontiers journal series is a multi-tier and interdisciplinary set of open-access, online journals, promising a paradigm shift from the current review, selection and dissemination processes in academic publishing. All Frontiers journals are driven by researchers for researchers; therefore, they constitute a service to the scholarly community. At the same time, the *Frontiers journal series* operates on a revolutionary invention, the tiered publishing system, initially addressing specific communities of scholars, and gradually climbing up to broader public understanding, thus serving the interests of the lay society, too.

Dedication to quality

Each Frontiers article is a landmark of the highest quality, thanks to genuinely collaborative interactions between authors and review editors, who include some of the world's best academicians. Research must be certified by peers before entering a stream of knowledge that may eventually reach the public - and shape society; therefore, Frontiers only applies the most rigorous and unbiased reviews. Frontiers revolutionizes research publishing by freely delivering the most outstanding research, evaluated with no bias from both the academic and social point of view. By applying the most advanced information technologies, Frontiers is catapulting scholarly publishing into a new generation.

What are Frontiers Research Topics?

Frontiers Research Topics are very popular trademarks of the *Frontiers journals series*: they are collections of at least ten articles, all centered on a particular subject. With their unique mix of varied contributions from Original Research to Review Articles, Frontiers Research Topics unify the most influential researchers, the latest key findings and historical advances in a hot research area.

Find out more on how to host your own Frontiers Research Topic or contribute to one as an author by contacting the Frontiers editorial office: frontiersin.org/about/contact

Hidden order behind cooperation in social systems

Topic editors

Dun Han — Jiangsu University, China

Jianbo Wang — Southwest Petroleum University, China

Jianrong Wang — Shanxi University, China

Citation

Han, D., Wang, J., Wang, J., eds. (2023). *Hidden order behind cooperation in social systems*. Lausanne: Frontiers Media SA. doi: 10.3389/978-2-8325-2206-6

Table of contents

| | |
|-----|------------------------------------------------------------------------------------------------------------------------------------------------------------------------------------------------------------------------------------------|
| 04 | Editorial: Hidden order behind cooperation in social systems Dun Han, Jianbo Wang and Jianrong Wang |
| 06 | A complex network study on Guangdong-Hong Kong-Macao Greater Bay Area based on economic development index Qingxiang Feng, Sha Zhu and Fujun Lai |
| 20 | A linear time series analysis of carbon price <i>via</i> a complex network approach Yuxia Hu, Chengbin Chu, Peng Wu and Jun Hu |
| 34 | Finite-time synchronization of Kuramoto-oscillator networks with a pacemaker based on cyber-physical system Pengchun Rao and Xiufeng Guo |
| 41 | Hitting time for random walks on the Sierpinski network and the half Sierpinski network Yu Sun, Xiaobei Liu and Xiaoyan Li |
| 50 | Assessment and prediction of railway station equipment health status based on graph neural network Jian Yao, Wei Bai, Guoyuan Yang, Zhikang Meng and Kaixuan Su |
| 65 | Measuring the impact of Wuhan's COVID-19 lockdown on the growth enterprise market in China Li Wang, Zeyu Huang and Yanan Wang |
| 78 | Increasing the prediction performance of temporal convolution network using multimodal combination input: Evidence from the study on exchange rates Xueling Lv, Xiong Xiong and Baojun Geng |
| 86 | Study on an SIR rumor propagation model with an interaction mechanism on WeChat networks Xinghua Chang |
| 95 | Investigating the searching behavior of Sino-U.S. relations in China based on complex network Jun Chen, Lei Wang and Wuyan Weng |
| 104 | An evolutionary game study on the cooperation behavior of the "government, banks, and guarantee institutions" in financing guarantee for China's new agricultural entities Jingjing Zhang, Zhu Mei, Fan Zhang and QiaoMei Zhou |
| 123 | Do global geopolitical risks affect connectedness of global stock market contagion network? Evidence from quantile-on-quantile regression Fujun Lai, Sicheng Li, Liang Lv and Sha Zhu |
| 142 | How do circadian rhythms and neural synchrony shape networked cooperation? Vaiva Vasiliauskaite and Carina I. Hausladen |



OPEN ACCESS

EDITED AND REVIEWED BY
Matjaž Perc,
University of Maribor, Slovenia

*CORRESPONDENCE

Dun Han,
✉ handunsir@163.com
Jianbo Wang,
✉ phyjbw@gmail.com
Jianrong Wang,
✉ wangjianronghappy@126.com

SPECIALTY SECTION

This article was submitted to Social
Physics, a section of the journal
Frontiers in Physics

RECEIVED 24 March 2023

ACCEPTED 29 March 2023

PUBLISHED 04 April 2023

CITATION

Han D, Wang J and Wang J (2023),
Editorial: Hidden order behind
cooperation in social systems.
Front. Phys. 11:1192856.
doi: 10.3389/fphy.2023.1192856

COPYRIGHT

© 2023 Han, Wang and Wang. This is an
open-access article distributed under the
terms of the [Creative Commons
Attribution License \(CC BY\)](#). The use,
distribution or reproduction in other
forums is permitted, provided the original
author(s) and the copyright owner(s) are
credited and that the original publication
in this journal is cited, in accordance with
accepted academic practice. No use,
distribution or reproduction is permitted
which does not comply with these terms.

Editorial: Hidden order behind cooperation in social systems

Dun Han^{1*}, Jianbo Wang^{2*} and Jianrong Wang^{3*}

¹School of Mathematical Sciences, Jiangsu University, Zhenjiang, Jiangsu, China, ²School of Computer Science, Southwest Petroleum University, Chengdu, Sichuan, China, ³School of Mathematical Sciences, Shanxi University, Taiyuan, Shanxi, China

KEYWORDS

cooperation, social systems, interaction, complex network, decision

Editorial on the Research Topic

Hidden order behind cooperation in social systems

Navigating the complexities of mobility and interaction, an agent's decision to cooperate or not can undergo evolutionary changes over time. Even though individuals are inherently selfish, cooperation behavior remains prevalent and serves as a crucial component of prosocial behavior. Quantitative analysis of cooperation behavior is of both theoretical and practical significance in modern science, with fields such as psychology, sociology, and economics emphasizing this research.

The global 2019-nCoV pandemic has once again highlighted the importance of analyzing virus transmission, prompting countries worldwide to focus on this Research Topic. To aid decision-making teams in implementing preventive measures, research into dynamic models for infectious diseases can aid in understanding transmission processes. Preventive vaccination is a fundamental and highly effective control measure for reducing transmission of infectious diseases and mortality rates. Under a voluntary vaccination scheme, the decision to vaccinate or not becomes an individual game decision, taking into account social environments, economic conditions, potential risks associated with vaccination, and other individuals' vaccination decisions. Understanding the cooperative phenomenon of egotism in disease propagation systems remains a major challenge.

As we live and cooperate within a complex and variable network of relationships, intricate interactions between individuals give rise to highly complex population dynamics. Complex network theory serves as a primary and effective tool for exploring these complex and interactive systems, offering a fresh perspective for studying evolutionary games in nature. This Research Topic in Frontiers in Physics aims to welcome contributions on cooperation behavior, encouraging papers that use network tools to provide meaningful references and insights into comprehending the rules and reasons behind social dilemmas. These findings have inspired the conception of the Research Topic, "Hidden Order Behind Cooperation in Social Systems." Within this Research Topic, [Vasiliauskaite et al.](#) investigated the impact of temporal changes at the individual and social levels on cooperation patterns in social networks. They discovered that temporal variation and synchrony can enhance or suppress cooperation in non-trivial ways, depending on parameter values. [Zhang et al.](#) employed an evolutionary game method to examine the cooperation behavior between government and banks. [Wang et al.](#) analyzed the impact of Wuhan's COVID-19 lockdown on the growth enterprise market in China, shedding light on the significance of digital inclusive finance for mitigating regional risks and financing issues. [Chang's](#) research on an SIR rumor propagation model with an interaction mechanism on WeChat networks provides significant insights for controlling the spread of rumors in WeChat

groups. [Chen et al.](#) examined the searching behavior of Sino-U.S. relations in China based on complex network analysis, offering a new perspective for analyzing the time series characteristics of Sino-U.S. relations.

Based on the contributions of these papers, it is evident that this research topic is highly valuable for understanding social systems. We hope that the theoretical models and practical applications presented in this research will encourage further exploration and development of cooperation in social systems.

Author contributions

All authors listed have made a substantial, direct, and intellectual contribution to the work and approved it for publication.

Conflict of interest

The authors declare that the research was conducted in the absence of any commercial or financial relationships that could be construed as a potential conflict of interest.

Publisher's note

All claims expressed in this article are solely those of the authors and do not necessarily represent those of their affiliated organizations, or those of the publisher, the editors and the reviewers. Any product that may be evaluated in this article, or claim that may be made by its manufacturer, is not guaranteed or endorsed by the publisher.



OPEN ACCESS

EDITED BY

Jianbo Wang,
Southwest Petroleum University, China

REVIEWED BY

Tsun Se Cheong,
Hang Seng University of Hong Kong,
Hong Kong SAR, China
Yunjia Chen,
Shanghai International Studies
University, China

*CORRESPONDENCE

Fujun Lai,
lfjlfj999@163.com

SPECIALTY SECTION

This article was submitted to Social
Physics,
a section of the journal
Frontiers in Physics

RECEIVED 12 August 2022

ACCEPTED 15 September 2022

PUBLISHED 05 October 2022

CITATION

Feng Q, Zhu S and Lai F (2022), A
complex network study on Guangdong-
Hong Kong-Macao Greater Bay Area
based on economic development index.
Front. Phys. 10:1018219.
doi: 10.3389/fphy.2022.1018219

COPYRIGHT

© 2022 Feng, Zhu and Lai. This is an
open-access article distributed under
the terms of the [Creative Commons
Attribution License \(CC BY\)](https://creativecommons.org/licenses/by/4.0/). The use,
distribution or reproduction in other
forums is permitted, provided the
original author(s) and the copyright
owner(s) are credited and that the
original publication in this journal is
cited, in accordance with accepted
academic practice. No use, distribution
or reproduction is permitted which does
not comply with these terms.

A complex network study on Guangdong-Hong Kong-Macao Greater Bay Area based on economic development index

Qingxiang Feng¹, Sha Zhu² and Fujun Lai^{3*}

¹School of Marxism, Sun Yat-sen University, Guangzhou, China, ²School of Statistics and Mathematics, Yunnan University of Finance and Economics, Kunming, China, ³School of Finance, Yunnan University of Finance and Economics, Kunming, China

City cluster, the most advanced spatial organization for urban development in the mature stage, is an important carrier for regional economic development. This paper researched into the correlation of economic development changes among cities in the Guangdong-Hong Kong-Macao Greater Bay Area through a new complex network approach. First, Principal Component Analysis was adopted to downscale the economic indicators of each city in the Greater Bay Area, and then we construct an economic development index on this basis; Second, through a TVS-VAR-SV model, a complex network of economic development changes within the city clusters in the Greater Bay Area was built based on the economic development index of each city mentioned above. It can be concluded from the study that Macao, firstly, is the biggest beneficiary of the complex network. Secondly, the most important node in the network is Guangzhou, whose development has a multiply effect on the development of the whole system. Thirdly, Hong Kong and Shenzhen enjoy the highest level of economic development, but their spillover effect on the city cluster system is much lower than that of Guangzhou.

KEYWORDS

Guangdong-Hong Kong-Macao Greater Bay Area, city cluster, economic development index, complex network, principal component analysis method, TVP-VAR-SV model

Introduction

Guangdong-Hong Kong-Macao Greater Bay Area, located in South China, consists of “9 + 2” cities, namely Guangzhou, Shenzhen, Zhuhai, Foshan, Zhongshan, Dongguan, Huizhou, Jiangmen and Zhaoqing, as well as Hong Kong Special Administrative Region and Macao Special Administrative Region. Boasting a total area of 56,000 square kilometers and a population of over 80 million, the Greater Bay Area has become one of the places with the highest degree of openness and the best economic vigor in China for its high population mobility, a close interaction of production factors and the resulting high GDP. Under the framework of “one country, two systems”, each city in the Greater Bay Area has its own social division of labor and central function. At present, a complete and comprehensive industrial manufacturing chain and value allocation system has

basically been formed, for example, Guangzhou's trade network, Shenzhen's scientific and technological innovation, Hong Kong's financing and investment, Macao's gambling and tourism, and Dongguan and Huizhou's high-end manufacturing. At the same time, the central government and local governments actively cooperate with the national development strategy, and according to the resource endowment, cultural foundation and regional advantages of each city, they have issued corresponding social policies to support the construction of Guangdong-Hong Kong-Macao Greater Bay Area.

Globalization and the development of modern communication technology have helped the flow of inter-city factors break through the boundaries of cities and tightened the economic relationships increasingly. The city cluster is essentially an urban functional area with a high concentration of population, industry, resources and other factors. Based on the realistic conditions and the social development law, the city cluster has become an inevitable trend of China's urban modernization. Guangdong-Hong Kong-Macao Greater Bay Area is a megapolis of 11 cities, where the population mobility, industrial chain upgrading, and resource integration are trying to break through the limit of one single city and turn to network development, which in return is conducive to driving and radiating a wider area. Though governments all over the world have paid more and more attention to the development of city cluster, the theory and method of the economic association network in the Bay Area are obviously lagging behind, and accordingly, fails to explain the current situation, changes and trends of the rapid development of city clusters. In view of this, based on Principal Component Analysis and TVP-VAR-SV model, this paper tried to explore the economic development index and the association network law of Guangdong-Hong Kong-Macao Greater Bay Area in response to the theoretical appeal and practical concern.

Literature review

As the level of urbanization is increasing around the world, the study of urban complex networks has become a research hot topic at home and abroad in recent years. As early as in the 1990s, Castells [1] keenly captures the trend of the rise of the complex network society and proposes that the world city refers to a process of production and reproduction by the globalized network, and the global urban system is created by the mobile space. By replacing the analytical framework of "spatial place" with "flowing space", this point of view breaks through the limitations of previous explanatory research featuring "attribute hierarchy", and turns a new page on urban observation through "network dynamics". For the theory centered on the study of urban networks, Taylor [2] names it as "central flow theory". He argues that based on the central place theory, traditional urban systems research is thus hierarchical.

"Central flow theory" views the relationship between cities as networked, which means it is not contradictory to the central place theory, as the former emphasizes more on global space while the latter more on local space and both of them are complementary to each other.

The rising globalization has seen science and technology changing with each passing day, labor, land, resources, and information flowing in the urban economic networks. The development potential of one single city no longer depends solely on its own population size and economic strength but on its ability to associate with other cities, namely, the strength and density of network links [3]. As an organic whole, cities are originally interconnected and influenced by each other. When "association networks" become the spatial component of modern urban systems, the effective regional organization mechanisms (or institutional integration) can improve the overall organizational capacity of the region, so that the available resources can be shared in a more effective way [4]. The major progress in the study of urban association network theory provides new ideas in solving the problems of unbalanced regional development and exploring the path of regional integration development for the whole world.

Guangdong-Hong Kong-Macao Greater Bay Area, one of China's major national development strategies, aims to build an international top bay area and a world-class city cluster. Among it, economic growth remains the priority in the construction of the Greater Bay Area, while the city clusters are increasingly becoming an important lever for economic development. Based on the extension and application of the theory of city complex networks, many scholars have analyzed the network characteristics, factor associations, and operation mechanisms of the economies in the Guangdong-Hong Kong-Macao Greater Bay Area from different perspectives. The comprehensive development level of Guangdong-Hong Kong-Macao Greater Bay Area's economy is fluctuating rapidly, and the economic index of Hong Kong and Macao has always been the highest in the Bay Area, with a fast growth rate in Guangzhou and Shenzhen [5]. The spatial economic network of the Greater Bay Area is featured with a reasonable and orderly "core-semi-edge-outer edge" hierarchical spatial structure [17]. Four kinds of factors, such as the distance between cities, the diffusion and agglomeration of factors, industrial structure and economic globalization, have significant influence on Guangdong-Hong Kong-Macao Greater Bay Area's economic network [6]. The increase in network density and network hierarchy as well as the decrease in network efficiency can effectively enhance the economic relations within the Guangdong-Hong Kong-Macao Greater Bay Area. While point centrality, intermediate centrality and proximity centrality can all strengthen the economic bonds in the Greater Bay Area [7]. Therefore, to promote regional coordinated development, we should adhere to the concept of "interconnection and intercommunication", weaken the scope of administrative boundaries [8], improve the radiation capacity of

the core cities of city clusters in the Greater Bay Area, build a hub-and-spoke network pattern, and innovate institutional mechanisms [9].

To sum up, the current research on regional economic complex networks features a combination of quantitative and qualitative as well as a combination of theory and practice. These thoughts offer important theoretical insights and a useful analytical framework for this paper. How to measure the economic development level of each city in the Greater Bay Area? How do the economic factors between them interact and influence each other? How to find out the key nodes of the economic complex network of city clusters? However, these questions have not been adequately explained in the related studies, either theoretically or methodologically. Therefore, what this paper discovers may deepen the study of complex networks by providing enlightenment for the economic development of the Greater Bay Area.

Model construction

The research goal of this paper is to build an economic development complex network among cities in Guangdong-Hong Kong-Macao Greater Bay Area and then adopt an empirical analysis of this network. The establishment of the model can be divided into two steps: first, this paper used the Principal Component Analysis (PCA) to reduce the dimension of classified data of economic development of cities in Guangdong-Hong Kong-Macao Greater Bay Area and then built the economic development index of each city through the Principal Component Factor Analysis. Second, the changes of economic development index of each city in the Greater Bay Area mentioned above was used to build the complex network of economic development among cities in Guangdong-Hong Kong-Macao Greater Bay Area by the TVP-VAR-SV model.

Construction of economic development index of cities in Guangdong-Hong Kong-Macao Greater Bay Area

This section will describe the methodology used to construct the economic development index of cities in the Guangdong-Hong Kong-Macao Greater Bay Area (the Greater Bay Area). In this paper, the principal component analysis method will be used to construct the comprehensive evaluation index of economic development. Principal component analysis (PCA) is a statistical procedure with the core idea of transforming multiple variables into a few principal components through dimensionality reduction techniques, and these principal components retain most of the information of the original variables. To this end, we can evaluate the economic development of the urban

agglomeration in the Greater Bay Area by leveraging the principal component information.

The evaluation is mainly divided into three steps: In the first step, standardized processing will be carried out on the data. Before measuring the comprehensive level of economic development, it is necessary to adjust the value of the indicators to make it co-trended and dimensionless, so as to eliminate the deviation caused by the different nature and dimension of the index. Because we will use PCA to reduce the dimension of the data later, we choose economic condition variables which we can collect and add them into the model. In the second step, principal component analysis and dimensionality reduction are carried out for the standardized indicators. The principal component analysis is carried out on the treated indicators, and the number of principal components is determined (generally) according to the principle that the cumulative variance contribution rate is not less than 85%, and the scores of each principal component are calculated. In the third step, a comprehensive evaluation index is constructed, that is, the economic development index of cities in the Greater Bay Area. The principal component scores of each city are weighted and summed to obtain a comprehensive evaluation of the economic level of each city, which is the economic development index we have constructed. The weight is the proportion of the variance contribution rate of each principal component in the cumulative variance contribution rate of the extracted principal component.

The detailed process and steps are as follows

1) Data standardization.

Ten indicators related to economic development in 11 cities in the Greater Bay Area are collected, and these original indicators are standardized (in time series). The data obtained after standardization is recorded as x_{ij} . The specific equation is:

$$x_{ij} = \frac{z_{ij} - \text{mean}_j}{\text{sd}_j} \quad (1)$$

Where, $i = 1, 2, \dots, n$; $j = 1, 2, \dots, p$. z_{ij} represents the original data with dimensions, i represents the i th sample, with a total of n samples, and j represents the j th indicator variable, with a total of p indicator variables. x_{ij} represents the original data after dimension elimination. mean_j indicates the sample average value of the j th indicator variable, sd_j indicates the sample standard deviation of the j th indicator variable.

2) Principal component analysis

(a) First, a covariance matrix is constructed using the standardized dimensionless data.

The standardized data matrix is set to X , where each column vector (standardized variable) has an expectation of 0 and a variance of 1. A dimensionless covariance matrix $\text{Cov} =$

$\frac{1}{n-1}X^T X = (r_{ij})_{p \times p}$ of the variables is built using the standardized data x_{ij} , where,

$$r_{ij} = \frac{1}{n-1} \sum_{k=1}^n (x_{ki} - \bar{x}_i)(x_{kj} - \bar{x}_j) \quad (2)$$

Where, x_{ki} indicates the data in the k row and i column of dimensionless data, \bar{x}_i indicates the average value in the i column of dimensionless data.

b) Then, the eigenvalues and eigenvectors of the covariance matrix are calculated by eigenvalue decomposition: $\lambda_1 \geq \dots \geq \lambda_p > 0$, w_1, w_2, \dots, w_p .

Since $\text{Cov} = \frac{1}{n-1}X^T X$ is a real symmetric matrix, we can decompose the eigenvalue of the real symmetric matrix by using a property of the real symmetric matrix. The eigenvalues of $\text{Cov} = \frac{1}{n-1}X^T X$ are decomposed and sorted in descending order to form a new covariance matrix Σ , and the corresponding eigenvectors (unit orthogonal bases) form the transformation matrix W . Therefore, $\text{Cov} = W\Sigma W^T$ can be obtained by eigenvalue decomposition, where $W = [w_1, w_2, \dots, w_p]$; $\Sigma = \text{diag}(\lambda_1, \lambda_2, \dots, \lambda_p)$. Generally, the eigenvalues of Σ are arranged in descending order in the eigenvalue decomposition.

c) The number of principal components is determined, and the scores of each principal component are obtained.

To realize the final data dimensionality reduction, m principal components are reasonably selected from all p principal components. Generally, the variance contribution rate $G(m) = \frac{\sum_{i=1}^m \lambda_i}{\sum_{i=1}^p \lambda_i}$ is used to explain the amount of information reflected by principal component F . We need to choose the value of m reasonably so that the cumulative contribution rate $G(m) = \frac{\sum_{i=1}^m \lambda_i}{\sum_{i=1}^p \lambda_i}$ reaches a large enough threshold (usually 85%).

The scores of each principal component can be obtained by dimensionless data matrix and feature vector matrix:

$$F = [F_1, F_2, \dots, F_p] = XW$$

$$= \begin{pmatrix} x_{11} & x_{12} & \dots & x_{1p} \\ x_{21} & x_{22} & \dots & x_{2p} \\ \vdots & \vdots & & \vdots \\ x_{n1} & x_{n2} & \dots & x_{np} \end{pmatrix} \begin{pmatrix} w_{11} & w_{12} & \dots & w_{1p} \\ w_{21} & w_{22} & \dots & w_{2p} \\ \vdots & \vdots & & \vdots \\ w_{p1} & w_{p2} & \dots & w_{pp} \end{pmatrix} \quad (3)$$

Where, x_{ij} represents the original data after dimension elimination, and W corresponds to the feature vector. According to the cumulative contribution rate $G(m)$, the scores of the first m principal components can be selected to construct a comprehensive evaluation index.

d) Finally, a comprehensive evaluation index is constructed according to the principal components.

Taking the proportion of variance contribution rate corresponding to m principal components in the cumulative variance contribution rate as the weight, the scores of principal

components are weighted and summed up, and the comprehensive evaluation index of the economic level of cities in the Greater Bay Area is obtained, which is the economic development index we constructed.

Comprehensive evaluation index

$$= F_1 \cdot \frac{\lambda_1}{\sum_{i=1}^m \lambda_i} + F_2 \cdot \frac{\lambda_2}{\sum_{i=1}^m \lambda_i} + \dots + F_m \cdot \frac{\lambda_m}{\sum_{i=1}^m \lambda_i} \quad (4)$$

Construction of complex network of economic development index of cities in Guangdong-Hong Kong-Macao Greater Bay Area

In the following content, this section will construct the economic development complex network of the urban agglomeration in the Greater Bay Area by using the variation of the economic development index previously constructed.

1) TVP-VAR-SV model

Diebold and Yilmaz [10–12] put forward the method of the Vector Autoregressive Model (VAR) to construct an information spillover networks among financial institutions. Despite being easy to use, this method still retains the shortcomings of the fixed-parameter VAR model. First, the model parameters of VAR are fixed in the window period; Second, the time window must be long enough, and a large number of samples need to be used for estimation. As the data samples of the economic development index of 11 cities in the Greater Bay Area were only established in 2010, such a short time span limits the application of the above methods. To effectively address the above two deficiencies, this paper assumes that the data is generated by the TVP-VAR-SV process, and then performs parameter estimation by using the Bayesian Analysis method and MCMC sampling.

Primiceri [13] proposed a time-varying parameter vector autoregressive model (TVP-VAR-SV) in which all parameters change with time. The model is evolved from the traditional VAR model, and its parameters are given time-varying characteristics, which overcomes many limitations of the traditional VAR model in practical application.

The basic form of a traditional time-invariant VAR(p) model with p -order lag is as follows:

$$Ay_t = F_1 y_{t-1} + F_2 y_{t-2} + \dots + F_p y_{t-p} + \mu_t, \quad t = p+1, \dots, n \quad (5)$$

Where, y_t is a $k \times 1$ dimensional observation variable, A and F_i are a $k \times k$ dimensional coefficient matrix, and the random disturbance term μ_t is a $k \times 1$ dimensional structural impact, and it is set that $\mu_t \sim (0, \Sigma)$. Assume that A is a lower triangular matrix with all main diagonal elements of 1, that is:

$$A = \begin{pmatrix} 1 & 0 & \cdots & 0 \\ \alpha_{21} & 1 & \ddots & \vdots \\ \vdots & \ddots & \ddots & 0 \\ \alpha_{k1} & \cdots & \alpha_{kk-1} & 1 \end{pmatrix}, \text{ meanwhile, } \Sigma = \begin{pmatrix} \sigma_1 & 0 & \cdots & 0 \\ 0 & \sigma_2 & \ddots & \vdots \\ \vdots & \ddots & \ddots & 0 \\ 0 & \cdots & 0 & \sigma_k \end{pmatrix}$$

If the structural impact of the contemporaneous relationship is identified by the recursive method, Equation 1 can be rewritten as:

$$y_t = B_1 y_{t-1} + B_2 y_{t-2} + \cdots + B_p y_{t-p} + A^{-1} \Sigma \varepsilon_t, \varepsilon_t \sim (0, I_k) \quad (6)$$

If the parameters in Eq. 6 are given time-varying characteristics, then the TVP-VAR-SV model can be expressed as:

$$y_t = B_{1,t} y_{t-1} + B_{2,t} y_{t-2} + \cdots + B_{p,t} y_{t-p} + A_t^{-1} \Sigma_t \varepsilon_t, \varepsilon_t \sim (0, I_k) \quad (7)$$

Where, $B_{i,t} = A_t^{-1} F_{i,t}$, $i = 1, 2, \dots, p$, the elements of the matrix $B_{i,t}$ are stacked according to the row vector to obtain the vector $\beta_t (k^2 s \times 1)$. Besides, if we define $X_t = I_k \otimes (y_t' y_{t+2}' \cdots y_{t-p}')$, where \otimes represents the Kronecker product, then the TVP-VAR-SV model can be further abbreviated as:

$$y_t = X_t \beta_t + A_t^{-1} \Sigma_t \varepsilon_t, t = p+1, \dots, n \quad (8)$$

In this TVP-VAR-SV model, the parameters β_t , A_t and Σ_t are time-varying. Where, A_t and Σ_t are:

$$A_t = \begin{pmatrix} 1 & 0 & \cdots & 0 \\ \alpha_{21,t} & 1 & \ddots & \vdots \\ \vdots & \ddots & \ddots & 0 \\ \alpha_{k1,t} & \cdots & \alpha_{kk-1,t} & 1 \end{pmatrix}, \Sigma_t = \begin{pmatrix} \sigma_{1,t} & 0 & \cdots & 0 \\ 0 & \sigma_{2,t} & \ddots & \vdots \\ \vdots & \ddots & \ddots & 0 \\ 0 & \cdots & 0 & \sigma_{k,t} \end{pmatrix}$$

According to Primiceri [13], let α_t be the row stacking of the lower triangular off-diagonal elements of the matrix A_t , that is:

$$\alpha_t = (\alpha_{21,t}, \alpha_{31,t}, \alpha_{32,t}, \alpha_{41,t}, \dots, \alpha_{kk-1,t})' \quad (9)$$

And let $h_t = (h_{1t}, h_{2t}, \dots, h_{kt})$, where $h_{jt} = \log \sigma_{jt}^2$, $j = 1, 2, \dots, k$, and $t = p+1, \dots, n$.

Meanwhile, it is assumed that the parameters in the TVP-VAR-SV model follow the random walk process:

$$\beta_{t+1} = \beta_t + \mu_{\beta_t}, \alpha_{t+1} = \alpha_t + \mu_{\alpha_t}, h_{t+1} = h_t + \mu_{h_t}, \quad (10)$$

$$\text{Where: } \begin{pmatrix} \varepsilon_t \\ \mu_{\beta_t} \\ \mu_{\alpha_t} \\ \mu_{h_t} \end{pmatrix} \sim N \left(0, \begin{pmatrix} I_k & 0 & 0 & 0 \\ 0 & \Sigma_{\beta} & 0 & 0 \\ 0 & 0 & \Sigma_{\alpha} & 0 \\ 0 & 0 & 0 & \Sigma_h \end{pmatrix} \right)$$

However, $t = p+1, \dots, n$, Σ_{β} , Σ_{α} and Σ_h are all positive definite diagonal matrices, and the initial values $\beta_{p+1} \sim N(\mu_{\beta_0}, \Sigma_{\beta_0})$, $\alpha_{p+1} \sim N(\mu_{\alpha_0}, \Sigma_{\alpha_0})$, $h_{p+1} \sim N(\mu_{h_0}, \Sigma_{h_0})$. Besides, ε_t , μ_{β_t} , μ_{α_t} and μ_{h_t} are all independent of each other.

In view of the low sample time span, in order to avoid “over-parameterization” in the time-varying model, this paper directly

sets the lag order of the model to 1 with reference to the practice of other scholars. The TVP-VAR-SV model described above can be estimated by the Bayesian Analysis method and MCMC sampling, as discussed in detail by Primiceri [13] and Nakajima et al. [14]. For MCMC samples, the posterior mean is used as the estimated value. Therefore, we can estimate the time-varying parameter matrix $B_{1,t}$, $B_{2,t}$, \dots , $B_{p,t}$; A_t and Σ_t . According to the estimated parameters of the TVP-VAR-SV model, the Impulse Response Function (IRF) and Generalized Forecast Error Variance Decomposition (GFEVD) which change with time can be calculated. Finally, using the estimated parameters, the complex network matrix based on the variance decomposition of generalized prediction errors can be constructed.

2) Complex network of economic development index variation of urban agglomeration

Diebold and Yilmaz [10–12] defined the information spillover effect as the variance contribution of prediction error, that is, the proportion of y_i 's H-step prediction error variance that can be explained by y_j 's shock after y_j 's shock has an impact on y_i under the condition that $i \neq j$. This proportion reflects the degree to which the change of the variable y_i is affected by other variables in the system. Before calculating the contribution of the H-step prediction error, it is necessary to obtain the connectedness matrix of the impulse response function. To calculate the time-varying impulse response function, Eq. 5 is converted into the representation of its Vector Moving Average (VMA):

$$Y_t^* = \sum_{i=0}^{\infty} \Psi_{i,t} u_{t-i} \quad (11)$$

Where, $Y_t^* = y_t - \bar{y}$, and $u_t = A_t^{-1} \Sigma_t \varepsilon_t$. And the $k \times k$ coefficient matrix $\Psi_{i,t}$ can be obtained by recursive calculation.

$$\Psi_{h,t} = B_{1,t} \Psi_{h-1,t} + B_{2,t} \Psi_{h-2,t} + \dots + B_{p,t} \Psi_{h-p,t} \quad (12)$$

For $t = p+1, p+2, \dots, t$, where $\Psi_{0,t} = I_k$, if $j < 0$, then $\Psi_{j,t} = 0$. Then, the time-varying impulse response function at time t is $\text{IRF}_h = \Psi_{h,t} A_t^{-1} \Sigma_t$.

And let $d_{ij,t}^{gH}$ be the degree to which y_j contributes to the variance of the H-step generalized prediction error of y_i at time t , indicate the degree to which the change of variable y_i is affected by y_j .

$$d_{ij,t}^g(H) = \frac{\sigma_{jj,t}^{-1} \sum_{h=0}^{H-1} (e_i' \Psi_{h,t} \Sigma_{ut} e_j)^2}{\sum_{h=0}^{H-1} (e_i' \Psi_{h,t} \Sigma_{ut} \Psi_{h,t}' e_i)} \quad (13)$$

Where, e_j is a selection vector with the j th element being one and the other elements being 0; $\Psi_{h,t}$ represents the coefficient matrix in the impulse response function; $\Sigma_{ut} = A_t^{-1} \Sigma_t (A_t^{-1})'$ is the variance matrix of u_t ; $\sigma_{jj,t}$ represents the diagonal elements of

TABLE 1 The connectedness effect of economic development index.

| | y_1 | y_2 | ... | y_k | Receiving effect |
|------------------|------------------------------------------------|------------------------------------------------|----------|------------------------------------------------|------------------------------------------------|
| y_1 | $\tilde{d}_{11,t}^{gH}$ | $\tilde{d}_{12,t}^{gH}$ | ... | $\tilde{d}_{1k,t}^{gH}$ | $\sum_{j=1}^k \tilde{d}_{1j,t}^{gH}, j \neq 1$ |
| y_2 | $\tilde{d}_{21,t}^{gH}$ | $\tilde{d}_{22,t}^{gH}$ | ... | $\tilde{d}_{2k,t}^{gH}$ | $\sum_{j=1}^k \tilde{d}_{2j,t}^{gH}, j \neq 2$ |
| \vdots | \vdots | \vdots | \ddots | \vdots | \vdots |
| y_k | $\tilde{d}_{k1,t}^{gH}$ | $\tilde{d}_{k2,t}^{gH}$ | ... | $\tilde{d}_{kk,t}^{gH}$ | $\sum_{j=1}^k \tilde{d}_{kj,t}^{gH}, j \neq k$ |
| Diffusion Effect | $\sum_{i=1}^k \tilde{d}_{i1,t}^{gH}, i \neq 1$ | $\sum_{i=1}^k \tilde{d}_{i2,t}^{gH}, i \neq 2$ | ... | $\sum_{i=1}^k \tilde{d}_{ik,t}^{gH}, i \neq k$ | |

the matrix Σ_{ut} at time t . This generalized variance decomposition method of prediction error makes the order of variables in the VAR model no longer affect the results of variance decomposition so that we no longer need to stick to the order of variables in the model, and it is more convenient for us to analyze related results [12,15,16].

But since $\sum_{j=1}^k \tilde{d}_{ij,t}^{gH} \neq 1$, in order to match the traditional variance decomposition results, we can add each element in the variance decomposition matrix of generalized prediction error by row and standardize it.

$$\tilde{d}_{ij,t}^g(H) = \frac{\tilde{d}_{ij,t}^{gH}(H)}{\sum_{j=1}^N \tilde{d}_{ij,t}^{gH}(H)} \quad (14)$$

By constructing $\sum_{j=1}^N \tilde{d}_{ij,t}^g(H) = 1$ and $\sum_{i,j=1}^N \tilde{d}_{ij,t}^g(H) = N$, we can calculate the connectedness matrix $\tilde{D}_t^g(H)$ of the economic development index for H -step at each time t .

$$\tilde{D}_t^g(H) = \begin{pmatrix} \tilde{d}_{11,t}^{gH} & \tilde{d}_{12,t}^{gH} & \cdots & \tilde{d}_{1k,t}^{gH} \\ \tilde{d}_{21,t}^{gH} & \tilde{d}_{22,t}^{gH} & \ddots & \tilde{d}_{2k,t}^{gH} \\ \vdots & \vdots & \ddots & \vdots \\ \tilde{d}_{k1,t}^{gH} & \tilde{d}_{k2,t}^{gH} & \cdots & \tilde{d}_{kk,t}^{gH} \end{pmatrix} \quad (15)$$

Specifically, in the variance decomposition matrix $\tilde{D}_t^g(H)$, the off-diagonal elements reflect the connected degree of economic development index between city i and city j . For example, the i -row and the j -column in $\tilde{D}_t^g(H)$ show the spillover effect of the economic development of city j on city i ; The j -row and the i -column in $\tilde{D}_t^g(H)$ show the spillover effect of the economic development of city i on city j . It should also be reminded that the TVP-VAR-SV model is used in this paper to estimate the prediction error variance matrix, so there is a prediction error variance matrix for each period t in this paper. This is an important difference between this paper and the traditional VAR method in constructing the prediction variance matrix.

For the off-diagonal sum of elements in the i -row in $\tilde{D}_t^g(H)$:

$$C_{i \leftarrow \bullet,t}^H = \sum_{j=1}^k \tilde{d}_{ij,t}^{gH}, j \neq i \quad (16)$$

Then, $C_{i \leftarrow \bullet,t}^H$ represents the degree to which city i is affected by the economic development indexes of other $k-1$ cities. So we can call $C_{i \leftarrow \bullet,t}^H$ the receiving effect of city i .

Similarly, for the off-diagonal sum of elements in the i -column in $\tilde{D}_t^g(H)$:

$$C_{\bullet \leftarrow i,t}^H = \sum_{j=1}^k \tilde{d}_{ij,t}^{gH}, i \neq j \quad (17)$$

Then, the sum $C_{\bullet \leftarrow i,t}^H$ in the i -column represents the spillover effect of city i 's economic development index on other $k-1$ cities' economic development indexes. So we call $C_{\bullet \leftarrow i,t}^H$ diffusion effect of city i . See Table 1 for details.

On this basis, we can define the net spillover effect and total connectedness effect of city i 's economic development index. The net spillover effect can be expressed as:

$$C_{i,t}^{\text{Net}} = C_{\bullet \leftarrow i,t}^H - C_{i \leftarrow \bullet,t}^H \quad (18)$$

The net spillover effect is obtained by subtracting the receiving effect from the diffusion effect of the city, so it reflects the net radiation ability of the economic development index of the city to the economic development indexes of other cities in the urban agglomeration. If the net spillover effect of city i is greater than 0, then the influence of city i on other cities is greater than that of other cities, which indicates that city i occupies a central position in the urban agglomeration, and its influence and radiation capacity are greater; On the contrary, if the net spillover effect of city i is less than 0, it means that city i is in a marginal position in the urban agglomeration, with weak influence and radiation power.

The total spillover effect can be expressed as:

$$C_{i,t}^{\text{Total}} = C_{\bullet \leftarrow i,t}^H + C_{i \leftarrow \bullet,t}^H \quad (19)$$

The total correlation effect is obtained by adding the diffusion effect and receiving effect of the city, so it can reflect the importance of the city in the process of communication and integration within the urban agglomeration in the Greater Bay Area. The larger the value, the more important the city i is in the Bay Area urban agglomeration. The closer the communication

TABLE 2 Variable definition.

| Variable name | Meaning |
|----------------|-----------------------------------------------------------------------------------|
| Export | Total exports/USD 100 million |
| Import | Total imports/USD 100 million |
| Excargo | Proportion of goods exports in the total exports of the Greater Bay Area/% |
| Imcargo | Proportion of goods imports in the total imports of the Greater Bay Area/% |
| FDI | Amount of foreign direct investment (FDI)/10,000 yuan |
| Finance | Loan-to-deposit ratio in local and foreign currencies of financial institutions/% |
| PortsVolume | Port cargo throughput/10,000 tons |
| Tourists | Total number of tourists/10,000 tourists |
| InboundTourist | Proportion of inbound tourists to the total number of tourists/% |
| TourismRevenue | Total tourism revenue/100 million yuan |

TABLE 3 Explanation of total variance.

| Component part | Eigenvalue | Difference of eigenvalues | Contribution rate | Cumulative contribution rate |
|----------------|------------|---------------------------|-------------------|------------------------------|
| Comp1 | 7.08464 | 5.44082 | 0.7085 | 0.7085 |
| Comp2 | 1.64381 | 0.821186 | 0.1644 | 0.8728 |
| Comp3 | 0.822629 | 0.624486 | 0.0823 | 0.9551 |
| Comp4 | 0.198143 | 0.032351 | 0.0198 | 0.9749 |
| Comp5 | 0.165792 | 0.116066 | 0.0166 | 0.9915 |
| Comp6 | 0.049726 | 0.025656 | 0.005 | 0.9965 |
| Comp7 | 0.02407 | 0.015734 | 0.0024 | 0.9989 |
| Comp8 | 0.008335 | 0.005876 | 0.0008 | 0.9997 |
| Comp9 | 0.002459 | 0.002065 | 0.0002 | 1 |
| Comp10 | 0.000394 | | 0 | 1 |

relationship in the urban agglomeration, the deeper the degree of mutual learning, competition and reference.

Empirical results

Construction results of economic development index

Because we will use PCA to reduce the dimension of the data later, we choose economic condition variables which we can collect and add them into the model. Table 2 details the meanings of the related variables we used to construct the economic development index. By using Stata software, the 10 original index variables are standardized by Z-score to get the standardized variables, and then the subsequent principal component analysis is carried out on these standardized variables.

We found that the first three eigenvalues were greater than or close to 1, and the cumulative variance contribution rate reached 95.51%, so we chose $m = 3$, that is, dimension reduction of the

TABLE 4 Eigenvectors of the first three principal components.

| Variable | Comp1 | Comp2 | Comp3 |
|----------------|--------|---------|---------|
| Export | 0.3615 | -0.1275 | 0.1018 |
| Import | 0.3639 | -0.1826 | 0.0438 |
| Excargo | 0.3593 | -0.1396 | 0.103 |
| Imcargo | 0.3627 | -0.1909 | 0.0396 |
| FDI | 0.3358 | -0.27 | -0.0342 |
| Finance | 0.1608 | 0.294 | 0.8966 |
| PortsVolume | 0.2329 | 0.5698 | -0.1599 |
| Tourists | 0.3038 | 0.3474 | -0.2358 |
| InboundTourist | 0.3346 | -0.2772 | -0.1852 |
| TourismRevenue | 0.2813 | 0.4614 | -0.2346 |

first three principal components. The variance contribution rate reaches 95.51%, indicating that these three factors can explain variables. The contribution rate of specific principal components is shown in Table 3.

TABLE 5 Economic development index.

| year | DongGuan | FoShan | GuangZhou | HongKong | HuiZhou | JiangMen | Macao | ShenZhen | ZhongShan | ZhouQing | ZhuHai |
|------|----------|----------|-----------|----------|----------|----------|----------|----------|-----------|----------|----------|
| 2010 | -0.91865 | -1.30896 | 0.808154 | 4.158358 | -1.32879 | -1.84488 | -1.57641 | 1.397716 | -1.69102 | -1.46987 | -1.26329 |
| 2011 | -0.8218 | -1.12081 | 0.964983 | 4.608636 | -1.25102 | -1.73515 | -1.45748 | 1.652942 | -1.56303 | -1.33719 | -1.18476 |
| 2012 | -0.70845 | -1.0727 | 1.052721 | 4.938371 | -1.06128 | -1.58116 | -1.54422 | 1.798581 | -1.49509 | -1.2246 | -1.18807 |
| 2013 | -0.68568 | -1.0405 | 1.170917 | 5.185219 | -0.94291 | -1.52012 | -1.43721 | 2.043477 | -1.42877 | -1.26493 | -1.30154 |
| 2014 | -0.53956 | -0.84609 | 1.498392 | 5.606448 | -0.72696 | -1.32182 | -1.19574 | 1.993717 | -1.21291 | -1.20674 | -1.16448 |
| 2015 | -0.48978 | -0.8391 | 1.580754 | 5.323792 | -0.73254 | -1.20717 | -1.08242 | 1.431982 | -1.14301 | -1.13967 | -1.08729 |
| 2016 | -0.50784 | -0.84497 | 1.737865 | 5.235643 | -0.74204 | -1.06908 | -1.02091 | 1.612893 | -1.11079 | -1.36023 | -0.70565 |
| 2017 | -0.47526 | -0.74426 | 2.152914 | 5.754495 | -0.55958 | -0.88137 | -0.97137 | 1.831731 | -0.97692 | -1.24732 | -0.57146 |
| 2018 | -0.33296 | -0.62011 | 2.627814 | 5.950539 | -0.30805 | -0.65648 | -0.80287 | 2.170822 | -0.92672 | -1.03706 | -0.51096 |

TABLE 6 Estimation results of TVP-VAR-SV model parameters.

| Parameter | Mean | Stdev | 95%L | 95%U | Geweke | Inef |
|-----------|--------|--------|--------|--------|--------|------|
| sb1 | 0.0225 | 0.0018 | 0.0193 | 0.0263 | 0.664 | 1.12 |
| sb2 | 0.0226 | 0.0018 | 0.0194 | 0.0265 | 0.328 | 1.75 |
| sa1 | 0.0777 | 0.0224 | 0.0477 | 0.1325 | 0.118 | 5.35 |
| sh1 | 0.0565 | 0.0115 | 0.0391 | 0.0838 | 0.806 | 1.06 |
| sh2 | 0.0566 | 0.0117 | 0.039 | 0.0848 | 0.006 | 1 |

Finally, using the eigenvectors in Table 4, we can calculate the scores of the first three most important principal components. Then, the economic development index is obtained by the following formula:

$$\begin{aligned} \text{Economic development index} &= F_1 \cdot \frac{\lambda_1}{\sum_{i=1}^m \lambda_i} + F_2 \cdot \frac{\lambda_2}{\sum_{i=1}^m \lambda_i} + \dots \\ &\quad + F_m \cdot \frac{\lambda_m}{\sum_{i=1}^m \lambda_i} \\ &= (0.7085 \cdot \text{Comp1} + 0.1644 \cdot \text{Comp2} + 0.0823 \cdot \text{Comp3}) / 0.9551 \end{aligned}$$

Table 5 shows the economic development level of cities in the Greater Bay Area.

Analysis of complex network parameter estimation results

In this paper, the Bayesian estimation framework and MCMC sampling method are used to estimate the parameters of the TVP-VAR-SV model. Among them, the total number of MCMC samples is 11,000, the first 1,000 samples are used for the burning period, and the last 10,000 samples for parameter estimation. Table 6 shows the parameter estimation results of the TVP-VAR-SV model. Among them, CD convergence value (Geweke) and inefficiency factors are the indicators to measure the effect of MCMC. Geweke index is used to measure the convergence of the Markov Chain, while inefficiency factors are used to measure the number of irrelevant samples generated by model simulation.

As can be seen from Table 3, the average values of relevant parameters are all in the 95% confidence interval. However, the CD convergence values (Geweke) are all less than 1.96 (the critical value of 5%), which indicates that we can accept the original assumption of convergence to the posterior distribution, that is, 10,000 MCMC samples are enough to make effective parameter estimation. In addition, the invalid influence factors in Table 6 are all small values, which indicates that the samples produced in the MCMC sampling process are valid.

Figure 1 shows the autocorrelation coefficient, sample value path and posterior density of MCMC samples. It can be seen from Figure 1 that the autocorrelation coefficient of the sample

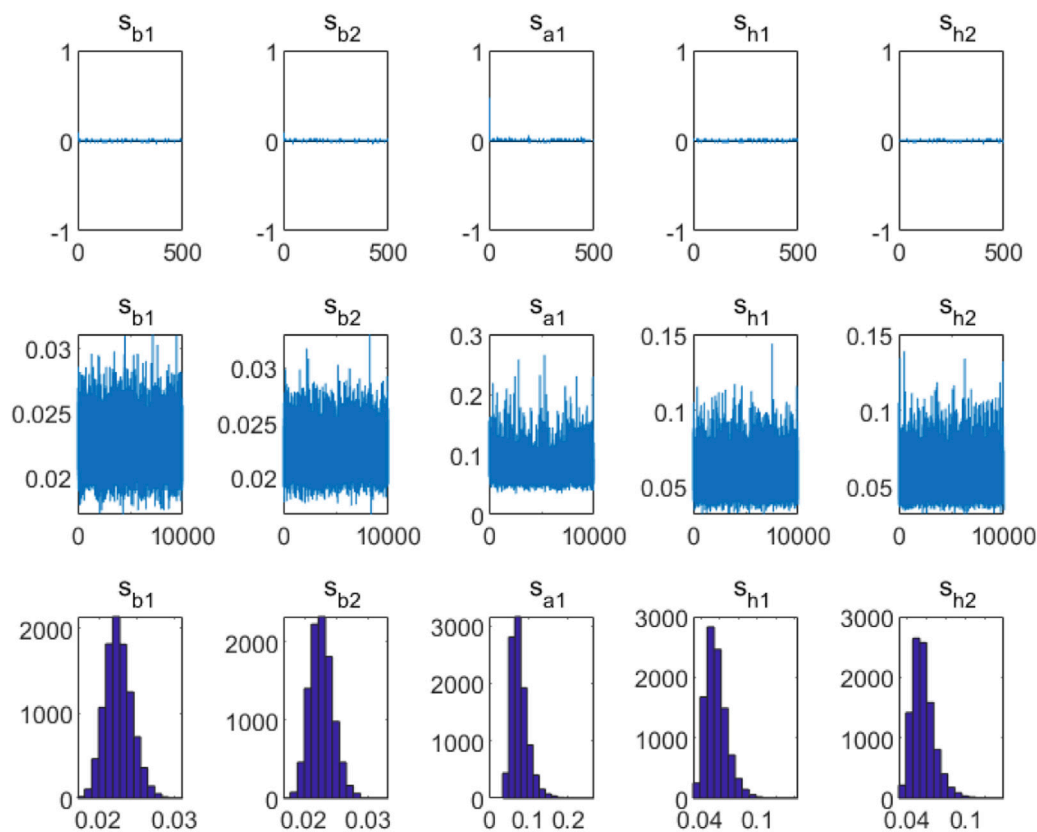


FIGURE 1
Estimation results of parameters of TVP-VAR-SV model.

changes around the value of 0, and the sampling path also changes smoothly around its mean value. The results in Table 6 and Figure 1 show that the model has achieved good estimation results.

The characteristics of the economic development network of cities in Guangdong-Hong Kong-Macao Greater Bay Area

Table 7 illustrates the average complex network of economic development variation among cities in Guangdong-Hong Kong-Macao Greater Bay Area in sample period. We estimated the connectedness of economic development among cities whose predicted step number $H = 10$ and lag order $p = 1$. The ij element in the table indicates the impact of the economic development variation in the city j on the economic development variation in the city i . Column sum without diagonal lines (“Diffusion Effect”) indicates the total impact on other cities from city j ; Row sum without diagonal lines (“Receiving Effect”) shows the total impact from other cities to city i .

As far as “Receiving Effect” is concerned, according to Table 7, Macao accounts for 99.63% - the biggest recipient (beneficiary) in Guangdong-Hong Kong-Macao Greater Bay Area’s economic development association network, followed by Shenzhen and Foshan, with 98.30 and 97.22% respectively, which means that compared with other cities in the Greater Bay Area, these three benefit most from the economic development of other cities and gain more from the overall development of the system.

As far as “Diffusion Effect” is concerned, Guangzhou is the largest transmitter (radiator) among 11 cities in the Greater Bay Area, hitting 401.64%, far more than Jiangmen (187.24%) and Dongguan (117.10%), the second and third. It demonstrates that in the overall development of Guangdong-Hong Kong-Macao Greater Bay Area, Guangzhou, a promoter for other cities, is playing a vital role in the development of the whole bay area system.

As far as “Net Spillover” is concerned, Table 7 indicates that among the 11 cities in the Greater Bay Area, Guangzhou is the most powerful economic engine in the development of the whole system, followed by Jiangmen and Dongguan. These three cities’ economic strengths can help gain huge economic momentum for the development of the whole system. If the economy of these

TABLE 7 Complex network for economic development of Guangdong-Hong Kong-Macao greater bay area.

| | DongGuan | FoShan | GuangZhou | HongKong | HuiZhou | JiangMen | Macao | ShenZhen | ZhongShan | ZhaoQing | ZhuHai | Receiving effect |
|------------------|----------|--------|-----------|----------|---------|----------|--------|----------|-----------|----------|--------|------------------|
| DongGuan | 0.00 | 2.78 | 40.64 | 2.57 | 5.19 | 18.64 | 0.39 | 1.17 | 3.02 | 9.95 | 3.76 | 88.11 |
| FoShan | 11.79 | 0.00 | 40.41 | 2.67 | 5.19 | 18.87 | 0.37 | 1.21 | 3.06 | 9.90 | 3.76 | 97.22 |
| GuangZhou | 11.93 | 2.73 | 0.00 | 2.60 | 5.24 | 18.71 | 0.35 | 1.15 | 2.99 | 9.77 | 3.59 | 59.06 |
| HongKong | 11.50 | 2.63 | 39.26 | 0.00 | 5.25 | 19.29 | 0.41 | 1.38 | 3.15 | 10.16 | 3.96 | 97.01 |
| HuiZhou | 11.79 | 2.71 | 40.39 | 2.66 | 0.00 | 18.83 | 0.36 | 1.23 | 3.04 | 9.99 | 3.74 | 94.73 |
| JiangMen | 11.89 | 2.78 | 40.84 | 2.64 | 5.12 | 0.00 | 0.36 | 1.13 | 3.03 | 9.72 | 3.67 | 81.17 |
| Macao | 11.95 | 2.79 | 41.05 | 2.57 | 5.13 | 18.75 | 0.00 | 1.12 | 3.02 | 9.60 | 3.65 | 99.63 |
| ShenZhen | 10.92 | 2.67 | 37.53 | 3.33 | 5.81 | 18.41 | 0.89 | 0.00 | 3.03 | 11.34 | 4.38 | 98.30 |
| ZhongShan | 11.83 | 2.73 | 40.53 | 2.75 | 5.06 | 19.15 | 0.32 | 1.18 | 0.00 | 9.55 | 3.73 | 96.84 |
| ZhaoQing | 11.66 | 2.60 | 40.02 | 3.06 | 5.74 | 17.88 | 0.85 | 1.61 | 2.92 | 0.00 | 3.67 | 90.00 |
| ZhuHai | 11.84 | 2.98 | 40.97 | 2.80 | 4.92 | 18.72 | 0.51 | 1.02 | 3.00 | 9.41 | 0.00 | 96.16 |
| Diffusion Effect | 117.10 | 27.41 | 401.64 | 27.64 | 52.65 | 187.24 | 4.80 | 12.20 | 30.28 | 99.37 | 37.90 | Total: 998.23 |
| Net Spillover | 28.99 | -69.82 | 342.58 | -69.37 | -42.08 | 106.07 | -94.83 | -86.1 | -66.56 | 9.37 | -58.27 | |

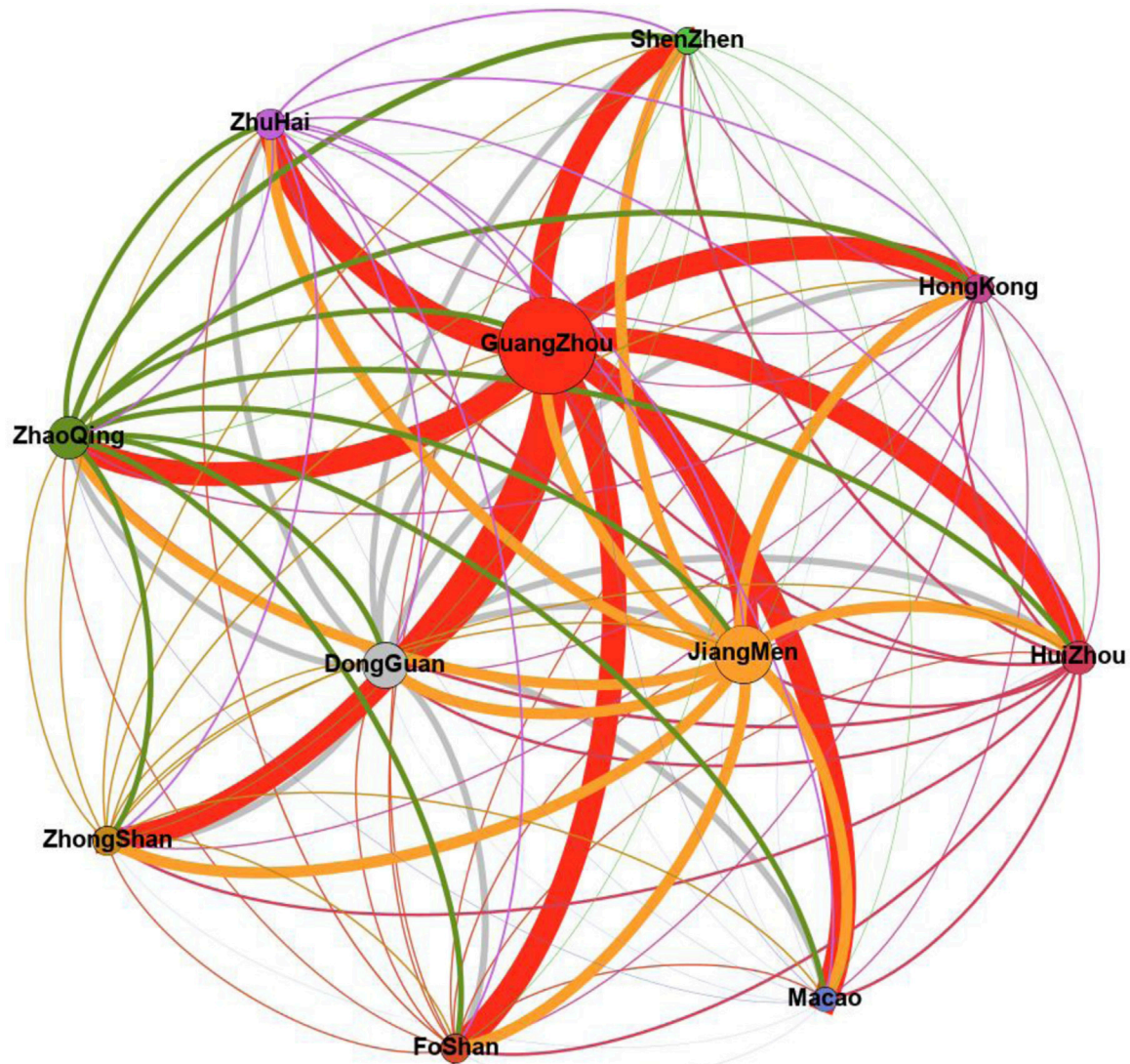


FIGURE 2
Complex network for economic development of Guangdong-Hong Kong-Macao greater bay area.

three cities can be further improved, then other cities can get more net benefits from their economic and social development.

Figure 2 obviously shows the key nodes in the economic development network of 11 cities in Guangdong-Hong Kong-Macao Greater Bay Area. The size of nodes in Figure 2 refers to the Net Spillover's influence of economic development. The larger the node is, the stronger the Net Spillover effect is. The direction of the edge is the same as the net spillover direction of the node, and the color of the edge is the same as that of its starting node. The size of the edge indicates the scale of Net Spillover. In this light, the thicker the edge is, the stronger the Net Spillover effect is.

The results of this complex network figure are in line with that of Table 7. From the figure, it is obvious that Guangzhou is

the most influential city in the economic network, and it is also the key node of Guangdong-Hong Kong-Macao Greater Bay Area's economic development. In other words, as the leader of Guangdong-Hong Kong-Macao Greater Bay Area's development, Guangzhou's economic and social development will have the greatest additional boost to the other 10 cities and accordingly promote the whole Greater Bay Area in an effective way.

Further discussion

The above results indicate the following problems:

Why is Shenzhen's economic role less important than expected?

According to “Diffusion Effect”, Shenzhen hits 12.20%, indicating the driving effect of economic development of Shenzhen on other cities - it is much lower than expected - it is over 30 times lower than Guangzhou, the top one. This shows that Shenzhen has been in the expressway of economic growth during the past 10 years (its total GDP replaced Guangzhou in 2017 as the third largest city in China), however, these economic achievements have just kept in Shenzhen without significant radiation or spillover to other cities in Greater Bay Area. The reason is that Shenzhen is not only a prefecture-level city in Guangdong Province, but also a city under separate state planning. As a special economic zone in China, it implements special economic policies, flexible economic measures and a special economic management system with the aim of developing an export-oriented economy. In terms of fiscal revenue, for example, as a city under separate planning, Shenzhen only pays taxes to the central government rather than to Guangdong. Its retained taxes and financial returns are more than those of other cities in the Greater Bay Area. Thanks to the independence of policy status and the extroversion of the industrial chain, Shenzhen is actually “de-embedded” in the Pearl River Delta economic framework and thus has a greater impact on the overall state economy than that of the local. In other words, the economic spillover effect of Shenzhen on Guangdong-Hong Kong-Macao Greater Bay Area cities might be diluted or diverted by the national economic system.

Why is it difficult for Hong Kong to integrate deeply into the Greater Bay Area economies?

Hong Kong scores 27.64% according to “Diffusion Effect” - it is the fourth lowest, though higher than Shenzhen, indicating that Hong Kong has not contributed much to the overall economic development of the Greater Bay Area in the past 10 years, and has not played a leading role in promoting the mainland cities in the Greater Bay Area, and the degree of integration is not high. The problems lie in that since the implementation of the Development Plan Outline of the Greater Bay Area, the administrative and policy thinking between Guangdong, Hong Kong and Macao remains the same as in the past. Central Government supports the integration of Hong Kong and Macao into the overall development of China and has introduced a number of measures to facilitate the development of Hong Kong and Macao residents on the mainland by taking advantage of the opportunities in the Greater Bay Area development. However, the deep-rooted “binary distinction and different treatment”

in the governance of Hong Kong and Macao has not been eliminated entirely. Concepts, norms and laws that highlight the differences between the “two systems” can still be seen in the practice of construction of Guangdong-Hong Kong-Macao Greater Bay Area, such as Hong Kong and Macao have always been regarded as overseas, Hong Kong and Macao residents as foreign citizens, Hong Kong capital as foreign capital in the “one country” system. The result is that there is a lack of awareness of deep mutual trust in the community of the Greater Bay Area. If the dilemma of “the gate is open while the door is closed” persists in urban mobility, all efforts to promote the integration of Hong Kong and Macao may become passive role planning and obedience, in return, Hong Kong and Macao's role in Greater Bay Area tend to be more blurred. As a result, there is still a gap in the policy status given to Hong Kong and Macao by the central government.

Why is Macao the biggest beneficiary of the economic development network of Guangdong-Hong Kong-Macao Greater Bay Area?

According to “Receiving Effect”, the value of Macao is 99.63%, which indicates that Macao has benefited most from the economic development of other cities. The reason can be found in Macao's population size, industrial structure and functional orientation. By the end of 2020, Macao had a total population of 683,200, with a per capita GDP of more than 80,000 USD, making it the city with the highest per capita GDP in China. Macao's industrial structure is dominated by the service industry, accounting for more than 90% of the regional GDP, which is characterized by service intensive. Compared with other cities in the Greater Bay Area, Macao's economy is small but extroverted, and it is closely connected with the international market. Thanks to its urban orientation as a free international trade port and its economic policy of low tax rate, capital, logistics and personnel flow freely in Macau. At the same time, Macao's unique historical culture, cultural landscape and ecological foundation have laid its unique advantages in tourism resources and provided an important bridge for trade and cultural exchanges between China and Portuguese-speaking countries. Driven by Guangdong-Hong Kong-Macao Greater Bay Area's strategy, with the implementation of major policies such as Hong Kong-Zhuhai-Macao Bridge and Hengqin Free Trade Zone, Macao has entered the fast lane of development in recent years. Under the principle of “one country, two systems”, Macao's small but sophisticated economic route and social strategy of actively integrating into the country enable it to gain more benefits from the overall development of the system.

Why is Guangzhou the most important node in the economic development connectedness network of Guangdong-Hong Kong-Macao Greater Bay Area?

Guangzhou is the largest in both “Diffusion Effect” and “Net Spillover”, indicating that Guangzhou’s economic development has placed a huge radiation spillover effect on other cities in Guangdong-Hong Kong-Macao Greater Bay Area - it is several times or even dozens of times the economic impact of other cities in this area. It is because Guangzhou is the capital of Guangdong Province and an important central city, international business center and comprehensive transportation hub in China. Boasting an advanced trade logistics network, Guangdong is able to allocate labor, land, resources, information, technology and other production factors in a reasonable association both in both spatial and timely manner. At the same time, Guangdong provincial government tries to open the channels of logistics, population mobility, capital flow and information flow in Guangdong-Hong Kong-Macao Greater Bay Area through institutional innovation, so that the circulation efficiency is up, circulation cost is down, the social resources put into production transform into productivity in a higher speed. Moreover, As a national historic and cultural city, this powerhouse of South China enjoys a second to none level of education, medical care, old-age care and entrepreneurship. In sum, Guangzhou gathers not only “things” but also “people”, it attracts the social resources of the surrounding cities, and radiates and feeds back the generated economic fruits to the surroundings even the whole country.

From the above, it can be concluded that in order to achieve a systematic development of Guangdong-Hong Kong-Macao Greater Bay Area in a way of twice the results for half the effort, we should give full play to Guangzhou’s role as a key node during the process of developing the related policies. In light of the uneven economic development and marketization among cities in the Guangdong-Hong Kong-Macao Greater Bay Area and the limited bargaining chips and ability for macroeconomic regulation and control of local governments, huge and continuous public financial expenditure is needed to achieve mutual integration and system optimization among the cities. Therefore, the central government should pay attention to the structural contradiction of the “fiscal division” between Guangzhou and Shenzhen in the policy arrangement. In addition, policy adjustment should focus on raising Guangzhou’s general budget revenue to enhance Guangzhou’s internal and external driving force of investment in the economy and people’s well-being projects of the Greater Bay Area, so that Guangzhou is able to play a leading role in the development of the Guangdong-Hong Kong-Macao Greater Bay Area.

Conclusion

As the attention paid by governments over the globe to the role of city clusters in regional development increased, an in-depth

study of the complex network of economic growth within city clusters can further enhance the city clusters’ development. This paper took the Guangdong-Hong Kong-Macao Greater Bay Area city cluster as the research object and studied the connectedness network of economic development among 11 cities from the perspective of complex networks. Firstly, 10 indicators about cities’ economic development were chosen in the beginning and were decomposed by Principal Component Analysis into three main components, which were further built into a comprehensive evaluation index of the economic development of the cities. Secondly, a new method—the TVP-VAR-SV model and MCMC method - were adopted to build a complex network of these economic development variation. This MCMC-based complex network can effectively solve the problem of failing to build a complex network due to the lack of sample data. This paper found that Macao, on one hand, is the largest beneficiary of the complex network of economic development in the Greater Bay Area. Guangzhou, on the other hand, performs as the largest radiator in this complex network of economic development. That is to say, when making the development policies of the Guangdong-Hong Kong-Macao Greater Bay Area, we must make full use of Guangzhou’s role as a key node to achieve an effective systematic development. Meanwhile, Shenzhen and Hong Kong enjoy more advanced economic development compared with other cities in the city cluster, the spillover effects of these two most developed cities, however, are much lower than that of Guangzhou, which is not in line with their economic status. To pursue high-quality development of the whole Bay Area city cluster, Shenzhen and Hong Kong should perform their leading roles in the economy by improving their integration with other cities, and further promoting the integration of economic development in the Greater Bay Area.

Data availability statement

The original contributions presented in the study are included in the article/supplementary material, further inquiries can be directed to the corresponding author.

Author contributions

QF performed the funding acquisition and data collection, wrote the original formal draft, performed editing. SZ performed the writing-review; editing. FL proposed the methodology, gave the formal data analysis and wrote the original formal draft.

Funding

This research was financially supported by the National Social Science Fund of China (20CKS056): Research on Strengthening the

National Identity of Hong Kong and Macao Teenagers under the New Situation of “One Country, Two Systems”.

Conflict of interest

The authors declare that the research was conducted in the absence of any commercial or financial relationships that could be construed as a potential conflict of interest.

References

1. Castells M. *The rise of the network society*. Oxford: Blackwell (1996).
2. Taylor PJ. *The challenge facing world city network analysis*[EB/OL]. *GaWC Res Bull* (2012) 409:09–25.
3. He DH, Yuan Y, Liu YT, Wang XM. The urban development strategy of cross-regional integration based on the network connection: A case of yangjiang city surrounding Guangdong-Hong Kong-Macao greater bay area. *Development Small Cities Towns* (2021) 39(10):15–22. doi:10.3969/j.issn.1009-1483.2021.10.003
4. Meijers E, Hoogerbrugge M, Cardoso R. Beyond polycentricity: Does stronger integration between cities in polycentric urban regions improve performance? *J Econ Hum Geogr* (2018) 109(1):1–21.
5. Zhou CS, Luo LJ, Shi CY, Wang JH. Spatio-temporal evolutionary characteristics of the economic development in the Guangdong-Hong Kong-Macao greater bay area and its influencing factors. *Trop Geogr* (2017) 37(6):802–13.
6. Wang FF, Yang HH. Research on the urban agglomeration spatial economic network structure of guangdong - hongkong - Macao greater bay area and its influencing factors: Based on analytic network process. *J South China Normal Univ (Social Sci Edition)* (2018) 63(04) 110–20.
7. Liu QF, Wang ZF. Evolution and network effects of economic spatial correlation in the Guangdong-Hong Kong-Macao greater bay area. *Geogr Geo-Information Sci* (2022) 38(2):55–62. doi:10.3969/j.issn.1672-0504.2022.02.008
8. Meng F, Lu ZG, Qin YR. Spatio-temporal evolution and influencing factors of economic differences in Guangdong-Hong Kong-Macao greater bay area. *Stat Decis* (2021) 37(08):116–20. doi:10.13546/j.cnki.tjyjc.2021.08.025
9. Shi XG, Hu LT. Research on the evolution of logistics network spatial structure of urban agglomeration—based on data analysis of Guangdong-Hong Kong-Macao greater bay area. *Price Theor Pract* (2022) 42(01) 152–5. doi:10.19851/j.cnki.CN11-1010/F.2022.01.014
10. Diebold FX, Yilmaz K. Measuring financial asset return and volatility spillovers, with application to global equity markets. *Econ J* (2009) 119:158–71.
11. Diebold FX, Yilmaz K. Better to give than to receive: Predictive directional measurement of volatility spillovers. *Int J Forecast* (2012) 28:57–66.
12. Diebold FX, Yilmaz K. On the network topology of variance decompositions: Measuring the connectedness of financial firms. *J Econom* (2014) 182(1):119–34. doi:10.1016/j.jeconom.2014.04.012
13. Primiceri GE. Time varying structural vector autoregressions and monetary policy. *Rev Econ Stud* (2005) 72:821–52.
14. Nakajima J, Kasuya M, Watanabe T. Bayesian analysis of time-varying parameter vector autoregressive model for the Japanese economy and monetary policy. *J Jpn Int Economies* (2011) 25:225–45.
15. Koop G, Pesaran MH, Potter SM. Impulse response analysis in nonlinear multivariate models. *J Econom* (1996) 74:119–47.
16. Pesaran HH, Shin Y. Generalized impulse response analysis in linear multivariate models. *Econ Lett* (1998) 58:17–29.
17. Sun QM, Fang FY, Li Y. Research on spatial economic network and core-edge structure of bay area urban agglomeration-comparative analysis between Guangdong-Hong Kong-Macao greater bay area and beibu gulf. *Study & Exploration* (2021) 314(09):113–22.

Publisher's note

All claims expressed in this article are solely those of the authors and do not necessarily represent those of their affiliated organizations, or those of the publisher, the editors and the reviewers. Any product that may be evaluated in this article, or claim that may be made by its manufacturer, is not guaranteed or endorsed by the publisher.



OPEN ACCESS

EDITED BY

Jianbo Wang,
Southwest Petroleum University, China

REVIEWED BY

Zhi-Qiang Jiang,
East China University of Science and
Technology, China
Zhao-Long Hu,
Zhejiang Normal University, China

*CORRESPONDENCE

Peng Wu,
wupeng88857@gmail.com

SPECIALTY SECTION

This article was submitted to Social
Physics,
a section of the journal
Frontiers in Physics

RECEIVED 27 August 2022

ACCEPTED 14 October 2022

PUBLISHED 03 November 2022

CITATION

Hu Y, Chu C, Wu P and Hu J (2022), A
linear time series analysis of carbon
price via a complex network approach.
Front. Phys. 10:1029600.
doi: 10.3389/fphy.2022.1029600

COPYRIGHT

© 2022 Hu, Chu, Wu and Hu. This is an
open-access article distributed under
the terms of the [Creative Commons
Attribution License \(CC BY\)](#). The use,
distribution or reproduction in other
forums is permitted, provided the
original author(s) and the copyright
owner(s) are credited and that the
original publication in this journal is
cited, in accordance with accepted
academic practice. No use, distribution
or reproduction is permitted which does
not comply with these terms.

A linear time series analysis of carbon price *via* a complex network approach

Yuxia Hu, Chengbin Chu, Peng Wu* and Jun Hu

School of Economics and Management, Fuzhou University, Fuzhou, China

Identifying the essential characteristics and forecasting carbon prices is significant in promoting green transformation. This study transforms the time series into networks based on China's pilots by using the visibility graph, mining more information on the structure features. Then, we calculate nodes' similarity to forecast the carbon prices by link prediction. To improve the predicted accuracy, we notice the node distance to introduce the weight coefficient, measuring the impact of different nodes on future nodes. Finally, this study divides eight pilots into different communities by hierarchical clustering to study the similarities between these pilots. The results show that eight pilots are the "small world" networks except for Chongqing and Shenzhen pilots, all of which are "scale-free" networks except for Shanghai and Tianjin pilots. Compared with other predicted methods, the proposed method in this study has good predicted performance. Moreover, these eight pilots are divided into three clusters, indicating a higher similarity in their price-setting schemes in the same community. Based on the analysis of China's pilots, this study provides references for carbon trading and related enterprises.

KEYWORDS

carbon market price, visibility graph, link prediction, community detection, complex network

1 Introduction

To effectively control CO₂ emissions, an emission trading scheme (ETS) was established by the EU in 2005, as a commodity to excise emission rights based on greenhouse gas emission reductions [1]. Since its launch, the EU has continuously optimized the carbon trading mechanism and subsequently formed a mature trading system. It is the most successful carbon trading system, covering 31 countries, bringing many experiences to China's ETS [2].

"The 14th Five-Year Plan" pointed out that carbon dioxide emissions will strive to achieve a "carbon peak" by 2030 and "carbon neutral" by 2060. During the 14th Five-Year Plan, a stronger trading policy will be introduced to accelerate the transformation of a high-carbon into a low-carbon nation, laying the foundation for "carbon neutrality" [3]. In the past 20 years, China's CO₂ emissions have increased six times faster than other regions, accounting for about 70% of global CO₂ emissions. Since 2020, China's per capita

CO₂ emissions have exceeded the EU [4]. Therefore, introducing a carbon trading mechanism has become an urgent task [5]. Subsequently, China established the Shenzhen pilot, Shanghai pilot, Beijing pilot, Guangdong pilot, Tianjin pilot, Hubei pilot, Chongqing pilot, and Fujian pilot since 2013, which is an important means to address climate problems and fulfil the international emission reduction commitments [6].

Due to China's ETS pilots' late opening, the mechanism is not mature enough to be applied effectively [7]. Many professors studied EU ETS, whereas a few researchers analyzed China's ETS pilots. In addition, there are lot of research works about the factors affecting carbon price, but they seldom predict it. Moreover, many studies have been conducted for one pilot and not eight pilots, resulting in a less in-depth analysis of the whole carbon market.

Recently, the complex network has attracted more attention. The visibility graph is a bridge between time series and complex networks, and the networks would retain the structural features of the time series [8]; [9]; [10]. However, if there are no direct links between two nodes, it is unknown whether they will create a connection in the future. To address this problem, the study in [11] proposed the link prediction based on the local random walk (LRW) to evaluate the similarity between two nodes, thus determining whether there is a link between them.

This study collects the daily carbon price in China's eight pilots and transforms the time series into eight networks by visibility graph. Then, we analyze the network structures and forecast the carbon prices based on link prediction. However, we consider the importance of the node distance to introduce the weight coefficient, which improves the predicted performance further. Finally, this study divides these pilots into different communities by hierarchical clustering, providing a special perspective to study the similarity between eight pilots.

Compared with existing studies, our contributions and core work in this study are mainly in three aspects. (1) A few researchers have studied the eight pilots in China together, but we evaluate them as a whole. To further explore them, we introduce the visibility graph to transform the time series. Based on the network structure, we mine more node information to analyze the features. (2) Most scholars only predicted the carbon prices and did not analyze the network structure to extract more information. We predict the carbon prices by link prediction and analyze the predicted performance according to the network features. Moreover, this study considers the importance of the node distance to introduce the weights, improving the forecasting accuracy. (3) Few studies have classified these pilots into different communities, and this study divides them into several sub-markets and analyzes their similarities.

The rest of this article is organized as follows: Section 2 provides a literature review of China's ETS analysis; Section 3 introduces some concepts about network science and link prediction. In Section 4, the proposed method and the data

are illustrated in detail; Section 5 shows the results and analysis, and we conclude our work in Section 6.

2 Literature review

Most academic research on carbon prices has focused on the causes that affect it and made predictions about it. Therefore, we introduce the two aspects in Section 2.1 and Section 2.2. Moreover, to further study the changing dynamic of the carbon prices in China's ETS pilots, we analyze the relevant research in Section 2.3.

2.1 The influencing factors of the carbon prices

Many researchers have analyzed the reasons that induce the dynamic of carbon prices, which are mainly divided into three categories: energy, climate, and macroeconomic events [12].

The study in [13] found that carbon prices are positive to crude oil and natural gas prices and insignificantly influenced by coal prices. In addition, they concluded that energy is the main influencing factor in carbon prices. The study in [14] used quantile regression to study the nonlinear effects of coal, oil, natural gas, and other energy prices on carbon prices.

Moreover, the study in [13] concluded that temperature extremes positively affect carbon prices. The study in [15] found that changes in temperature at freezing temperatures have a greater impact on carbon prices than shallow temperatures, and high temperatures do not have such an effect.

The authors of [16] thought the macroeconomic environment would affect carbon prices. When the economic situation arises, industrial production activities increase, the demand for carbon emission rights increases, and carbon prices increase accordingly. Conversely, carbon prices will also decrease when the financial situation declines. The study in [17] analyzed the impact of industrial output on carbon trading prices. They found that the only industries in the EU's industrial output significantly affecting carbon prices are the combustion and steel industries.

2.2 The forecasting of the carbon prices

To further analyze carbon prices, many experts have predicted prices that provide some experiences to control CO₂ emissions. There are three main methods to forecast time series: statistical models, artificial intelligence algorithms, and ensemble models. Statistical models are the methods to forecast the samples' trend, including the generalized auto-regressive conditional heteroskedasticity (GARCH) model, auto-regressive integrated moving average (ARIMA) model, grey model GM (1,1), and so on. The authors of the study in [18]

made a comparative analysis based on the daily data of the Europe Climate Exchange by using the GARCH model. The process is simple in statistical models, but there are also unavoidable drawbacks; hence, they are not suitable for non-linearity and non-stationary problems.

To address the limits of the statistical models, artificial intelligence algorithms are widely used to capture samples' features. They mainly include back-propagation neural networks (BPNN), least squares support vector regression (LSSVR), and long short-term memory networks (LSTM). The authors of the study in [2] thought that the dynamics of the carbon prices were chaotic and proposed a multi-layer perceptron network prediction model to forecast the third phase prices in the EU. The study in [19] used ARIMA and LSSVM models to predict carbon prices. Moreover, particle swarm optimization (PSO) is used to find the best parameters for LSSVM to improve predicted accuracy.

To obtain a better performance in forecasting carbon prices, ensemble models that decompose the time series are proposed. The ensemble models mainly conclude empirical mode decomposition (EMD), variational mode decomposition (VMD), and so on. The authors of the study in [20] forecasted the carbon prices in the Guangdong pilot by back-propagation (BP), support vector machines (SVM), and a hybrid model of EMD-BP-DNN, respectively. In addition, they compared the forecasting performances of these models.

2.3 Relevant studies on China's ETS pilots

The existing research on China's ETS pilots also considered two aspects: the influencing factors and predictions in the carbon prices. Although there is not much research on eight pilots, it still has reference values.

Unlike the EU market, China's carbon prices are mainly affected by coal rather than crude oil. The authors of the study in [21] examined the relationship between China's ETS pilot and its influencing variables: coal price, economy, temperature, and the EU's carbon prices. The results show a long-term co-integration relationship between them, and coal prices are the dominant factor. The study in [22] discussed the price drivers in ETS pilots by structural mutation testing and an auto-regressive distributed lag model. They proved that oil prices are positively correlated with carbon prices, while coal prices are negatively correlated. The study in [23] studied the driving factors (macroeconomic risks, environmental factors, and energy) in China's carbon prices by quantitative analysis and the causes affecting price by the dynamic correlation measurement method.

Moreover, there are many methods to predict carbon prices. The authors of the study in [24] proposed a model based on a combination of an empirical modal decomposition algorithm (EMD) and a generalized auto-regressive condition heteroscedasticity model (GARCH), which predicted five pilots' prices after 2016. The authors of the study in [25]

proposed a combination forecasting model based on the hybrid interval multi-scale decomposition method and its application to forecasting interval-valued carbon prices. To mine the relationship between these pilots, the authors of the study in [26] visually analyzed the seven pilots by visibility graph and studied the similarity and heterogeneity.

3 Preliminary

3.1 Visibility graph algorithm

The authors of the study in [27] proposed a visibility graph algorithm, transforming the time series into visibility graphs. In the study, China's ETS daily carbon prices as the time series values were mapped to each visual node in the network and then the linkages between all nodes were constructed by using the visibility graph algorithm [28]. Assuming a given time series $T = \{(t_1, y_1), (t_2, y_2), \dots, (t_N, y_N)\}$, y_N is the value at t_N correspondingly. If there is a node (t_b, y_b) between node (t_a, y_a) and (t_c, y_c) and it satisfied $t_a < t_b < t_c$, then whether two nodes construct a link depends on the following equation:

$$y_b < y_a + (y_c - y_a) \frac{(t_b - t_a)}{(t_c - t_a)}. \quad (1)$$

Commonly, if there is a link between two nodes in a histogram, they can also be linked in a network. For example, if any two vertical bars can see each other's top, then these 2 bars are supposed to take a linkage [29]; [30]. Next, we can create an adjacent metric based on the corresponding time series. Finally, a network is constructed by network science, as shown in Figure 1.

3.2 Topological measures of the VG

3.2.1 Average degree

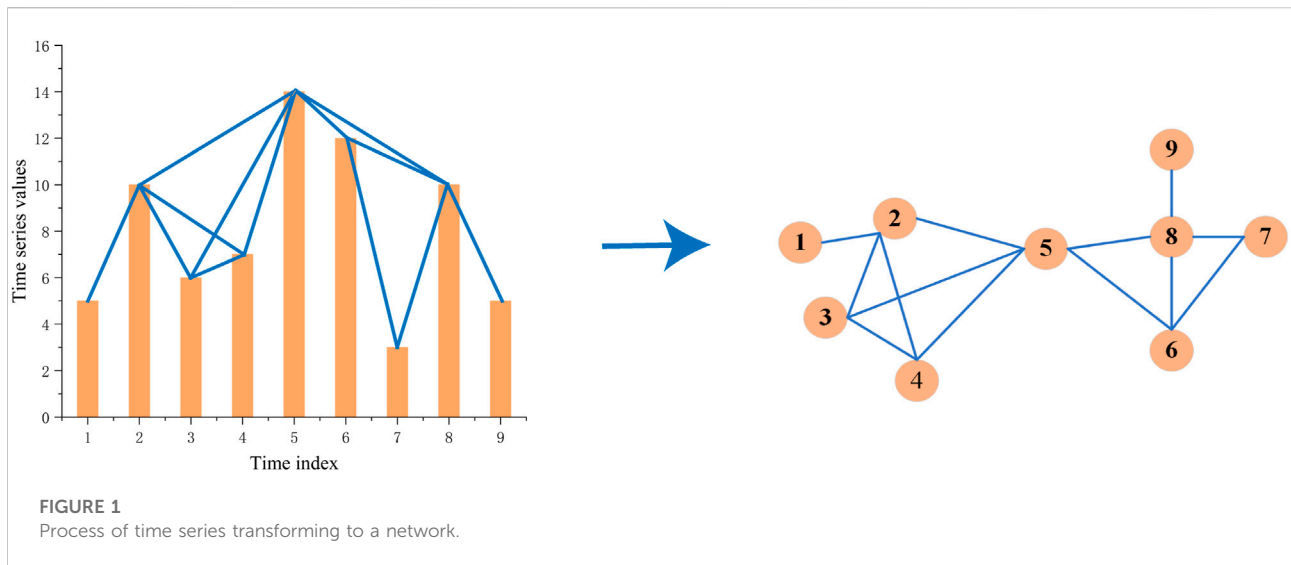
The average degree is the average value of all the nodes' degree in a network. K_i is the degree of node i , describing the number of nodes directly connected to it. Commonly, the larger the node degree, the more communication the node and the larger the average degree, demonstrating that the network is more frequently communicated. The average degree is calculated by Eq. 2 and denoted by $\langle k \rangle$.

$$\langle k \rangle = \frac{1}{N} \sum_{i=0}^N k_i. \quad (2)$$

It also can be expressed as follows:

$$\langle k \rangle = \frac{2E}{N}, \quad (3)$$

where E represents the number of edges in a network and N is the number of nodes in a network.



3.2.2 Network diameter

The network diameter is a measure that the maximum value of distance between all nodes in a network, denoted as D , and expressed as

$$D = \max(d_{ij}), \quad (4)$$

where d_{ij} is the shortest distance of node i and node j , which defined as the least number of edges from node i to node j .

3.2.3 Average path length

The average path length is a vital character in a network, meaning the average of the shortest distance between any two nodes, denoted by L . The smaller the average path length, the more frequent communication between all nodes in the network. The calculation formula is shown as follows:

$$L = \frac{2}{N(N-1)} \sum_{i \geq j} d_{ij}. \quad (5)$$

3.2.4 Network density

The network density is used to measure the closeness in the network, denoted by D_g . The higher the D_g , the more tightly connected the network. D_g is expressed by

$$D_g = \frac{E}{N(N-1)}. \quad (6)$$

3.2.5 Average clustering coefficient

The average clustering coefficient refers to the clustering coefficient of the whole network, denoted as C ($0 \leq C \leq 1$), which means that the clustering coefficients of all nodes are averaged. In a network, suppose node i is connected to k_i nodes and we denote

the actual number of edges existing between these k_i nodes as E_i ; then, we can define the clustering coefficient of node i as the ratio of E_i to the total maximum possible proportion of the number of edges $k_i(k_i-1)/2$, and the calculation formula of C_i is as follows:

$$C_i = \frac{2E_i}{k_i(k_i-1)}. \quad (7)$$

Then, the average clustering coefficient is denoted by

$$C = \frac{1}{N} \sum_{i=1}^N C_i. \quad (8)$$

3.2.6 Community structure

To further explore the network, we introduce the community structure. Nodes are tightly connected between the same communities while sparsely connected between different communities [31]. Usually, the modularity Q function is used to describe the accuracy of community division, which was devised by the authors of the study in reference [32]. The closer the Q takes to 1, the more obvious the community structure is [33], which is expressed as follows:

$$Q = \frac{1}{2E} \sum_{i,j} \left(a_{ij} - \frac{k_i k_j}{2E} \right) \delta(g_i, g_j). \quad (9)$$

Moreover, the function $\delta(g_i, g_j)$ is defined as: if node i and node j belong to the same community, $\delta(g_i, g_j) = 1$, otherwise $\delta(g_i, g_j) = 0$ [34]

3.3 Link prediction

Link prediction is a method to forecast the likelihood of two unlinked nodes establishing a link in the future based on the

existing network analysis. Since a time series converts into a network, then the time series prediction map into a network prediction. In addition, most link prediction methods are based on node similarity, such as common neighbors (CN), resource allocation index (RA), and so on. The authors of the study in [11] proposed a competitive prediction method based on the local random walk (LRW), which measures the similarity by a walker walking randomly in the network. Correspondingly, the higher similarity between two nodes, the higher probability they will connect in the future.

3.3.1 Local random walk

In the method, a visibility graph is described as an unweighted network $G(V, E)$, where V is the set of nodes and E is the set of edges. Then, the transition probability matrix that a random walker stays at node x and moves to node y in one step, denoted by P_{xy} and obtained by

$$P_{xy} = \frac{a_{xy}}{k_x}, \quad (10)$$

where $a_{xy} = 1$ if node x is connected to node y , otherwise $a_{xy} = 0$. k_x is the degree of node x .

After t steps, the probability $\vec{\pi}_x(t)$ that the walker moves from node x to node y is calculated by

$$\vec{\pi}_x(t) = P^T \vec{\pi}_x(t), \quad (11)$$

where P^T is the transposition of matrix P . Suppose there is a N length time series and an $N \times 1$ vector with the x th element equaling to one and others to 0, then the vector is devoted by $\vec{\pi}_x(0)$, representing that the walker starts walk from node x .

Then, the similarity between node x and node y based on LRW is calculated by

$$S_{xy}^{LRW}(t) = \frac{k_x}{2E} \pi_{xy}(t) + \frac{k_y}{2E} \pi_{yx}(t). \quad (12)$$

However, there is a problem that a random walker will walk too far away from node x to node y even though node x is adjacent to node y , resulting in unsatisfactory predictions. To address the issue, a higher similarity method is proposed, which ensures a random walker walks in a local part rather than other parts of the network. Superposed random walk (SRW) similarity between node x to node y is denoted by S_{xy}^{SRW} , as follows:

$$S_{xy}^{SRW}(t) = \sum_{l=1}^t S_{xy}^{LRW}(l). \quad (13)$$

Then, $S_{xy}^{LRW}(n) = S_{yx}^{LRW}(n)$ and $S_{xy}^{SRW}(t) = S_{yx}^{SRW}(t)$.

3.3.2 Node distance

According to the method proposed in [35], the distance $d_{i \rightarrow j}$ between node t_i and node t_j is calculated by Eq. (14), which corresponding time values in point (t_i, y_i) and (t_j, y_j) , respectively.

$$d_{i \rightarrow j} = |t_i - t_j|. \quad (14)$$

4 Method and data

The method is proposed to predict carbon prices utilizing the visibility graph and link prediction, which will be illustrated in detail and divided into three parts. In Section 4.1, the preliminary work based on visibility graph and link prediction will be introduced. In Section 4.2, an initial prediction will be obtained based on the node similarity. In Section 4.3, node distance will be taken into consideration to improve initial predicted accuracy.

4.1 Preliminary work

The preliminary work including three main steps as follows:

Step 1: Transforming a time series to a visibility graph

A given time series $T = \{(t_1, y_1), (t_2, y_2), \dots, (t_N, y_N)\}$ can map into a network by visibility graph algorithm, as illustrated in Eq. (1).

Step 2: Calculating the node similarity based on LRW

The similarity between any two nodes based on LRW model is first calculated by Eqs (10)–(12). Then, to sum, the results of $S^{SRW} = [S_{1N}, S_{2N}, \dots, S_{(N-1)N}]$ will obtain the similarities between the last node N and all previous $(N - 1)$ nodes by using Eq. 13.

Step 3: Finding out the most similar nodes

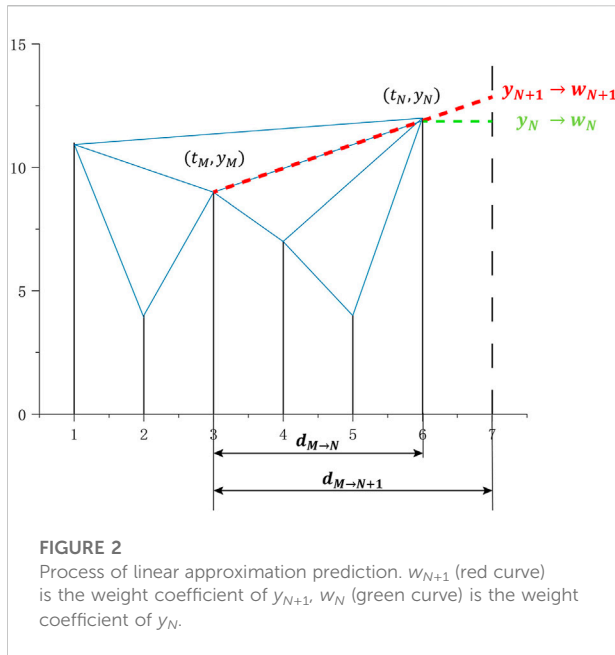
The maximum value of S^{SRW} is denoted by S_{MN} , and then node (t_M, y_M) is the most similar point to node (t_N, y_N) .

4.2 Initial forecasting

Suppose to forecast the future node (t_{N+1}, y_{N+1}) , and it is the closest to the last observed node (t_N, y_N) , namely, it will be directly influenced by node (t_N, y_N) . However, the future node is not only influenced by the nearest node but also previously observed values. In Section 4.1, the higher similarity node (t_M, y_M) is obtained, and it is the most similar point to node (t_N, y_N) , meaning it represents the previous data. Therefore, it is considered to carry all the historical information to forecast the future nodes.

As node (t_M, y_M) and node (t_N, y_N) have the most similarity in the network, they will directly link to forecast the future node (t_{N+1}, y_{N+1}) , the calculation of y_{N+1} by Eq. 15 according to the study in [36].

$$y_{N+1} = \frac{y_N - y_M}{t_N - t_M} (t_{N+1} - t_M) + y_M. \quad (15)$$



As shown in Figure 2, it describes the process of the linear approximation prediction. Clearly, node (t_3, y_3) are the most similar point to (t_6, y_6) , which determines the future node (t_7, y_7) .

4.3 Improved forecasting

To improve the predicted accuracy, the node distance is considered to this method based on the initial forecasting, which determines the weight coefficients of y_{N+1} and y_N , respectively.

Step 1: Calculating the node distance

The distance between node (t_M, y_M) and node (t_N, y_N) is determined by Eq. 16, denoted by $d_{M \rightarrow N}$.

$$d_{M \rightarrow N} = |t_M - t_N|, \quad (16)$$

where t_M and t_N are corresponding time values ($M < N$).

Similarly, the distance between node (t_M, y_M) and node (t_{N+1}, y_{N+1}) , node (t_N, y_N) , and node (t_{N+1}, y_{N+1}) is calculated by

$$d_{M \rightarrow N+1} = |t_M - t_{N+1}|, \quad (17)$$

$$d_{N \rightarrow N+1} = |t_N - t_{N+1}|. \quad (18)$$

Step 2: Determination of the weight coefficient

Furthermore, the closer the node (t_M, y_M) and node (t_N, y_N) , the less importance the node (t_M, y_M) . However, node (t_M, y_M) contains less historical information about past, which has the same effect as node (t_N, y_N) to predict future information. Conversely, if node (t_M, y_M) is far away from node (t_N, y_N) ,

the importance of node (t_M, y_M) is higher because it carries more historical information for further predictions [37].

Then, the weight coefficients are defined by

$$w_N = \frac{d_{M \rightarrow N}}{d_{M \rightarrow N+1}}, \quad (19)$$

$$w_{N+1} = 1 - w_N, \quad (20)$$

where w_{N+1} denotes the weight coefficient of the predict value y_{N+1} and w_N denotes the weight coefficient of the last observed value y_N . Figure 2 gives a more vivid interpretation.

Step 3: Final weighted prediction

Commonly, the larger the $d_{M \rightarrow N}$, the larger $d_{M \rightarrow N+1}$ and the smaller the w_N , demonstrating node (t_M, y_M) with more useful historical information. Therefore, the final predicted results are calculated by

$$\hat{y}_{N+1} = w_{N+1} * y_{N+1} + w_N * y_N. \quad (21)$$

4.4 Data

The seven pilots' carbon prices per day from January 2014 to June 2021 are collected from China's Carbon Emission Trading Network (<http://k.tanjiaoyi.com/>) except the Fujian pilot. Because the Fujian pilot was constructed to operate in 2016, the pilot's daily carbon prices are collected from January 2017 to June 2021. In addition, the transaction prices are used as the carbon prices except the Shenzhen pilot. Since six allowances (SZA-2013 to SZA-2019) traded in the Shenzhen market, it takes the average transaction prices as the carbon prices. Missing data are added by moving the average in the previous week. Therefore, these eight China pilots' carbon prices are shown in Figure 3.

5 Results and analysis

This section will analyze the data from January 2014 to June 2021 between China's pilots. First, to realize the link prediction, this study transforms the time series into a visibility graph by the VG model and studies the network structures in the carbon price of eight pilots. In addition, we predict carbon prices by the proposed methods. To verify the predicted accuracy, the error indicators are used to analyze. Finally, we introduce hierarchical clustering to study the similarity between these eight pilots in China.

5.1 The network structure results

We construct eight networks by the data of Beijing, Fujian, Shanghai, Chongqing, Hubei, Shenzhen, Guangdong, and

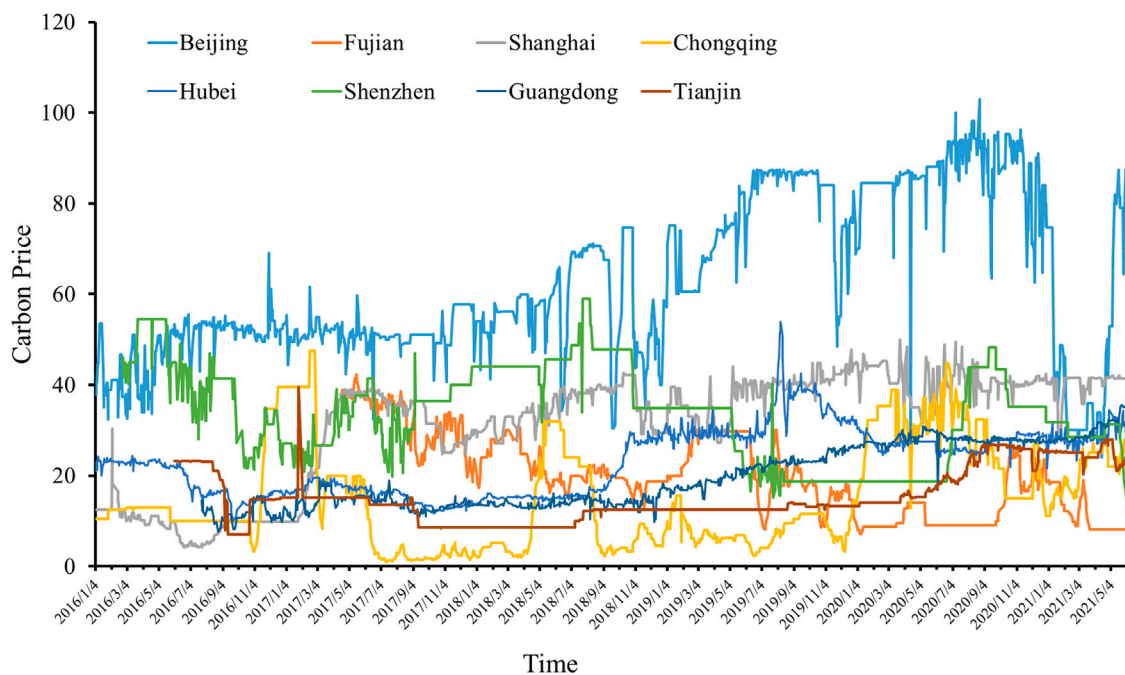


FIGURE 3
Carbon prices in China's ETS pilots; the different colors represent different pilots.

TABLE 1 Characteristic statics of eight China's ETS pilots.

| | Beijing | Fujian | Shanghai | Chongqing | Hubei | Shenzhen | Guangdong | Tianjin |
|--------------------------------|---------|--------|----------|-----------|--------|----------|-----------|---------|
| Diameter | 9 | 8 | 2 | 13 | 7 | 13 | 9 | 7 |
| Average degree | 10.504 | 16.587 | 6.04 | 18.992 | 16.184 | 6.334 | 11.16 | 26.634 |
| Average path length | 4.087 | 3.945 | 1.996 | 5.745 | 3.418 | 6.156 | 3.987 | 2.625 |
| Modularity | 0.804 | 0.769 | 0.242 | 0.734 | 0.583 | 0.85 | 0.731 | 0.483 |
| Average clustering coefficient | 0.761 | 0.753 | 0.834 | 0.71 | 0.728 | 0.774 | 0.746 | 0.692 |

Tianjin pilots, respectively. After mapping the time series to eight networks by visibility graph, we calculate the characteristic statistics by Eqs 2-9, as shown in Table 1.

Usually, the average degree reflects the importance of a node in networks. The average degree is the largest in Tianjin pilot, whereas Shanghai and Shenzhen pilots are small, reflecting that the carbon prices in Tianjin pilot are much affected by previous price fluctuations. The Shanghai pilot has the smallest diameter. The diameter of Chongqing and Shenzhen pilots is 13, indicating that the Shanghai pilot is easily influenced by the near prices. However, Chongqing and Shenzhen pilots are easily affected by earlier prices. Correspondingly, the changing trend of the average path length is as same as the diameter. In addition, the density is ranged from 0.004 to 0.017, which illustrates the tightness of the network. The average clustering coefficient indicates the aggregation of the network

structure, ranging from 0.692 to 0.834. Moreover, the modularity of Beijing and Shenzhen pilots surpasses 0.8, reflecting that their community structures are apparent. The modularity in the Shanghai pilot is the lowest, indicating that the community structure is insignificant.

5.2 "Small world" and "scale-free" properties

As seen in Table 1, except Chongqing and Shenzhen pilots, these networks have a considerable average clustering coefficient and small average path length, showing "small world" characters. It reflects that the future carbon prices are easily affected by the historical prices, and are mainly influenced by the hubs in the networks.

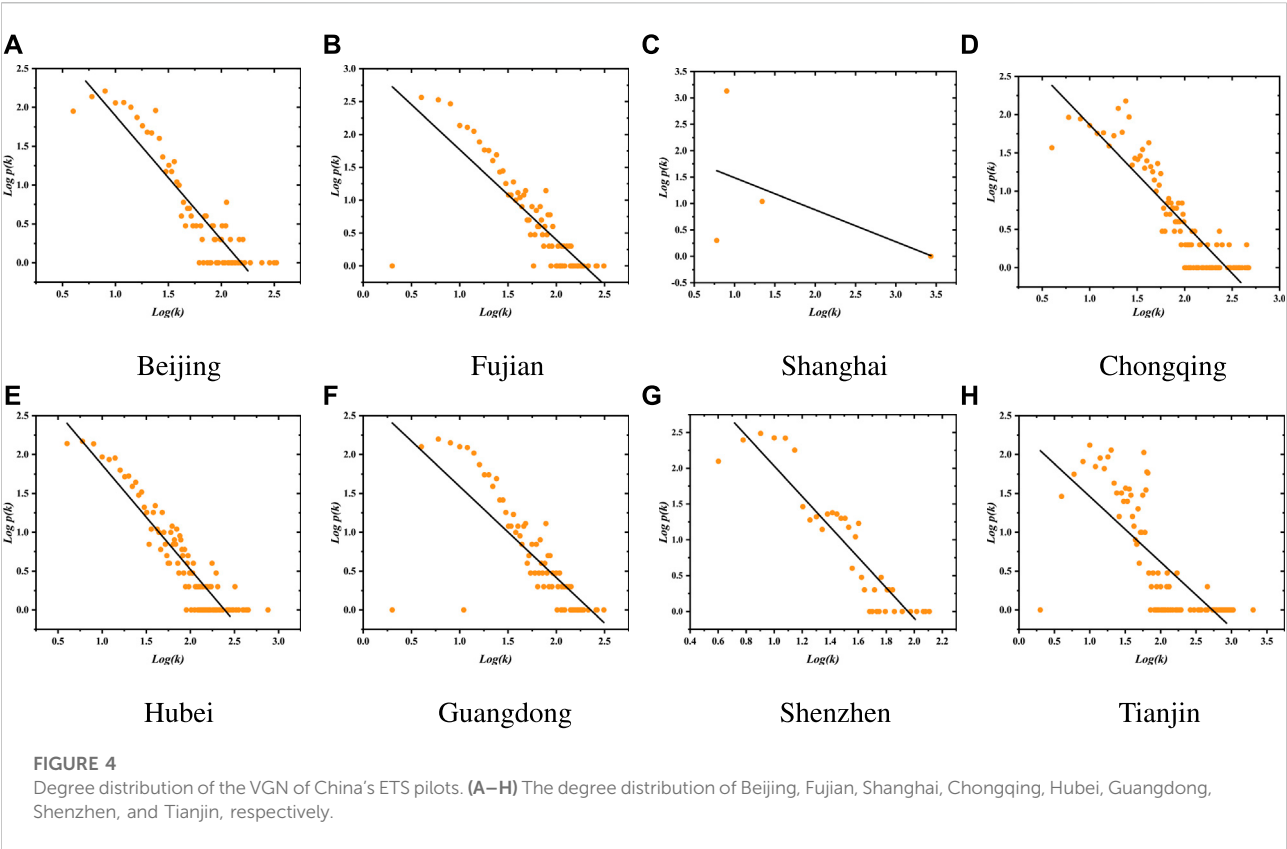


TABLE 2 Exponent of power-law degree distribution and the fitting goodness.

| | Beijing | Fujian | Shanghai | Chongqing | Hubei | Shenzhen | Guangdong | Tianjin |
|----------|---------|--------|----------|-----------|-------|----------|-----------|---------|
| γ | 1.593 | 1.371 | 0.606 | 1.294 | 1.339 | 2.128 | 1.172 | 0.844 |
| R^2 | 0.831 | 0.677 | 0.382 | 0.806 | 0.866 | 0.843 | 0.603 | 0.567 |

Figure 4 and Table 2 show the power-law degree distribution of China's ETS pilots, where γ is the exponent of the power-law degree distribution and R^2 is the fitting goodness. Clearly, the larger the fitting goodness, the more conforms to the "scale-free" properties. The "scale-free" network shows that only a few nodes have a large degree, whereas most nodes in the network have little linkage to other nodes, which reflects a severe heterogeneity in degree distribution. In this study, the properties indicate that future carbon prices will be affected easily by highly degree nodes, which have many linkages with other nodes in the network.

Usually, the exponent γ is between 1 and 2. Beijing, Fujian, Chongqing, Hubei, Guangdong, and Shenzhen pilots are the "scale-free" network, except Shanghai and Tianjin pilots. To further mine their features, we analyze the topology network for Beijing and Shanghai pilots in Figure 5. However, the nodes' degrees are described by different colors. The larger the degree, the large the node size is. Clearly, there are a few hubs and many low-degree nodes in the Beijing pilot, whereas there are many

hubs and a few low-degree nodes in Shanghai. It proves that our experimental results are correct.

The "scale-free" pilots show that the nodes with a high degree are easily affected by previous prices, and they also easily affect future carbon prices. Moreover, the carbon prices of pilots are not easily affected by events because there are a few hubs that would be influenced. Moreover, the fitting goodness of Fujian and Guangdong is about 60%, and others are all higher than 80%. Hubei shows the highest R^2 , and the value is 0.866. However, in Shanghai and Tianjin pilots, γ is 0.606 and 0.844, respectively. In addition, Shanghai and Tianjin have a low R^2 , meaning the fitting effect has a bad performance. As the financial technology center, the Shanghai topology network is different from others not with "scale-free" features. It communicates with many cities, and there are many carbon-reducing technologies here. Due to these characters, the carbon prices in Shanghai are easily affected by emergency events because there are many hubs that would be attacked.

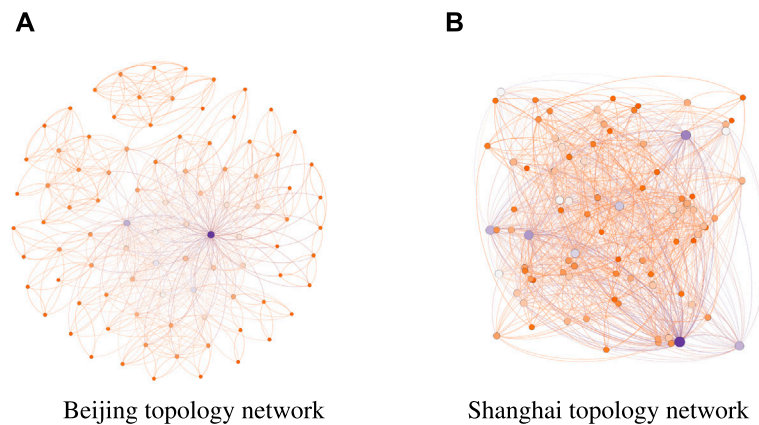


FIGURE 5

Different colors indicate nodes with different degree; the higher the degree, the larger the node size. (A) There are a few hubs and many low-degree nodes in Beijing. (B) There are a few low-degree nodes and many hubs in Shanghai.

5.3 Carbon price forecasting

In this section, we calculate the average carbon price in a month as the monthly price, and then the proposed method is adopted to forecast the monthly carbon prices in China's pilots. Specifically, we divide China's ETS pilots into a Universe dataset T from January 2014 to June 2021. First, the data from January 2014 to September 2015 are selected as a training set to predict October 2015. Then, the actual value of October 2015 will be added to the training set to forecast the next value. Above all, this process will be repeated until the value of June 2021 is predicted. Finally, we will obtain the predicted set from January 2016 to June 2021. Particularly, the Fujian pilot dataset is from January 2017 to June 2021. The training set is from January 2017 to September 2018, predicting the carbon prices from October 2018 to June 2021. The process of the method is shown in Algorithm 1.

Algorithm 1: The forecasting process of China's ETS carbon prices

Input: Time series dataset T : N data values

Output: The predicted values

```

1 for  $j=20$  to  $N-1$  do
2   Training set= $x|x \in T(i), i = 1, 2, \dots, j$ ;
3   Calculate node similarity  $S_{xy}^{SRW}$ ;
4   Find two most similar nodes  $(t_m, y_m)$  and  $(t_j, y_j)$ ;
5   Determine node distance  $d_{m \rightarrow j}$ ;
6   Calculate weighted coefficient  $w_j$  and  $w_{j+1}$ ;
7    $y_{j+1} \leftarrow \frac{(y_j - y_m)}{(t_j - t_m)}(t_{j+1} - t_m) + y_m$ ;
8    $\hat{y}_{j+1} \leftarrow w_{j+1} * y_{j+1} + w_j * y_j$ ;
9   Return  $(y_{j+1}, \hat{y}_{j+1})$ ;
10  Add  $T_{j+1}$  to training set
11 end

```

To verify the efficiency of the improved method, we compare two forecasting methods and the results in

Figure 6. In this panel, (A–H) represents the predicted results in Beijing, Fujian, Shanghai, Chongqing, Hubei, Shenzhen, Guangdong, and Tianjin pilots, respectively.

As can be seen, the blue line is the initial predicted values, the green line is the improved predictions, and the red line is the actual values. If the red line is close to the blue line or green line, indicating that the predicted accuracy of the proposed method is high. Conversely, the farther away the red line from the blue line, the worse the predicted accuracy. Moreover, if the green line is closer to the red line than the blue line, the improved method has a better predicted performance in a network.

To evaluate the predicted accuracy of the proposed method, this study adopts three error measures: mean absolute difference (MAD), root mean square error ($RMSE$), and mean absolute percentage error ($MAPE$). These error indicators are denoted by

$$MAD = \frac{1}{N} \sum_{t=1}^N |\hat{y}_t - y_t|, \quad (22)$$

$$RMSE = \sqrt{\frac{1}{N} \sum_{t=1}^N (\hat{y}_t - y_t)^2}, \quad (23)$$

$$MAPE = \frac{1}{N} \sum_{t=1}^N \frac{|\hat{y}_t - y_t|}{y_t}, \quad (24)$$

where N is the number of predicted values, $\hat{y}(t)$ represents the predicted value at t time, and $y(t)$ is the actual value at t time.

The predicted accuracy is high if the results exhibit a low MAD , $RMSE$, or $MAPE$. Namely, the proposed method has a

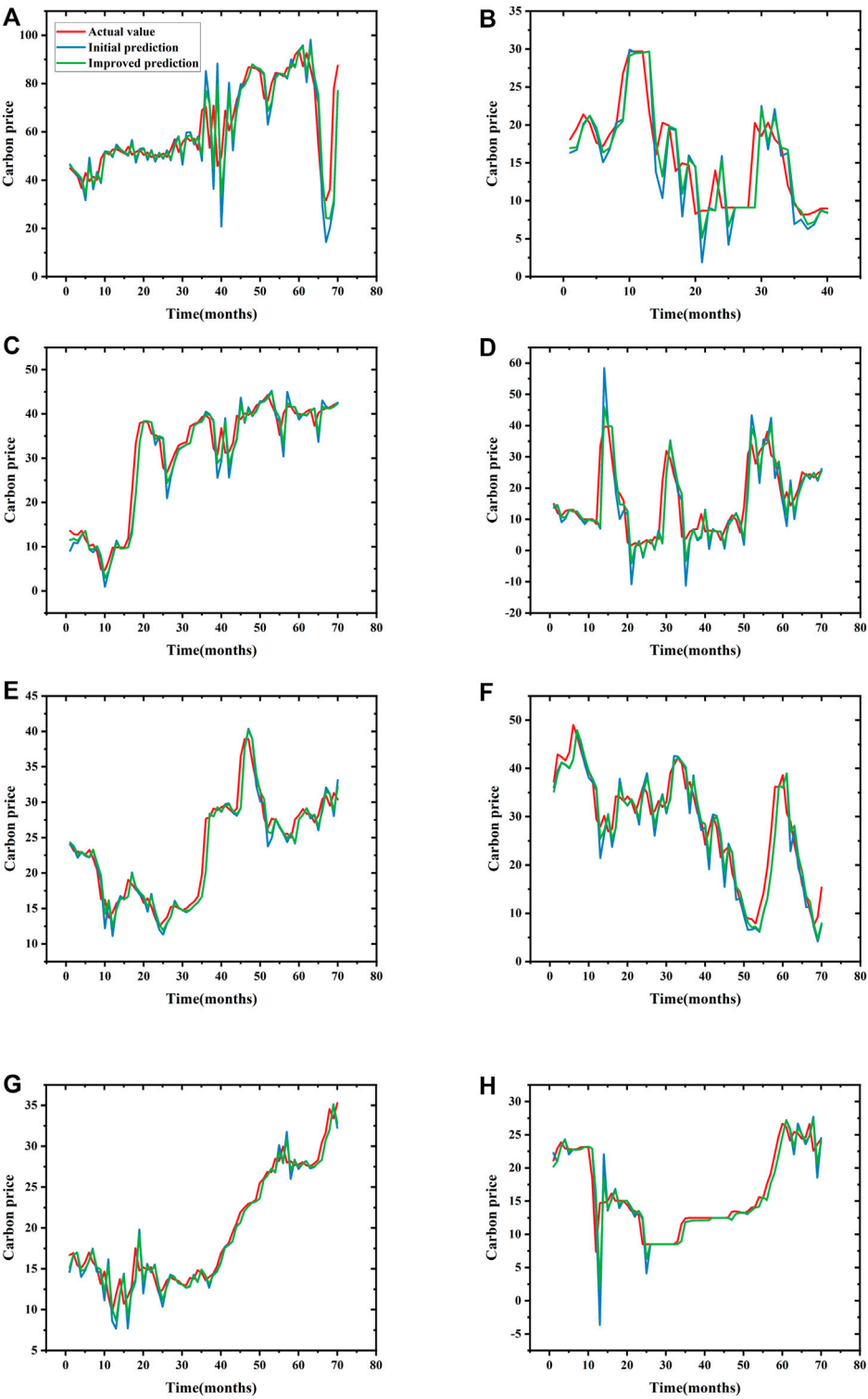
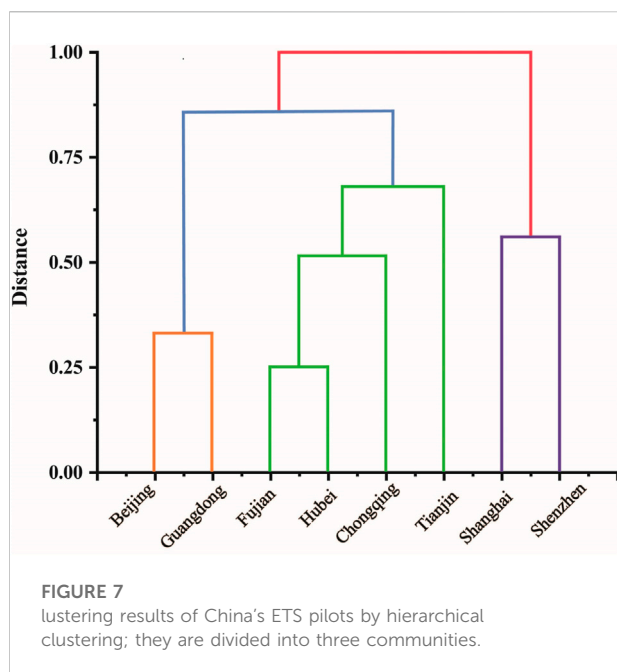


FIGURE 6
The forecasting results in panel. (A–H) The predicted results in Beijing, Fujian, Shanghai, Chongqing, Hubei, Shenzhen, Guangdong, and Tianjin pilots, respectively.



good prediction performance. To verify its forecasting performance further, we introduce the moving average (MA) method, a linear combination of residual terms to forecast. The order of MA is determined by ACF, which describes the correlation between the current and past values. Moreover, we compare three strategies of the initial predictions, the improved predictions, and the MA predictions in eight pilots, as shown in Table 3.

According to these data, the order of MA is 2. From Table 3, the performance of predicted values by MA(2) is worse than the method proposed by this study. The improved method has a better predicted capacity, showing that the node distance is also an important character in networks, so it is

necessary to consider the weight coefficient. Moreover, the result explains that future prices will be affected by historical issues, not only recent events. The price fluctuations in the Hubei, Guangdong, and Tianjin pilots are flat, and the MAD(b) are all less than 1. These pilots start with a low price and actively encourage enterprises to reduce emissions. They are not easily affected by related events based on their “scale-free” features, so the carbon prices are stable to obtain a good forecasting performance.

Conversely, the forecasting performance in Beijing, Chongqing, and Shenzhen pilots is the worst, the RMSE(b) exceeds 3 because their prices fluctuate greatly. Beijing as the highest pilot with the worst MAD(b) and RMSE(b), 4.966 and 9.077, respectively. It cooperates with many enterprises with rich trading products, so there are a lot of uncertain factors to affect forecasting validity. Similarly, the Shenzhen pilot is the first carbon trading market, covering 40% of carbon emissions. In addition, it is one of the pilot areas with the largest number of enterprises and the most active transactions, so its prices are easily affected by other factors, such as coal, climate, and economic events. Moreover, Shenzhen and Chongqing pilots are not the “small world” networks with poor communication, inducing a bad predicted performance.

Besides, we have to consider the impact of the COVID-19 epidemic on carbon market trading, and the emergency has affected the predicted accuracy. Due to the abruptness of the COVID-19 outbreak, we cannot precisely estimate the trend of carbon prices. Thus, we cannot obtain a good forecasting performance.

5.4 Cluster results

Hierarchical clustering is a method to analyze the nodes' similarity, measured by node distances. The steps are as follows:

TABLE 3 Error measurements of carbon prices forecasting in eight pilots. (A–C) The initial forecasting method, improved forecasting method, and MA (2), respectively.

| | Beijing | Fujian | Shanghai | Chongqing | Hubei | Shenzhen | Guangdong | Tianjin |
|---------|---------|--------|----------|-----------|-------|----------|-----------|---------|
| MAD(a) | 5.915 | 2.242 | 1.930 | 3.775 | 1.054 | 2.434 | 1.022 | 1.135 |
| MAD(b) | 4.966 | 1.838 | 1.626 | 3.201 | 0.952 | 2.212 | 0.882 | 0.975 |
| MAD(c) | 8.327 | 4.876 | 4.622 | 4.516 | 2.793 | 3.092 | 8.883 | 3.135 |
| RMSE(a) | 10.731 | 3.586 | 3.131 | 6.312 | 1.740 | 3.536 | 1.597 | 2.615 |
| RMSE(b) | 9.077 | 3.128 | 2.766 | 5.431 | 1.611 | 3.212 | 1.359 | 2.097 |
| RMSE(c) | 15.325 | 13.569 | 9.087 | 7.677 | 5.033 | 5.368 | 13.688 | 5.462 |
| MAPE(a) | 0.104 | 0.159 | 0.085 | 0.441 | 0.047 | 0.101 | 0.061 | 0.076 |
| MAPE(b) | 0.085 | 0.127 | 0.071 | 0.352 | 0.042 | 0.091 | 0.052 | 0.067 |
| MAPE(c) | 0.142 | 0.367 | 0.270 | 0.349 | 0.123 | 0.095 | 0.407 | 0.190 |

- Step 1: Each node is considered a cluster
- Step 2: The distances between each cluster is calculated, and the two closet clusters are merged into a group
- Step 3: The previous operations are repeated until all clusters are merged into a cluster
- Step 4: The final cluster results are obtained

We divide eight pilots into three communities, which are seen as each sub-market, as shown in [Figure 7](#). The higher the similarity between these pilots divided into a cluster, so they in the same sub-market are similar in price dynamics, and we use different colors to denote different groups. Beijing and Guangdong pilots are a community with the most similarity to China's pilots because they encourage companies to save energy with a good performance to reduce emissions. Likewise, Shanghai and Shenzhen pilots belong to a cluster with a high GDP, illustrating that their operational mechanisms are similar. They cover the more comprehensive industries, and their penalties are also strict. Then, the rest of these pilots belong to a sub-market. They operate from a low price and trade in a single product with an inactive performance.

6 Conclusion

Carbon emission reduction has promoted the global carbon market development. To further control CO₂ emission effectively, this study analyzes the eight pilots in China based on network science. According to the network structures of eight pilots, we conclude that most pilots show the “scale-free” and “small world” features. Meanwhile, we predict the carbon prices by introducing the weight coefficient that measures the node distance, acquiring a better performance than before. We combine network science and link prediction, providing an effective method to forecast carbon prices. Finally, to study the similarity between these pilots, this study divides eight pilots into different communities by hierarchical clustering.

In this study, our analysis supplies experiences and policies among these pilots, providing crucial theoretical guidance for market participants to participate actively. The carbon pricing tool is a mechanism to stimulate markets to reduce emissions. Thus, it is important to predict carbon prices, which can stimulate innovation and improve productivity. However, the sudden outbreak of COVID-19 affects carbon market trading, so it is necessary to forecast carbon prices to change policies for decision makers. But, the uncontrollability and instability result in worse forecasting performance.

The subsequent research work would like to progress in the following areas: (1) This study predicts monthly carbon prices based on eight pilots. However, we will next consider forecasting the daily data in a pilot, maintaining more topology features to obtain a better predicted performance. (2) EEMD will be introduced to decompose the time series to mine the data features. After getting different IMFs and a residue, we predict them by different methods and integrate the results to obtain a final result. (3) To improve the accuracy, we can transform unweighted networks into weighted networks by different similarity indices in link prediction, even considering the reliability of the communication route.

To further respond effectively to global warming, China's carbon market can be considered from the following aspects: First, the cooperation with the global carbon market should be deepened and we should start exploring the internationalization path, accelerating the internationalization of China's pilots. At the same time, as the largest carbon market, China's carbon market is expected to play a scale advantage in construction. Second, we should strengthen the construction of the basic legal system and improve the system specification. Third, we should take the carbon market as the leading market mechanism for coordinating energy conservation, emission reduction, and promote positive synergy.

Data availability statement

The original contributions presented in the study are included in the article/[Supplementary Material](#); further inquiries can be directed to the corresponding author.

Author contributions

YH: visualization, drawing, writing, and software. CC: investigation and validation. PW: conceptualization and methodology. JH: writing—reviewing and editing and software.

Funding

This study was supported in part by the National Natural Science Foundation of China under Grant 71871159, in part by the Humanities and Social Science Foundation of the Chinese Ministry of Education under Grant 21YJA630096, in part by the second Fujian Young Eagle Program Youth Top Talent Program, in part by the Natural Science Foundation of Fujian Province, China, under Grant 2022J01075, and in part by the Fujian science and technology economic integration service platform.

Conflict of interest

The authors declare that the research was conducted in the absence of any commercial or financial relationships that could be construed as a potential conflict of interest.

Publisher's note

All claims expressed in this article are solely those of the authors and do not necessarily represent those of their affiliated

organizations, or those of the publisher, the editors, and the reviewers. Any product that may be evaluated in this article, or claim that may be made by its manufacturer, is not guaranteed or endorsed by the publisher.

Supplementary material

The Supplementary Material for this article can be found online at: <https://www.frontiersin.org/articles/10.3389/fphy.2022.1029600/full#supplementary-material>

References

- Alberola E, Chevallier J, Chèze B. The eu emissions trading scheme: The effects of industrial production and co2 emissions on carbon prices. *Economie internationale* (2008) n° 116:93–125. doi:10.3917/ecoi.116.0093
- Fan X, Li S, Tian L. Chaotic characteristic identification for carbon price and an multi-layer perceptron network prediction model. *Expert Syst Appl* (2015) 42: 3945–52. doi:10.1016/j.eswa.2014.12.047
- Chen J, Li C, Ristovski Z, Milic A, Gu Y, Islam MS, et al. A review of biomass burning: Emissions and impacts on air quality, health and climate in China. *Sci Total Environ* (2017) 579:1000–34. doi:10.1016/j.scitotenv.2016.11.025
- Hu J, Chen J, Zhu P, Hao S, Wang M, Li H, et al. Difference and cluster analysis on the carbon dioxide emissions in China during Covid-19 lockdown via a complex network model. *Front Psychol* (2022) 12:795142. doi:10.3389/fpsyg.2021.795142
- Rong T, Zhang P, Zhu H, Jiang L, Li Y, Liu Z. Spatial correlation evolution and prediction scenario of land use carbon emissions in China. *Ecol Inform* (2022) 71: 101802. doi:10.1016/j.ecoinf.2022.101802
- Adedoyin FF, Gumede MI, Bekun FV, Etokakpan MU, Balsalobre-Lorente D. Modelling coal rent, economic growth and co2 emissions: Does regulatory quality matter in brics economies? *Sci Total Environ* (2020) 710:136284. doi:10.1016/j.scitotenv.2019.136284
- Liu L, Chen C, Zhao Y, Zhao E. China's carbon-emissions trading: Overview, challenges and future. *Renew Sustain Energy Rev* (2015) 49:254–66. doi:10.1016/j.rser.2015.04.076
- Mao S, Hu Y, Yuan X, Zhang M, Qiu Q, Wu P. Analysis of patent application attention: A network analysis method. *Front Phys* (2022):342.
- Hu J, Chu C, Xu L, Wu P, Lia H-J. Critical terrorist organizations and terrorist organization alliance networks based on key nodes founding. *Front Phys* (2021) 9:687883.
- Wang Y, Meng K, Wu H, Hu J, Wu P. Critical airports of the world air sector network based on the centrality and entropy theory. *Int J Mod Phys B* (2021) 35: 2150081.
- Liu W, Lü L. Link prediction based on local random walk. *Europhys Lett* (2010) 89:58007. doi:10.1209/0295-5075/89/58007
- Ji C-J, Hu Y-J, Tang B-J. Research on carbon market price mechanism and influencing factors: A literature review. *Nat Hazards (Dordr)* (2018) 92:761–82. doi:10.1007/s11069-018-3223-1
- Mansanet-Bataller M, Pardo A, Valor E. Co2 prices, energy and weather. *Energy J* (2007) 28. doi:10.5547/issn0195-6574-ej-vol28-no3-5
- Hammoudeh S, Nguyen DK, Sousa RM. Energy prices and co2 emission allowance prices: A quantile regression approach. *Energy policy* (2014) 70:201–6. doi:10.1016/j.enpol.2014.03.026
- Alberola E, Chevallier J, Chèze B. Price drivers and structural breaks in European carbon prices 2005–2007. *Energy policy* (2008) 36:787–97. doi:10.1016/j.enpol.2007.10.029
- Christiansen AC, Arvanitakis A, Tangen K, Hasselknippe H. Price determinants in the eu emissions trading scheme. *Clim Pol* (2005) 5:15–30. doi:10.1080/14693062.2005.9685538
- Chèze B, Chevallier J, Alberola E. Climate change and energy policy. *J Policy Modeling* (2009) 31 (3):446–462. doi:10.1016/j.jpolmod.2008.12.004
- Byun SJ, Cho H. Forecasting carbon futures volatility using garch models with energy volatilities. *Energy Econ* (2013) 40:207–21. doi:10.1016/j.eneco.2013.06.017
- Zhu B, Chevallier J. Carbon price forecasting with a hybrid arima and least squares support vector machines methodology. In: *Pricing and forecasting carbon markets*. Berlin/Heidelberg, Germany; Springer (2017). p. 87–107.
- Yan M, Wang C. Prediction of carbon trading price based on multi-scale integrated model—Take guangzhou carbon emission trading centre as an example. *J Tech Econ Manag* (2020) 5:19–24.
- Zhao X, Zou Y, Yin J, Fan X. Cointegration relationship between carbon price and its factors: Evidence from structural breaks analysis. *Energy Proced* (2017) 142: 2503–10. doi:10.1016/j.egypro.2017.12.190
- Ji C-J, Hu Y-J, Tang B-J, Qu S. Price drivers in the carbon emissions trading scheme: Evidence from Chinese emissions trading scheme pilots. *J Clean Prod* (2021) 278:123469. doi:10.1016/j.jclepro.2020.123469
- Wen F, Zhao H, Zhao L, Yin H. What drive carbon price dynamics in China? *Int Rev Financial Anal* (2022) 79:101999. doi:10.1016/j.irfa.2021.101999
- Li W, Lu C. The research on setting a unified interval of carbon price benchmark in the national carbon trading market of China. *Appl Energy* (2015) 155: 728–39. doi:10.1016/j.apenergy.2015.06.018
- Liu J, Wang P, Chen H, Zhu J. A combination forecasting model based on hybrid interval multi-scale decomposition: Application to interval-valued carbon price forecasting. *Expert Syst Appl* (2022) 191:116267. doi:10.1016/j.eswa.2021.116267
- Fan X, Li X, Yin J, Tian L, Liang J. Similarity and heterogeneity of price dynamics across China's regional carbon markets: A visibility graph network approach. *Appl Energy* (2019) 235:739–46. doi:10.1016/j.apenergy.2018.11.007
- Lacasa L, Luque B, Ballesteros F, Luque J, Nuno JC. From time series to complex networks: The visibility graph. *Proc Natl Acad Sci U S A* (2008) 105: 4972–5. doi:10.1073/pnas.0709247105
- Hu J, Zhang Y, Wu P, Li H. An analysis of the global fuel-trading market based on the visibility graph approach. *Chaos, Solitons & Fractals* (2022) 154:111613. doi:10.1016/j.chaos.2021.111613
- Feng Q, Wei H, Hu J, Xu W, Li F, Lv P, et al. Analysis of the attention to covid-19 epidemic based on visibility graph network. *Mod Phys Lett B* (2021) 35: 2150081.
- Cui X, Hu J, Ma Y, Wu P, Zhu P, Li H-J. Investigation of stock price network based on time series analysis and complex network. *Int J Mod Phys B* (2021) 35:2150171.

31. Jiao J, Wang J, Jin F, Wang H. Impact of high-speed rail on inter-city network based on the passenger train network in China, 2003–2013. *Acta Geogr Sin* (2016) 71:265–80.
32. Newman ME. Modularity and community structure in networks. *Proc Natl Acad Sci U S A* (2006) 103:8577–82. doi:10.1073/pnas.0601602103
33. Hu J, Xia C, Li H, Zhu P, Xiong W. Properties and structural analyses of USA's regional electricity market: A visibility graph network approach. *Appl Maths Comput* (2020) 385:125434. doi:10.1016/j.amc.2020.125434
34. Cui M, Hu J, Wu P, Hu Y, Zhang X. Evolutionary analysis of international student mobility based on complex networks and semi-supervised learning. *Front Phys* (2022):538.
35. Fei L, Wang H, Chen L, Deng Y. A new vector valued similarity measure for intuitionistic fuzzy sets based on owa operators. *Iranian J Fuzzy Syst* (2019) 16: 113–26.
36. Zhang R, Ashuri B, Shyr Y, Deng Y. Forecasting construction cost index based on visibility graph: A network approach. *Physica A: Stat Mech Its Appl* (2018) 493: 239–52. doi:10.1016/j.physa.2017.10.052
37. Xu H, Wang M. A novel carbon price fluctuation trend prediction method based on complex network and classification algorithm. *Complexity* (2021) 2021: 1–19. doi:10.1155/2021/3052041



OPEN ACCESS

EDITED BY
Jianbo Wang,
Southwest Petroleum University, China

REVIEWED BY
Zhao-Long Hu,
Zhejiang Normal University, China
Rongzhong Yu,
Jiujiang University, China

*CORRESPONDENCE
Pengchun Rao,
pcrao@ecjtu.edu.cn

SPECIALTY SECTION
This article was submitted to Social
Physics,
a section of the journal
Frontiers in Physics

RECEIVED 22 October 2022
ACCEPTED 09 November 2022
PUBLISHED 24 November 2022

CITATION
Rao P and Guo X (2022), Finite-time
synchronization of Kuramoto-oscillator
networks with a pacemaker based on
cyber-physical system.
Front. Phys. 10:1077045.
doi: 10.3389/fphy.2022.1077045

COPYRIGHT
© 2022 Rao and Guo. This is an open-
access article distributed under the
terms of the [Creative Commons
Attribution License \(CC BY\)](#). The use,
distribution or reproduction in other
forums is permitted, provided the
original author(s) and the copyright
owner(s) are credited and that the
original publication in this journal is
cited, in accordance with accepted
academic practice. No use, distribution
or reproduction is permitted which does
not comply with these terms.

Finite-time synchronization of Kuramoto-oscillator networks with a pacemaker based on cyber-physical system

Pengchun Rao* and Xiufeng Guo

School of Science, East China Jiaotong University, Nanchang, China

In this paper, we study the finite-time synchronization problem of a Kuramoto-oscillator network with a pacemaker. By constructing a cyber-physical system (CPS), the finite-time phase agreement and frequency synchronization of the network are explored for identical and non-identical oscillators, respectively. According to the Lyapunov stability analysis, sufficient conditions are deduced for ensuring the phase agreement and frequency synchronization for arbitrary initial phases and/or frequencies under distributed strategies. Furthermore, the upper bound estimations of convergence time are obtained accordingly, which is related to the initial phases and/or frequencies of oscillators. Finally, numerical examples are presented to verify the effectiveness of the theoretical results.

KEYWORDS

finite-time, synchronization, Kuramoto-oscillator, pacemaker, cyber-physical system (CPS)

1 Introduction

Synchronization of complex networks has been extensively investigated by researchers due to its numerous practical applications. As one of the most celebrated periodic-oscillator models, Kuramoto model [1] and its variations have been widely used for explaining various synchronization phenomena, and they have attracted considerable attention from researchers in diverse fields ranging from biology [2, 3], mathematics [4], physics [5, 6] and engineering [7–10]. In the past decade, many progresses concerning on the synchronization of Kuramoto-oscillator networks have been made by researchers in the control community [10–20], where synchronization criteria with respect to constraints on coupling strengths and initial phases have been developed. For example, in [10], the relationship between the algebraic connectivity of a connected Kuramoto-oscillator network and critical coupling was revealed. In [11], Chopra and Spong showed that initial relative phases should be confined to $\pi/2$ and a critical coupling strength should be satisfied, which guaranteed the frequency synchronization of an all-to-all connected Kuramoto network.

In [14, 15, 17, 20], researchers have taken the pacemaker (i.e. the so-called leader) into consideration, where synchronization criteria were related to not only the constraint on coupling strengths and initial phases, but also the selection of direct controlled oscillators. Since the interactions between oscillators are usually in the sinusoidal form of phase

differences, the theoretical results mentioned above were based on the requirements of initial phases, and only local stability analyses were provided. Based on the framework of cyber-physical systems [21, 22], distributed linear controllers have been adopted to synchronize Kuramoto-oscillator networks in [23, 24], where the derived stability conditions were independent of the initial phases such that the global synchronization was achieved. In [24], sufficient criteria were established for the Kuramoto-oscillator network with a pacemaker under distributed linear control.

The results aforementioned merely focused on the asymptotical synchronization, which indicated that synchronization was realized when $t \rightarrow \infty$. Recently, in [18, 19, 25–27], more researchers have focused on the finite-time synchronization of Kuramoto-oscillator networks, which is also of significance in practical applications. For example, power grids need to get rid of local power failures as soon as possible in order to avoid the cascading failure. In [27], Wu and Li investigated the finite-time and fixed-time synchronization of Kuramoto-oscillator networks by employing a novel multiplex control. However, the finite-time synchronization of Kuramoto-oscillator network in presence of a pacemaker has not been investigated so far.

Inspired by the above literatures, it is worth investigating the finite-time synchronization of Kuramoto-oscillator network with a pacemaker. In this paper, we aim to explore finite-time synchronization criteria of such network by adopting distributed schemes based on CPS. The main contributions of this paper are summarized as follows: Firstly, effective criteria are established to deal with finite-time phase agreement and frequency synchronization for Kuramoto-oscillator network with a pacemaker, and the upper bound of synchronization time is also provided; Secondly, synchronization can be achieved for arbitrary initial phases, which only influence the upper bound of synchronization time; Finally, the requirement on the connectivity of physical system is relaxed, even if it is an unconnected network.

The remainder of this paper is organized as follows. In Section 2, the framework of CPS is constructed, which consists of the physical Kuramoto-oscillator network system and the cyber (controlling) system. Furthermore, two definitions and some necessary mathematical preliminaries are encompassed in Section 2. Finite-time phase agreement in an identical Kuramoto-oscillator network and frequency synchronization in a non-identical Kuramoto-oscillator network cover the heart body of Section 3 and Section 4, respectively. Section 5 presents the numerical simulation results, and Section 6 concludes the whole paper.

2 Model and preliminaries

In the framework of CPS, a Kuramoto-oscillator network consisting of N oscillators with control input u_i can be described as

$$\dot{\theta}_i = \omega_i + \sum_{j=1}^N a_{ij} \sin(\theta_j - \theta_i) + u_i, i \in I, \quad (1)$$

where $I = \{1, \dots, N\}$, θ_i and ω_i are the phase and natural frequency of the i th oscillator, respectively. $A = (a_{ij})_{N \times N}$ denotes the adjacency matrix of an undirected network, where $a_{ij} = a_{ji}$ ($i \neq j$) > 0 iff there is an edge between oscillator i and oscillator j ; otherwise, $a_{ij} = 0$. Let $\mathcal{L}_A = D^A - A$ be the Laplacian matrix associated with the adjacency matrix A , where $D^A \in \mathbb{R}^{N \times N}$ is a diagonal matrix with $D_{ii}^A = \sum_{j=1}^N a_{ij}$ ($\forall i \in I$). The network associated with the adjacency matrix A is called physical network.

Assume that there is a pacemaker with dynamics

$$\dot{\theta}_0 = \omega_0,$$

where θ_0 and ω_0 are the phase and natural frequency of the pacemaker, respectively.

In this paper, we concern phase agreement and frequency synchronization with respect to the pacemaker in finite time.

Definition 1. Network Eq. 1 with control input u_i achieves (pacemaker-based) finite-time phase agreement, if there exists a settling time $T > 0$ depending on the initial states $\theta_i(0)$ ($i \in \{0\} \cup I$), such that

$$\lim_{t \rightarrow T} (\theta_i - \theta_0) = 0, i \in I, \quad (2)$$

and $\theta_i - \theta_0 \equiv 0$ for $t \geq T$.

Definition 2. Network Eq. 1 with control input u_i achieves (pacemaker-based) finite-time frequency synchronization, if there exists a settling time $T > 0$ depending on the initial states $\dot{\theta}_i(0)$ ($i \in \{0\} \cup I$), such that

$$\lim_{t \rightarrow T} (\dot{\theta}_i - \dot{\theta}_0) = 0, i \in I, \quad (3)$$

and $\dot{\theta}_i - \dot{\theta}_0 \equiv 0$ for $t \geq T$.

In order to obtain the sufficient conditions, the following Lemmas are needed.

Lemma 1. [28] For an undirected graph \mathcal{G} with N nodes, $x^T \mathcal{L} x = \frac{1}{2} \sum_{i=1}^N \sum_{j=1}^N a_{ij} (x_i - x_j)^2$ holds, where $x = (x_1, x_2, \dots, x_N)^T$ and \mathcal{L} is the Laplacian matrix of \mathcal{G} .

Lemma 2. [29] Consider the system of differential equation

$$\dot{x}(t) = f(x(t)) \quad (4)$$

where $f: \mathcal{D} \rightarrow \mathbb{R}^n$ is continuous on an open neighborhood $\mathcal{D} \subseteq \mathbb{R}^n$ of the origin and $f(0) = 0$. A continuously differentiable function $x: I \rightarrow \mathcal{D}$ is said to be a solution of Eq. 4 on the interval $I \subset \mathbb{R}$ if x satisfies Eq. 4 for all $t \in I$.

If there exists a continuous function $V(x): \mathcal{D} \rightarrow \mathbb{R}$ such that (1) $V(x)$ is positive definite;

(2) There exist real numbers $c > 0$, $0 < \rho < 1$, and an open neighborhood $\mathcal{D}_0 \subseteq \mathcal{D}$ of the origin such that $\dot{V}(x) \leq -cV^\rho(x)$, $x \in \mathcal{D}_0 \setminus \{0\}$.

Then, the origin is a finite-time stable equilibrium of Eq. 4 and the finite settling time T satisfies

$$T \leq \frac{V^{1-\rho}(x(0))}{c(1-\rho)}.$$

If in addition $\mathcal{D}_0 = \mathcal{D} = \mathbb{R}^N$, the origin is globally finite-time stable equilibrium.

For the sake of convenience, let $\xi_i = \theta_i - \theta_0$, then $\dot{\xi}_i = \dot{\theta}_i - \dot{\theta}_0 = \dot{\theta}_i - \omega_0$. For a real symmetric matrices \mathcal{L} , let $\lambda_{\min}(\mathcal{L})$ be the minimum eigenvalue of matrix \mathcal{L} . Denote $\text{sig}(x)^\alpha = \text{sign}(x)|x|^\alpha$, where the signum function $\text{sign}(x)$ is defined as

$$\text{sign}(x) = \begin{cases} 1, & \forall x > 0, \\ 0, & x = 0, \\ -1, & \forall x < 0. \end{cases}$$

3 Finite-time phase agreement for identical Kuramoto oscillators

In this section, we first concentrate on the case of oscillators with identical natural frequency, i.e., $\omega_i = \omega_0$, $\forall i \in I$. Thus, network Eq. 1 with control input u_i becomes

$$\dot{\theta}_i = \omega + \sum_{j=1}^N a_{ij} \sin(\theta_j - \theta_i) + u_i, i \in I. \quad (5)$$

For achieving finite-time phase agreement, a distributed control strategy is constructed as

$$u_i = \sum_{j=1}^N b_{ij}(\theta_j - \theta_i) + f_i \text{sig}(\theta_0 - \theta_i)^\alpha, \quad (6)$$

where $B = (b_{ij})_{N \times N}$ denotes the adjacency matrix of an undirected network with elements b_{ij} defined similar to a_{ij} , $f_i \geq 0$, and parameter $0 < \alpha < 1$. The network associated with the connections between the oscillators in the controller Eq. 6 is called cyber network. Let \mathcal{L}_B be the Laplacian matrix associated with the adjacency matrix B , where its elements are defined similar to \mathcal{L}_A .

By transforming θ_i into ξ_i , network Eq. 5 with distributed control strategy Eq. 6 becomes

$$\dot{\xi}_i = \sum_{j=1}^N a_{ij} \sin(\xi_j - \xi_i) + \sum_{j=1}^N b_{ij}(\xi_j - \xi_i) - f_i \text{sig}(\xi_i)^\alpha. \quad (7)$$

Theorem 1. Network Eq. 1 with identical oscillator under distributed control strategy Eq. 6 achieves finite-time phase agreement with the settling time bounded by

$$T_1 \leq \frac{\|\xi(0)\|^{1-\alpha}}{(1-\alpha)f_{\min}}, \quad (8)$$

if

$$\lambda_{\min}(\cos \gamma \cdot \mathcal{L}_A + \mathcal{L}_B) \geq 0,$$

where $f_{\min} = \min\{f_1, \dots, f_N\}$, $\|\xi(0)\|^2 = \sum_{i=1}^N [\xi_i(0)]^2$ and $\gamma \in (\pi, 2\pi)$ satisfies $\tan \gamma = \gamma$.

Proof 1. Consider the following Lyapunov functional candidate

$$V_1 = \frac{1}{2} \xi^T \xi = \frac{1}{2} \sum_{i=1}^N \xi_i^2.$$

The derivation of V_1 along trajectories Eq. 7 gives

$$\begin{aligned} \dot{V}_1 &= \sum_{i=1}^N \xi_i \dot{\xi}_i = \sum_{i=1}^N \sum_{j=1}^N a_{ij} \xi_i \sin(\xi_j - \xi_i) + \sum_{i=1}^N \sum_{j=1}^N b_{ij} \xi_i \sin(\xi_j - \xi_i) \\ &\quad - \sum_{i=1}^N f_i \xi_i \text{sig}(\xi_i)^\alpha. \end{aligned} \quad (9)$$

According to Lemma 1 and the fact $\frac{\sin(\theta_j - \theta_i)}{(\theta_j - \theta_i)} \in [\cos \gamma, 1]$, we can obtain

$$\begin{aligned} \sum_{i=1}^N \sum_{j=1}^N a_{ij} \xi_i \sin(\xi_j - \xi_i) &= \frac{1}{2} \sum_{i=1}^N \sum_{j=1}^N a_{ij} (\xi_i - \xi_j) \sin(\xi_j - \xi_i) \\ &= -\frac{1}{2} \sum_{i=1}^N \sum_{j=1}^N a_{ij} \frac{\sin(\xi_j - \xi_i)}{(\xi_j - \xi_i)} (\xi_j - \xi_i)^2 \\ &\leq -\frac{\cos \gamma}{2} \cdot \sum_{i=1}^N \sum_{j=1}^N a_{ij} (\xi_j - \xi_i)^2 \\ &= -\cos \gamma \cdot \xi^T \mathcal{L}_A \xi. \end{aligned} \quad (10)$$

And,

$$\sum_{i=1}^N \sum_{j=1}^N b_{ij} \xi_i (\xi_j - \xi_i) = -\frac{1}{2} \sum_{i=1}^N \sum_{j=1}^N b_{ij} (\xi_j - \xi_i)^2 = -\xi^T \mathcal{L}_B \xi, \quad (11)$$

$$\sum_{i=1}^N f_i \xi_i \text{sig}(\xi_i)^\alpha = \sum_{i=1}^N f_i \xi_i \text{sign}(\xi_i) |\xi_i|^\alpha \leq \sum_{i=1}^N f_i |\xi_i|^{1+\alpha}. \quad (12)$$

Combining Eqs. 10–12, Eq. 9 yields

$$\dot{V}_1 \leq -\xi^T (\cos \gamma \cdot \mathcal{L}_A + \mathcal{L}_B) \xi - \sum_{i=1}^N f_i |\xi_i|^{1+\alpha}.$$

If $\lambda_{\min}(\cos \gamma \cdot \mathcal{L}_A + \mathcal{L}_B) \geq 0$, we get

$$\begin{aligned} \dot{V}_1 &\leq -\sum_{i=1}^N f_i |\xi_i|^{1+\alpha} \\ &= -\sum_{i=1}^N f_i \left[|\xi_i|^2 \right]^{\frac{1+\alpha}{2}} \\ &\leq -f_{\min} 2^{\frac{1+\alpha}{2}} \left[\frac{1}{2} \sum_{i=1}^N |\xi_i|^2 \right]^{\frac{1+\alpha}{2}} \\ &= -2^{\frac{1+\alpha}{2}} f_{\min} V_1^{\frac{1+\alpha}{2}}. \end{aligned}$$

By Lemma 2 and Definition 1, network Eq. 1 with identical oscillator under distributed control strategy Eq. 6 achieves finite-time phase agreement with the settling time bounded by

$$T_1 \leq \frac{\left[\sum_{i=1}^N (\xi_i(0))^2 \right]^{\frac{1-\alpha}{2}}}{(1-\alpha)f_{\min}} = \frac{\|\xi(0)\|^{1-\alpha}}{(1-\alpha)f_{\min}}.$$

This completes the proof.

Remark 1. According to (8), we find that the upper bound of synchronization time is proportionate to initial state $\|\xi(0)\|$, and is inversely proportional to f_{\min} . According to Theorem 1, it is sufficient to achieve finite-time phase agreement if $\lambda_{\min}(\cos \gamma \cdot \mathcal{L}_A + \mathcal{L}_B) \geq 0$. Therefore, even if the physical network is not connected, phase agreement could be also achieved with the help of cyber network, which relaxes the requirement on the connectivity of the physical network.

4 Finite-time frequency synchronization for non-identical Kuramoto oscillators

Now we further concentrate on the case of oscillators with non-identical natural frequencies, i.e., there exists some $i \in I$ such that $\omega_i \neq \omega_0$. For achieving finite-time frequency synchronization, a distributed control strategy u_i is designed as

$$u_i = \sum_{j=1}^N b_{ij}(\theta_j - \theta_i) + U_i, \quad (13)$$

where $\dot{U}_i = f_i \text{sig}(\dot{\theta}_0 - \dot{\theta}_i)^\alpha$, $f_i \geq 0$, parameter $0 < \alpha < 1$, and b_{ij} denotes the same as that in Eq. 6. Let \mathcal{L}_B be the Laplacian matrix associated with the adjacency matrix B , where its elements are defined similar to \mathcal{L}_A .

Theorem 2. Network Eq. 1 with non-identical oscillators under distributed control strategy Eq. 13 achieves frequency synchronization with the settling time bounded by

$$T_2 \leq \frac{\|\dot{\xi}(0)\|^{1-\alpha}}{(1-\alpha)f_{\min}}, \quad (14)$$

if

$$\lambda_{\min}(\mathcal{L}_B - \mathcal{L}_A) \geq 0,$$

where $\|\dot{\xi}(0)\|^2 = \sum_{i=1}^N [\dot{\xi}_i(0)]^2$.

Proof 2. By taking the derivation of Eq. 1, we obtain

$$\ddot{\xi}_i = \ddot{\theta}_i = \sum_{j=1}^N a_{ij} \cos(\xi_j - \xi_i)(\dot{\xi}_j - \dot{\xi}_i) + \dot{u}_i. \quad (15)$$

Consider the following Lyapunov functional candidate

$$V_2 = \frac{1}{2} \dot{\xi}^T \dot{\xi} = \frac{1}{2} \sum_{i=1}^N \dot{\xi}_i^2.$$

The derivation of V_2 along trajectories Eq. 15 gives

$$\begin{aligned} \dot{V}_2 &= \sum_{i=1}^N \dot{\xi}_i \ddot{\xi}_i = \sum_{i=1}^N \dot{\xi}_i \left[\sum_{j=1}^N a_{ij} \cos(\xi_j - \xi_i)(\dot{\xi}_j - \dot{\xi}_i) + \dot{u}_i \right] \\ &= \sum_{i=1}^N \dot{\xi}_i \left[\sum_{j=1}^N a_{ij} \cos(\xi_j - \xi_i)(\dot{\xi}_j - \dot{\xi}_i) + \sum_{j=1}^N b_{ij}(\dot{\xi}_j - \dot{\xi}_i) - f_i \text{sig}(\dot{\xi}_i)^\alpha \right] \\ &= \sum_{i=1}^N \sum_{j=1}^N \dot{\xi}_i a_{ij} \cos(\xi_j - \xi_i)(\dot{\xi}_j - \dot{\xi}_i) + \sum_{i=1}^N \sum_{j=1}^N b_{ij} \dot{\xi}_i (\dot{\xi}_j - \dot{\xi}_i) \\ &\quad - \sum_{i=1}^N \dot{\xi}_i \text{sig}(\dot{\xi}_i)^\alpha. \end{aligned} \quad (16)$$

According to Lemma 1 and the fact $|\cos(\theta_j - \theta_i)| \leq 1$, we can obtain

$$\begin{aligned} \sum_{i=1}^N \sum_{j=1}^N \dot{\xi}_i a_{ij} \cos(\xi_j - \xi_i)(\dot{\xi}_j - \dot{\xi}_i) &= -\frac{1}{2} \sum_{i=1}^N \sum_{j=1}^N a_{ij} (\dot{\xi}_j - \dot{\xi}_i)^2 \cos(\xi_j - \xi_i) \\ &\leq \frac{1}{2} \sum_{i=1}^N \sum_{j=1}^N a_{ij} (\dot{\xi}_j - \dot{\xi}_i)^2 = \dot{\xi}^T \mathcal{L}_A \dot{\xi}. \end{aligned} \quad (17)$$

And,

$$\sum_{i=1}^N \sum_{j=1}^N b_{ij} \dot{\xi}_i (\dot{\xi}_j - \dot{\xi}_i) = -\frac{1}{2} \sum_{i=1}^N \sum_{j=1}^N b_{ij} (\dot{\xi}_j - \dot{\xi}_i)^2 = -\dot{\xi}^T \mathcal{L}_B \dot{\xi}, \quad (18)$$

$$\sum_{i=1}^N \dot{\xi}_i \text{sig}(\dot{\xi}_i)^\alpha = \sum_{i=1}^N f_i \dot{\xi}_i \text{sig}(\dot{\xi}_i) |\dot{\xi}_i|^\alpha \leq \sum_{i=1}^N f_i |\dot{\xi}_i|^{\alpha+1}. \quad (19)$$

Combining Eqs. 17–19, Eq. 16 yields

$$\dot{V}_2 \leq -\dot{\xi}^T (\mathcal{L}_B - \mathcal{L}_A) \dot{\xi} - \sum_{i=1}^N f_i |\dot{\xi}_i|^{\alpha+1}.$$

If $\lambda_{\min}(\mathcal{L}_B - \mathcal{L}_A) \geq 0$, we get

$$\begin{aligned} \dot{V}_2 &\leq -\sum_{i=1}^N f_i |\dot{\xi}_i|^{\alpha+1} \\ &= -\sum_{i=1}^N f_i \left[|\dot{\xi}_i|^2 \right]^{\frac{\alpha+1}{2}} \\ &= -f_{\min} 2^{\frac{1+\alpha}{2}} \left[\frac{1}{2} \sum_{i=1}^N |\dot{\xi}_i|^2 \right]^{\frac{1+\alpha}{2}} \\ &= -2^{\frac{1+\alpha}{2}} f_{\min} V_2^{\frac{1+\alpha}{2}}. \end{aligned}$$

By Lemma 2 and Definition 2, network Eq. 1 with non-identical oscillators under distributed control strategy Eq. 13 achieves finite-time frequency synchronization with the settling time bounded by

$$T_2 \leq \frac{\left[\sum_{i=1}^N (\dot{\xi}_i(0))^2 \right]^{\frac{1-\alpha}{2}}}{(1-\alpha)f_{\min}} = \frac{\|\dot{\xi}(0)\|^{1-\alpha}}{(1-\alpha)f_{\min}}.$$

This completes the proof.

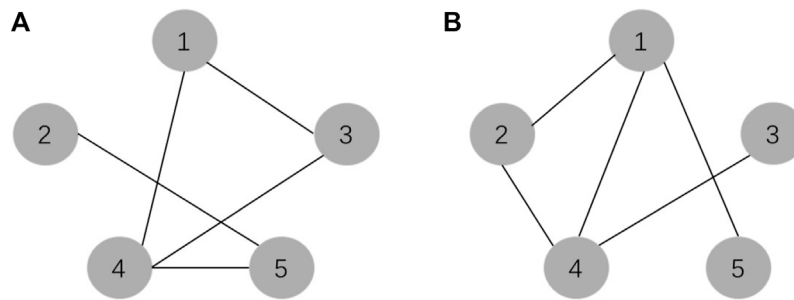


FIGURE 1

(A) Network associated with adjacency matrix A. (B) Network associated with adjacency matrix B.

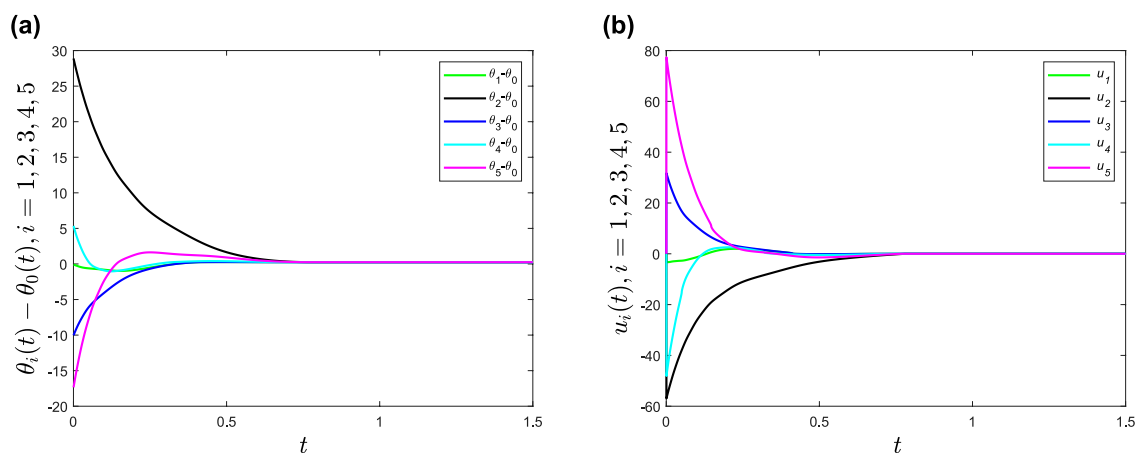


FIGURE 2

(A) Time evolutions of phase differences $\theta_i - \theta_0$ ($i = 1, 2, 3, 4, 5$) under distributed control strategy Eq. 6. (B) Time evolutions of the distributed control strategy Eq. 6.

Remark 2. According to Eq. 14, we find that the upper bound of synchronization time is proportionate to initial state $\|\dot{\xi}(0)\|$, and is inversely to the f_{\min} . According to Theorem 2, it is sufficient to achieve finite-time frequency synchronization if $\lambda_{\min}(\mathcal{L}_B - \mathcal{L}_A) \geq 0$. Therefore, even if the physical network is not connected, frequency synchronization could be also achieved with the help of cyber network, which relaxes the requirement on the connectivity of the physical network.

5 Numerical simulation

In this section, we assume networks associated with adjacency matrices A and B as shown in Figures 1A,B, respectively.

We first verify Theorem 1. Obviously, $\lambda_{\min}(\cos \gamma \cdot \mathcal{L}_A + \mathcal{L}_B) = 0$. For simplicity, set $\omega_i = 0$ ($i = 0, 1, 2, 3, 4, 5$), $\alpha = 0.5$, $f_i = 2$ ($i = 1, 2, 3, 4, 5$), and $(\theta_0(0), \theta_1(0), \theta_2(0), \theta_3(0), \theta_4(0), \theta_5(0)) = (0.25, -0.1028, 28.8866, -10.0289, 5.3575, -17.3534)^T$.

In Figure 2A, phase differences $\theta_i - \theta_0$ converge to zero, which means finite-time phase agreement is achieved. Besides, it also shows phase agreement is achieved about 2.2s, which is less than the upper bound of settling time $T_1 = 5.9600$ s. Time evolutions of the controller Eq. 6 of each oscillator are shown in Figure 2B.

Secondly, we verify Theorem 2. Obviously, $\lambda_{\min}(\mathcal{L}_B - \mathcal{L}_A) = 0$. Set $\alpha = 0.5$, $f_i = 2$ ($i = 1, 2, 3, 4, 5$), $\dot{\theta}_0(0) = \omega_0 = 2$, $(\omega_1, \omega_2, \omega_3, \omega_4, \omega_5) = (-10, -4, 0, 4, 10)^T$, and $(\dot{\theta}_1(0), \dot{\theta}_2(0), \dot{\theta}_3(0), \dot{\theta}_4(0), \dot{\theta}_5(0)) = (44.5324, -4.2299, 17.8956, -39.9282, -18.2699)^T$. In Figure 3A frequency differences $\dot{\theta}_i - \dot{\theta}_0$ converge to zero, which means finite-time frequency synchronization is achieved. Besides, it also shows frequency synchronization is achieved about 0.825s, which is less than the upper bound of settling time bound $T_2 = 2.1147$ s. Time evolutions of the controller Eq. 13 of each oscillator are shown in Figure 3B.

Finally, we move to see the influence of parameter α on synchronization time. In the simulations, we set $\alpha = 0.1, 0.3, 0.5$,

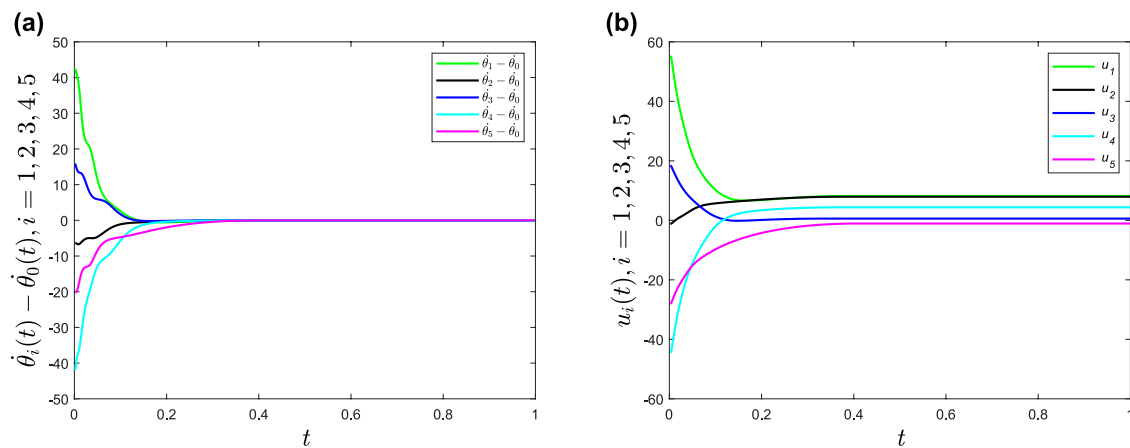


FIGURE 3

(A) Time evolutions of frequencies differences $\dot{\theta}_i - \dot{\theta}_0$ ($i = 1, 2, 3, 4, 5$) under distributed control strategy Eq. 13. (B) Time evolutions of the distributed control strategy Eq. 13.

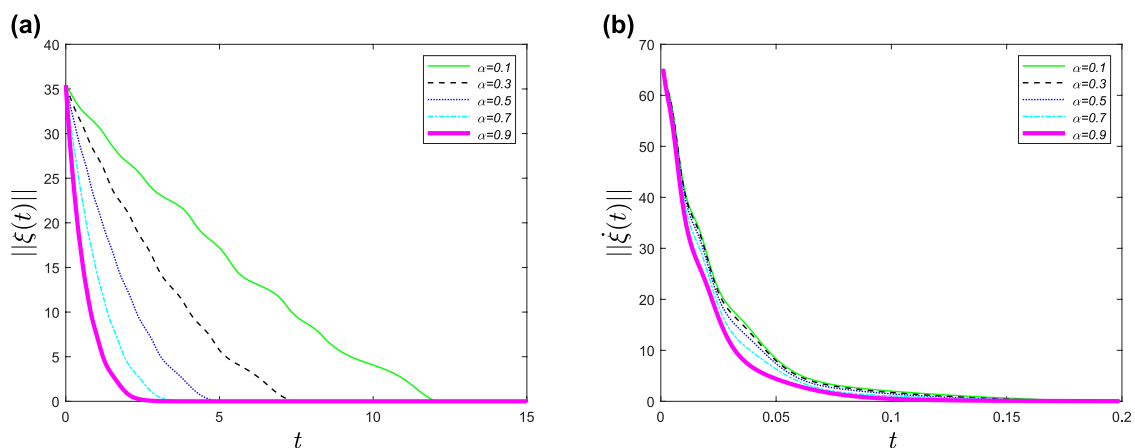


FIGURE 4

(A) Time evolutions of $\|\xi(t)\|$ under the distributed control strategy Eq. 6 with respect to different parameters $\alpha = 0.1, 0.3, 0.5, 0.7, 0.9$. (B) Time evolutions of $\|\dot{\xi}(t)\|$ under the distributed control strategy Eq. 13 with respect to different parameters $\alpha = 0.1, 0.3, 0.5, 0.7, 0.9$.

0.7, 0.9. In Figure 4, it is showed that the synchronization time decreases as α grows.

6 Conclusion

In this paper, the problems of finite-time phase agreement and frequency synchronization of Kuramoto-oscillator networks with a pacemaker have been investigated. Two distributed control strategies, based on the CPS, have been designed to drive the Kuramoto-oscillator networks. In the light of finite-time stability theory, the sufficient criteria have been derived for

guaranteeing the phase agreement and frequency synchronization of identical and non-identical Kuramoto-oscillator networks with a pacemaker. At the same time, the upper bounds estimation of convergence time of Kuramoto-oscillator networks have been given accordingly. Numerical examples have validated the effectiveness of the derived theoretical results.

However, the convergence time estimations of this paper are heavily related to initial phases and/or frequencies of oscillators. Therefore, it is urgent to explore the fixed-time synchronization of Kuramoto model with a pacemaker in the future.

Data availability statement

The original contributions presented in the study are included in the article/Supplementary Material; further inquiries can be directed to the corresponding author.

Author contributions

All authors listed have made a substantial, direct, and intellectual contribution to the work and approved it for publication.

Funding

This work is supported by National Natural Science Foundation of China (Grant No. 61903142), the Science and

Technology Project of Jiangxi Education Department (Grant No. GJJ180356).

Conflict of interest

The authors declare that the research was conducted in the absence of any commercial or financial relationships that could be construed as a potential conflict of interest.

Publisher's note

All claims expressed in this article are solely those of the authors and do not necessarily represent those of their affiliated organizations, or those of the publisher, the editors and the reviewers. Any product that may be evaluated in this article, or claim that may be made by its manufacturer, is not guaranteed or endorsed by the publisher.

References

- Kuramoto Y. *Chemical oscillators, waves, and turbulence*. Berlin, Germany: Springer (1984).
- Liu C, Weaver DR, Strogatz SH, Reppert SM. Cellular construction of a circadian clock: period determination in the suprachiasmatic nuclei. *Cell* (1997) 91: 855–60. doi:10.1016/s0092-8674(00)80473-0
- Chen C, Liu S, Shi X-Q, Chaté H, Wu YL. Weak synchronization and large-scale collective oscillation in dense bacterial suspensions. *Nature* (2017) 542:210–4. doi:10.1038/nature20817
- Kim J-H, Park J-H. Exponential synchronization of Kuramoto oscillators using spatially local coupling. *Physica D: Nonlinear Phenomena* (2014) 277:40–7. doi:10.1016/j.physd.2014.03.006
- Wiesenfeld K, Colet P, Strogatz SH. Frequency locking in josephson arrays: connection with the Kuramoto model. *Phys Rev E* (1998) 57:1563–9. doi:10.1103/physreve.57.1563
- Daido H. Quasientrainment and slow relaxation in a population of oscillators with random and frustrated interactions. *Phys Rev Lett* (1992) 68:1073–6. doi:10.1103/physrevlett.68.1073
- Sun W, Lü JH, Yu XH, Chen Y, Chen SH. Cooperation of multiagent systems with mismatch parameters: a viewpoint of power systems. *IEEE Trans Circuits Syst* (2016) 63:693–7. doi:10.1109/tcsii.2016.2530178
- Seyboth GS, Wu JB, Qin JH, Yu CB, Allgöwer F. Collective circular motion of unicycle type vehicles with non-identical constant velocities. *IEEE Trans Control Netw Syst* (2014) 1:167–76. doi:10.1109/tcns.2014.2316995
- Sepulchre R, Paley DA, Leonard NE. Stabilization of planar collective motion: all-to-all communication. *IEEE Trans Automat Contr* (2007) 52:811–24. doi:10.1109/tac.2007.898077
- Dörfler F, Bullo F. Synchronization in complex networks of phase oscillators: a survey. *Automatica* (2014) 50:1539–64. doi:10.1016/j.automatica.2014.04.012
- Chopra N, Spong MW. On exponential synchronization of Kuramoto oscillators. *IEEE Trans Automat Contr* (2009) 54:353–7. doi:10.1109/tac.2008.2007884
- Ha S-Y, Li ZC, Xue XP. Formation of phase-locked states in a population of locally interacting Kuramoto oscillators. *J Differential Equations* (2013) 255: 3053–70. doi:10.1016/j.jde.2013.07.013
- Li HQ, Chen G, Liao XF, Huang TW. Attraction region seeking for power grids. *IEEE Trans Circuits Syst* (2017) 64:201–5. doi:10.1109/tcsii.2016.2561410
- Li X, Rao PC. Synchronizing a weighted and weakly-connected Kuramoto oscillator digraph with a pacemaker. *IEEE Trans Circuits Syst* (2015) 62:899–905. doi:10.1109/tcsi.2014.2382193
- Rao PC, Li X, Ogorzalek MJ. Stability of synchronous solutions in a directed Kuramoto-Oscillator network with a pacemaker. *IEEE Trans Circuits Syst* (2017) 64:1222–6. doi:10.1109/tcsii.2017.2679216
- Jadbabaie A, Motee N, Barahona M. On the stability of the Kuramoto model of coupled nonlinear oscillators. *Proc Amer Control Conf* (2004) 5.
- Tong DB, Rao PC, Chen QY, Ogorzalek MJ, Li X. Exponential synchronization and phase locking of a multilayer Kuramoto-oscillator system with a pacemaker. *Neurocomputing* (2018) 308:129–37. doi:10.1016/j.neucom.2018.04.067
- Wu J, Liu MQ, Wang XF, Ma R-R. Achieving fixed-time synchronization of the Kuramoto model via improving control techniques. *J Korean Phys Soc* (2021) 79:998–1006. doi:10.1007/s40042-021-00302-z
- Wu J, Li X. Global stochastic synchronization of Kuramoto-oscillator networks with distributed control. *IEEE Trans Cybern* (2021) 51:5825–35. doi:10.1109/tcyb.2019.2959854
- Wang YQ, Doyle FJ. Exponential synchronization rate of Kuramoto oscillators in the presence of a pacemaker. *IEEE Trans Automat Contr* (2013) 58:989–94. doi:10.1109/tac.2012.2215772
- Derler P, Lee EA, Vincentelli AS. Modeling cyber-physical systems. *Proc IEEE* (2012) 100:13–28. doi:10.1109/jproc.2011.2160929
- Lee EA. *Computing foundations and practice for cyber-physical systems: a preliminary report*. California: University of California (2007).
- Zhang W-Y, Yang C, Guan Z-H, Liu Z-W, Chi M, Zheng G-L. Bounded synchronization of coupled Kuramoto oscillators with phase lags via distributed impulsive control. *Neurocomputing* (2016) 218:216–22. doi:10.1016/j.neucom.2016.08.054
- Rao PC, Li X. Pacemaker-based global synchronization of Kuramoto oscillators via distributed control. *IEEE Trans Circuits Syst* (2018) 65:1768–72. doi:10.1109/tcsii.2017.2763184
- Dong J-G, Xue XP. Finite-time synchronization of Kuramoto-type oscillators. *Nonlinear Anal Real World Appl* (2015) 26:133–49. doi:10.1016/j.nonrwa.2015.05.006
- Zhang XX, Sun ZY, Yu CB. Finite-time synchronization of networked Kuramoto-like oscillators. In: *Proceedings of Australian Control Conference*; 3–4 Nov; Newcastle (2016).
- Wu J, Li X. Finite-time and fixed-time synchronization of kuramoto-oscillator network with multiplex control. *IEEE Trans Control Netw Syst* (2019) 6:863–73. doi:10.1109/tcns.2018.2880299
- Olfati-Saber R, Murray RM. Consensus problems in networks of agents with switching topology and time-delays. *IEEE Trans Automat Contr* (2004) 49:1520–33. doi:10.1109/tac.2004.834113
- Bhat SP, Bernstein DS. Finite-time stability of continuous autonomous systems. *SIAM J Control Optim* (2000) 38:751–66. doi:10.1137/s0363012997321358



OPEN ACCESS

EDITED BY
Dun Han,
Jiangsu University, China

REVIEWED BY
Lifeng Xi,
Ningbo University, China
Zu-Guo Yu,
Xiangtan University, China
Min Niu,
University of Science and Technology
Beijing, China

*CORRESPONDENCE
Yu Sun,
sunyu88sy@163.com

SPECIALTY SECTION
This article was submitted to Social
Physics, a section of the journal
Frontiers in Physics

RECEIVED 21 October 2022
ACCEPTED 23 November 2022
PUBLISHED 09 December 2022

CITATION
Sun Y, Liu X and Li X (2022), Hitting time
for random walks on the Sierpinski
network and the half Sierpinski network.
Front. Phys. 10:1076276.
doi: 10.3389/fphy.2022.1076276

COPYRIGHT
© 2022 Sun, Liu and Li. This is an open-
access article distributed under the
terms of the [Creative Commons
Attribution License \(CC BY\)](#). The use,
distribution or reproduction in other
forums is permitted, provided the
original author(s) and the copyright
owner(s) are credited and that the
original publication in this journal is
cited, in accordance with accepted
academic practice. No use, distribution
or reproduction is permitted which does
not comply with these terms.

Hitting time for random walks on the Sierpinski network and the half Sierpinski network

Yu Sun*, Xiaobei Liu and Xiaoyan Li

School of Mathematical Sciences, Jiangsu University, Zhenjiang, China

We consider the unbiased random walk on the Sierpinski network ($S_n \circ N$) and the half Sierpinski network ($HS_n \circ N$), where n is the generation. Different from the existing works on the Sierpinski gasket, $S_n \circ N$ is generated by the nested method and $HS_n \circ N$ is half of $S_n \circ N$ based on the vertical cutting of the symmetry axis. We study the hitting time on $S_n \circ N$ and $HS_n \circ N$. According to the complete symmetry and structural properties of $S_n \circ N$, we derive the exact expressions of the hitting time on the n th generation of $S_n \circ N$ and $HS_n \circ N$. The curves of the hitting time for the two networks are almost consistent when n is large enough. The result indicates that the diffusion efficiency of $HS_n \circ N$ has not changed greatly compared with $S_n \circ N$ at a large scale.

KEYWORDS

hitting time, half Sierpinski networks, vertical cutting, random walk, fractal

1 Introduction

In recent decades, complex networks have attracted great interest in the scientific community [1,2] and are considered valuable tools for describing real-world systems in the nature and society [3]. They also have a significant impact on mobility patterns, network sampling, community detection, signal transmission, virus spreading, epidemic control, and link prediction [4,5]. In recent years, complex networks have not only been studied in the field of mathematics due to their intersectionality and complexity but also more scholars in other disciplines have begun to pay attention to them, which involves system science, statistical physics, computer and information science, etc. [6–9]. Common analysis methods and tools include the graph theory, combinatorial mathematics, matrix theory, probability theory, and stochastic process.

A fractal is a rough or fragmented geometric shape that can be divided into multiple parts, and each part is approximately a reduced-version copy of the whole. According to this definition, a fractal feature is a property known as self-similarity, which means that a fractal has self-similarity [10–13]. In recent years, fractals have attracted a surge of attention in various scientific fields [14,15]. The fractal theory [16,17] has always been a very popular and active theory. This is due to the self-similar structure that exists and the crucial impact of the idea of fractals on a large variety of scientific disciplines, such as molecular biology, pharmaceutical chemistry, optics, economics, and ecology [18]. In addition, many complex networks and real networks are generated by the self-similar fractal network [19–22]. There are many classical fractal models, such as the Cantor set,

the Koch curve, and the Sierpinski gasket [23,24]. These structures have obviously become the focus of research, and many potential characterizations have been discovered. In 25–36, the network evolved from the Sierpinski carpet and some vital properties of the Sierpinski gasket were considered.

It has a great theoretical and practical significance to study the hitting time of random walks, which is the mean of the first-passage time of a random walker starting from any site on the network to a trap (a perfect absorber). It can characterize various other dynamical processes taking place on the network, such as mobility patterns and virus spreading. For example, in the communication and information industry, the hitting time of a random walk model can be used to study and simulate information transmission and latency, data collection, quantification and the prediction of communication and search costs, etc. In the field of biology, random walk models can be used to study and describe the spread of infectious diseases and metabolic fluxes among organisms. In the computer industry, the study of characteristics results in community detection, computer vision, collaborative recommendation, and image segmentation. It also describes the diffusion efficiency of different networks. Kozak and Balakrishnan [37,38] studied random walks on a two-dimensional Sierpinski gasket, three-dimensional Sierpinski tower, and d -dimensional Sierpinski model and gave the analytical expression of the hitting time. Wu [39] studied the random walk on the half Sierpinski gasket and gave the formula for the hitting time. Qi [40] got the expression of the hitting time for several absorbing random walks on Sierpinski graphs and hierarchical graphs.

In this paper, we study random walks and discuss the hitting time on the Sierpinski network model ($S_n \circ N$) and the half Sierpinski network model ($HS_n \circ N$) obtained by vertically cutting $S_n \circ N$ based on the symmetry axis. Compared with $S_n \circ N$, the global self-similarity structure of $HS_n \circ N$ is lost, and only the local self-similarity is preserved. We expect to obtain the exact expression of the hitting time on $HS_n \circ N$ from the complete symmetry of $S_n \circ N$ and show whether there is any effect on the diffusion efficiency of the cut network. The mathematical combination method and fractal theory are applied. The remainder of this paper is organized as follows: in Section 2, we introduce our models. In Section 3, we have a detailed calculation of the hitting time of $S_n \circ N$. Also, the detailed calculation of the hitting time of $HS_n \circ N$ is given in Section 4. In the last section, we draw the conclusion.

2 Preliminaries

In this section, we introduce the structure of $S_n \circ N$ and $HS_n \circ N$ and some concepts about several types of random walks, which will be used in the following.

2.1 The structure of $S_n \circ N$ and $HS_n \circ N$

Actually, $S_n \circ N$ can be constructed in a nested manner with a self-similar structure. We separately define a triangle and a 3-regular graph as S and N . As shown in Figure 1, we can make three copies of the 3-regular graph N and then embed N into S by nodes to obtain the initial generation, which is recorded as $S_1 \circ N$. Making three copies of $S_1 \circ N$ and then embedding the initial generation $S_1 \circ N$ into S to produce the second generation is known as $S(S_1 \circ N)$. For the convenience of the following description, the second generation is abbreviated as $S_2 \circ N$. We get the n th generation $S(S_{n-1} \circ N)$ by repeating the aforementioned process, making three copies of $S_{n-1} \circ N$ and then embedding the $(n-1)$ th generation $S_{n-1} \circ N$ into S , which is abbreviated as $S_n \circ N$. Specifically, $S_n \circ N$ is divided into three parts marked as $S_{n-1}^{(i)} \circ N$ with $i = 1, 2$, and 3 , according to the structure and iteration method. The upper half of Figure 2 shows the first two generations of $S_n \circ N$. It should be noted that all nodes will be labeled sequentially from the top to the bottom by the site index i . The corner node 1 is the trap node, also called the target node. Otherwise, the corner node 1, the left-hand corner node, and the right-hand corner node of the bottom row on $S_n \circ N$ are represented by the set A . Therefore, it is convenient to refer to these three corner nodes as 1, L , and R , respectively. Also, the hitting time is represented by $T_1^{(n)}$, $T_L^{(n)}$, and $T_R^{(n)}$, where n is the generation.

As shown in the lower half of Figure 2, $HS_n \circ N$ is obtained by cutting the corresponding $S_n \circ N$ along the vertical symmetry axis. The cutting method of the network cannot equally divide all the nodes because vertices on the partition line will be retained during segmentation.

From the aforementioned construction, we can easily derive the total number of nodes on $S_n \circ N$ and $HS_n \circ N$ to be

$$N_n = \frac{5 \cdot 3^n + 3}{2}, \quad (1)$$

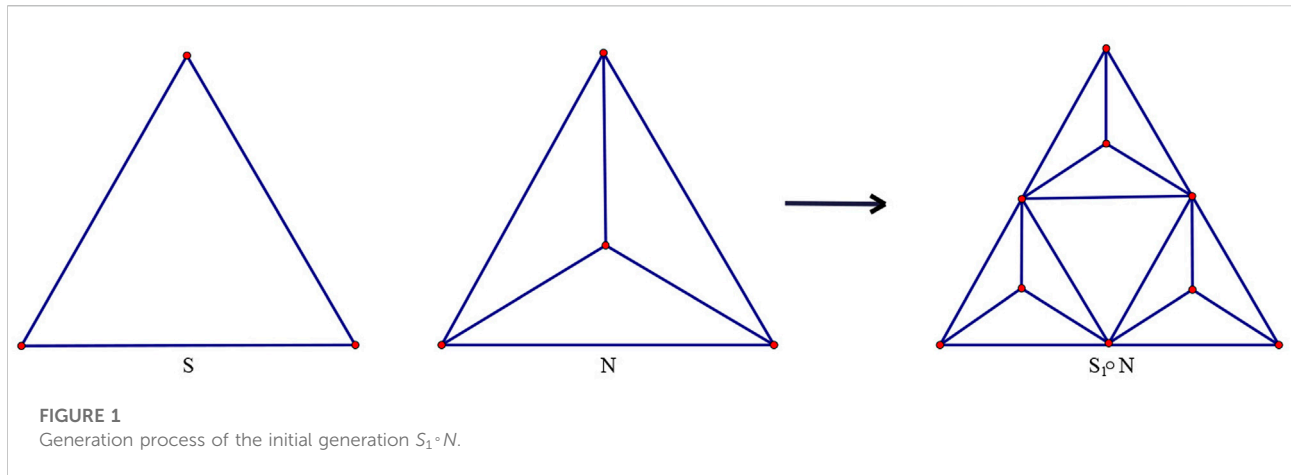
$$H_n = \frac{N_n - (n+2)}{2} + (n+2) = \frac{5 \cdot 3^n + 2n + 7}{4}. \quad (2)$$

The three connecting vertices C_1 , C_2 , and C_3 , which are named after connecting the three regions $S_{n-1}^{(i)} \circ N$ ($i = 1, 2, 3$) on $S_n \circ N$, are marked separately by the numbers as follows: $C_1 = \frac{5 \cdot 3^{n-1} + 3 - 2^n}{2}$, $C_2 = C_1 + 2^{n-1} = \frac{5 \cdot 3^{n-1} + 3}{2}$, and $C_3 = C_2 + 5 \cdot 3^{n-1} = \frac{5 \cdot 3^n + 3 - 2^n}{2}$. According to the position of the three connecting nodes relative to the trap node 1, we divide them into two categories, denoted by sets Ω_n^1 and Ω_n^2 , i.e.,

$$\Omega_n^1 = \{C_1, C_2\}, \quad (3)$$

$$\Omega_n^2 = \{C_3\}. \quad (4)$$

In addition, we use Ω_n^f to denote the set of n non-trap nodes on the vertical secant line, except site 2.



2.2 Calculation of intermediate quantities

The hitting time is the mean of the first-passage time of a random walker starting from any site on the network to a trap node. In order to determine the hitting time for $S_n \circ N$, we introduce the following intermediate quantities, all of which are the probability of a Markov chain on $S_n \circ N$ ending at corner node 1. In the process, the chain starts at a certain vertex and stops whenever it visits any of the three corner nodes of $S_n \circ N$, where n is the generation.

p_n : The starting state is a corner node other than site 1. At least one transition is performed.

$p_1(n)$: The starting state is a special vertex belonging to Ω_n^1 .

$p_2(n)$: The starting state is a special vertex belonging to Ω_n^2 .

$$\begin{cases} p_{n+1} = p_n p_2(n+1) + p_n p_1(n+1), \\ p_1(n+1) = \frac{1}{2} [p_n + (1-p_n)p_1(n+1)] \\ \quad + \frac{1}{2} [p_n p_2(n+1) + (1-2p_n)p_1(n+1)], \\ p_2(n+1) = \frac{1}{2} [p_n p_1(n+1) + (1-2p_n)p_2(n+1)] \\ \quad + \frac{1}{2} [p_n p_1(n+1) + (1-2p_n)p_2(n+1)]. \end{cases} \quad (5)$$

The first equality of the equation group is explained. A random walk in $S_{n+1} \circ N$, starting from the corner node L and ending whenever the walker reaches any three corner nodes of $S_{n+1} \circ N$, is limited to jumping at least one step. By definition, the walker stops at the corner node R or 1 with probability p_{n+1} . In addition, the walker must first reach a connecting vertex C_1 or C_3 in order to reach one of the corner nodes R or 1 . By definition and symmetry, the probability of reaching each of the connecting vertices C_1 or C_3 is p_n , where the connecting vertex C_1 belongs to Ω_{n+1}^1 and the other connecting vertex C_3 belongs to Ω_{n+1}^2 , and the walker has the remaining probability $1-2p_n$ returning to the corner node L , where it stops walking. Therefore, the first equality is obtained.

We next certify the second equality in the equation system (Eq. 5). Considering a random walk in $S_{n+1} \circ N$, which starts from the connecting vertex C_1 and ends whenever the walker reaches any three corner nodes of $S_{n+1} \circ N$, it jumps at least one step. By definition, the probability that the walker stops at corner node 1 is $p_1(n+1)$. The probability of getting in $S_n^{(1)} \circ N$ and $S_n^{(2)} \circ N$ is $\frac{1}{2}$. If it enters $S_n^{(1)} \circ N$, it has a probability of p_n to arrive at corner node 1 , where the walker stops jumping. Also, the walker reaches the other two corner nodes of $S_n^{(1)} \circ N$ with probability $1-p_n$, i.e., connecting vertices C_1 and C_2 belonging to Ω_{n+1}^1 . As a result, we can write the first item on the right side of the second equality. Similarly, if it enters $S_n^{(2)} \circ N$, it reaches the corner node L or the connecting vertex C_3 with the same probability p_n . When it reaches the corner node L , it stops walking. When it reaches the connecting vertex C_3 , it will continue to walk to the target node. Then, the walker has a probability $1-2p_n$ of returning to the connecting vertex C_1 . Therefore, we can write the second item on the right side of the second equality. From these analyses, the aforementioned equality is obtained.

Ultimately, we testify to the third equality of the system of Eq. 5. A random walk in $S_{n+1} \circ N$, starting from the connecting vertex C_3 and ending whenever the walker reaches any three corner nodes of $S_{n+1} \circ N$, jumps at least one step. By definition, the probability that the walker stops at corner node 1 is $p_2(n+1)$. The probability of getting into $S_n^{(2)} \circ N$ and $S_n^{(3)} \circ N$ is $\frac{1}{2}$. If it enters $S_n^{(2)} \circ N$, the probability of the walker reaching the corner node L is p_n , and the walker will stop walking at this point. In addition, the probability of the walker reaching the connecting vertex C_1 is p_n , and the probability of returning to the starting site C_3 is $1-2p_n$. As a result, we can draw up the primary item on the right side of the last equality in the system of Eq. 5. Due to the complete symmetry of $S_{n+1} \circ N$, the random walk on $S_n^{(3)} \circ N$ is the same as that of $S_n^{(2)} \circ N$. Therefore, the last equation is true.

It is easy to know that the initial value $p_1 = \frac{4}{15}$. Through simplification, the final solution is obtained:

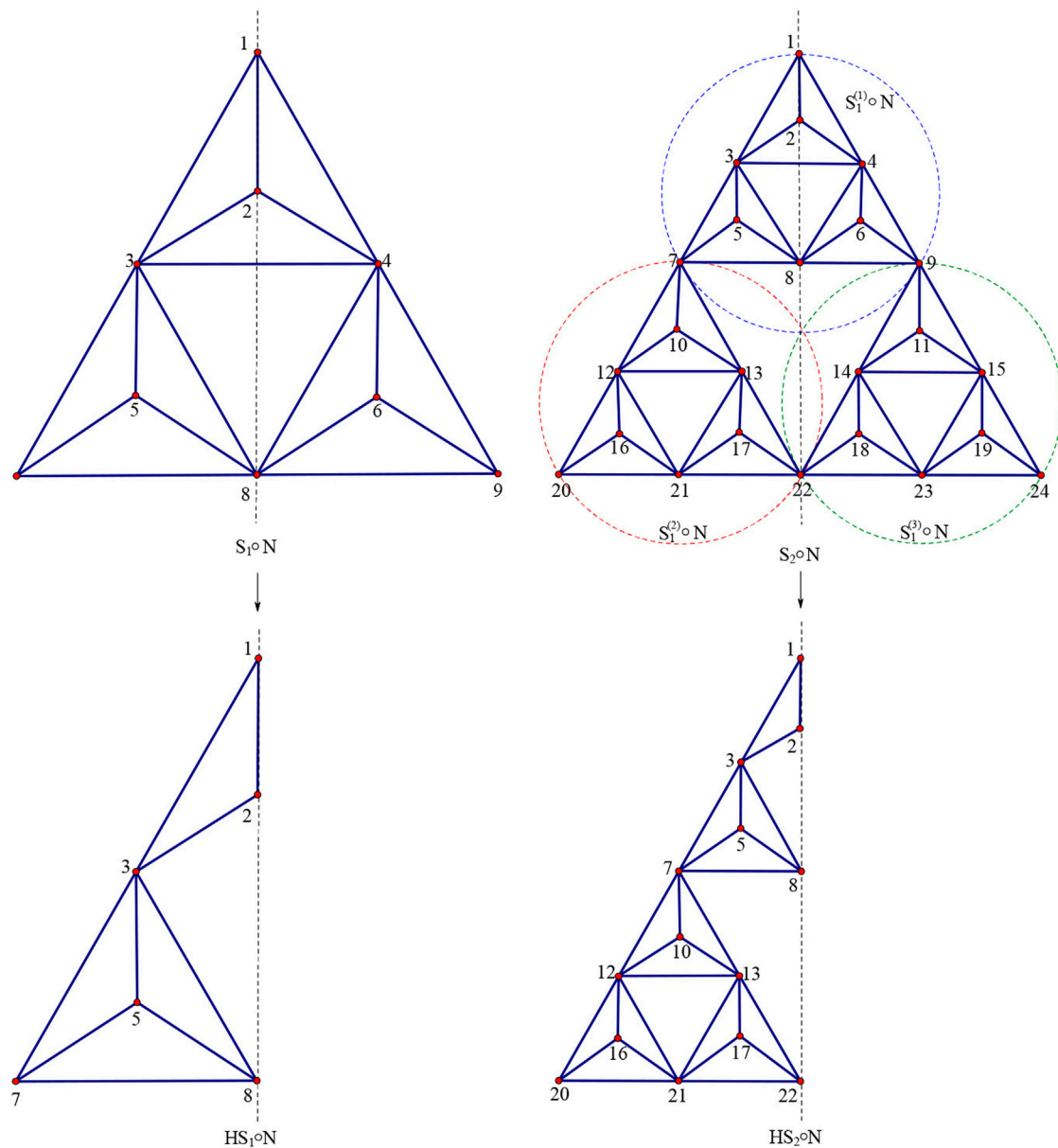


FIGURE 2
First two generations of $S_n^o N$ and $HS_n^o N$ for $n = 1$ and 2 .

$$\begin{cases} p_n = \frac{4}{15} \left(\frac{3}{5}\right)^{n-1}, \\ p_1(n) = \frac{2}{5}, \\ p_2(n) = \frac{1}{5} \end{cases} \quad (6)$$

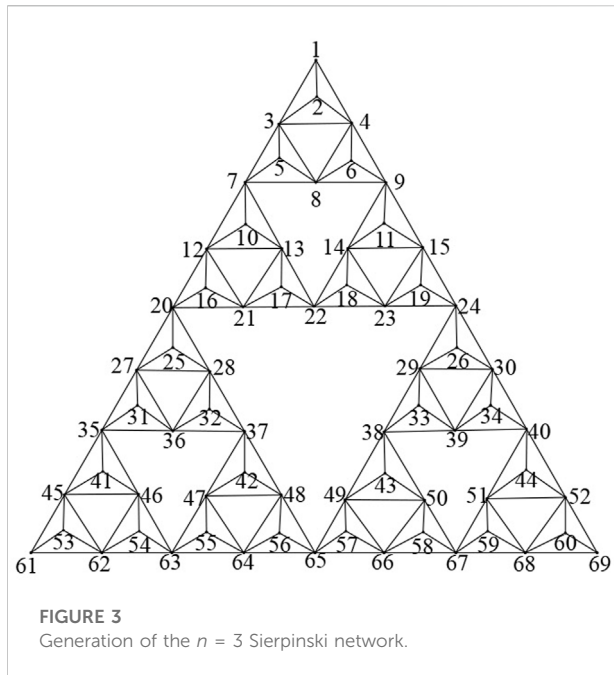
We next define the corresponding hitting time. Corner nodes $1, L$, and R are represented by set A , where site 1 is set as

the trap node; connecting vertices C_1, C_2 , and C_3 are indicated by set I .

$T_{L \rightarrow 1}(n)$: The hitting time from the corner node L to the corner node 1 in the n th generation.

$T_{L \rightarrow A}(n)$: The hitting time from the corner node L to any node in set A in the n th generation.

$T_{I \rightarrow A}(n)$: The hitting time from any vertex in set I to any node in set A in the n th generation.



$$\begin{cases} T_{L \rightarrow 1}(n) = T_{L \rightarrow A}(n) + (1 - p_n)T_{L \rightarrow 1}(n), \\ T_{L \rightarrow A}(n+1) = T_{L \rightarrow A}(n) + 2p_n T_{L \rightarrow A}(n+1), \\ T_{L \rightarrow A}(n+1) = \frac{1}{2} [T_{L \rightarrow A}(n) + (1 - p_n)T_{L \rightarrow A}(n+1)] \\ \quad + \frac{1}{2} [T_{L \rightarrow A}(n) + (1 - p_n)T_{L \rightarrow A}(n+1)]. \end{cases} \quad (7)$$

We now attest to the first equality in the equation system (Eq. 7). $T_{L \rightarrow 1}(n)$ is the hitting time for a random walk in $S_n \circ N$ starting from the corner node L and ending at the trap node 1. According to the structure of $S_n \circ N$, the walker must first reach any of the three corner nodes of $S_n \circ N$ in order to reach trap node 1, taking expected timesteps $T_{L \rightarrow A}(n)$. In such a process, the probability of reaching destination node 1 is p_n , where the walker stops jumping. Also, the probability of reaching corner nodes R and L is $1 - p_n$, from which the walker must continue to bounce $T_{L \rightarrow 1}(n)$ steps to reach trap node 1. Thus, we get the first expression.

Subsequently, we prove the second equality in the equation system (Eq. 7). $T_{L \rightarrow A}(n+1)$ is the hitting time for a random walk starting from the corner node L to any of the three corner nodes of $S_{n+1} \circ N$ for the first time, under the limitation that the walker jumps at least one step. In order to reach any of corner nodes in $S_{n+1} \circ N$, the walker starting from the corner node L must first visit one of the corner nodes in $S_n \circ N$. It is worth noting that these points belong to $S_n^{(2)} \circ N$. This process is expected of $T_{L \rightarrow A}(n)$ timesteps. In this process, there is the same probability of reaching the connecting vertices C_1 and C_3 , which is p_n . The probability of returning to the corner node L is $1 - 2p_n$, stopping at this point. If the walker reaches any of the connecting vertices C_1 and C_3 , it will continue to jump $T_{L \rightarrow A}(n+1)$ steps to visit any of the corner nodes of $S_{n+1} \circ N$.

Ultimately, we testify to the third equality of the system in Eq. 7. Consider a random walk, which starts from any one of the connecting nodes C_1 , C_2 , and C_3 and ends whenever it reaches any corner nodes on $S_{n+1} \circ N$. By definition, the hitting time is $T_{I \rightarrow A}(n+1)$. We now study the random walk from the connecting vertex C_3 , which may perform the following two processes. Both processes happen with the probability of $\frac{1}{2}$. In the first process, the walker goes inside $S_n^{(2)} \circ N$, taking $T_{L \rightarrow A}(n)$ timesteps to reach the three corner nodes of $S_n^{(2)} \circ N$. The probability of reaching the corner node L is p_n , where the walking process is over. Also, the probability of reaching the other two corner nodes belonging to $S_n^{(2)} \circ N$ is $1 - p_n$, i.e., the connecting vertices C_1 and C_3 . The walker needs to take further $T_{I \rightarrow A}(n+1)$ timesteps before being absorbed. According to the symmetry of $S_n \circ N$, the second process is the same as the first one.

By substituting the value of $p_n = \frac{4}{15} (\frac{3}{5})^{n-1}$ into the aforementioned equation and simplifying it. In addition, it is easy to know $T_{L \rightarrow A}(1) = 4$, so we can get the following:

$$\begin{cases} T_{L \rightarrow 1}(n) = 3 \cdot 5^n, \\ T_{L \rightarrow A}(n) = 4 \cdot 3^{n-1}, \\ T_{I \rightarrow A}(n) = 3 \cdot 5^{n-1}. \end{cases} \quad (8)$$

3 Formula of hitting time on $S_n \circ N$

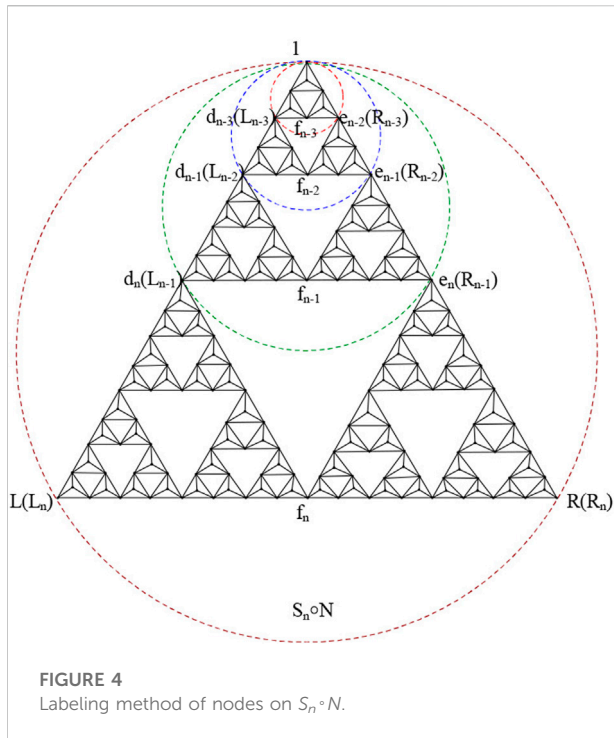
The Sierpinski network in any given generation n , using arrays (a, b, c) to represent a piece of interior points, for instance, $(2, 5, 6)$ or $(10, 16, 17)$, as shown in Figure 3; let (I_1, J_1, K_1) label the three vertices of the smallest triangle containing the three interior points (a, b, c) , simultaneously, for instance, $(1, 7, 9)$ or $(7, 20, 22)$. According to the numerical results, the hitting time can be rewritten as follows:

$$T_a(n) + T_b(n) + T_c(n) = T_{I_1}(n) + T_{J_1}(n) + T_{K_1}(n) + 9. \quad (9)$$

Let (i_1, j_1, k_1) label the three sites, which are one of any minimum size 1 lacunary triangle on $S_n \circ N$. For example, $(3, 4, 8)$ or $(12, 13, 21)$; (I_1, J_1, K_1) also label the three vertices of the triangle containing (i_1, j_1, k_1) as its central lacunary region, such as $(1, 7, 9)$ or $(7, 20, 22)$, referring to Figure 3. According to the numerical results, it is easy to see the following:

$$T_{i_1}(n) + T_{j_1}(n) + T_{k_1}(n) = T_{I_1}(n) + T_{J_1}(n) + T_{K_1}(n) + 9 \cdot 5^0. \quad (10)$$

In the same way, we now let (i_2, j_2, k_2) denote the three vertices of a lacunary region of size 2 in the network, such as $(7, 9, 22)$ or $(35, 37, 63)$; (I_2, J_2, K_2) label the three vertices of the triangle containing (i_2, j_2, k_2) as its central lacunary region, such as $(1, 20, 24)$ or $(20, 61, 65)$. It then follows the scaling derived previously that is as follows:



$$T_{i_2}(n) + T_{j_2}(n) + T_{k_2}(n) = T_{I_2}(n) + T_{J_2}(n) + T_{K_2}(n) + 9 \cdot 5^1. \quad (11)$$

Therefore, moving up the hierarchy, if (i_r, j_r, k_r) are the sites demarcating a lacunary triangle of size r in the ascending order of size, starting from the smallest in size 1, and if (I_r, J_r, K_r) label the vertices of the triangle with (i_r, j_r, k_r) as the central lacunary region, then

$$T_{i_r}(n) + T_{j_r}(n) + T_{k_r}(n) = T_{I_r}(n) + T_{J_r}(n) + T_{K_r}(n) + 9 \cdot 5^{r-1}. \quad (12)$$

The foregoing suggests how the hitting time $T_{total}(n)$ may be computed for the arbitrary n . This is carried out by suitably regrouping the terms in the sum $\sum_{i=2}^{N_n} T_i(n)$ and systematically and repeatedly using Eq. 12 as one moves upward through triangles of increasing sizes. It needs some combinatorics and involves the enumeration of the number of lacunary triangles of each size in the network. The final result can be expressed entirely in terms of the known numerical factors and the combination $(T_1(n) + T_L(n) + T_R(n))$. Since $T_1(n) \equiv 0$, while $T_L(n) = T_R(n) = 3 \cdot 5^n$, this leads directly to the desired expression for $T_{total}(n)$. As an illustration of the procedure, consider the network of generation $n = 3$, with $N_n = 69$. Dropping for a moment the generation superscript for brevity and with $L = 61$ and $R = 69$, as shown in Figure 3, we obtain the following:

$$\begin{aligned} T_{total}(3) &= \sum_{i=2}^{69} T_i(3) \\ &= 3(T_1 + T_L + T_R) + 3^2 \cdot 9 + 3^2 \cdot 9 \cdot 5^0 \\ &\quad + 5\{3^0(T_1 + T_L + T_R) + 3^1 \cdot 9 \cdot 5^1 + 3^1 \\ &\quad [(T_1 + T_L + T_R) + 3^0 \cdot 9 \cdot 5^2]\}. \end{aligned} \quad (13)$$

Thus, $T_{total}(3)$ has been recast in terms of the sum $(T_1 + T_L + T_R)$ of the hitting time from the three primary sites. The meaning of 3^2 of the second term on the right side of the equation is that there are nine pieces of interior points in $S_3^o N$. It should be noted that the modulus 3^2 of the third term represents the number of regions of size 1, the coefficient 3^1 of the factor multiplying $9 \cdot 5^1$ is the number of lacunary triangles of size 2, and 3^0 of the factor multiplying $9 \cdot 5^2$ is the number of lacunary triangles of size 3 on the $n = 3$ network.

We may now carry out a similar procedure for the case of general n . The analog of Eq. 13 yields the following:

$$\begin{aligned} T_{total}(n) &= \sum_{i=2}^{N_n} T_i(n) \\ &= \left(3 + 5 \cdot \sum_{m=0}^{n-2} 3^m\right) (T_1(n) + T_L(n) + T_R(n)) \\ &\quad + 2 \cdot 3^{n-1} \cdot 9 + (3^{n-2} \cdot 9 \cdot 5) \sum_{m=1}^{n-1} 5^m. \end{aligned} \quad (14)$$

The numerical value is substituted to get the following result:

$$T_{total}(n) = \frac{25}{4} \cdot 5^n \cdot 3^n + 3 \cdot 5^n - \frac{1}{4} \cdot 3^n. \quad (15)$$

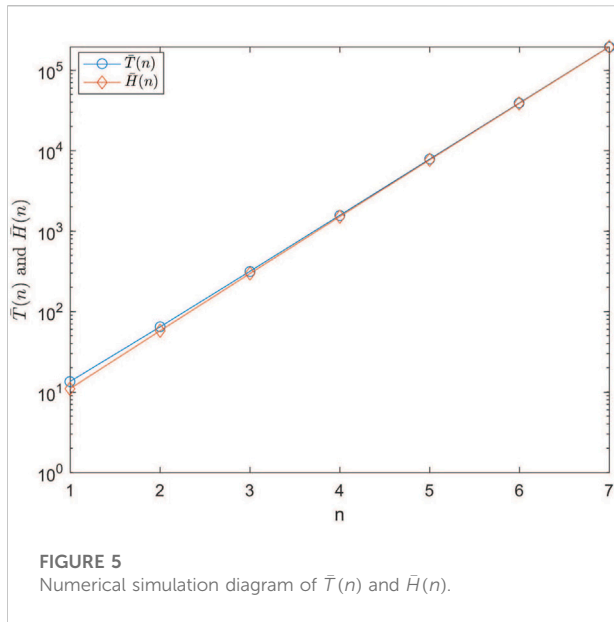
Therefore, the hitting time on $S_n^o N$ is as follows:

$$\begin{aligned} \bar{T}(n) &= \frac{1}{N_n - 1} T_{total}(n) \\ &= \frac{1}{N_n - 1} \sum_{i=2}^{N_n} T_i(n) \\ &= \frac{25 \cdot 5^n \cdot 3^n + 12 \cdot 5^n - 3^n}{2(3^n \cdot 5 + 1)}. \end{aligned} \quad (16)$$

4 Formula of hitting time on $HS_n^o N$

We divide the random walk into two processes on $S_n^o N$ and $HS_n^o N$, except node 2. The first process is that a walker starts from the starting point to node 3 or 4, which is the sum of the hitting time called $T_g(n)$. The second procedure is a random walk from node 3 or 4 to the trap node, which is called $T_3(n)$. In addition, $T_2(n)$ denotes the hitting time from site 2 to trap node 1.

Similarly, the first process of $HS_n^o N$ is a random walk from any site to node 3, and the hitting time of this process is recorded as $H_g(n)$. The second process is recorded as $H_3(n)$, and $H_2(n)$



represents the hitting time from site 2 to trap node 1 on $HS_n \circ N$. Thence, we have the following equations:

$$\begin{cases} T_{total}(n) = T_g(n) + (N_n - 2)T_3(n) + T_2(n), \\ H_{total}(n) = H_g(n) + (H_n - 2)H_3(n) + H_2(n). \end{cases} \quad (17)$$

Let $T_r(n)$ be the mean of the first return time for a random walker starting from node 3 in the first process of $HS_n \circ N$. Then, $T_r(n)$ can also be the mean of the first return time to node 3 or 4 in the first process of $S_n \circ N$. Therefore, according to the structure of $HS_n \circ N$ and $S_n \circ N$, we have the following relationship:

$$\begin{cases} T_3(n) = \frac{1}{6} + \frac{1}{6}[1 + T_2(n)] + \frac{1}{6}[1 + T_3(n)] + \frac{3}{6}[T_r(n) + T_3(n)], \\ H_3(n) = \frac{1}{5} + \frac{1}{5}[1 + H_2(n)] + \frac{3}{5}[T_r(n) + H_3(n)]. \end{cases} \quad (18)$$

Moreover, from the numerical results, we have $T_2(n) = 3 \cdot 3^n$ and $H_2(n) = 2 \cdot 3^n$. So, we get the following relation:

$$T_3(n) - H_3(n) = \frac{1}{2}(3^n + 1).$$

Because the nodes on the cut line are retained, the hitting time $T_i(n)$ from any node i on the secant line to the goal node 1 is also divided into two parts. The first process is a random walk from node i to node 3 or 4, which is denoted as $T_{i \rightarrow 3,4}(n)$. The hitting time of the second process is denoted as $T_3(n)$, which represents a random walk from site 3 to destination node 1. Therefore, $T_i(n)$ can be rewritten as follows:

$$T_i(n) = T_{i \rightarrow 3,4}(n) + T_3(n). \quad (19)$$

Consequently, the formula for the hitting time of nodes that belong to Ω_n^f is as follows:

$$\begin{aligned} T^f(n) &= \sum_{i \in \Omega_n^f} (T_{i \rightarrow 3,4}(n) + T_3(n)) \\ &= \bar{T}^f(n) + n \cdot T_3(n). \end{aligned} \quad (20)$$

In $S_n \circ N$, in addition to the nodes on the secant line, other nodes are evenly divided on both the sides in the segmentation process. $HS_n \circ N$ contains the nodes on the left half of the secant line and the nodes in set Ω_n^f . Therefore, it can be obtained by the following:

$$H_g(n) = \frac{1}{2} [T_g(n) - \bar{T}^f(n)] + \bar{T}^f(n). \quad (21)$$

Eqs 17 and 20 are inserted into the aforementioned formula to get the following solution:

$$H_g(n) = \frac{1}{2} [T_{total}(n) - (N_n + n - 2)T_3(n) - T_2(n) + T^f(n)]. \quad (22)$$

Then, substituting the aforementioned expression (Eq. 22) into the second formula in the equation group (Eq. 17), we get the following:

$$\begin{aligned} H_{total}(n) &= H_g(n) + (H_n - 2)H_3(n) + H_2(n) \\ &= \frac{1}{2} [T_{total}(n) - (N_n + n - 2)T_3(n) - T_2(n) + T^f(n)] \\ &\quad + (H_n - 2)H_3(n) + H_2(n) \\ &= \frac{1}{2} \left[T_{total}(n) - \frac{3^n + 1}{2} (N_n + n - 2) + 3^n + T^f(n) \right]. \end{aligned} \quad (23)$$

We focus on solving the expression of $T^f(n)$. In order to facilitate the calculation, we rewrite the three connecting vertices C_1 , C_2 , and C_3 of $S_n \circ N$ as d_n , e_n , and f_n , respectively. According to the structural characteristics of $S_n \circ N$, the sites d_n and e_n in the n th generation can be labeled as the corner nodes L_{n-1} and R_{n-1} in the $(n-1)$ th generation. The labeling method of nodes on $S_n \circ N$ can be seen in Figure 4.

If corner nodes 1, L_n , and R_n are set as goal nodes, then the walker starting from site f_y ($y = 1, \dots, n$) is captured by the trap set A after $3 \cdot 5^{y-1}$ random walks on average in $S_n \circ N$, which can be seen from the analysis of the equation group (Eq. 7) and results. In addition, the arriving node L_y or R_y has a probability of $\frac{2}{5}$. Thus, $T_{f_y}(n)$ ($y = 1, \dots, n$) can be denoted as follows:

$$\begin{aligned} T_{f_y}(n) &= 3 \cdot 5^{y-1} + \frac{2}{5}T_{L_y}(n) + \frac{2}{5}T_{R_y}(n) \\ &= 3 \cdot 5^{y-1} + \frac{4}{5}T_{L_y}(n) \\ &= 3 \cdot 5^{y-1} + \frac{4}{5}T_{d_{y+1}}(n). \end{aligned}$$

Similarly, starting from the point d_{y+1} ($y = 1, \dots, n$) and getting to the site L_y or R_y has a probability of $\frac{2}{5}$ after $3 \cdot 5^y$ random walks on average. Then, the walker is captured by the trap set A . In addition, there are $\frac{2}{5}$ and $\frac{1}{5}$ probabilities reaching

nodes L_{y+1} and R_{y+1} , respectively. Therefore, the aforementioned equation can be expressed as follows:

$$\begin{aligned}
 T_{f_y}(n) &= 3 \cdot 5^{y-1} + \frac{4}{5} \left[3 \cdot 5^y + \frac{2}{5} T_{L_{y+1}}(n) + \frac{1}{5} T_{R_{y+1}}(n) \right] \\
 &= 3 \cdot 5^{y-1} + \frac{4}{5} \cdot 3 \cdot 5^y + \frac{4}{5} \cdot \frac{3}{5} T_{L_{y+1}}(n) \\
 &= \dots \\
 &= 3 \cdot 5^{y-1} + 4 \cdot 5^{y-1} \sum_{k=1}^{n-y} 3^k + \frac{4}{5} \cdot \left(\frac{3}{5}\right)^{n-y} T_{L_n}(n) \quad (24) \\
 &= 3 \cdot 5^{y-1} + 4 \cdot 5^{y-1} \sum_{k=1}^{n-y} 3^k + \frac{4}{5} \cdot \left(\frac{3}{5}\right)^{n-y} \cdot 3 \cdot 5^n \\
 &= 18 \cdot 5^{y-1} \cdot 3^{n-y} - 3 \cdot 5^{y-1}.
 \end{aligned}$$

Here, $T_{L_n}(n) = 3 \cdot 5^n$ and the expression for the hitting time of nodes that belong to Ω_n^f is as follows:

$$\begin{aligned}
 T^f(n) &= \sum_{i \in \Omega_n^f} T_i(n) \\
 &= \sum_{y=1}^n T_{f_y}(n) \quad (25) \\
 &= \sum_{y=1}^n (18 \cdot 5^{y-1} \cdot 3^{n-y} - 3 \cdot 5^{y-1}) \\
 &= \frac{33}{4} \cdot 5^n + 9 \cdot 3^n + \frac{3}{4}.
 \end{aligned}$$

Therefore, substituting Eq. 15 and Eq. 25 into Eq. 23, the expression of $H_{total}(n)$ is as follows:

$$H_{total}(n) = \frac{1}{2} \left[\frac{25}{4} \cdot 5^n \cdot 3^n + \frac{45}{4} \cdot 5^n - \frac{37}{4} \cdot 3^n - \frac{5}{4} \cdot 3^{2n} - \frac{n(3^n+1)}{2} + 1 \right]. \quad (26)$$

Then, the hitting time on $HS_n \circ N$ is as follows:

$$\begin{aligned}
 \bar{H}(n) &= \frac{1}{H_n - 1} H_{total}(n) \\
 &= \frac{1}{H_n - 1} \sum_{i=2}^{H_n} H_i(n) = \frac{2}{5 \cdot 3^n + 2n + 3} \\
 &\quad \left[\frac{25}{4} \cdot 5^n \cdot 3^n + \frac{45}{4} \cdot 5^n - \frac{37}{4} \cdot 3^n - \frac{5}{4} \cdot 3^{2n} - \frac{n(3^n+1)}{2} + 1 \right]. \quad (27)
 \end{aligned}$$

In order to compare it with the exact formula for the hitting time of a random walk on $S_n \circ N$ and $HS_n \circ N$, we draw the numerical simulation diagram of $\bar{T}(n)$ and $\bar{H}(n)$ for $n = 1, 2, \dots, 7$, as shown in Figure 5. The figure shows that the difference in the hitting time between $S_n \circ N$ and $HS_n \circ N$ is small when n is large enough. Therefore, the curves of both the networks are nearly merged for large scales, which indicate that the diffusion efficiency of $HS_n \circ N$ is consistent with $S_n \circ N$ for a large scale.

5 Conclusion

In this paper, we study analytically the unbiased random walk on the Sierpinski network ($S_n \circ N$) and the half Sierpinski

network ($HS_n \circ N$), which is obtained by vertically cutting $S_n \circ N$ along the symmetry axis. After cutting, the global self-similarity of $S_n \circ N$ is destroyed, but only the local self-similarity is maintained. We have analytically obtained the closed-form expression of the hitting time for a random walk on the n th generation $HS_n \circ N$, which is $\bar{H}(n) = \frac{2}{5 \cdot 3^n + 2n + 3} \left[\frac{25}{4} \cdot 5^n \cdot 3^n + \frac{45}{4} \cdot 5^n - \frac{37}{4} \cdot 3^n - \frac{5}{4} \cdot 3^{2n} - \frac{n(3^n+1)}{2} + 1 \right]$. However, the hitting time of $S_n \circ N$ is found to be $\bar{T}(n) = \frac{25 \cdot 5^n \cdot 3^n + 12 \cdot 5^n - 3^n}{2(3^n+1)}$. The hitting time is the quantity that characterizes the diffusion efficiency of the network. The curves of the two networks show that the hitting time of $HS_n \circ N$ is practically similar compared with $S_n \circ N$ when n is large enough, and our results show that the diffusion efficiency of $HS_n \circ N$ has little effect compared with $S_n \circ N$ at a large scale. Our work is further helpful in understanding the properties of Sierpinski networks.

Data availability statement

The original contributions presented in the study are included in the article/Supplementary Material, further inquiries can be directed to the corresponding author.

Author contributions

All authors listed have made a substantial, direct, and intellectual contribution to the work and approved it for publication.

Conflict of interest

The authors declare that the research was conducted in the absence of any commercial or financial relationships that could be construed as a potential conflict of interest.

The handling editor declared a shared affiliation with the authors at the time of review.

Publisher's note

All claims expressed in this article are solely those of the authors and do not necessarily represent those of their affiliated organizations, or those of the publisher, the editors, and the reviewers. Any product that may be evaluated in this article, or claim that may be made by its manufacturer, is not guaranteed or endorsed by the publisher.

References

- Strogatz SH. Exploring complex networks. *nature* (2001) 410:268–76. doi:10.1038/35065725
- Wang XF, Chen G. Synchronization in scale-free dynamical networks: Robustness and fragility. *IEEE Trans Circuits Syst* (2002) 49:54–62. doi:10.1109/81.974874
- Guimerà R, Amaral LAN. Functional cartography of complex metabolic networks. *nature* (2005) 433:895–900. doi:10.1038/nature03288
- Grubesić TH, Matisziw TC, Zook MA. Global airline networks and nodal regions. *GeoJournal* (2008) 71:53–66. doi:10.1007/s10708-008-9117-0
- Deng F-G, Li X-H, Li C-Y, Zhou P, Zhou H-Y. Quantum secure direct communication network with einstein–podolsky–rosen pairs. *Phys Lett A* (2006) 359:359–65. doi:10.1016/j.physleta.2006.06.054
- Batool A, Pál G, Danku Z, Kun F. Transition from localized to mean field behaviour of cascading failures in the fiber bundle model on complex networks. *Chaos, Solitons & Fractals* (2022) 159:112190. doi:10.1016/j.chaos.2022.112190
- Cotilla-Sanchez E, Hines PD, Barrows C, Blumsack S, Patel M. Multi-attribute partitioning of power networks based on electrical distance. *IEEE Trans Power Syst* (2013) 28:4979–87. doi:10.1109/tpwrs.2013.2263886
- Jung J, Jin W, Kang U. Random walk-based ranking in signed social networks: Model and algorithms. *Knowl Inf Syst* (2020) 62:571–610. doi:10.1007/s10115-019-01364-z
- Bai S, Niu M. Spectral properties of a class of treelike networks generated by motifs with single root node. *Mod Phys Lett B* (2022) 36:2250038. doi:10.1142/s0217984922500385
- Li B-G, Yu Z-G, Zhou Y. Fractal and multifractal properties of a family of fractal networks. *J Stat Mech* (2014) 2014:P02020. doi:10.1088/1742-5468/2014/02/P02020
- Zhou Y, Leung Y, Yu Z-G. Relationships of exponents in two-dimensional multifractal detrended fluctuation analysis. *Phys Rev E* (2013) 87:012921. doi:10.1103/physreve.87.012921
- Chen J, Dai M, Wen Z, Xi L. A class of scale-free networks with fractal structure based on subshift of finite type. *Chaos* (2014) 24:043133. doi:10.1063/1.4902416
- Wang Q, Xi L, Zhang K. Self-similar fractals: An algorithmic point of view. *Sci China Math* (2014) 57:755–66. doi:10.1007/s11425-013-4767-x
- Babić M, Mihelić J, Cali M. Complex network characterization using graph theory and fractal geometry: The case study of lung cancer dna sequences. *Appl Sci* (2020) 10:3037. doi:10.3390/app10093037
- Wang Z, Zhou Y, Bajenaid AS, Chen Y. Design of wireless sensor network using statistical fractal measurements. *Fractals* (2022) 30:2240092. doi:10.1142/s0218348x22400928
- Klafter J, Blumen A, Zumofen G. Fractal behavior in trapping and reaction: A random walk study. *J Stat Phys* (1984) 36:561–77. doi:10.1007/bf01012922
- Zhang P, Zhang Y, Huang Y, Xia Y. Experimental study of fracture evolution in enhanced geothermal systems based on fractal theory. *Geothermics* (2022) 102:102406. doi:10.1016/j.geothermics.2022.102406
- Blumen A, Klafter J, Zumofen G. Trapping and reaction rates on fractals: A random-walk study. *Phys Rev B* (1983) 28:6112–5. doi:10.1103/physrevb.28.6112
- Rammal R. Random walk statistics on fractal structures. *J Stat Phys* (1984) 36:547–60. doi:10.1007/bf01012921
- Hughes B, Montroll E, Shlesinger M. Fractal and lacunary stochastic processes. *J Stat Phys* (1983) 30:273–83. doi:10.1007/bf01012302
- Mandelbrot BB, Mandelbrot BB. *The fractal geometry of nature*, 1. New York: W. H. Freeman (1982).
- Chen J, Dai M, Wen Z, Xi L. Trapping on modular scale-free and small-world networks with multiple hubs. *Physica A: Stat Mech its Appl* (2014) 393:542–52. doi:10.1016/j.physa.2013.08.060
- Barlow MT, Bass RF. Transition densities for brownian motion on the sierpiński carpet. *Probab Theor Relat Fields* (1992) 91:307–30. doi:10.1007/bf01192060
- Zhou Z, Wu M. The hausdorff measure of a sierpiński carpet. *Sci China Ser A-math* (1999) 42:673–80. doi:10.1007/bf02878985
- Kajino N. Heat kernel asymptotics for the measurable riemannian structure on the sierpiński gasket. *Potential Anal* (2012) 36:67–115. doi:10.1007/s11118-011-9221-5
- Grabner PJ. Functional iterations and stopping times for brownian motion on the sierpiński gasket. *Mathematika* (1997) 44:374–400. doi:10.1112/s0025579300012699
- Wu S, Zhang Z, Chen G. Random walks on dual sierpiński gaskets. *Eur Phys J B* (2011) 82:91–6. doi:10.1140/epjb/e2011-20338-0
- Wu S, Zhang Z. Eigenvalue spectrum of transition matrix of dual sierpiński gaskets and its applications. *J Phys A: Math Theor* (2012) 45:345101. doi:10.1088/1751-8113/45/34/345101
- Guyon R. Diffusion on the sierpiński gaskets: A random walker on a fractally structured object. *Phys Rev A (Coll Park)* (1984) 29:2751–5. doi:10.1103/physreva.29.2751
- Hattori K. Displacement exponent for loop-erased random walk on the sierpiński gasket. *Stochastic Process their Appl* (2019) 129:4239–68. doi:10.1016/j.spa.2018.11.021
- Lara PCS, Portugal R, Boettcher S. Quantum walks on sierpiński gaskets. *Int J Quan Inform* (2013) 11:1350069. doi:10.1142/s021974991350069x
- Bedrosian SD, Sun X. Theory and application of pascal-sierpiński gasket fractals. *Circuits Syst Signal Process* (1990) 9:147–59. doi:10.1007/bf01236448
- Shima T. On eigenvalue problems for the random walks on the sierpiński pre-gaskets. *Jpn J Ind Appl Math* (1991) 8:127–41. doi:10.1007/bf03167188
- Chen J, Gao F, Le A, Xi L, Yin S. A small-world and scale-free network generated by sierpiński tetrahedron. *Fractals* (2016) 24:1650001. doi:10.1142/s0218348x16500018
- Chen J, Le A, Wang Q, Xi L. A small-world and scale-free network generated by sierpiński pentagon. *Physica A: Stat Mech its Appl* (2016) 449:126–35. doi:10.1016/j.physa.2015.12.089
- Xi L. Differentiable points of sierpiński-like sponges. *Adv Math* (2020) 361:106936. doi:10.1016/j.aim.2019.106936
- Kozak JJ, Balakrishnan V. Analytic expression for the mean time to absorption for a random walker on the sierpiński gasket. *Phys Rev E* (2002) 65:021105. doi:10.1103/physreve.65.021105
- Kozak JJ, Balakrishnan V. Exact formula for the mean length of a random walk on the sierpiński tower. *Int J Bifurcation Chaos* (2002) 12:2379–85. doi:10.1142/s0218127402006138
- Wu B, Zhang Z. The average trapping time on a half sierpiński gasket. *Chaos, Solitons & Fractals* (2020) 140:110261. doi:10.1016/j.chaos.2020.110261
- Qi Y, Dong Y, Zhang Z, Zhang Z. Hitting times for random walks on sierpiński graphs and hierarchical graphs. *Comp J* (2020) 63:1385–96. doi:10.1093/comjnl/bxz080



OPEN ACCESS

EDITED BY

Dun Han,
Jiangsu University, China

REVIEWED BY

Dawei Zhang,
Shandong University, China
Fengping An,
Beijing Institute of Technology, China
Haitao Xu,
University of Science and Technology
Beijing, China
Yunyun Yang,
Taiyuan University of Technology, China

*CORRESPONDENCE

Wei Bai,
baiweisxu@126.com

SPECIALTY SECTION

This article was submitted to Social
Physics,
a section of the journal
Frontiers in Physics

RECEIVED 26 October 2022

ACCEPTED 21 November 2022

PUBLISHED 16 December 2022

CITATION

Yao J, Bai W, Yang G, Meng Z and Su K
(2022), Assessment and prediction of
railway station equipment health status
based on graph neural network.
Front. Phys. 10:1080972.
doi: 10.3389/fphy.2022.1080972

COPYRIGHT

© 2022 Yao, Bai, Yang, Meng and Su.
This is an open-access article
distributed under the terms of the
[Creative Commons Attribution License](https://creativecommons.org/licenses/by/4.0/)
(CC BY). The use, distribution or
reproduction in other forums is
permitted, provided the original
author(s) and the copyright owner(s) are
credited and that the original
publication in this journal is cited, in
accordance with accepted academic
practice. No use, distribution or
reproduction is permitted which does
not comply with these terms.

Assessment and prediction of railway station equipment health status based on graph neural network

Jian Yao¹, Wei Bai^{2*}, Guoyuan Yang², Zhikang Meng³ and
Kaixuan Su⁴

¹Postgraduate Department, China Academy of Railway Sciences, Beijing, China, ²Institute of Computing Technology, China Academy of Railway Sciences Corporation Limited, Beijing, China, ³School of Automation and Software Engineering, Shanxi University, Taiyuan, China, ⁴School of Mathematical Sciences, Shanxi University, Taiyuan, China

The equipment in railway station is complicated and diverse, and the health status assessment and prediction of equipment is crucial to the safe and stable operation of stations. Graph Neural Networks (GNNs) effectively combine graph data with deep learning technology, which has stronger data and knowledge representation capability and can efficiently handle some non-Euclidean spatial data problems with irregular station equipment associated network structure. Based on this, this paper takes the automatic gate machine and X-ray security checker as an example and proposes a health status assessment and prediction scheme for railway passenger station equipment based on Graph Long Short-Term Memory (G-LSTM) neural network. This paper first analyzes the main factors affecting the health status of passenger station equipment, as well as the correlation between the equipment. Then, the initial graph network structure of the passenger station equipment is constructed, and the G-LSTM model is used to evaluate and predict the health status of the passenger station equipment. Finally, this paper takes the automatic gate machine and X-ray security checker of a high-speed railway station in Beijing as an example to verify the proposed method. The experimental results show that all evaluation metrics perform well, indicating that the G-LSTM model has high accuracy in assessing and predicting the health status of automatic gate machine and X-ray security checker. This paper realizes the health status assessment and prediction of railway passenger station equipment, which can provide some reference for the Prognostics and Health Management (PHM) of equipment in railway stations.

KEYWORDS

deep learning, graph neural network, G-LSTM, status assessment, status prediction

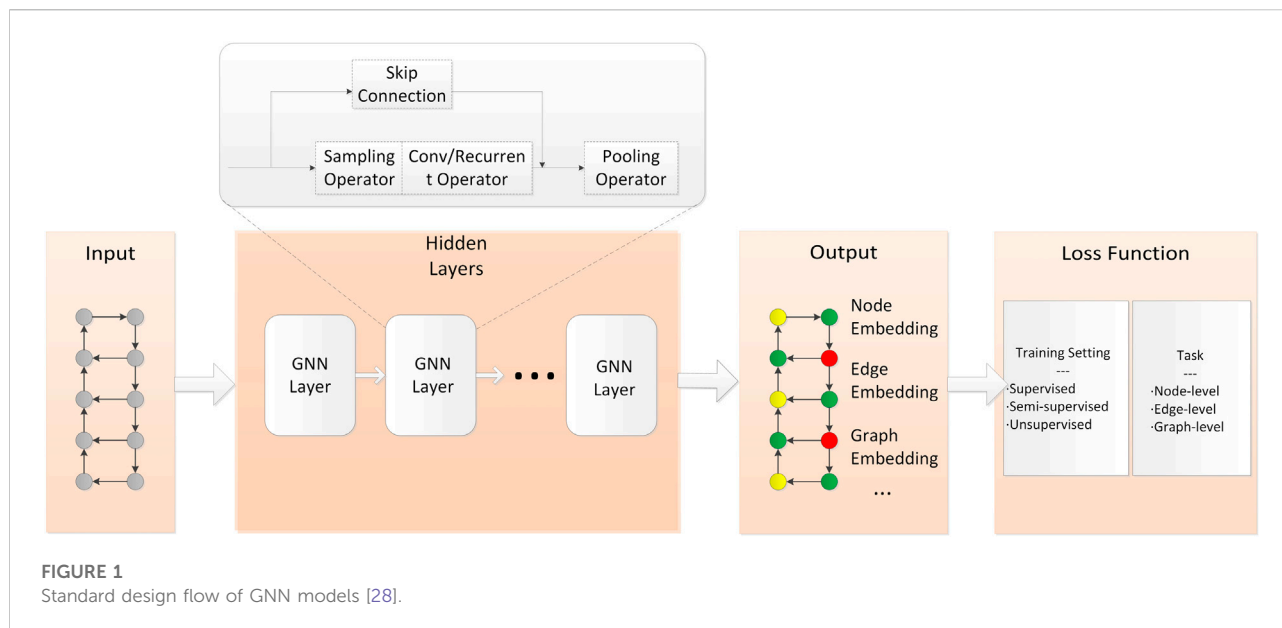
1 Introduction

In recent years, with the rapid improvement of China's high-speed railway intelligence level, the dependence of railway passenger station transportation production and passenger transportation organization on equipment and facilities has been increasing, and railway passenger station equipment has gradually shown the characteristics of diversification, complexity, integration and intelligence, etc. The safe and stable operation of passenger station equipment has become an important guarantee for the safety of passenger station operation and the improvement of passenger service quality. Therefore, it is important to fuse and analyze the status information of railway passenger station equipment, access the health status, gain insight into and predict system failures, and then avoid risks.

For the problem of equipment health assessment and prediction, some experts and scholars have conducted in-depth studies using traditional machine learning methods, such as dynamic Bayesian networks [1, 2], support vector machine regression [3–5], hidden Markov models [6–9], pattern recognition [10], fuzzy sets and rough sets [11–13], and so on. In-depth understanding of the mechanism of equipment health status for different application environments can effectively build a relational model through the health indicators of equipment performance degradation to achieve the evaluation and prediction of equipment health status. In recent years, with the rapid development of the information age, the various types of monitoring and state operation information formed by diverse-complex-intelligent equipment in long-term service present typical big data characteristics with time-series characteristics. Based on this, many experts and scholars have carried out research related to equipment health management with the powerful modeling and data processing capabilities of deep learning, and it has been widely used in many fields. For Prognostics and Health Management (PHM) of equipment, a center task is to predict the Remaining Useful Life (RUL). Yang et al. [14] proposed a double-CNN framework for intelligent RUL prediction. The method takes the original vibration signals as input, which can solve the feature extraction problem while preserving the operational information. Peng et al. [15] proposed a Bayesian Deep-Learning-based (BDL-based) method for health prognostics with uncertainty quantification. The paper extended the existing deep learning models to Bayesian Neural Networks (BNNs) and proposed a BNNs learning and inference method based on variational inference. Chen et al. [16] proposed an attention-based deep learning framework for machine's RUL prediction. In addition, a feature fusion framework was developed to combine handcrafted features with automatically learned features to improve the performance of the RUL prediction. Ma et al.

[17] proposed a new extension of Long Short-Term Memory (LSTM) network with convolutional operation integrated, named CLSTM, and used it for ball bearing RUL prediction, which is crucial to PHM of various rotating machines. A pure data-driven method for bearing RUL prediction with little prior knowledge was proposed in [18]. In this method, a recurrent neural network based on encoder-decoder framework with attention mechanism was proposed to predict Health Indicate (HI) values that are closely related to RUL values. Ren et al. [19] transformed feature values into feature maps as the input of deep convolutional neural networks to effectively predict the RUL of bearings. Li et al. [20] constructed hierarchical gated recurrent networks by stacking multiple hidden layers to capture nonlinear features and evaluate the health condition to achieve health prediction of rolling bearings. Chen [21] addressed the core problem of fault prediction and health management of equipment systems under complex operating conditions, and combined LSTM networks to investigate in depth the data-driven health condition assessment modeling method and RUL prediction method. Zhang et al. [22] used a Long Short-Term Memory-Recurrent Neural Network (LSTM-RNN) to synthesize a data-driven RUL predictor, and the constructed LSTM-RNN can be used for offline data training to predict the battery RUL. Costa et al. [23] proposed a deep learning method for domain adaptation in prognostics based on a Long Short-Term Memory Neural Network and a Domain Adversarial Neural Network (LSTM-DANN). The proposed method provides a promising approach to performing domain adaptation in practical PHM applications. For multiple sensors data environments, Shi et al. [24] proposed a Dual-LSTM framework for degradation analysis and RUL prediction using LSTM. A novel sensor data-driven RUL prediction method was introduced in [25] by using a Deep Long Short-Term Memory (DLSTM) network-based model. The method integrates multiple sensory signals by using the DLSTM to achieve more accurate and robust predictions. She et al. [26] proposed a Bidirectional Gated Recurrent Unit (BiGRU) RUL prediction method based on bootstrap method, and obtained the confidence interval of RUL by bootstrap method. Since traditional RUL prediction methods are not effective in complex systems with multiple components, multiple states and a large number of parameters, Chen et al. [27] first used Kernel Principal Component Analysis (KPCA) for nonlinear feature extraction; then, Gated Recurrent Unit (GRU) was used to predict RUL.

Traditional neural networks have obvious advantages in dealing with regular structured Euclidean spatial data, but are slightly inadequate in dealing with some non-Euclidean spatial data with irregular association network structure. Graph Neural Networks (GNNs) effectively combine graph data with deep learning technology, which has stronger data and knowledge representation capability and can efficiently solve the problem of



assessing and predicting the health status of railway passenger station equipment, however, there are few related studies. Therefore, this paper proposes a Graph Long Short-Term Memory (G-LSTM) method for evaluating and predicting the health status of railway passenger station equipment, taking the automatic gate machine and X-ray security checker (hereinafter referred to as “gate” and “security checker”) as an example. Firstly, we analyze the factors influencing the health status of railway passenger station equipment and the association rules between equipment. Then, the initial graph structure of passenger station equipment is constructed based on the equipment association relationship, and the health status of passenger station equipment is evaluated and predicted by using graph neural network model. Finally, we realize the health monitoring management of passenger station equipment operation status.

2 Preliminary

2.1 Graph neural networks

A graph is a data structure that models a set of objects (nodes) and their relationships (edges). In recent years, research on analyzing graphs with machine learning has received increasing attention due to their powerful expressive power, and a large number of studies and applications have been carried out in several fields, such as social networks, recommender systems, protein-protein interaction networks, knowledge graphs, causal inference, etc. GNNs are deep

learning-based methods that operate on the graph domain [28] and focus on tasks such as analyzing node (graph) classification, node (graph) regression, link prediction, node state prediction, node clustering, graph partitioning, and graph visualization. The standard design flow of GNN models is shown in Figure 1.

GNNs are usually classified into Graph Convolution Neural Network (GCNN), Graph Recurrent Neural Network (GRNN), Graph Attention Network (GAT), Graph Auto Encoder (GAE), Graph Generative Network (GGN), Graph Spatial-Temporal Network (GSTN), etc. [29]. In addition, based on the above basic graph neural networks, numerous variants of graph neural networks have been derived, such as Adaptive Graph Convolutional Neural Network (AGCNN) [30], Graph Long Short-Term Memory Network (Graph LSTM) [31], Gated Graph Neural Network (GGNN) [32], etc.

For the problem studied in this paper, the main advantages of GNNs compared to traditional deep learning algorithms are as follows.

2.1.1 Broader application scenarios

Traditional deep learning toolbox is designed for regular Euclidean data like sequences and grids with translation invariance, while GNNs are mainly applied to graph data in non-Euclidean space with extremely irregular structure, and graph data no longer satisfy translation invariance. In the real world, graph data are prevalent. Railway passenger stations have diverse equipment and complex relationships with each other, which are more appropriately described using graph data.

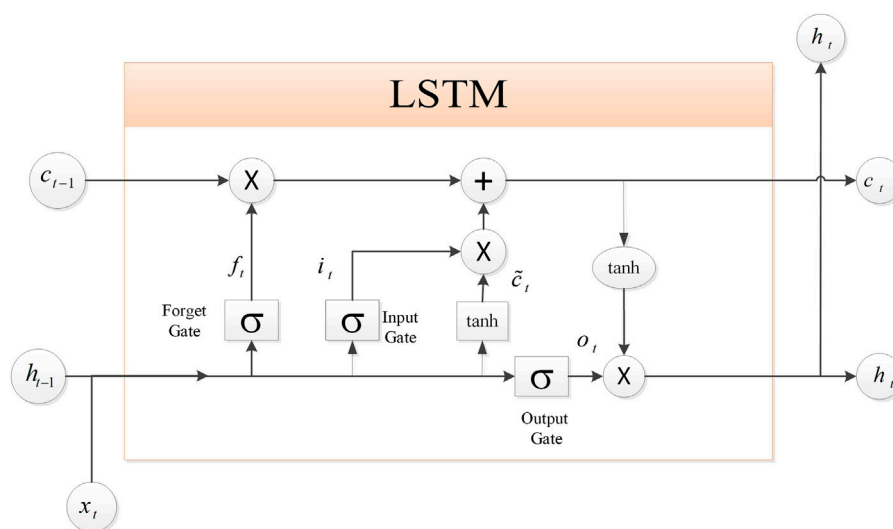


FIGURE 2
Schematic diagram of LSTM cell structure.

However, traditional deep learning algorithms perform much less well on graph data than GNNs.

2.1.2 Efficient utilization of structural features

Compared with traditional deep learning models, GNNs are more universal in information mining and data modeling because graph data contain richer information. Graph data consist of a series of nodes and edges. The nodes are connected by edges, which can effectively and fully express the information such as dependencies between nodes, thus maximizing the structural features of realistic graphs. In the railway passenger station environment, various types of equipment can be regarded as nodes. Through GNNs, we can better characterize the correlations between devices, explore the potential connections between them, and enhance the understanding of knowledge.

2.1.3 Reasoning and cognitive ability

GNNs can effectively handle various relationships and generate reasoning graphs from various unstructured data, which is expected to help improve the performance of various knowledge reasoning tasks and solve a series of problems such as relational reasoning that cannot be handled by traditional deep learning methods. The application of GNNs to railway passenger station environment is a positive attempt to promote “railway passenger station intellectualization.” To be sure, it needs more extensive and in-depth research by subsequent scholars to realize the real intelligent equipment that can reason and think.

GNNs also have many application scenarios in railway passenger station operation management, such as GCNN-based cross-video personnel tracking, GCNN-based face and voice emotion recognition, knowledge inference-based equipment fault assessment and prediction, GNN-based equipment knowledge graph representation, GNN-based passenger information advisory recommendation system, etc.

2.2 Long short-term memory neural network

LSTM neural network [33] is an improvement of the traditional Recurrent Neural Networks (RNNs), which is effective in processing time series data, it can preserve the information so that it can be used later, solve the gradient disappearance problem, realize the memory of historical states, and has better performance in time series prediction, thus LSTM neural networks are widely used in many fields.

The LSTM is basically the same as the RNN, but the difference is that the LSTM has a relatively more refined processing unit inside the LSTM, which can effectively store important information, discard unnecessary information, and update the information at each time step. The schematic diagram of the LSTM unit structure is shown in Figure 2, in which there is a memory unit to store historical information, corresponding to the neurons in the hidden layer of the original RNN. Furthermore, it includes

forget gate, input gate and output gate for updating the information.

As shown in Figure 2, the specific definitions of each part in the LSTM cell are given as follows.

$$f_t = \sigma(W_f \cdot [h_{t-1}, x_t] + b_f) \quad (1)$$

$$i_t = \sigma(W_i \cdot [h_{t-1}, x_t] + b_i) \quad (2)$$

$$o_t = \sigma(W_o \cdot [h_{t-1}, x_t] + b_o) \quad (3)$$

$$\tilde{c}_t = \tanh(W_c \cdot [h_{t-1}, x_t] + b_c) \quad (4)$$

$$c_t = f_t \circ c_{t-1} + i_t \circ \tilde{c}_t \quad (5)$$

$$h_t = o_t \circ \tanh(c_t) \quad (6)$$

where, x_t represents the input vector in time t ; c_t is the cell state; h_t is the hidden layer output vector; f_t , i_t and o_t are the activation vectors of forget gate, input gate and output gate, respectively; W_f , W_i , W_o and W_c are the weight matrices; b_f , b_i , b_o and b_c are the bias matrices; σ is the sigmoid activation function; \circ denotes the Hadamard product.

Then, the reverse transmission of the error term along time is given by

$$\delta_{t-1} = \delta_{o,t}^T W_{oh} + \delta_{f,t}^T W_{fh} + \delta_{i,t}^T W_{ih} + \delta_{\tilde{c},t}^T W_{ch} \quad (7)$$

where, W_{oh} , W_{fh} , W_{ih} and W_{ch} are weight matrices.

According to the definitions of $\delta_{o,t}$, $\delta_{f,t}$, $\delta_{i,t}$, $\delta_{\tilde{c},t}$, it is known that

$$\delta_{o,t}^T = \delta_t^T \circ \tanh(c_t) \circ o_t \circ (1 - o_t) \quad (8)$$

$$\delta_{f,t}^T = \delta_t^T \circ o_t \circ (1 - \tanh(c_t))^2 \circ c_{t-1} \circ f_t \circ (1 - f_t) \quad (9)$$

$$\delta_{i,t}^T = \delta_t^T \circ o_t \circ (1 - \tanh(c_t))^2 \circ \tilde{c}_t \circ i_t \circ (1 - i_t) \quad (10)$$

$$\delta_{\tilde{c},t}^T = \delta_t^T \circ o_t \circ (1 - \tanh(c_t))^2 \circ i_t \circ (1 - \tilde{c}^2) \quad (11)$$

According to the above equations, the equation for passing the error term forward to any k time can be obtained as:

$$\delta_k^T = \prod_{j=k}^{t-1} \delta_{o,j}^T W_{oh} + \delta_{f,j}^T W_{fh} + \delta_{i,j}^T W_{ih} + \delta_{\tilde{c},j}^T W_{ch} \quad (12)$$

The weight gradient is calculated with the following equations.

$$\frac{\partial E}{\partial b_o} = \sum_{j=1}^t \delta_{o,j} \quad (13)$$

$$\frac{\partial E}{\partial b_i} = \sum_{j=1}^t \delta_{i,j} \quad (14)$$

$$\frac{\partial E}{\partial b_f} = \sum_{j=1}^t \delta_{f,j} \quad (15)$$

$$\frac{\partial E}{\partial b_c} = \sum_{j=1}^t \delta_{\tilde{c},j} \quad (16)$$

The weights are updated with the following equation.

$$W_{ji} \leftarrow W_{ji} - \eta \frac{\partial E_d}{\partial W_{ji}} \quad (17)$$

where, η denotes the learning rate.

2.3 Graph structure representation

In order to ensure the safe and stable operation of railway passenger station environment, this paper mainly evaluates and predicts the health status of railway passenger station equipment based on the graph structure method.

In the structural representation of the equipment graph, the equipment related to the passenger station is considered as nodes, and the connections or potential relationships between equipment and equipment are used as connected edges. The graph \mathcal{G} consists of an ordered quaternion $(\mathcal{V}, \mathcal{D}, \mathcal{O}, \mathcal{A})$, where \mathcal{V} denotes the non-empty set of nodes, \mathcal{D} denotes the set of edges that do not intersect with \mathcal{V} , \mathcal{O} denotes the association function (each edge in \mathcal{G} corresponds to an unordered vertex pair of \mathcal{G}), and \mathcal{A} denotes the set of attributes of the nodes (the main factors influencing the health status of equipment nodes). The health status graph representation of railway passenger station equipment is shown in Figure 3. The shape of the nodes in the diagram represents the type of equipment, such as a square represents a gate, a triangle represents a security checker, etc. The different colors of the nodes indicate the different health status of the equipment, and the connected edges between the nodes indicate a certain association relationship between the health status of different equipment.

The healthy operation data of railway passenger station equipment shows obvious time-series characteristics with the changes of each influencing factor. To address this problem, this paper proposes a G-LSTM neural network-based method for assessing and predicting the health status of railway passenger station equipment, focusing on two types of associated equipment (gates and security checkers) to carry out related research.

3 A G-LSTM based method for assessing the health status of railway station equipment

3.1 Factors influencing the health status of equipment

In the railway passenger station environment, there are many different equipment. In addition to the above-mentioned gates and security checkers, other common railway passenger station equipment includes: ticket vending machine, archway metal

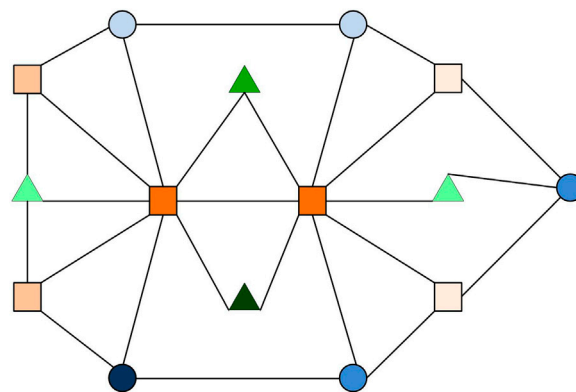


FIGURE 3
Initial health status of railway passenger station equipment.

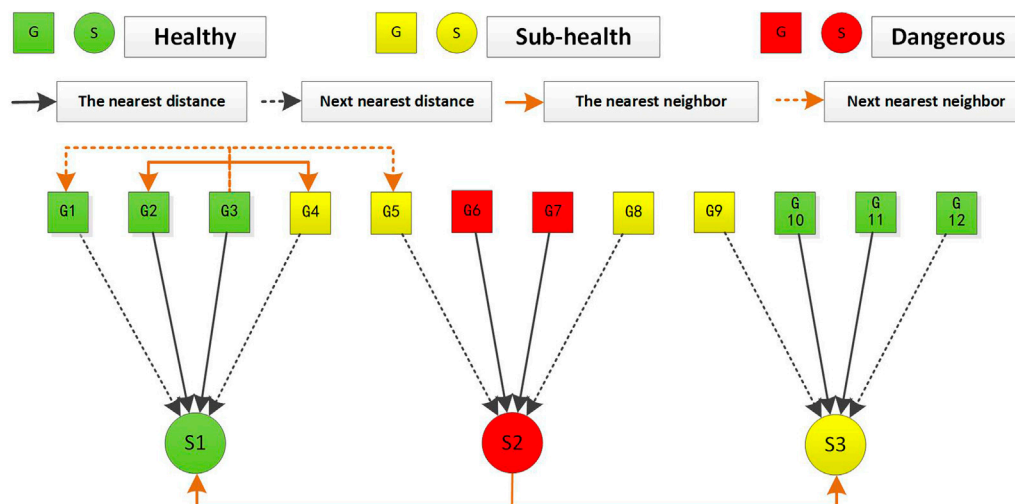


FIGURE 4
The association structure of gates and security checkers in railway passenger station. (G, Gates; S, Security Checkers).

detector, train information display, monitoring system, voice broadcasting system, escalator or elevator, etc. With the global coronavirus (COVID-19) pandemic, many railway passenger stations have also placed infrared thermal imaging thermometers at their entrances. A variety of equipment forms a very complex association graph. On the one hand, all passengers have to check their tickets and undergo rigorous security checks when entering the station. As a vital part of the station automation system, gates and security checkers play a key role as “gatekeepers.” For this reason, compared to other equipment, gates and security checkers are subjected to greater passenger pressure and are more likely to be damaged, so the assessment and prediction of their health status is of great

significance. On the other hand, there are clear correlations between gates and gates, between gates and security checkers, and between security checkers and security checkers (Figure 4). This scenario is well suited to be described using graph data. In conclusion, the subsequent parts of the paper will take gates and security checkers as an example to build the model, and then access and predict their health status. It is worth noting that the health status prediction method proposed in this paper is not only applicable to gates and security checkers, but can also be extended to other railway passenger station equipment.

There are many factors affecting the health status of gates and security checkers in railway passenger station, which are usually divided into human factors and inherent factors. Human factors

refer to the wrong operation of equipment management personnel, operating irregularities and other operational misconduct; inherent factors mainly include rated life, production time, frequency of use/running time, maintenance, troubleshooting, etc. This paper will focus on the frequency of use/running time, maintenance, production time and other inherent factors on the health status of the equipment to analyze and study.

3.2 Equipment health status correlation modeling based on frequency of use/running time

The association structure of gates and security checkers in railway passenger stations is shown in Figure 4, where the square nodes represent the gate devices and the circular nodes represent the security checkers. When passengers pass through the gates and security checkers, they follow the nearest distance principle, that is, passengers choose the nearest neighboring equipment to pass; when the gates and security checkers have too much traffic or are closed, the nearest neighbor traffic distribution and the next nearest neighbor traffic distribution scheme is adopted to distribute the flow of people to other equipment of the same type.

In the normal operation of the equipment, as the frequency of use of the gate and the running time of the security checker have a greater relationship with the flow of passengers through the equipment, this paper analyzes the impact of frequency of use and running time on the health status of the equipment by the flow of passengers. Among them, the gate can directly express its frequency of use by the passenger flow data, and evaluate the status of the equipment; the health status of the security checker is mainly related to its running time, which can convert the passenger flow into its running time, and then realize the evaluation and prediction of the equipment status.

According to Figure 4, it can be seen that there is a spatio-temporal uniformity between the gates and the security checkers. Since the health status of the two types of equipment is closely related to the passenger flow, the passenger flow data of each security checker can be deduced from the passenger flow data passing through each gate. According to the passenger flow rules, it is known that: assuming that each security checker is associated with four gates, the passenger flow of the security checker can be obtained from the number of passengers passing through its neighboring gates, defined as:

$$y_j = w_1(x_i + x_{i+1}) + w_2(x_{i-1} + x_{i+2}), i = 1, 2, \dots, n, j = 1, 2, \dots, m \quad (18)$$

where, y_j denotes the passenger flow through the j -th security checker; $x_{i-1}, x_i, x_{i+1}, x_{i+2}$ denotes the passenger flow of the four gates close to the j -th security checker; w_1 denotes the constraint weight of the passenger flow of the two gates nearest to the j -th

security checker and w_2 denotes the constraint weight of the passenger flow of the two gates next nearest to the j -th security checker, satisfying $w_1 + w_2 = 1$.

By using the daily passenger flow data of each security checker, the running time of each security checker per day can be predicted. Assuming that the daily passenger flow through a certain security checker is the highest, and setting the running time of that security checker to T hours, then after the data regularization process, we can use Eq. 19 to obtain the running time of each security checker per day.

$$f_1: \begin{cases} y_j^T = T \times \frac{y_i}{y_{\max}}, j = 1, 2, \dots, m, \\ y_j^{\hat{T}} = T - y_j^T, j = 1, 2, \dots, m, \end{cases} \quad (19)$$

where, y_j^T denotes the running time of the security checker under load; $y_j^{\hat{T}}$ denotes the running time of the security checker without load; y_{\max} denotes the maximum passenger flow through a security checker per day; then $w_i y_j^T + w_{ii} y_j^{\hat{T}}$ can indicate the effective working time of the security checker, w_i and w_{ii} are adjustable parameters.

3.3 Equipment health status correlation modeling based on maintenance and production time

Equipment in railway passenger stations is usually maintained using regular schedules, and experience-based management methods such as regular maintenance and preventive maintenance have an impact on the safe operation and O&M (Operation and Maintenance) costs of the equipment. In addition, the difference in equipment brands and production time also has an impact on the health status of the equipment.

Maintenance refers to the inspection and upkeep of passenger station equipment in accordance with equipment inspection, overhaul plans and requirements. Maintenance can prevent or timely detect equipment failures, reduce the probability of equipment failures and extend the equipment life cycle. Eq. 20 is used here to express the evaluation rule of maintenance on the service life of equipment.

$$f_2: y_m = e^{-\mu x} \quad (20)$$

where, y_m denotes the frequency/time of use obtained by maintaining the equipment; μ denotes the fitness factor; and x denotes the input characteristics of each node, i.e., the maintenance cycle.

The situation varies for equipment with different production time, when its rated service life is fixed, and will be updated by Eq. 21.

$$f_3: y_b = w_{\text{brand}} u_1 - w_{\text{year}} u_2 + f_2(x_m) \quad (21)$$

where, y_b denotes the expected remaining frequency/time of use of the equipment after production; u_1 denotes the equipment

brand (quantified as a numerical feature); u_2 denotes the used years; w_{brand} and w_{year} denote the weight coefficients of the equipment brand and the used years, respectively; and $f_2(x_m)$ is the output of Eq. 20.

3.4 Equipment health status correlation modeling based on troubleshooting

During operation, since the equipment is subject to its own quality problems, operational normality, human damage, sudden changes in the operating environment and other factors, it can result in sudden or episodic failure problems and affect the normal operation of the equipment. Therefore, the frequency of equipment troubleshooting within a certain cycle is also an important factor affecting the health status of the equipment.

The correlation function of the troubleshooting frequency on equipment health in a given cycle can be defined as follows.

$$f_4: y_r = \begin{cases} k_1 v, 0 \leq v \leq s_1, \\ k_2 v^\alpha, s_1 < v < s_2, \end{cases} \quad (22)$$

where, y_r denotes the impact of troubleshooting frequency on the health status of the equipment; k_1, k_2, α is the fitness factor; s_1 refers to the steady state threshold of the equipment, within which the equipment performance is stable; s_2 refers to the threshold of the equipment in a damaged state, beyond which the equipment is in a dangerous state at any time; v is the troubleshooting frequency of equipment during the cycle.

3.5 Comprehensive assessment model for the health status of passenger station equipment

Through the correlation modeling analysis of the above-mentioned factors on the equipment status, Eqs 18–21 are evaluated comprehensively, and the comprehensive evaluation model of the gates and the security checkers is obtained as follows.

$$g^1 = \omega_1 x + \omega_2 f_2 + \omega_3 f_3 \quad (23)$$

$$g^2 = \varphi_1 f_1 + \varphi_2 f_2 + \varphi_3 f_3 \quad (24)$$

where, g^1 denotes the integrated usage frequency of gates, g^2 denotes the integrated running time of security checkers, and ω_i, φ_i denotes the fitness weight, where $i = 1, 2, 3$.

In addition, when establishing the assessment model for the health status of equipment, the influence of the troubleshooting in Eq. 22 on the equipment health status needs to be considered comprehensively. We use research and analysis to develop the health status assessment rules of the equipment, and combine the above comprehensive evaluation model to assess the health status of the gates and security

TABLE 1 Rules for evaluating the health status of gates.









| C_1/v_1 | Health status | Node color marking |
|---------------------------------------------------------------|---------------------|-------------------------------------------------------------------------------------|
| $[0, \frac{2}{3}\mathcal{N}_1]/[0, 2]$ | Healthy |  |
| $(\frac{2}{3}\mathcal{N}_1, \frac{3}{4}\mathcal{N}_1]/(2, 5]$ | Hidden danger |  |
| $(\frac{3}{4}\mathcal{N}_1, \mathcal{N}_1]/(5, 8]$ | Dangerous |  |
| $(\mathcal{N}_1, +\infty)/(8, +\infty)$ | Seriously dangerous |  |

TABLE 2 Rules for evaluating the health status of security checkers.

| C_2/v_2 | Health status | Node color marking |
|---------------------------------------------------------------|---------------------|--------------------------------------------------------------------------------------|
| $[0, \frac{2}{3}\mathcal{N}_2]/[0, 2]$ | Healthy |  |
| $(\frac{2}{3}\mathcal{N}_2, \frac{3}{4}\mathcal{N}_2]/(2, 5]$ | Hidden danger |  |
| $(\frac{3}{4}\mathcal{N}_2, \mathcal{N}_2]/(5, 8]$ | Dangerous |  |
| $(\mathcal{N}_2, +\infty)/(8, +\infty)$ | Seriously dangerous |  |

checkers in two dimensions, as shown in Table 1 and Table 2. At a certain moment, when the evaluation rules of the two dimensions are inconsistent, the relatively poor evaluation result is chosen as the health status of the equipment in order to ensure the safe operation of the equipment to the greatest extent.

3.5.1 Rules for evaluating the health status of gates

The evaluation rules for the health status of the gate are shown in Table 1, where \mathcal{N}_1 indicates the total number of the gate openings and closings, C_1 indicates the cumulative number of uses of the gate, and v_1 indicates the number of troubleshooting of the gate per year.

3.5.2 Rules for evaluating the health status of security checkers

The evaluation rules for the health status of the security checker are shown in Table 2, where \mathcal{N}_2 indicates the total operating hours of the security checker, C_2 indicates the cumulative hours of use of the security checker, and v_2 indicates the number of troubleshooting of the security checker per year.

Based on the comprehensive assessment model for the health status of equipment, after obtaining the time-series

TABLE 3 The data set of passenger flow at gates of a high-speed railway station in Beijing.

| Date | NUM | Machine No. | Position |
|------------|-----|-------------|------------|
| 1/10/2018 | 319 | 001 | Group 1-1 |
| 1/10/2018 | 354 | 002 | Group 1-2 |
| 1/10/2018 | 368 | 003 | Group 1-3 |
| ... | ... | ... | ... |
| 26/12/2019 | 339 | 049 | Group 2-49 |
| 26/12/2019 | 89 | 050 | Group 2-50 |
| 26/12/2019 | 207 | 051 | Group 2-51 |

input of the factors influencing the operation status of equipment in passenger station, it is transformed into an information matrix, and then the LSTM neural network is used to evaluate and predict the operation status of equipment in passenger station. At the same time, the health status structure diagram of equipment in railway passenger station is updated by the above status assessment rules.

4 Experiments

4.1 Experimental data set and experimental environment

The experimental data in this paper are mainly selected from the basic biographical information of the equipment of the gates and security checkers at the entrance of a high-speed railway passenger station in Beijing, and the daily passenger flow through the gates during the period from October 2018 to December 2019. In order to reflect the diversity of experimental data, two passenger station area devices of group 1 (18 gates and 5 security checkers) and group 2 (16 gates and 4 security checkers) are selected as experimental objects, and the actual valid experimental data are about 15,300 items after processing certain missing items and abnormal items, which are divided into training set, validation set and test set according to the ratio of 6:2:2.

The passenger flow data set of the gates contains four columns of data: DATE, NUM, Machine No., and Position, where the NUM column is used as the input vector. In order to facilitate the neural network processing, all data are normalized before the experiment, i.e., the time series of each gate is subtracted from its mean value and divided by its standard deviation. The details are shown in Table 3.

The experimental environment in this paper is Ubuntu 20.04.4 LTS operating system, NVIDIA graphics card GTX 1650, and the software versions used are: CUDA 11.6, cuDNN 8.3, Python 3.6.13, Tensorflow 2.5.0, Keras 2.7.0.

4.2 Initial graph construction

The initial graph of the health status of equipment will be used as the initial input graph of the G-LSTM model, focusing on the evaluation and prediction of the health status of equipment at a certain moment in time. Using the previous graph structure representation method to construct the initial graph, gates and security checkers will be used as nodes, and the association relationship between the equipment will be represented by edges. Using the experimental data set, the health status of the equipment at a given moment can be obtained by correlation modeling based on influencing factors and the health status evaluation rules.

Specifically, firstly, according to the basic biographical information of equipment, a structure graph without equipment health information is constructed; Then, the experimental dataset of this paper is transformed into information on the frequency of use of gates and the running time of security checkers by the content of Section 2.2, and the above information is weighted and accumulated with the number of maintenance, brand and other influencing factors to obtain the initial comprehensive measurement data of the equipment; Next, the current health status of all equipment is obtained according to the rules for evaluating the health status of equipment; Finally, the initial graph of the health status of each equipment in the passenger station at a certain moment is plotted using Networkx, as shown in Figure 5, where the gates are labeled 0-33 and the security checkers are labeled a-i.

4.3 Model training and testing

In this paper, we mainly use the Keras framework with TensorFlow as the back-end engine to implement the health status prediction of equipment, and the core algorithm used is LSTM. Two LSTM recurrent layers are stacked in the training network to improve the expressiveness of the network, while dropout is used in each LSTM layer to suppress the overfitting effect, which effectively improves the accuracy of the experimental results. The model is compiled with the root mean square prop (RMSPProp) and adaptive momentum (Adam), using Mean Absolute Error (MAE) as the loss function and Mean Square Error (MSE) and Mean Absolute Percentage Error (MAPE) as the evaluation metrics. When the MAE is smaller, it means the loss is smaller, and when the MSE and MAPE are smaller, it means the prediction accuracy is higher. The specific formula is shown below.

$$MAE = \frac{1}{N} \sum_{i=1}^N (|g_i^1 - g_{act}|) \quad (25)$$

$$MSE = \frac{1}{N} \sum_{i=1}^N (g_i^1 - g_{act})^2 \quad (26)$$

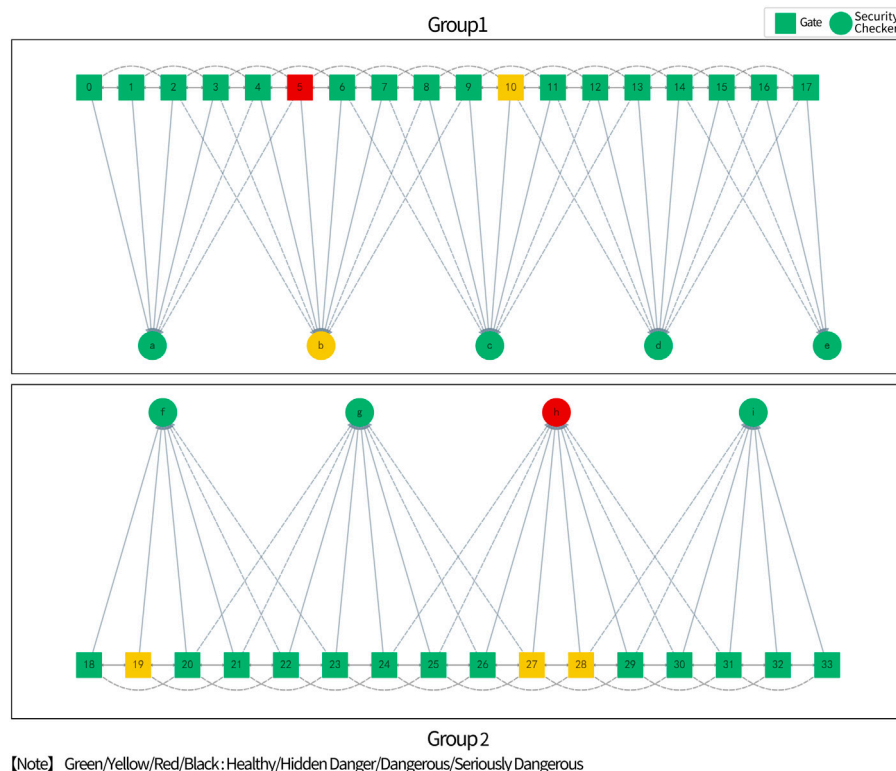


FIGURE 5
Initial graph of the health status of equipment in railway passenger station.

$$MAPE = \frac{100\%}{N} \sum_{i=1}^N \left(\left| \frac{g_i^1 - g_{act}}{g_{act}} \right| \right) \quad (27)$$

where, g_i^1 denotes the predicted value of the integrated usage frequency of gates or integrated running time of security checkers; g_{act} is the actual value; and N is the total number of samples.

For all the gates and security checkers in the passenger station, their comprehensive measurement data are input into the network model in this paper for training separately, and during the training process, the hyperparameters (the number of units per layer or the learning rate of the optimizer) are continuously adjusted for each equipment to find the best configuration. Taking gate 1-1 (corresponding to “Group 1-1” in Table 3) as an example, after 200 epochs of training, the comparison image of training MAE and verification MAE, and the comparison image of training MSE and verification MSE are shown in Figure 6.

As shown in Figure 6, the experimental effect of the method is similar in the training dataset and validation dataset samples, and the correlation error gradually decreases as the number of iterations increases. When the

training iterations are about 200, the decreasing trend of the validation MAE and validation MSE of this gate is basically smooth, around 0.20 and 0.10, respectively, which achieves better experimental results.

The optimal model obtained on the training set was used to conduct experiments on the test set. The change curves of the predicted and real values obtained from the test set through the network were monitored in the experiment, indicating that the model has a good predictive capability. Taking gate 1-1 and security checker a as an example, Figure 7 below shows the prediction performance of both on the test set.

Meanwhile, the MAE, MSE, and MAPE of the gates and security checkers are evaluated on all test set samples, respectively, and their average values are taken as shown in Table 4, and the experiments show that the G-LSTM has high prediction accuracy.

4.4 Experimental prediction

Since the equipment manufacturers and production time of passenger stations are different, and their service life and

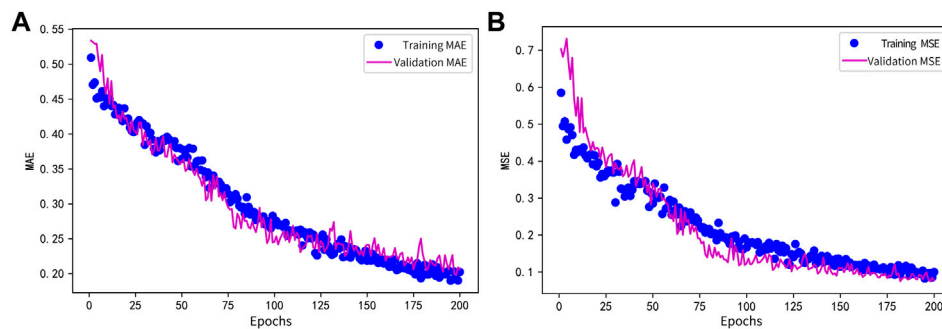


FIGURE 6
Comparison of training and validation. (A) Training MAE and Validation MAE; (B) Training MSE and Validation MSE.

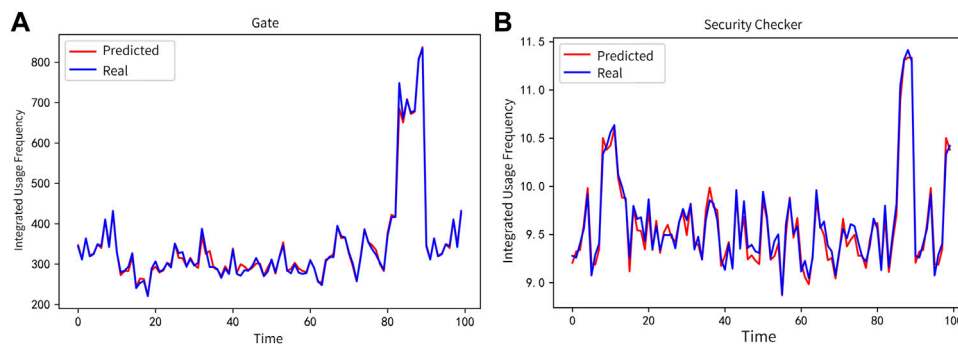


FIGURE 7
Prediction effect of the G-LSTM on the test set. (A) Gate; (B) Security checker.

TABLE 4 Test results of G-LSTM

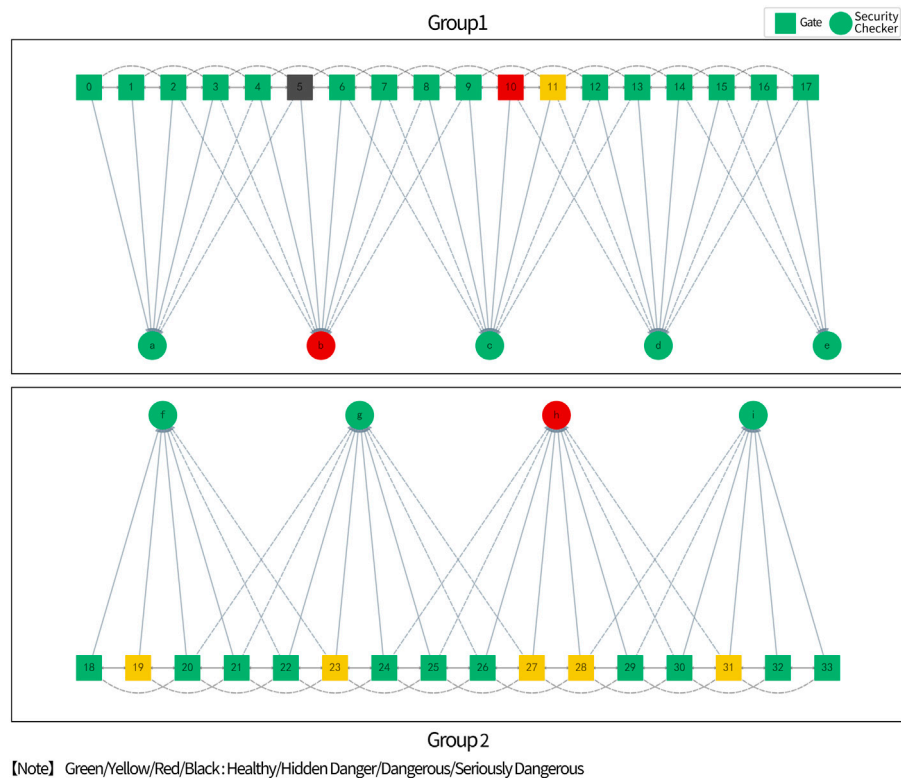
| | Average MAE | Average MSE | Average MAPE (%) |
|-------------------|-------------|-------------|------------------|
| Gates | 0.2318 | 0.1176 | 5.57 |
| Security checkers | 0.2504 | 0.2610 | 2.04 |

rated life also differ, the health status of the two types of equipment in the future period is predicted using the method in this paper.

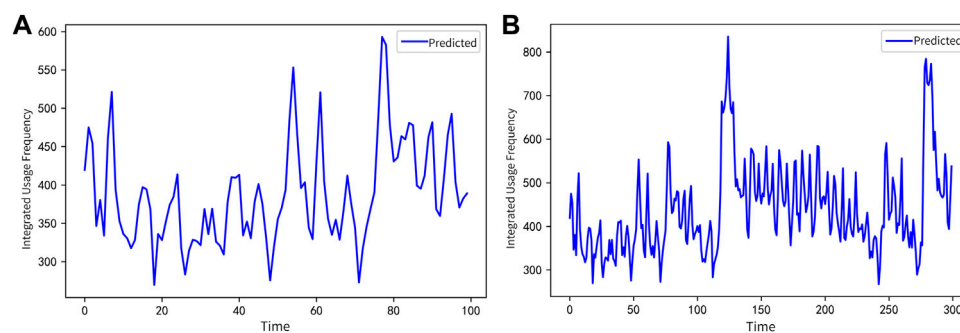
First, based on the initial graph of equipment in Figure 5, the equipment health status is predicted for 100 days thereafter using the data predicted based on the test set samples. At the same time, it is compared with the real test set samples. The experimental results show that the same graph of the health status of equipment can be obtained using both types of experimental data, as shown in Figure 8.

In addition, the model in this paper can be applied to predict the experimental scenarios for the next 100, 300, 500, and 700 days, by the rolling prediction method, i.e., continuously using the data obtained from our prediction as the real data, and thus further predicting the next data. Figure 9 shows the forecast for gate 1-1 in the next 100 and 300 days.

Based on the numerical results obtained from the prediction, the future health status of the equipment can be predicted. Figure 10 below shows the possible health status of the equipment after 100 days (Figure 10A), 300 days

**FIGURE 8**

The health status graph of equipment in railway passenger station after 100 days.

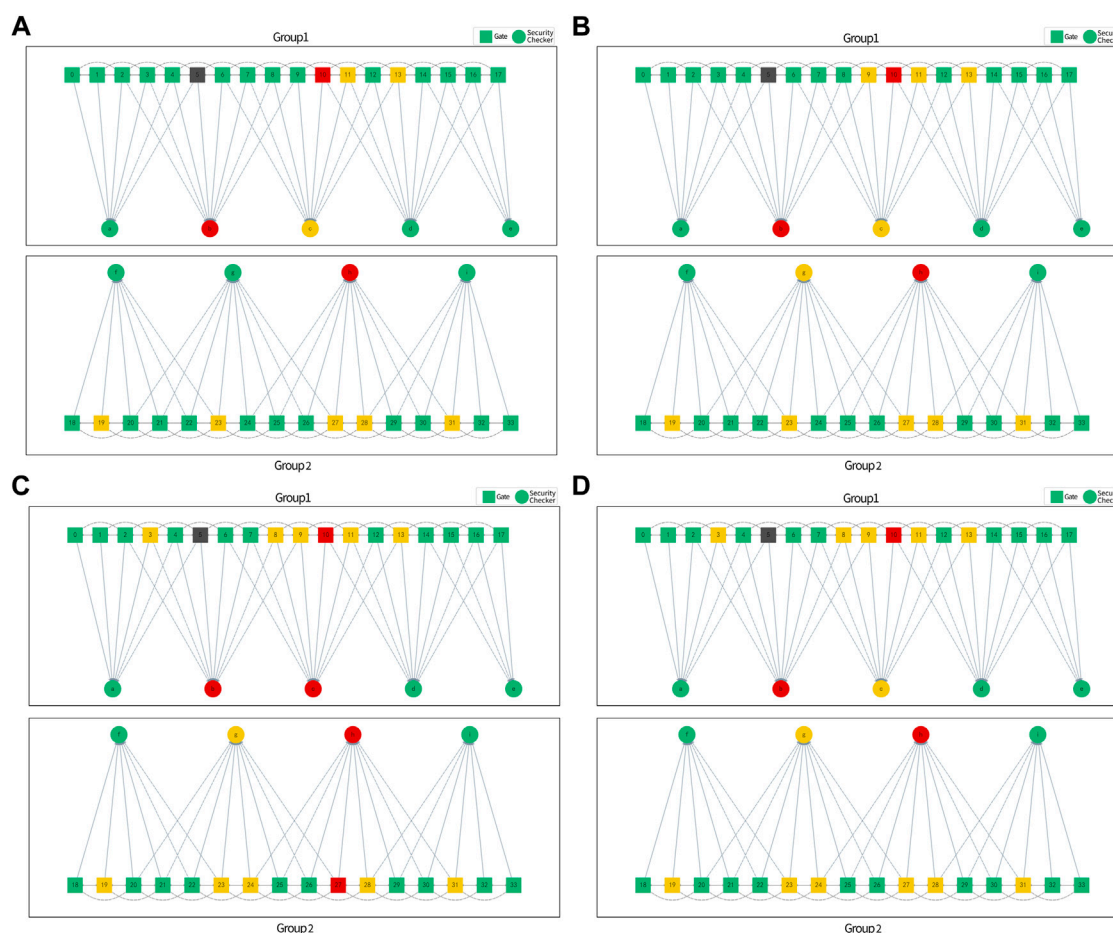
**FIGURE 9**

The forecast for the next 100 and 300 days. (A) 100 days; (B) 300 days.

(Figure 10B), 500 days (Figure 10C) and 700 days (Figure 10D) in the future based on the initial graph of Figure 8, which provides a reference basis for the maintenance of the equipment.

4.5 Analysis of experimental results

In this paper, we conduct experimental verification for gates and security checkers in a high-speed railway passenger station.

**FIGURE 10**

Equipment health status prediction. (A) Health status prediction after 100 days; (B) Health status prediction after 300 days; (C) Health status prediction after 500 days; (D) Health status prediction after 700 days.

The experimental results show that the G-LSTM model proposed in this paper obtains the average MAE: 0.2318, 0.2504, average MSE: 0.1176, 0.2610 and average MAPE: 5.57%, 2.04% for the gates and security checkers on the test set samples, realizing the assessment and prediction of the health status of railway passenger station equipment. The method in this paper can be extended to other equipment in passenger stations to reflect the health status of railway passenger station equipment more comprehensively, which has good application value. In addition, on the one hand, we can provide a decision basis for passenger station managers based on the health status prediction results. Managers can combine the health status of equipment at different locations in passenger stations for dynamic guidance of passenger flow to avoid inconvenience to passengers due to potential equipment failure. On the other hand, according to the current health status and deterioration trend of equipment, it provides differential maintenance strategies for passenger station

equipment managers to avoid equipment failure to the greatest extent and ensure the safety of passenger stations.

5 Summary

In this paper, we combine graph data and deep learning technology and propose a G-LSTM based method for assessing and predicting the health status of equipment in passenger stations. This paper mainly describes the health assessment and prediction of gates and security checkers. Firstly, we analyzed the correlation modeling of the factors influencing the health status of equipment in railway passenger station. Then, we constructed a comprehensive assessment model for the health status of equipment in passenger station. Finally, we selected gates and security checkers in a high-speed railway passenger station for experimental verification. The experimental results show that the G-LSTM model can be used to evaluate and predict the health

status of equipment with high experimental accuracy. The method proposed in this paper realizes the health management such as abnormal status warning, remaining life prediction, etc.

In the future, we will continue to optimize and improve the method proposed in this paper, and extend its application to all kinds of equipment in passenger stations to realize the health management of all equipment. At the same time, we can explore the application of various GNNs in multiple scenarios in passenger stations, such as recommendation algorithms based on GNNs to provide personalized information push services for passengers, and equipment link prediction of passenger stations based on spatio-temporal graph convolutional neural networks for detecting key equipment information and early warning prediction of paralysis, etc. In addition, although GNNs have carried out applied research in many fields, challenges still exist due to the complexity of the graph structure, and there is plenty of room for continuous optimization in model structure.

Data availability statement

The original contributions presented in the study are included in the article/Supplementary Material, further inquiries can be directed to the corresponding author.

Author contributions

JY and GY mainly uses G-LSTM neural network to model and analyze the prediction of the railway station equipment health status. WB mainly proposes the assessment of the railway station equipment health status. ZM and KS are mainly responsible for building the experimental platform and numerical simulation for the assessment and prediction of railway station equipment health status.

References

1. Li X, Zhang Y, Li Y, Zhan Y, Yang L. Health state prediction and performance evaluation of belt conveyor based on dynamic Bayesian network in underground mining. *Shock and Vibration* (2021) 2021:6699611. doi:10.1155/2021/6699611
2. Wang X, Guo H, Wang J, Wang L. Predicting the health status of an unmanned aerial vehicles data-link system based on a Bayesian network. *Sensors* (2018) 18(11):3916. doi:10.3390/s18113916
3. Yang B-S, Widodo A. Support vector machine for machine fault diagnosis and prognosis. *J Syst Des Dyn* (2008) 2(1):12–23. doi:10.1299/jsdd.2.12
4. Zhang L, Liu Z, Luo D, Li J, Huang H. Review of remaining useful life prediction using support vector machine for engineering assets. In: Proc. Int. Conf. Qual. Rel. Risk Maint. Safety Eng. (QR2MSE); 15–18 July 2013; Chengdu, China. IEEE (2013). p. 1793–9.
5. Xiong Y, Jiang Z, Fang H, Fan H. Research on health condition assessment method for spacecraft power control system based on SVM and cloud model. In: Proc. Progn. Syst. Health Manag. Conf. (PHM-Paris); 02–05 May 2019; Paris, France. IEEE (2019). p. 143–9.
6. Ghasemi A, Yacout S, Ouali M. -S. Evaluating the reliability function and the mean residual life for equipment with unobservable states. *IEEE Trans Reliab* (2010) 59(1):45–54. doi:10.1109/TR.2009.2034947
7. Martins A, Fonseca I, Farinha J, Reis J, Cardoso A. Maintenance prediction through sensing using hidden Markov models—a case study. *Appl Sci (Basel)* (2021) 11(16):7685. doi:10.3390/app11167685
8. Dong M, He D, Banerjee P, Keller J. Equipment health diagnosis and prognosis using hidden semi-Markov models. *Int J Adv Manuf Technol* (2006) 30(7–8):738–49. doi:10.1007/s00170-005-0111-0
9. Liu Q, Dong M, Lv W, Geng X, Li Y. A novel method using adaptive hidden semi-Markov model for multi-sensor monitoring equipment health prognosis. *Mech Syst Signal Process* (2015) 64–65:217–32. doi:10.1016/j.ymssp.2015.03.029
10. Orchard ME, Vachtsevanos GJ. A particle-filtering approach for on-line fault diagnosis and failure prognosis. *Trans Inst Meas Control* (2009) 31(3–4):221–46. doi:10.1177/0142331208092026
11. Zhao F, Chen J, Guo L, Li X. Neuro-fuzzy based condition prediction of bearing health. *J Vib Control* (2009) 15(7):1079–91. doi:10.1177/1077546309102665
12. Soualhi A, Makdessi M, German R, Echeverria FR, Razik H, Sari A, et al. (2018). Health monitoring of capacitors and supercapacitors using the neo-fuzzy neural approach. *IEEE Trans Industr Inform* 14(1):24–34. doi:10.1109/TII.2017.2701823

Funding

This work was supported by the National Key Research and Development Program of China under Grant 2020YFF0304100, Research Project of China Academy of Railway Sciences Group Co., Ltd. under Grant 2021YJ183, Research Project of Beijing Jingwei Information Technologies Limited Company under Grant DZYF21-56 and DZYF22-11 and China Postdoctoral Science Foundation under Grant 2021M692400.

Conflict of interest

Authors WB and GY were employed by China Academy of Railway Sciences Corporation Limited.

The authors declare that this study received funding from the research project of China academy of railway sciences group Co., Ltd. and the research project of Beijing Jingwei information technologies limited company. JY, WB and GY are all members of the above three funded projects. JY and GY mainly uses G-LSTM neural network to model and analyze the prediction of the railway station equipment health status. WB mainly proposes the assessment of the railway station equipment health status.

Publisher's note

All claims expressed in this article are solely those of the authors and do not necessarily represent those of their affiliated organizations, or those of the publisher, the editors and the reviewers. Any product that may be evaluated in this article, or claim that may be made by its manufacturer, is not guaranteed or endorsed by the publisher.

13. Zhao Z, Jiang W, Gao W. Health evaluation and fault diagnosis of medical imaging equipment based on neural network algorithm. *Comput Intell Neurosci* (2021) 2021:1–9. doi:10.1155/2021/6092461
14. Yang B, Liu R, Zio E. Remaining useful life prediction based on a double-convolutional neural network architecture. *IEEE Trans Ind Electron* (2019) 66(12):9521–30. doi:10.1109/TIE.2019.2924605
15. Peng W, Ye Z-S, Chen N. Bayesian deep-learning-based health prognostics toward prognostics uncertainty. *IEEE Trans Ind Electron* (2020) 67(3):2283–93. doi:10.1109/TIE.2019.2907440
16. Chen Z, Wu M, Zhao R, Guretno F, Yan R, Li X. Machine remaining useful life prediction via an attention-based deep learning approach. *IEEE Trans Ind Electron* (2021) 68(3):2521–31. doi:10.1109/TIE.2020.2972443
17. Ma M, Mao Z. Deep-Convolution-based LSTM network for remaining useful life prediction. *IEEE Trans Industr Inform* (2021) 17(3):1658–67. doi:10.1109/TII.2020.2991796
18. Chen Y, Peng G, Zhu Z, Li S. A novel deep learning method based on attention mechanism for bearing remaining useful life prediction. *Appl Soft Comput* (2020) 86:105919. doi:10.1016/j.asoc.2019.105919
19. Ren L, Sun Y, Wang H, Zhang L. Prediction of bearing remaining useful life with deep convolution neural network. *IEEE Access* (2018) 6:13041–9. doi:10.1109/ACCESS.2018.2804930
20. Li X, Jiang H, Xiong X, Shao H. Rolling bearing health prognosis using a modified health index based hierarchical gated recurrent unit network. *Mech Mach Theor* (2019) 133:229–49. doi:10.1016/j.mechmachtheory.2018.11.005
21. Chen Z. Research on equipment health assessment and remaining useful life prediction method based on LSTM. M.S. thesis. China: University of Science and Technology of China (2019).
22. Zhang Y, Xiong R, He H, Pecht MG. Long short-term memory recurrent neural network for remaining useful life prediction of lithium-ion batteries. *IEEE Trans Veh Technol* (2018) 67(7):5695–705. doi:10.1109/TVT.2018.2805189
23. da Costa PRde O, Akçay A, Zhang Y, Kaymak U. Remaining useful lifetime prediction via deep domain adaptation. *Reliability Eng Syst Saf* (2020) 195:106682. doi:10.1016/j.res.2019.106682
24. Shi Z, Chehade A. A dual-LSTM framework combining change point detection and remaining useful life prediction. *Reliability Eng Syst Saf* (2021) 205:107257. doi:10.1016/j.res.2020.107257
25. Wu J, Hu K, Cheng Y, Zhu H, Shao X, Wang Y. Data-driven remaining useful life prediction via multiple sensor signals and deep long short-term memory neural network. *ISA Trans* (2020) 97:241–50. doi:10.1016/j.isatra.2019.07.004
26. She D, Jia M. A BiGRU method for remaining useful life prediction of machinery. *Measurement* (2021) 167:108277. doi:10.1016/j.measurement.2020.108277
27. Chen J, Jing H, Chang Y, Liu Q. Gated recurrent unit based recurrent neural network for remaining useful life prediction of nonlinear deterioration process. *Reliability Eng Syst Saf* (2019) 185:372–82. doi:10.1016/j.res.2019.01.006
28. Zhou J, Cui G, Hu S, Zhang Z, Yang C, Liu Z, et al. (2020). Graph neural networks: A review of methods and applications. *AI Open* 1:57–81. doi:10.1016/j.aiopen.2021.01.001
29. Wu Z, Pan S, Chen F, Long G, Zhang C, Yu PS. A comprehensive survey on graph neural networks. *IEEE Trans Neural Netw Learn Syst* (2021) 32(1):4–24. doi:10.1109/TNNLS.2020.2978386
30. Li Y, Tarlow D, Brockschmidt M, Zemel RS. Gated graph sequence neural networks. In: Proc. Int. Conf. Learn. Represent.; 05 May 2016; Paris, France. IEEE (2016). p. 1–20.
31. Zayats V, Ostendorf M. Conversation modeling on reddit using a graph-structured LSTM. *Trans Assoc Comput Linguist* (2018) 6:121–32. doi:10.1162/tacl_a_00009
32. Li R, Wang S, Zhu F, Huang J. Adaptive graph convolutional neural networks. In: Proc. 32nd AAAI Conf. Artif. Intell.; 13 March 2018; New Orleans, LA, United states. AAAI (2018). p. 3546–52.
33. Hochreiter S, Schmidhuber J. Long short-term memory. *Neural Comput* (1997) 9(8):1735–80. doi:10.1162/neco.1997.9.8.1735



OPEN ACCESS

EDITED BY

Jianbo Wang,
Southwest Petroleum University, China

REVIEWED BY

Zhiwu Hong,
China University of Political Science and
Law, China
Liyun Zhou,
South China Agricultural University,
China
Xian Fang,
Institute of industrial economics, Jinan
University, China

*CORRESPONDENCE

Yanan Wang,
✉ wangyn518@sina.com

SPECIALTY SECTION

This article was submitted to Social
Physics,
a section of the journal
Frontiers in Physics

RECEIVED 27 October 2022

ACCEPTED 14 December 2022

PUBLISHED 06 January 2023

CITATION

Wang L, Huang Z and Wang Y (2023),
Measuring the impact of Wuhan's
COVID-19 lockdown on the growth
enterprise market in China.
Front. Phys. 10:1081615.
doi: 10.3389/fphy.2022.1081615

COPYRIGHT

© 2023 Wang, Huang and Wang. This is
an open-access article distributed
under the terms of the [Creative
Commons Attribution License \(CC BY\)](#).
The use, distribution or reproduction in
other forums is permitted, provided the
original author(s) and the copyright
owner(s) are credited and that the
original publication in this journal is
cited, in accordance with accepted
academic practice. No use, distribution
or reproduction is permitted which does
not comply with these terms.

Measuring the impact of Wuhan's COVID-19 lockdown on the growth enterprise market in China

Li Wang¹, Zeyu Huang² and Yanan Wang^{3*}

¹School of Economics, Faculty of Economics and Management, East China Normal University, Shanghai, China, ²School of Economics, Faculty of Economics, Renmin University of China, Beijing, China, ³School of Economics and Finance, South China University of Technology, Guangzhou, China

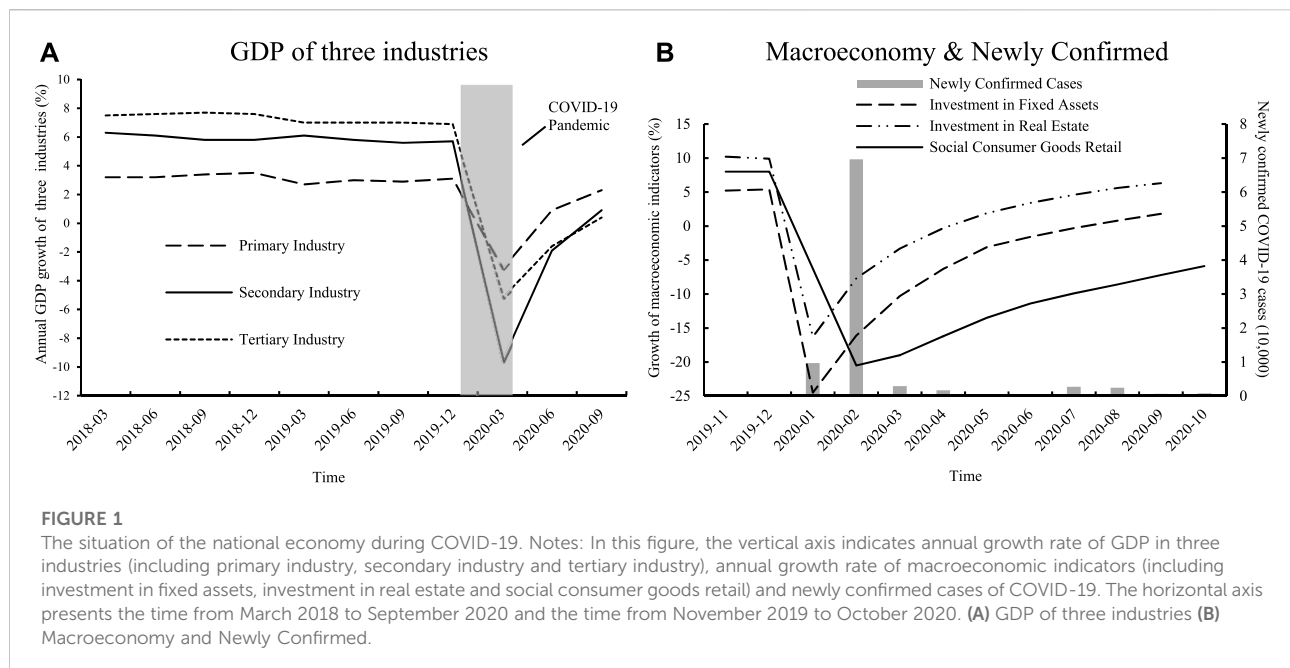
The outbreak of COVID-19 had a huge impact on the financial market. As a new growth point in China, it's necessary to study how SMEs (small and medium-sized enterprises) represented by listed companies on the GEM (growth enterprise market) can withstand sudden shocks. This paper examines the impact of Wuhan's COVID-19 lockdown on the financial markets based on the data of GEM listed companies and the method of event analysis. The results show that investors had a great response to epidemic related news. Compared with the interest rate cut policy, the targeted RRR reduction policy had a more significant positive influence on the financial markets. Furthermore, in the early stages of COVID-19, there was not a significant effect of distance on the firms' CARs (cumulative abnormal returns). In an improving epidemic environment, the farther the firms were from Wuhan City, the more positive the impact on their CARs would be. This paper provides new evidence and important enlightenment for preventing the impact of public health emergencies on the GEM market and highlights the significance of developing digital inclusive finance, which can mitigate regional risk and financing issues.

KEYWORDS

COVID-19 pandemic, Wuhan's lockdown, growth enterprise market, monetary policy, digital inclusive finance

1 Introduction

The COVID-19 epidemic broke out in Wuhan at the beginning of 2020. China managed to control the epidemic with its 2-month economic stagnation. However, enterprise, a key pillar of the national economy, had weathered tough times. Despite the medical pharmaceutical industry, which was directly related to epidemic prevention and control, the vast majority of enterprises could not operate normally. China's GDP fell 6.8% year-on-year in the first quarter of 2020, according to the National Bureau of Statistics. [Figure 1](#) illustrates the annual growth rate of China's sub-industrial GDP from March 2018 to September 2020, and the changes of China's macroeconomic indicators from November 2019 to October 2020. As can be seen from [Figure 1](#), the COVID-19 epidemic had a huge impact on a variety of industries in China. A sharp drop in



investment in real estate, fixed assets, and social consumer goods retail was also observed with the increase in newly confirmed COVID-19 cases.

A number of policies were issued by the State Council and People's Bank of China. These include tax reductions and exemptions, reductions of reserve ratios and interest rates, all aimed at encouraging enterprises to resume work and production and boost economic growth. At the same time, fiscal and monetary policies continued to make efforts, and domestic enterprises' resumption of work and production achieved remarkable results. According to the National Bureau of Statistics, China's GDP grew by 3.2% year-on-year and 11.5% quarter-on-quarter in the second quarter of 2020, with significant economic growth in high-tech manufacturing, modern services and Internet retail. China is reported to be the only major economy in the world to achieve positive growth in 2020, with a growth rate of 2.3 percent.¹

It is no denying that contagion effects have always been the focus of human disease and health network research [1–2] empirically analyzed three types networks of disease transmission, namely, temporary networks, static networks, and a fully connected topology. Results showed that time structure can affect disease transmission more than static network structure. Also, complex networks are always used to describe the spread of major disease in populations of interacting individuals [3]. Furthermore, considering that social activities

and infectivity are time phenomena, [4]. Believed that when these two processes are synchronized, diseases are most likely to spread. It can be seen that the existence of contagion networks and social networks will aggravate the impact of epidemics on the whole society. What's more, maintaining stable economic operation and active capital market is an important issue for a country to be concerned about, so the economic consequences of the epidemic need to be studied. Especially in the context of highly contagion during the incubation period, if there was no interference with any physical restrictions, the embedding of social network into life and business would lead to the spread of the contagion network, causing secondary damage.

The COVID-19 epidemic had several significant characteristics, such as suddenness, urgency, uncertainty, and unpredictable nature [5], which had a huge negative impact on the economy and social stability, especially the financial market [6]. Many of the existing studies about COVID-19 epidemics followed the ideas of SRAS, which focused on national economy and industrial economy in the long term. Through quantitative and empirical analysis, [7] examined the effects of COVID-19 on SMEs. Nevertheless, the epidemic was a widespread malignant public health emergency, causing a great deal of public concern. They did not examine the huge impact of COVID-19 on investor sentiment and financial markets. A second large group of recently emerging literature focused on the financial markets. And they consistently showed that stock markets around the world have reacted to the epidemic with strong negative yields [8–11]. For instance, [10] examined the data of ten stock markets and found that the market reaction caused by COVID-19 did not seem to be a recession but rather a stagnation.

¹ Source: <https://news.china.com/focus/2021quanguolianghui/13004116/20210305/39349372.html>.

[8] found the share prices of all firms in China declined due to the expected adverse economic outcomes of COVID-19. There is however no special attention given to Chinese growth enterprise market. Against the background of mass entrepreneurship and mass innovation in China, the innovative SMEs represented by GEM's listed companies are accelerating to become the new economic growth point in China. In addition, the impact of the epidemic on innovative SMEs during the growth period was more severe than the impact on other firms. With the yield on GEM as the starting point, we can show the overall situation of SMEs' survival under the epidemic.

By using the data of GEM listed companies from 18 June 2019 to 20 June 2020, we examine the performance of the medical and pharmaceutical industries as well as the non-medical and non-pharmaceutical industry stock yields during the epidemic through event analysis. Furthermore, we study how the direct distance between the business location of firms and Wuhan City affects the CARs (cumulative abnormal returns) under four events. This study will answer four questions: Firstly, whether the impact of epidemic-related events and monetary policies on the GEM is consistent with expectations during the outbreak of COVID-19. Secondly, whether there is industry heterogeneity in the above studies. Additionally, in the early stages of an outbreak, whether distances between firms and Wuhan City have an adverse effect on the CAR. Finally, whether digital inclusive finance can contribute to mitigating the effects of the COVID-19 epidemic on the financial markets.

We offer at least three contributions to the existing literature. Firstly, we focus on the growth enterprise market in China. Studies that examined the impact of the COVID-19 epidemic on China's economy tended to concentrate on long-term macroeconomic effects, and few studies considered the particularities of GEM policy. In addition, research about GEM focused primarily on the prospects of the listed companies in GEM, ignoring their substantial risk-resistance capabilities. In light of the COVID-19 epidemic, we analyze the GEM market's response and fluctuation. Secondly, we provide a complementary analysis to recent studies that examined government involvement in COVID-19. [9] used the daily data of 77 countries to assess the economic impact of various government interventions, such as social distancing measures, public awareness campaigns, testing policies, etc. We contribute to the existing literature by studying the effects of monetary policy implementation on the financial markets. Furthermore, as the result of the ongoing technological revolution driven by the explosion of information technology, the development of digital inclusive finance contributes to the economic recovery during these difficult times. It is also pertinent for scholars to examine the relationship between the COVID-19 epidemic and digital inclusive finance. We integrate digital inclusive finance into the analysis framework. In this way, it is explored whether digital inclusive finance can contribute to mitigating the negative impact on the financial markets.

2 Literature review

2.1 Public health emergency and macroeconomy

Studies have shown that public emergencies negatively affect a country's economy over the short and long term [12,13]. Epidemics, a kind of public health emergencies, however, also have unique adverse effects when compared to other public emergencies.

First of all, public health emergencies have a wide range of implications. In general, natural disasters and man-made disasters have local impacts, affecting mostly a few cities, provinces, or regions. However, epidemic diseases have the potential to spread everywhere, impacting the economies of a number of countries and regions. According to [14], the epidemic may cause a self-reinforcing panic and long-term economic weakness. Additionally, evidence from the Ebola virus in West Africa shows that public health emergencies can have a more long-term impact on developing countries [15]. Through the Growth at Risk (GaK), [16] analyzed how financial risk impacts economic growth under COVID-19. The impact of COVID-19 was mainly reflected in the negative impact of short-term economic growth, whereas its long-term impact was relatively small.

Further, public health emergencies hinder the flow of factors, especially labor factors. The most effective way to deal with the epidemic is to restrict people's movement and impose physical quarantine. As a result, people and businesses have difficulty getting to work. In particular, the epidemic will be a life-or-death challenge for industries that require a lot of human capital. [17] evaluated the short-term effects of the new H1N1 epidemic on the tourism and aviation industries in Mexico, and concluded that the aviation industry was more vulnerable to high-intensity negative impacts. Due to the COVID-19 epidemic, [18] also believed that the catering, tourism, transportation, entertainment, and manufacturing industries had suffered huge losses. Stagflation in some parts of the manufacturing supply chain caused an asymmetric demand imbalance between upstream and downstream, resulting in serious economic consequences.

2.2 Public health emergency and microeconomy

The impact of public emergencies on the economy is multilevel [19], which can not only have a huge impact on the long-term and stable operation of a country's economy, but also have a negative impact on enterprises, financial markets and individual behaviors.

From the perspective of enterprises, public health emergencies will affect the normal operation of enterprises

in the short term. In comparison to other enterprises, SMEs are more sensitive to public emergencies. Due to the size of SMEs, [20] believed that they were not well equipped to resist risks and to repair themselves. Therefore, public health emergencies have a greater impact on start-ups, which are more likely to be exposed to bankruptcy risk in a crisis [21]. In addition, compared with large enterprises, for a long time, SMEs are often faced with loan difficulties and financing difficulties. In other words, they are more in need of financial support in case of public emergency, but it is also more difficult for them to obtain financial support. Additionally, [22] believed that banks tended to face liquidity crunch and other problems in the context of public emergencies that may lead to economic recession. To adjust their balance sheets, they were more inclined to tighten credit to SMEs, which also increased the operating costs for enterprises in a crisis.

In terms of public emergencies, not only do they depend on objective characteristics of the event, but also on the response of society [23], so the financial market is highly likely to respond to unpredictable emergencies [24]. According to [25] and [26], public emergencies were a systematic risk and could affect the stock yield. [27] and [28] all pointed out that the COVID-19 case could arouse a significant increase in financial market volatility. Moreover, [29] found that overwhelming panic generated by the news media increased equity market volatility. Furthermore, most studies employ the event analysis method to analyze the impact of special events on the financial markets when faced with natural disasters, man-made disasters and public health emergencies. As an example, [30] investigated 43 insurance loss events and found that insurance managers receive abnormal returns on the day of the event. Under some special events, [31], [32], [33], and [34] also used event analysis to investigate share prices, spillover effects, and trade effects in financial markets.

As far as individual behavior is concerned, public health emergencies will likely cause widespread panic, accompanied by a herd effect. According to [35] and [36], vicious public emergencies can easily cause panic among investors and change their trading behavior. During the 2003 SARS epidemic in China, [37] studied the influence of rumors on individual economic behavior. They find that rumors were more frequent in hard-hit areas and triggered a number of knock-on effects, such as herd behavior of buying.

2.3 Summary

It is generally agreed that public emergencies can negatively impact a country's long-term macroeconomics and short-term financial markets. Among them, public health emergencies are further clarified as being distinct from other kinds of emergency. Furthermore, the emerging literature about the impact of

COVID-19 in China is primarily a descriptive summary of the great changes in national economy from a qualitative point of view, as well as suggestions and perspectives for future long-term public governance and policy formulation. Meanwhile, a small number of studies use micro-data to investigate the current state and policy demands of SMEs. Few studies, however, have considered how Chinese growth enterprise market responded to the epidemic news and monetary policies during COVID-19. Also, during the period of the epidemic, the strong development of digital inclusive finance ensures many conveniences and supports economic recovery under the new technological revolution, with artificial intelligence and digital technology at the forefront. In this light, it is also important to consider how to view the relationship between COVID-19 and digital inclusive finance.

3 Basic facts about the epidemic

3.1 Impact of COVID-19 epidemic on Chinese growth enterprise market

In Figure 2, we show the weighted yield on the GEM from 1 July 2019 to 30 June 2020. A shadow region presents the movement of the GEM since the epidemic outbreak. Compared with before the outbreak, the range and volatility of yields are much wider. The yield suffered several large fluctuations, once falling as low as -7.49% .² On the day Wuhan was officially closed down, the yield dropped from 1% to nearly -8% . It is clear that the outbreak of COVID-19 was a huge blow to China's growth enterprise market.

3.2 Monetary policies during COVID-19 epidemic

In response to COVID-19, People's Bank of China issued monetary policies to stabilize the money supply and maintained the country's economic system. As shown in Figure 3, China's money supply changed at various levels between November 2019 and September 2020. Before the outbreak, the money supply grew between 2% and 4% annually. When the outbreak occurred, M1's annual growth rate decreased suddenly, and then gradually picked up. Also, M2's growth rate became higher than before the epidemic. All evidence shows that the measures taken by People's Bank of China during the epidemic were successful in recovering the national economy.

² Source: CSMAR database.

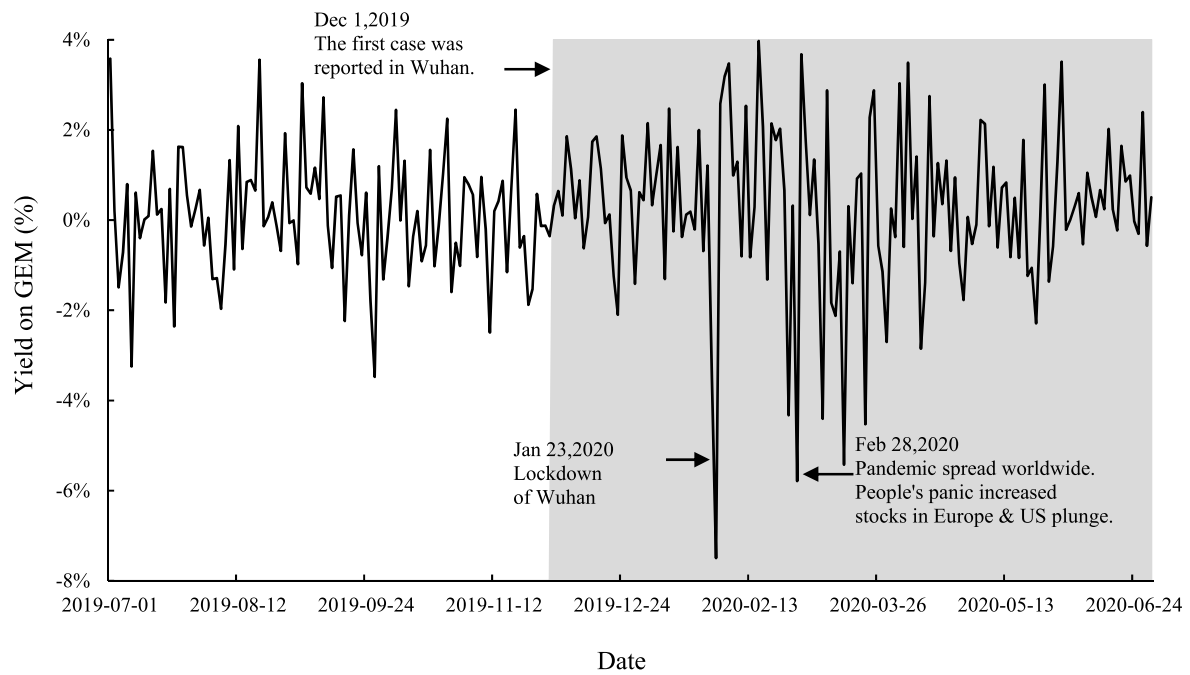


FIGURE 2
Yields on the GEM during COVID-19.

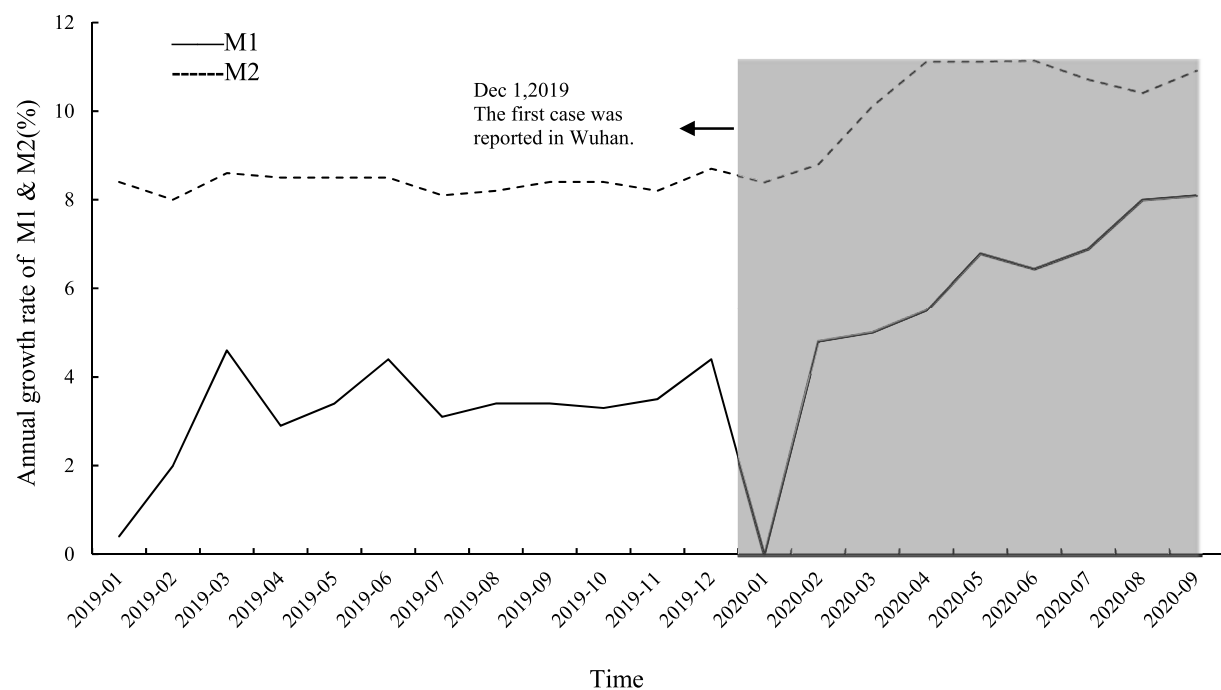


FIGURE 3
Money supply in China during COVID-19.

TABLE 1 Detail information of event dates.

| Event | Date | Content |
|-------|------------------|----------------------------------------------------------------------------------------------------------------------------------------------------------------------------------------------------------|
| 1* | 23 January 2020 | Lockdown of Wuhan City. ("Bad News") |
| 2* | 17 February 2020 | The State Council announced that the situation in the prevention and control of the epidemic was improving. ("Good News") |
| 3** | 13 March 2020 | The People's Bank of China reduced the RRR for inclusive finance by 0.5%–1%, releasing 550 billion yuan of long-term funds. ("RRR Reduction") |
| 4** | 30 March 2020 | The People's Bank of China lowered the 7-day reverse repurchase rate by 20 basis points and launched a 7-day reverse repurchase operation of 50 billion yuan through interest rate bidding. ("Rate Cut") |

Notes: Events marked * are epidemic news and events marked ** are monetary policies.

4 The GEM's response to the epidemic

4.1 Empirical strategy

According to [34], we use event analysis to study the impact of COVID-19 epidemic on the GEM listed companies. ARs (abnormal returns) and CARs (cumulative abnormal returns) of the GEM listed companies were also calculated in accordance with [38]. For calculating ARs of stock i , we use the market model to mitigate the impact of the overall market fluctuations. Here are the specific methods:

First of all, using the daily trading data of individual stocks, we calculate the daily stock yields according to Eq. 1:

$$Ret_{i,t} = \ln \frac{P_{i,t} - P_{i,t-1}}{P_{i,t-1}} \quad (1)$$

Where $Ret_{i,t}$ represents the daily stock yield of stock i on day t . $P_{i,t}$ and $P_{i,t-1}$ stand for the closing price of stock i on day t and day $t - 1$ respectively.

Secondly, we estimate the model parameters α_i , β_i and σ_ε^2 in the Eq. 2, and calculate the expected stock yield using the above parameters.

$$\begin{cases} E(Ret_{i,t}) = \alpha_i + \beta_i Market_Ret_t + \varepsilon_{i,t} \\ E(\varepsilon_{i,t}) = 0 \\ Var(\varepsilon_{i,t}) = \sigma_\varepsilon^2 \end{cases} \quad (2)$$

Among them, $Market_Ret_t$ represents the yield on the GEM in day t , and $E(Ret_{i,t})$ represents the expected stock yield of stock i on day t .

Finally, Eq. 3 is used to calculate $AR_{i,t}$:

$$AR_{i,t} = Ret_{i,t} - E(Ret_{i,t}) \quad (3)$$

$CAR_{i,m}$ of stock i in the event window $[0, m]$ can be expressed as:

$$CAR_{i,m} = \sum AR_{i,t} \quad (4)$$

In order to examine the GEM's responds to the epidemic news and monetary policies, four event days are selected. Event dates are determined on the basis of official media bulletins and reports from the official website of People's Bank of China, the Chinese government website and XINHUANET.

In the case of the lockdown of Wuhan City, 23 January 2020 is taken as the first event. Table 1 shows the description of four event days.³

[39] pointed out that choosing an estimate window with a time span of more than 100 days can guarantee the accuracy of parameter estimation. According to previous studies, the estimated window spans 100–300 days. Therefore, we select the time span from the first 150 days to the first 30 days of the event, a total of 120 days for the estimation window. Four event windows are included, that is, $[0, 1]$, $[0, 3]$, $[0, 5]$, and $[0, 7]$. For example, the event day and the following 7 trading days can be expressed as $[0, 7]$.

4.2 Responds to epidemic events

In Table 2 shows the GEM's respond to the "Bad News" (lockdown of Wuhan City). There was a significant negative impact on GEM's share price due to "Bad News". The reason is that measures like city closures, market strikes, household closures, and gathering bans were widely used to prevent the spread of COVID-19. Consequently, most industries in China suffered a huge blow as these measures increased transportation costs and reduced consumer demand. As for the medical and pharmaceutical industries, the CARs of GEM listed companies were significantly positive. In the epidemic, medical and pharmaceutical companies contributed greatly to the production of epidemic prevention products. They tried their best to meet consumers' demands for medical and pharmaceutical products. This gave investors a positive signal that this industry met an excellent opportunity for growth during the recession.

Table 3 presents the GEM's respond to the "Good News" (improving situation). A significant positive effect of "Good

³ On 3 Feb 2020, People's Bank of China launched an open market reverse repurchase operation with 1.2 trillion yuan. It was the monetary policy closest to the outbreak. Considering that the Chinese stock market is closed during the Spring Festival holiday, it was only one trading day between the announce of this policy and the lockdown. The pure effect of this monetary policy is hard to come by, so we have not included it in our event day list.

TABLE 2 The GEM's respond to "Bad News" (lockdown of Wuhan City).

| Event window | All industry | Medical and pharmaceutical industry | Non-medical and non-pharmaceutical industry |
|--------------|-------------------|-------------------------------------|---------------------------------------------|
| | (1) | (2) | (3) |
| [0,1] | -.0036 (-1.54) | .0508*** (4.48) | -.0104*** (-4.97) |
| [0,3] | -.0340*** (-9.10) | .0974*** (7.94) | -.0503*** (-14.71) |
| [0,5] | -.0275*** (-6.27) | .0508*** (4.48) | -.0404*** (-9.26) |
| [0,7] | -.0293*** (-7.13) | .0974*** (7.94) | -.0392*** (-9.23) |
| Observations | 758 | 84 | 674 |

Notes: *, ** and *** denote the 10, 5 and 1 percent significance levels, respectively. The value in parentheses is the t-value. The same below.

TABLE 3 The GEM's respond to "Good News" (improving situation).

| Event window | All industry | Medical and pharmaceutical industry | Non-medical and non-pharmaceutical industry |
|--------------|-----------------|-------------------------------------|---------------------------------------------|
| | (1) | (2) | (3) |
| [0,1] | .00703** (2.35) | .0508*** (4.48) | .00985*** (6.28) |
| [0,3] | .0202*** (4.48) | -.0312*** (-5.20) | .0157*** (6.36) |
| [0,5] | .0107*** (4.54) | -.0133*** (-3.26) | .0140*** (4.70) |
| [0,7] | .0192*** (5.64) | -.0312*** (-5.20) | .0234*** (6.37) |
| Observations | 761 | 84 | 677 |

TABLE 4 The GEM's respond to "Rate Cut".

| Event window | All industry | Medical and pharmaceutical industry | Non-medical and non-pharmaceutical industry |
|--------------|--------------------|-------------------------------------|---------------------------------------------|
| | (1) | (2) | (3) |
| [0,1] | -.00739*** (-4.64) | .00113 (0.24) | -.00852*** (-5.07) |
| [0,3] | -.00813*** (-4.34) | -.0199*** (-3.55) | -.00679*** (-3.44) |
| [0,5] | -.00684*** (-3.01) | .00746 (1.01) | -.00884*** (-3.73) |
| [0,7] | -.00113 (-0.47) | .0215*** (3.27) | -.00407 (-1.58) |
| Observations | 764 | 84 | 680 |

News" on the share price of GEM can be seen in the results. In the non-medical and non-pharmaceutical industries, the positive CARs all passed the significance level test of 1%. "Good News" indicated that the situation of the epidemic was gradually improving, and investors' confidence in the stock market was gradually increasing, which was why funds flowed into the GEM. As for the medical and pharmaceutical industries, "Good News" had a significant negative impact on share prices. Considering that investors' mood toward the medical pharmaceutical industry had been on the rise since the outbreak, "Good News" could release increased demand for medical products, leading investors to

sell some of the medical pharmaceutical stocks, resulting in a decline in the share prices of medical pharmaceutical companies.

Table 4 shows the GEM's respond to the "Rate Cut". Surprisingly, "Rate Cut" had a negative impact on the GEM overall. However, this policy could lead positive effects to the GEM medical and pharmaceutical industries to some degree. To sum up, we find that the interest rate cut policy had not much positive impact on innovative SMEs. In fact, this problem was homogenous with SMEs' financing difficulty. The SMEs were not capable of dealing with bank financing evaluations and were unable to effectively enjoy the policy

TABLE 5 The GEM's respond to "RRR Reduction".

| Event window | All industry | Medical and pharmaceutical industry | Non-medical and non-pharmaceutical industry |
|--------------|-----------------|-------------------------------------|---------------------------------------------|
| | (1) | (2) | (3) |
| [0,1] | .00448** (2.47) | .00694 (1.31) | .00435** (2.26) |
| [0,3] | .00196 (0.71) | -.00781 (-1.26) | .00332 (1.11) |
| [0,5] | .0110*** (3.56) | .00694 (1.31) | .0142*** (4.24) |
| [0,7] | .0144*** (4.10) | -.007811 (-1.26) | .0173*** (4.63) |
| Observations | 764 | 84 | 680 |

support of People's Bank of China. Due to this, the interest rate cut policy were difficult to apply to all types of small businesses.

Table 5 shows the GEM's respond to the "RRR Reduction". Within 1 week of implementing the RRR reduction policy, except for the event window [0,3], the CARs passed the significance level test of 5%, indicating that the targeted RRR reduction policy for inclusive finance had a positive impact on GEM. Compared with the interest rate cut policy, the RRR reduction policy was more effective for innovative SMEs. SMEs were more likely to raise funds and get financial support to tide over the epidemic because of the RRR reduction policy, which expanded the credit scale of commercial banks.

5 Distance from Wuhan City and market responds

As the epidemic was highly contagious and physical prevention measures were more effective than others, the distance from the epidemic center would seriously affect the development of enterprises. Wuhan lockdown would cause the enterprise upstream and downstream supply chain fracture and other serious economic consequences. Therefore, this section further studies the impact of distance from Wuhan on the response of GEM listed companies. Considering that the monetary policies were issued by the People's Bank of China, which was radiated throughout the country and less restricted by geographical location, this section only discusses the epidemic events, namely Event 1 ("Bad News") and Event 2 ("Good News").

5.1 Empirical strategy

5.1.1 Model

We establish the following regression model:

$$CAR_{i,t} = \gamma_0 + \gamma_1 Dist_{i,t} + \gamma_2 Cont_{i,t} + \mu_i + \gamma_t + \varepsilon_{i,t} \quad (5)$$

$$CAR_{i,t} = \theta_0 + \theta_1 Dist_{i,t} + \theta_2 Dist_{i,t} \times Clus_i + \theta_3 Cont_{i,t} + \mu_i + \gamma_t + \varepsilon_{i,t} \quad (6)$$

Where explained variable $CAR_{i,t}$ is calculated by event analysis. $Dist_{i,t}$ is the straight-line distance between a firm's business location and Wuhan. $Clus_i$ refers to a type of firm, in which $Phar_i$, Fin_i and $Trade_i$ represent the various classifications of firms. $Phar_i$ is used to determine whether a firm is in the medical or pharmaceutical industry. In case $Phar_i = 1$, the firm belongs to the medical or pharmaceutical industry, $Phar_i = 0$, otherwise. Fin_i divides the firm's business location according to the level of digital inclusive finance. $Fin_i = 1$ indicates an above-medium level of digital inclusive finance, $Fin_i = 0$, otherwise. $Trade_i$ describes whether or not a firm is engaged in trade. When $Trade_i = 1$, it represents a firm engaged in trade, $Trade_i = 0$, otherwise. $Cont_{i,t}$ represents a set of firm-level control variables, including firm age, equity nature (value is 1 for a private enterprise and value equal 0 otherwise), duality (value is 1 if the chairman of board holds the position of manager and value equal 0 otherwise), number of directors, the ratio of independent directors, leverage ratio, the return on assets, the return on capital, and number of employees (expressed in logarithmic form). μ_i , γ_t and $\varepsilon_{i,t}$ are industry fixed effect, span fixed effect and random error. In this model, i represents the GEM listed company and t represents the time span of event window.

5.1.2 Data

This paper focuses on Growth Enterprise Market listed companies. Basic information and financial data are retrieved from the CSMAR database, while share price data is gathered from the Wind database. Data is collected from 18 June 2019 to 7 April 2020. Also, the GEM listed companies with insufficient stock data, suspended for more than 3 months, with updated listings, or suspended longer than 3 months are excluded. A total of 764 GEM listed companies are obtained. According to the latitude and longitude data, we manually calculate the distance between firms and Wuhan City.

Following the *Guidelines on Industry Classification of Listed Companies (Revised in 2012)*, we initially classify pharmaceutical

TABLE 6 Descriptive statistics.

| Variables | Obs | Mean | Median | Std. Dev | Min | Max |
|----------------------|------|-------|--------|----------|--------|--------|
| CAR (Event 1) | 2920 | −.023 | −.043 | .103 | −.389 | .691 |
| CAR (Event 2) | 2928 | .012 | .006 | .071 | −.303 | .445 |
| CAR (Event 3) | 2924 | .008 | .001 | .079 | −.299 | .502 |
| CAR (Event 4) | 2922 | −.007 | −.114 | .056 | −.223 | .496 |
| <i>Dist</i> | 734 | 7.744 | 8.148 | 3.046 | 0 | 27.652 |
| <i>Phar</i> | 734 | .113 | 0 | .317 | 0 | 1 |
| <i>Fin</i> | 734 | .538 | 1 | .499 | 0 | 1 |
| <i>Trade</i> | 734 | .515 | 1 | .500 | 0 | 1 |
| <i>Age</i> | 734 | 7.467 | 7 | 2.908 | 2 | 12 |
| <i>Equity_nature</i> | 734 | .857 | 1 | .350 | 0 | 1 |
| <i>Dual</i> | 730 | .578 | 1 | .494 | 0 | 1 |
| <i>Board</i> | 732 | 7.870 | 8 | 1.453 | 5 | 13 |
| <i>Inde</i> | 732 | .385 | .375 | .055 | .25 | .667 |
| <i>Lev</i> | 732 | 1.852 | 1.542 | 1.631 | −2.268 | 25.411 |
| <i>ROA</i> | 732 | .004 | .003 | .015 | −.068 | .070 |
| <i>ROE</i> | 732 | .003 | .006 | .043 | −.800 | .106 |
| <i>Staff</i> | 732 | 7.093 | 7.034 | .939 | 3.970 | 11.551 |

TABLE 7 Impact of distance on the CARs under Event 1 (“Bad News”) and Event 2 (“Good News”).

| Variables | (1) | (2) | (3) | (4) |
|--------------|---------|---------|----------|----------|
| | Event1 | Event1 | Event2 | Event2 |
| <i>Dist</i> | −.0006 | −.0006 | .0014*** | .0012*** |
| | (.0006) | (.0006) | (.0004) | (.0004) |
| Controls | No | Yes | No | Yes |
| Industry FE | Yes | Yes | Yes | Yes |
| Span FEt | Yes | Yes | Yes | Yes |
| R-squared | .172 | .189 | .075 | .090 |
| Observations | 2,936 | 2,920 | 2,944 | 2,928 |

Notes: *Dist* is measured in units of 100 km *, ** and *** denote the 10, 5, and 1 percent significance levels, respectively. The value in parentheses is standard error. The same below.

manufacturing, scientific research, and health industry firms as medical and pharmaceutical industries. Furthermore, firms are manually divided according to the scope of their business, with 84 in the medical and pharmaceutical industry and 680 in the non-medical and non-pharmaceutical industry.

We determine the level of digital inclusive finance in each firm’s business location using the 2018 Digital Financial Index.

Following that, we divide the firms by their median index into two groups. A total of 398 companies are classified as having a digital inclusive finance level above the median level, and 341 companies are classified as having a digital inclusive finance level below the median level.

The business scope information of all GEM listed companies is manually gathered. Businesses involved in trade business are

classified as those with the word “import” “export”, “trade” or other related words in their business scope. The total number of firms involved in trade business is 380, and 359 are not.

The descriptive statistics of the main variables are shown in Table 6.

5.2 Baseline regression results

The baseline regression results are presented in Table 7. In Columns (1) and (2), the dependent variables are the CARs from Event 1, the lockdown of Wuhan City. The effect of distance on the CARs from Event 1 is not significant. This finding contradicts the view that companies at the epicenter of the outbreak were hard hit by COVID-19. This may be because, as a major public health emergency, the COVID-19 epidemic had a wide radiation range. The outbreak of epidemic had a serious impact on the overall economic trend of the whole country, causing investors to be indiscriminately negative about firms across the whole country. Therefore, in the early stage of the outbreak, whether the firm is located far away from Wuhan City or not, it suffered a severe economic impact.

Columns (3) and (4) examine the CARs from Event 2, the announcement that the epidemic situation was improving. The longer the distance between firms' business locations and Wuhan City, the greater the positive impact on CARs from Event 2. This finding is consistent with investors' belief that firms at the epicenter of the outbreak were more difficult to resume production and operations. Therefore, investors remain pessimistic about firms close to Wuhan City.

The epidemic had severely restricted the movement of factors such as labor. One of the most important ways to deal with the epidemic is to impose physical quarantines and restrict the movement of people, which would prevent employees from coming to work, greatly hinder the process of logistics, and disrupt firms' supply chains. Wuhan City was the epicenter of the epidemic, and restricting and sealing the city had become an important measure to stop the further spread of the epidemic. As a result, firms near Wuhan City were more likely to have employees unable to get to work. At the same time, considering the necessary transaction costs in business activities, such as distance cost, firms often choose to conduct business with those close to their business location. Therefore, distance also affected the smooth logistics and the integrity of the supply chain. All these would cause difficulties in enterprise operation and management, and then affected firm performance. In the short term, investors were more inclined to invest in firms further away from Wuhan City.

In addition, the impact of the epidemic could also bring about uncertainty and negative mood. On the one hand, investors might be more optimistic about the recovery of firms farther from Wuhan City. On the other hand, the confidence of entrepreneurs was crucial to restoring in production.

Entrepreneurs at the center of the epidemic would have more negative moods to the resumption of production, which was not conducive to the normal operation of the firm from a subjective perspective. And investors would take a wait-and-see attitude towards such firms in anticipation of this phenomenon. To sum up, distance indeed matters firms' CARs a lot.

5.3 Heterogeneity

We also explore some potential heterogeneity to see if distance between firms' business locations and Wuhan City impacts CARs across some key firm or industry characteristics. Heterogeneity regression results are presented in Table 8.

We first analyze an industrial heterogeneity. The interaction term between the pharmaceutical industry dummy and the distance is added to the regressions. As shown in Columns (1) and (2) of Table 8, the interaction term is significantly positive in Event 1, and significantly negative in Event 2. Due to the lockdown, raw materials for firms were limited, and the Spring Festival holiday made it difficult for firms to resume operations on time. However, firms in the medical and pharmaceutical industries restarted their operations immediately when faced with difficulties. They even continued on to work overtime to create medical products, resulting in the industry's recovery. Therefore, investors' expectations for the pharmaceutical and medical industry were raised, thereby alleviating the bad situation. Then, when the epidemic situation improved, companies in the medical and pharmaceutical industries no longer had higher market expectations than other industries, which provided more firms with good development prospects.

Columns (3) and (4) explore the heterogeneity of financial development. The regressions include the interaction term between the distance and the digital inclusive finance dummy. The coefficient of the interaction term is significantly positive during Event 1, but significantly negative during Event 2. This indicates that digital inclusive finance released the negative impact of the epidemic and slowed down the positive effects of good news on CARs. This may be due to the fact that digital inclusive finance reflects China's digital economy, which can alleviate regional inequalities more effectively. During a severe epidemic, when factors flowed relatively slowly, digital inclusive finance greatly facilitated the economic behaviors of individuals, enterprises, and governments, and could counteract the distance-related difference in CARs. In addition, digital inclusive finance can increase the coverage of financial services and reduce the cost of financial services [40], as well as make financial behaviors more accessible and convenient [41]. Particularly for SMEs with financing difficulties, digital inclusive finance reduced the likelihood of financial constraints [42,43] and allows SMEs to handle business shocks more effectively. This would make sure that SMEs of all sizes and regions could benefit more evenly from the policy, given the improving epidemic situation and looser monetary policy.

TABLE 8 Heterogeneity analysis: industry, level of financial development and business type.

| Variables | (1) | (2) | (3) | (4) | (5) | (6) |
|---------------------|----------------------|---------------------|---------------------|------------------------|-------------------|----------------------|
| | Event1 | Event2 | Event1 | Event2 | Event1 | Event2 |
| <i>Dist</i> | −.0021*** (.0006) | .0015*** (.0005) | −.0013** (.0006) | .0018*** (.0005) | −.0007 (.0007) | .0020*** (.0005) |
| <i>Dist × Phar</i> | .0096*** (.0011) | −.0020** (.0008) | | | | |
| <i>Dis × Fin</i> | | | .0020*** (.0005) | −0.0015*** (0.0003) | | |
| <i>Dist × Trade</i> | | | | | .0001 (.0004) | −.0013*** (.0003) |
| Controls | Yes | Yes | Yes | Yes | Yes | Yes |
| Industry FE | Yes | Yes | Yes | Yes | Yes | Yes |
| Span FE | Yes | Yes | Yes | Yes | Yes | Yes |
| R-squared | .211 | .189 | .194 | .097 | .189 | .095 |
| Observations | 2,920 | 2,920 | 2,920 | 2,920 | 2,920 | 2,928 |

Columns (5) and (6) examine the heterogeneity based on the type of firm's business. The interaction term between the distance and the trade business dummy is included in the regression. Under Event 1, the interaction term is insignificant. The epidemic was just breaking out, and the international environment was stable, so CARs did not suffer any effects from the trade business. Under Event 2, the interaction term is significantly negative. This may be because that Event 2 coincided with the time node when the overseas epidemic worsened. Many SMEs involved in import and export business were affected by the global spread of COVID-19.

6 Conclusion

Early 2020 marks the beginning of the COVID-19 epidemic. SMEs had a low level of risk resistance and self-healing ability, so public emergencies affected them more severely. Moreover, innovative firms are more likely to go bankrupt during crises [21]. As representative of innovative SMEs, GEM listed companies are contributing to China's economic growth. Thus, this paper uses event analysis to investigate the stock yield performance of GEM listed companies during the epidemic. Furthermore, this paper examines the effects of the straight-line distance between a firm's business location and Wuhan City on the CARs.

The empirical results indicate that: Firstly, "Good News" of epidemic made the GEM more optimistic, while "Bad News" of epidemic had a significantly negative impact on the GEM.

Secondly, a targeted RRR reduction policy was more beneficial to GEM listed companies than an interest rate reduction policy. Thirdly, the distance between the firms' business locations and Wuhan City did not significantly affect the CARs in the early stages of the outbreak. When the epidemic situation improves, the farther the firms' business locations are from Wuhan City, the more positive the impact on CARs. Finally, there were heterogeneous effects based on industry, inclusive finance, and business type. COVID-19's negative impact on CARs can be released by digital inclusive finance.

Based on these findings, this paper provides some recommendations on how to mitigate the negative impacts of public health emergencies on SMEs.

Firstly, the central government needs to grasp the benefits of policies and assist SMEs that are suffering large losses. In order to meet SMEs' needs, local governments should accelerate the implementation of policies. Additionally, they should provide loan guarantees for qualified SMEs to ease their lending and financing difficulties.

Secondly, the government must take action to stabilize the stock market during the epidemic, to ease investors' panic and to ensure the survival and development of GEM listed companies. The government could prioritize the stable shutdown of the stock market in case of a public emergency in order to stabilize the securities market. Moreover, government should ensure that information disclosure is timely and effective and the content of information is true and reliable. Securities regulatory authorities are supposed to send positive and correct signals to investors and listed companies, guiding market participants to invest rationally.

Thirdly, the central bank can prioritize RRR reduction policy over interest rate cuts. Based on the epidemic situation, the two policies could be implemented alternately, creating a superposition effect to complement one another. In addition, the central bank must pay attention to the tilt of innovative SMEs, deepening inclusive finance activities.

Lastly, the government should fully consider the effect of the distance factor on the production and operation activities of SMEs, as far as possible to achieve “one-industry, one-way” and “one firm, one policy”. The government should pay close attention to the medical and pharmaceutical industry, which is overheating in the early stages of the epidemic. Thus, overproduction would be avoided, and its steady and healthy development would be ensured.

There are limitations in this study. At the initial stage of the epidemic, various epidemic news and policies were released frequently. It is difficult for us to accurately test the impact of all events on the market and obtain a pure effect. Therefore, only four representative and comparative epidemic news and monetary policies are the main research objects. In addition, this paper only examines the short-term market performance within half a year after the outbreak of the epidemic, but did not track and study the medium and long-term market changes and economic conditions within 3 years since the outbreak. How to develop the capital market in the post epidemic era is an important future research direction. Finally, considering the high infectivity of the epidemic, the contagion network will be further expanded in business and interpersonal communication. On the basis of this fact, how various economic networks, such as production networks, will change is also a research direction worthy of attention.

Data availability statement

The raw data supporting the conclusion of this article will be made available by the authors, without undue reservation.

References

- Xu R. Statistical methods for the estimation of contagion effects in human disease and health networks. *Comput Struct Biotechnol J* (2020) 18:1754–60. doi:10.1016/j.csbj.2020.06.027
- Holme P. Temporal network structures controlling disease spreading. *Phys Rev E* (2016) 94:022305. doi:10.1103/PhysRevE.94.022305
- Iacopini I, Petri G, Barrat A, Latora V. Simplicial models of social contagion. *Nat Commun* (2019) 10:2485. doi:10.1038/s41467-019-10431-6
- Colman E, Spies K, Bansal S. The reachability of contagion in temporal contact networks: How disease latency can exploit the rhythm of human behavior. *BMC Infect Dis* (2018) 18:219. doi:10.1186/s12879-018-3117-6
- Yang Z, Chen Y, Zhang P. Macroeconomic shocks, financial risk transmission and governance response in major public emergencies. *Manag World* (2020) 36(5):13–35+7. (in Chinese). doi:10.19744/j.cnki.11-1235/f.2020.0067
- Gourio F. Disaster risk and business cycles. *Am Econ Rev* (2012) 102(6):2734–66. doi:10.1257/aer.102.6.2734
- Zhu W, Zhang P, Li P, Wang Z, Kong F, Fu P, et al. Novel macrolactams from a deep-sea-derived *streptomyces* species. *Manag World* (2020) 36(4):13–26. (in Chinese). doi:10.3390/md19010013
- Al-Awadhi AM, Alsaifi K, Al-Awadhi A, Alhamadi S. Death and contagious infectious diseases: Impact of the COVID-19 virus on stock market returns. *J Behav Exp Finance* (2020) 27:100326. doi:10.1016/j.jbef.2020.100326
- Ashraf BN. Economic impact of government interventions during the COVID-19 pandemic: International evidence from financial markets. *J Behav Exp Finance* (2020) 27:100371. doi:10.1016/j.jbef.2020.100371
- Estrada M, Koutroufas E, Lee M. Staggression: The economic and financial impact of the COVID-19 pandemic. *Contemp Econ* (2020) 15(1):19–33. doi:10.5709/ce.1897-9254.433
- Zhang D, Hu M, Ji Q. Financial markets under the global pandemic of COVID-19. *Finance Res Lett* (2020) 36:101528. doi:10.1016/j.frl.2020.101528
- Jackson EL. Response to earthquake hazard: The west coast of North America. *Environ Behav* (1981) 13(4):387–416. doi:10.1177/0013916581134001

Author contributions

All authors listed have made a substantial, direct, and intellectual contribution to the work. LW and YW contributed to conception and design of the study. LW organized the database. YW performed the statistical analysis. ZH wrote the first draft of the manuscript. All authors contributed to manuscript revision, read, and approved the submitted version.

Funding

This work is supported by Humanities and Social Sciences Project of the Ministry of Education of China (Grant numbers 22YJA790055, Grant numbers 21YJC790107), Guangdong Philosophy and Social Science Planning Project (Grant numbers GD22YYJ06), National Natural Science Foundation of China (Grant numbers 72073142).

Conflict of interest

The authors declare that the research was conducted in the absence of any commercial or financial relationships that could be construed as a potential conflict of interest.

Publisher's note

All claims expressed in this article are solely those of the authors and do not necessarily represent those of their affiliated organizations, or those of the publisher, the editors and the reviewers. Any product that may be evaluated in this article, or claim that may be made by its manufacturer, is not guaranteed or endorsed by the publisher.

13. Dessaint O, Matray A. Do managers overreact to salient risks? Evidence from hurricane strikes. *J Financial Econ* (2017) 126(1):97–121. doi:10.1016/j.jfineco.2017.07.002
14. Misici L, Filippo S. Epidemic propagation: An automaton model as the continuous SIR model. *Appl Math* (2013) 4(10C):84–9. doi:10.4236/am.2013.410A3011
15. Bausch DG, Schwarz L. Outbreak of Ebola virus disease in Guinea: Where ecology meets economy. *Plos Negl Trop Dis* (2014) 8(7):e3056. doi:10.1371/journal.pntd.0003056
16. Zhang X, Liu L, Ge Z, Zhao H, Miao L, Pan Y. The dimension and morphology of alveolar bone at maxillary anterior teeth in periodontitis: A retrospective analysis-using CBCT. *Econ Res J* (2020) 55(6):4–21. (in Chinese). doi:10.1038/s41368-019-0071-0
17. Rassy D, Smith RD. The economic impact of H1N1 on Mexico's tourist and pork sectors. *Health Econ* (2013) 22(7):824–34. doi:10.1002/hec.2862
18. He C, Wen Y, Chang Y, Geng X. Measurement analysis of the impact of the new coronavirus pneumonia outbreak on China's economy. *J Quantitative Tech Econ* (2020) 37(5):3–22. (in Chinese). doi:10.13653/j.cnki.jqte.2020.05.001
19. Worthington A, Valadkhani A. Measuring the impact of natural disasters on capital markets: An empirical application using intervention analysis. *Appl Econ* (2004) 36(19):2177–86. doi:10.1080/0003684042000282489
20. Mel S, McKenzie D, Woodruff C. Enterprise recovery following natural disasters. *Econ J* (2012) 122(559):64–91. doi:10.1111/j.1468-0297.2011.02475.x
21. Lee N, Sameen H, Cowling M. Access to finance for innovative smes since the financial crisis. *Res Pol* (2015) 44(2):370–80. doi:10.1016/j.respol.2014.09.008
22. Sannajust A. *Impact of the world financial crisis to SMEs: The determinants of bank loan rejection in Europe and USA. No 2014-327, Working Papers*. France: Department of Research, Ipag Business School (2014).
23. Zhang H, Tong X. Structural change in China's emergency management: Theoretical generalizations. *Social Sci China* (2016) 37(2):77–98. doi:10.1080/02529203.2016.1162010
24. Noy I. The macroeconomic consequences of disasters. *J Dev Econ* (2009) 88(2):221–31. doi:10.1016/j.jdeveco.2008.02.005
25. Hartmann P, Straetmans S, Vries CG. Asset market linkages in crisis periods. *Rev Econ Stat* (2004) 86(1):313–26. doi:10.1162/003465304323023831
26. Barunik J, Krehlik T. Measuring the frequency dynamics of financial connectedness and systemic risk. *J Financial Econ* (2018) 16(2):271–96. doi:10.1093/jjfinec/nby001
27. Albulescu CT. COVID-19 and the United States financial markets' volatility. *Finance Res Lett* (2021) 38:101699. doi:10.1016/j.frl.2020.101699
28. Baig AS, Butt HA, Haroon O, Rizvi SAR. Deaths, panic, lockdowns and US equity markets: The case of COVID-19 pandemic. *Finance Res Lett* (2021) 38:101701. doi:10.1016/j.frl.2020.101701
29. Haroon O, Rizvi SAR. COVID-19: Media Coverage and financial markets behavior-A sectoral inquiry. *J Behav Exp Finance* (2020) 27:100343. doi:10.1016/j.jbef.2020.100343
30. Ragin MA, Halek M. Market expectations following catastrophes: An examination of insurance broker returns. *J Risk Insurance* (2016) 83:849–76. doi:10.1111/jori.12069
31. Shelor RM, Anderson DC, Cross ML. Gaining from loss: Property liability insurer stock values in the aftermath of the 1989 California earthquake. *J Risk Insurance* (1992) 59(3):476–88. doi:10.2307/253059
32. Lamb RP. An exposure-based analysis of property-liability insurer stock values around Hurricane Andrew. *J Risk Insurance* (1995) 62(1):111–20. doi:10.2307/253695
33. Lanfear MG, Lioui A, Siebert MG. Market anomalies and disaster risk: Evidence from Extreme weather events. *J Financial Markets* (2019) 46:100477. doi:10.1016/j.finmar.2018.10.003
34. Xie H, Jiang T, Zhang W. Trade effects of political shocks - analysis of events with the election of trump. *China Econ Q* (2020) 19(1):233–60. (in Chinese). doi:10.13821/j.cnki.ceq.2019.04.11
35. Schweitzer R. How do stock returns react to special events? *Business Rev* (1989) 7:17–29.
36. Hood M, Kamesak A, Nofsinger J, Tamura T. Investor response to a natural disaster: Evidence from Japan's 2011 earthquake. *Pacific-Basin Finance J* (2013) 25:240–52. doi:10.1016/j.pacfin.2013.09.006
37. Tai Z, Sun T. The rumouring of SARS during the 2003 epidemic in China. *Sociol Health Illness* (2011) 33(5):677–93. doi:10.1111/j.1467-9566.2011.01329.x
38. Campbell JY, Lo AWC, Mackinlay AC. *The econometrics of financial markets*. Princeton, New Jersey: Princeton University Press (1997).
39. Corrado CJ, Zivney TL. The specification and power of the sign test in event study hypothesis tests using daily stock returns. *J Financial Quantitative Anal* (1992) 27(3):465–78. doi:10.2307/2331331
40. Sutherland A. Does credit reporting lead to a decline in relationship lending? Evidence from information sharing technology. *J Account Econ* (2018) 66(1):123–41. doi:10.1016/j.jacceco.2018.03.002
41. Jaksic M, Marinc M. Relationship banking and information technology: The role of artificial intelligence and fintech. *Risk Management-an Int J* (2019) 21(1):1–18. doi:10.1057/s41283-018-0039-y
42. Mollick E. The dynamics of crowdfunding: An exploratory study. *J Business Venturing* (2014) 29(1):1–16. doi:10.1016/j.jbusvent.2013.06.005
43. Li J, Wu Y, Xiao J. The impact of digital finance on household consumption: Evidence from China. *Econ Model* (2020) 86(C):317–26. doi:10.1016/j.econmod.2019.09.027



OPEN ACCESS

EDITED BY
Jianbo Wang,
Southwest Petroleum University, China

REVIEWED BY
Liang Wu,
Southwestern University of Finance and
Economics, China
Jun Hu,
Rey Juan Carlos University, Spain
Huijie Yang,
University of Shanghai for Science and
Technology, China

*CORRESPONDENCE
Xiong Xiong,
✉ xxpeter@tju.edu.cn

SPECIALTY SECTION
This article was submitted to Social
Physics,
a section of the journal
Frontiers in Physics

RECEIVED 31 July 2022
ACCEPTED 28 December 2022
PUBLISHED 12 January 2023

CITATION
Lv X, Xiong X and Geng B (2023), Increasing
the prediction performance of temporal
convolution network using multimodal
combination input: Evidence from the
study on exchange rates.
Front. Phys. 10:1008445.
doi: 10.3389/fphy.2022.1008445

COPYRIGHT
© 2023 Lv, Xiong and Geng. This is an
open-access article distributed under the
terms of the [Creative Commons
Attribution License \(CC BY\)](#). The use,
distribution or reproduction in other
forums is permitted, provided the original
author(s) and the copyright owner(s) are
credited and that the original publication in
this journal is cited, in accordance with
accepted academic practice. No use,
distribution or reproduction is permitted
which does not comply with these terms.

Increasing the prediction performance of temporal convolution network using multimodal combination input: Evidence from the study on exchange rates

Xueling Lv¹, Xiong Xiong^{1,2*} and Baojun Geng³

¹College of Management and Economics, Tianjin University, Tianjin, China, ²Laboratory of Computation and Analytics of Complex Management Systems (CACMS), Tianjin University, Tianjin, China, ³Pittsburgh Institute, Sichuan University, Chengdu, China

The currency market is one of the most important financial markets in the world. The exchange rate movement has effect on international trade and capital flow. This study presents a forecasting method for exchange rate based on multi-modal combination market trend. The method facilitates the more accurate identification of volatility link between exchange rates, unlike the conventional ones, in which only information related to itself is used as input. We select multiple characteristics of the exchange rate from other countries as input data. Then the Pearson correlation coefficient and random forest model are used to filter these characteristics. We integrate the data with higher correlation into the temporal convolutional network model to forecast the exchange rate. For the empirical samples, a nine-year period historical exchange rates of the Euro, Ruble, Australian dollar, and British pound corresponding to the Renminbi are used. The empirical results show the more stable effect using the forecasting method proposed in this study than the traditional models.

KEYWORDS

Pearson correlation coefficient, deep learning, random forest, artificial intelligence, exchange rate prediction

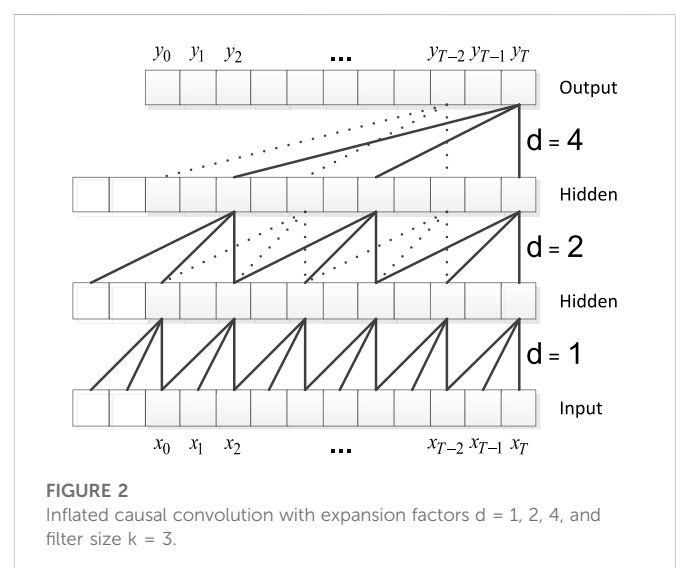
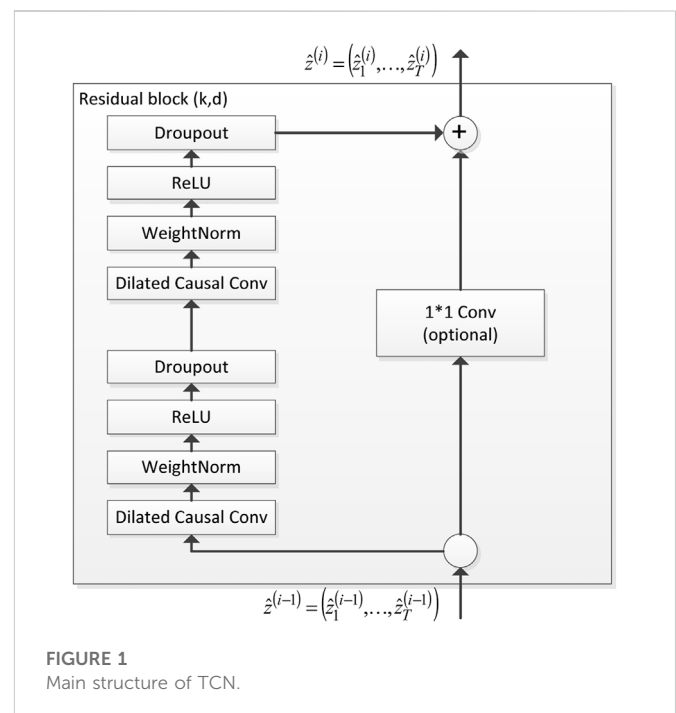
1 Introduction

Financial markets play an important role in the development of the global economy. And the currency market is an influential component of the financial market. Thus, exchange rate forecasting has come into one focus of the academia and economic [1, 2]. Several scholars have conducted studies on the exchange rates [3–5]. In addition, the study of exchange rate time-series data has been an invaluable component of time-series research. This involves the judgment and speculation of fluctuation ranges and trend changes in the exchange rate relationships.

Henrique B M et al. [6] analyzed the application of current commonly used machine learning methods in the field of financial forecasting. By analyzing machine learning models in many papers, the author shows that machine learning methods can predict the trend of financial prices. Sezer OB et al. [7] analyzed papers on machine learning models and deep learning models published in 2020 and before. The results show that the popularity of deep learning models in the field of financial forecasting is gradually improving, and the deep

learning model also has good prediction accuracy. However, traditional neural networks have defects. Deep neural network (DNN) is not proper to the time series. Recurrent neural network (RNN) cannot perform massively parallel processing. Convolutional neural network (CNN) has the advantage of massive parallel processing, regardless of the network's depth. Long short-term memory (LSTM) and gate recurrent unit (GRU) degrades to random guesses as the time length T grows. However, temporal convolutional network (TCN) [8] overcomes the shortcomings of the traditional models. The review of [9] introduces TCN and documents its application in the field of time series prediction. The fact that TCN does not utilize future information and that input and output lengths are equal makes TCN models of considerable interest to researchers. Soleymani and [10] proposed a novel deep learning framework called the QuantumPath for long-term stock-price forecasting. They also incorporated a TCN into the model to ensure causality. The experiments demonstrated the effectiveness of the proposed method. Totannanavar [11] used the TCN to predict stock prices. In relation to other neural networks, this model has several advantages. Wiese et al. [12] proposed data-driven models called quant generative adversarial networks (GANs). The model consists of a generator and a discriminator function and uses a TCN to capture long-term dependencies. To predict the stock prices, Janssen [13] combined a TCN with attention mechanisms. The study's finding shows a more significant effect of the combination of temporal attention and TCN. Tan et al. [14] developed a new financial time series GAN (FinGAN) based on TCN. The results show that the model can more accurately fit high-volatility convertible bonds. Lei et al. [15] constructed a deep TCN model to predict volatility under high-frequency financial data based on other trading information such as trading volume, trend indicators, and quote change rate. The results show that TCN model with investor attention provides better prediction accuracy than that of the TCN model without investor attention. Using a TCN, Dai et al. [16] classified price changes into several categories and predicted the conditional probability of each category. They also added a mechanism to the TCN architecture to model the time-varying distribution of stock price changes. Empirical evidence indicates that the proposed method outperforms the comparison model. According to Zhang et al. [17], the TCN is an effective method to predict return volatility and value-at-risk in exchange rate forecasting studies.

This study investigates the exchange rate changes among countries using TCN, considering the advantages of TCN in financial forecasting. Furthermore, although many studies have used several methods to predict exchange rates, none of them considers the correlation between the exchange rates from different countries. The progress in global economic integration have increasingly correlated the exchange rate movements between countries. As exchange rates have both linear and nonlinear behavioural characteristics, a single linear or nonlinear model can not predict exchange rates roundly. Instead of using only information related to the individual exchange rate as input, we use information related to exchange rate volatility as input. This enables us to determine the relationship between volatility and the exchange rate. We present a multimodal combination-based method for forecasting exchange rate market trends, using multiple exchange rate characteristics from other countries as input data. We also filter multiple exchange rate characteristics using a Pearson correlation



coefficient and a random forest model. We incorporate data with higher correlation to improve the accuracy and stability of exchange rate forecasting. Subsequently, we analyse the exchange rate prediction by considering the TCN model. In terms of the data, we select nine-years historical data of the exchange rate of the Euro (EUR), Ruble (RUB), Australian dollar (AUD), and the British pound (GBP) to RMB. Four evaluation indicators are applied to compare with other four from the traditional models. We test different datasets separately.

The contributions of this study are as follows. First, this study attempts a pure end-to-end approach to predict the movement of the exchange market. Specifically, this research utilizes a model combining feature extraction and TCN. Only the raw exchange rate data are used as input. Hence, it can eliminate the human

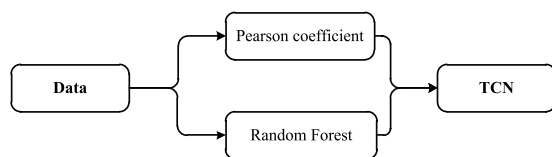


FIGURE 3
Model flow chart.

intervention. Second, this study identifies the characteristics of the movement of exchange rate based on the exchange rate in several other countries. We combine the Pearson correlation coefficient with a random forest to filter the multiple exchange rate characteristics. Then, we identify the characteristics with higher correlation from the filtered characteristics. As a result, we integrate the historical exchange rate data and exchange rate characteristics into one specific data set. The results demonstrate that the proposed method provides more stable prediction effect than the traditional models.

The rest of this article is organized as follows. [Section 2](#) reviews related methodologies. The data and the empirical results are provided in [Section 3](#). [Section 4](#) concludes the article.

2 Methodologies

2.1 Temporal convolutional networks

A RNN performs well on almost all time-series issues. However, in practice, RNN presents serious problems. Since the network can only process one time step at a time, the latter must wait until the processing is complete in the preceding step, before it can be computed. This problem means that an RNN cannot perform massive parallel processing, which implies that RNN is computationally demanding.

When a CNN processes an image, it treats the image as a two-dimensional *block* ($m \times n$ matrix). Moving to time series, time series can be viewed as a one-dimensional object ($1 \times n$ vector). Through the multilayer network structure, the CNN retrieves a sufficiently large receptive field. This practice deepens the model

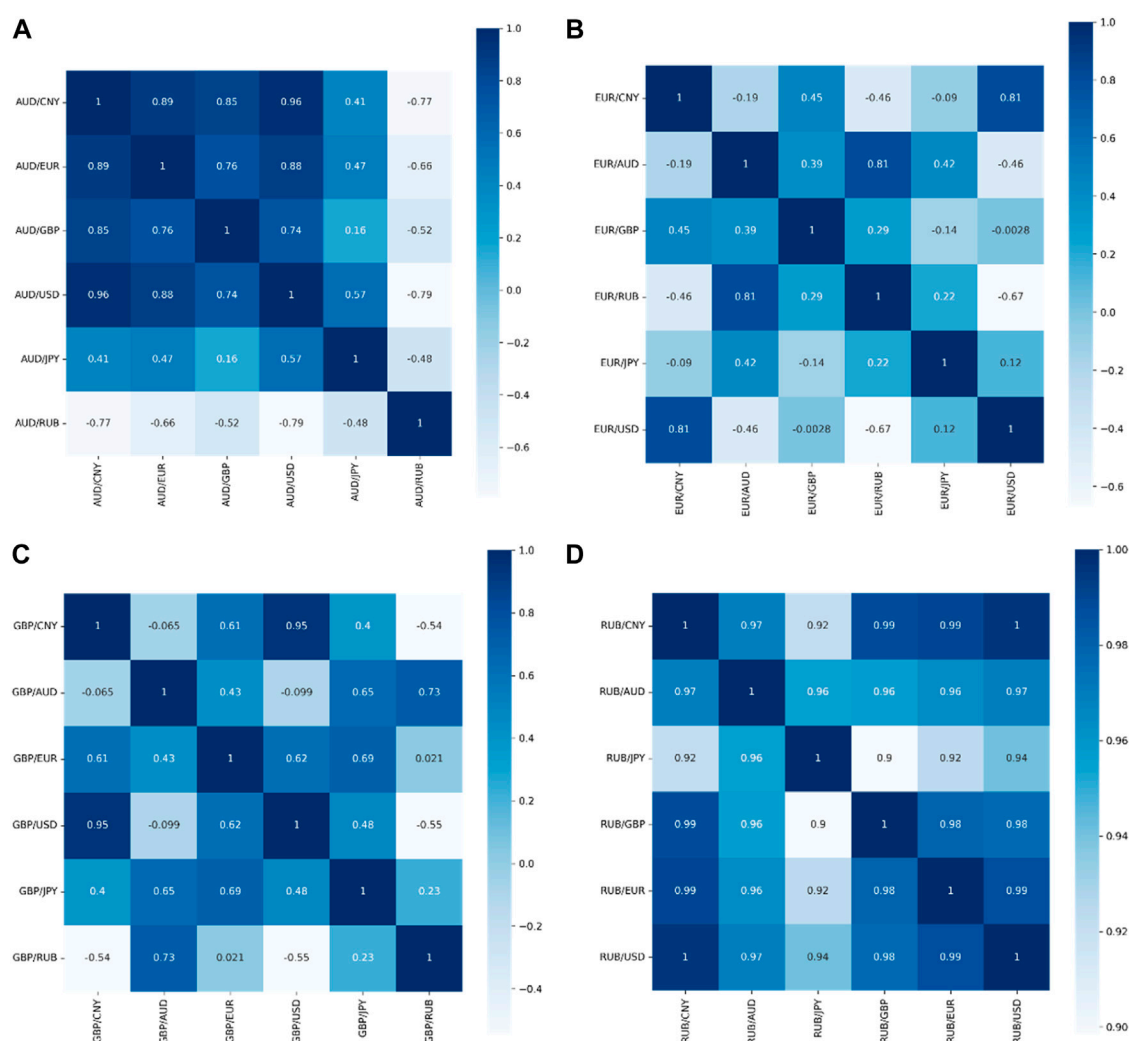


FIGURE 4
Plot of correlation coefficients for the foreign exchange dataset.

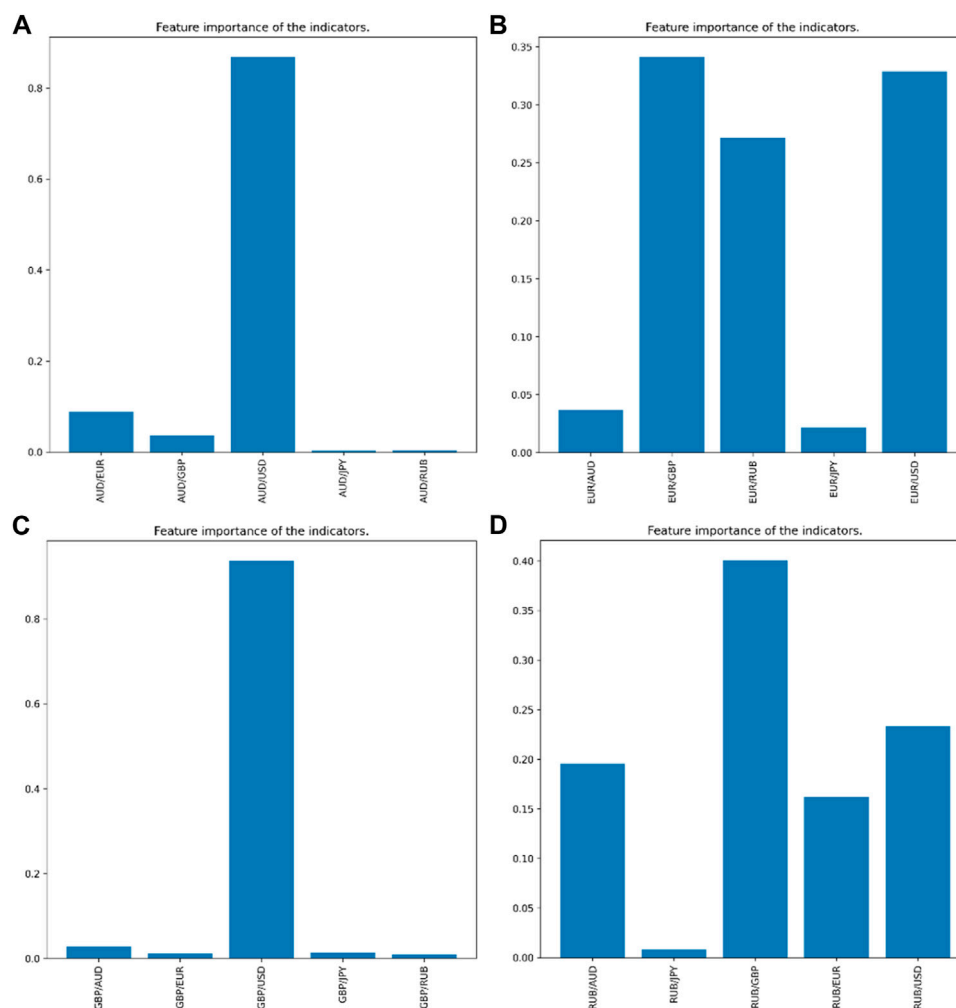


FIGURE 5
Random forest feature importance ranking.

structure of the CNN. However, the CNN saves time owing to the advantage of massive parallel processing, regardless of the network's depth.

The network combines the structural features of the RNN and CNN with more flexible perceptual fields, more stable gradient changes, and less memory usage. The main structure of the TCN is shown in Figure 1. The TCN mainly comprises five parts—the dilated causal convolutional, WeightNorm, activation function, and dropout layers and a residual connection block.

The dilated causal convolutional layer mines the data features for analysis. Figure 2 shows the structure of the dilated causal convolutional layer. The WeightNorm layer accelerates the model by rewriting the weights of the deep network. The activation function layer increases the nonlinearity of the network and improves the model's expressiveness. The dropout layer prevents model overfitting. The residual connection block is a 1×1 convolution block. The residual connection locks not only enable the network to transmit information across layers but also ensure the consistency of the input and output.

2.2 Multimodal combination-based method for forecasting exchange rate

With economic globalization, countries are becoming increasingly closely connected. This indicates an obvious correlation between the exchange rate prices from different economies. However, the differences in the relationships between countries yields different correlations between exchange rate prices of different countries. Some exchange rate data and forecast exchange rates have an obvious strong correlation, whereas others have an obvious weak correlation. Therefore, this study proposes a method for forecasting the trend of the exchange rate market based on a multimodal combination.

Figure 3 illustrates the specific process of the proposed model. First, we use the Pearson correlation coefficient to extract the features highly correlated with the predicted exchange rate in the input data. Pearson's correlation coefficient ranges from -1 to 1 . The closer the absolute value is to 1 , the stronger is the linear correlation between exchange rates.

TABLE 1 Predictors of different comparison models.

| | | MAE | MSE | RMSE | R^2_score |
|-----------------|----------------|----------|----------|-----------|--------------|
| AUD/RMB dataset | Our | 0.0173 4 | 0.0004 3 | 0.0208 4 | 0.9981 4 |
| | CNN | 0.0505 0 | 0.0032 9 | 0.0573 6 | 0.9859 3 |
| | LSTM | 0.0439 0 | 0.0029 5 | 0.0543 3 | 0.9873 7 |
| | CNN-LSTM | 0.0362 5 | 0.0018 8 | 0.0433 5 | 0.9919 6 |
| | Attention-LSTM | 0.0266 2 | 0.0011 6 | 0.0341 1 | 0.9950 2 |
| EUR/RMB Dataset | Our | 0.0373 3 | 0.0021 7 | 0.0465 3 | 0.9602 1 |
| | CNN | 0.0569 4 | 0.0043 4 | 0.0659 0 | 0.9202 1 |
| | LSTM | 0.0542 4 | 0.0042 6 | 0.0652 8 | 0.9217 1 |
| | CNN-LSTM | 0.0376 4 | 0.0020 3 | 0.0450 3 | 0.9627 4 |
| | Attention-LSTM | 0.0466 8 | 0.0033 2 | 0.0576 6 | 0.9389 1 |
| GBP/RMB Dataset | Our | 0.0407 2 | 0.0017 2 | 0.0414 7 | 0.9841 3 |
| | CNN | 0.0671 3 | 0.0055 5 | 0.0744 9 | 0.9488 2 |
| | LSTM | 0.0541 1 | 0.0045 2 | 0.0672 2 | 0.9583 1 |
| | CNN-LSTM | 0.0444 5 | 0.0027 9 | 0.0528 6 | 0.9742 2 |
| | Attention-LSTM | 0.0524 5 | 0.0037 9 | 0.0616 0 | 0.9649 9 |
| RUB/RMB Dataset | Our | 0.0018 9 | 0.0000 1 | 0.0023 6 | 0.9878 2 |
| | CNN | 0.0063 6 | 0.0000 5 | 12.4571 0 | 0.9011 2 |
| | LSTM | 0.0051 0 | 0.0000 3 | 12.5132 4 | 0.9383 5 |
| | CNN-LSTM | 0.0035 0 | 0.0000 1 | 12.3503 6 | 0.9678 3 |
| | Attention-LSTM | 0.0040 1 | 0.0000 2 | 0.0041 8 | 0.9617 6 |

TABLE 2 DM detection of the proposed model and other models.

| | | CNN | LSTM | CNN-LSTM | Attention-LSTM |
|-----------------|------------|-------------------------|-------------------------|-------------------------|-------------------------|
| AUD/RMB dataset | DM value | -13.366 | -8.972 | -10.731 | -8.120 |
| | p -value | 7.838×10^{-37} | 2.144×10^{-18} | 3.783×10^{-25} | 1.815×10^{-15} |
| EUR/RMB Dataset | DM value | -10.050 | -6.791 | 0.884 | -2.591 |
| | p -value | 2.092×10^{-22} | 2.231×10^{-11} | 0.377 | 0.010 |
| GBP/RMB Dataset | DM value | -11.834 | -5.768 | -3.945 | -9.333 |
| | p -value | 7.888×10^{-30} | 1.157×10^{-8} | 8.695×10^{-5} | 1.048×10^{-19} |
| RUB/RMB Dataset | DM value | -18.443 | -20.462 | -10.332 | -15.822 |
| | p -value | 2.730×10^{-63} | 8.744×10^{-75} | 1.545×10^{-23} | 4.309×10^{-49} |

The Pearson correlation coefficient is linear, reflecting the degree of linear correlation between the two quantities. However, the exchange rates of various countries are interrelated, and there is a nonlinear relationship between the exchange rate prices. Therefore, this study uses the random forest algorithm to analyse the impact of the closing price of the exchange rate of other countries on the predicted exchange rate.

Finally, we use the TCN to predict exchange rate changes by combining the Pearson correlation coefficient and random forest features.

3 Empirical results

3.1 Data

We collect the nine-years period data of the exchange rate data from the Wind database, from 1 January 2012 to 31 December 2021. The closing price of Australia's exchange rate to RMB (AUD/RMB), the closing price of the Euro exchange rate to RMB (EUR/RMB), the closing price of the Sterling's exchange rate to RMB (GBP/RMB), and the closing price of the Ruble's exchange rate to RMB (RUB/RMB) are selected as empirical data.

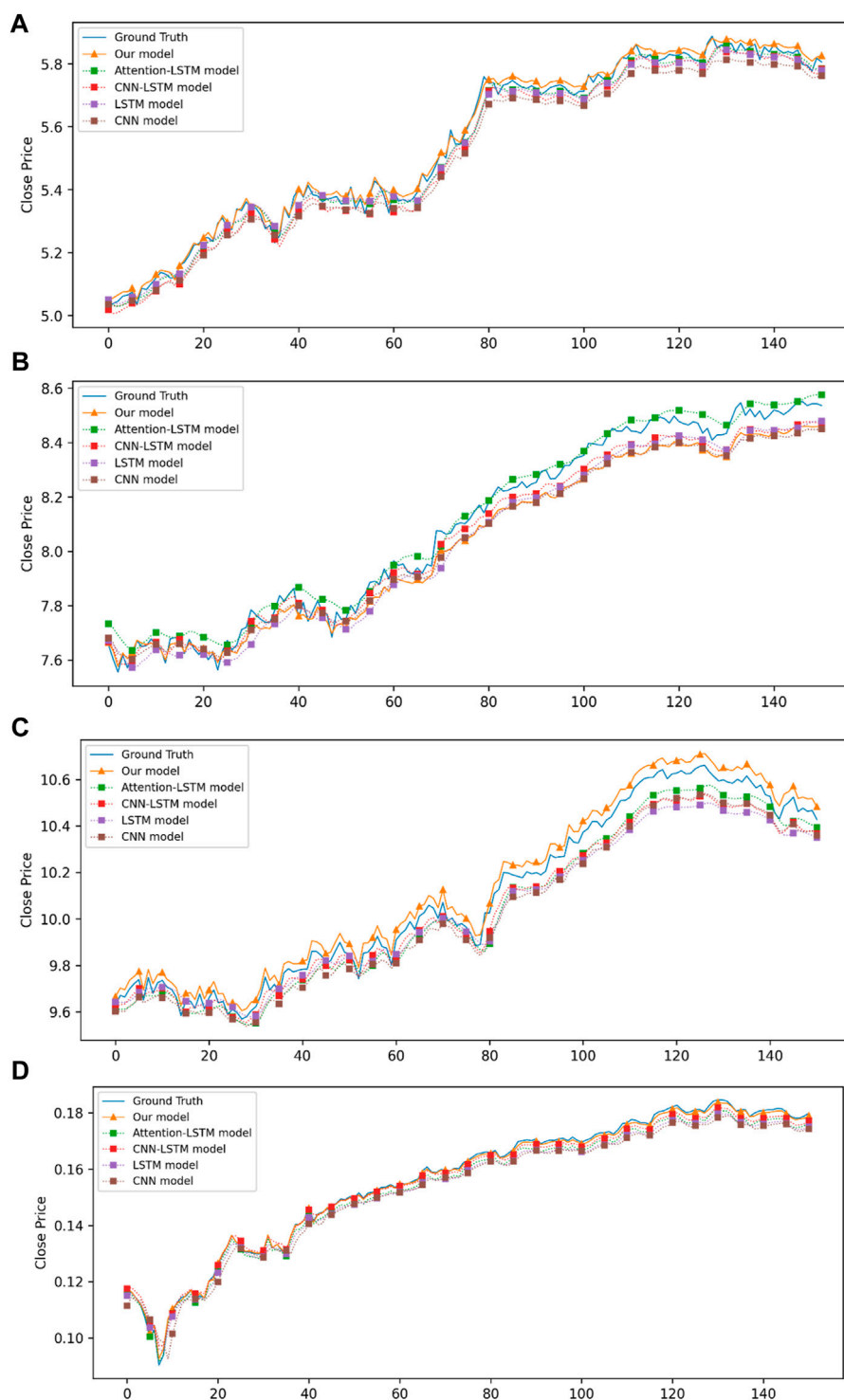


FIGURE 6
Plots of prediction results of each comparison model.

The data consists of two parts. The first part introduces the closing prices of exchange rates of other countries in each forecast data set. The second part consists of the closing, opening, lowest, and highest prices, which are extracted from the forecast data.

3.2 Test indicators

We use the mean absolute error (MAE), mean absolute percentage error (MSE), root mean squared error (RMSE), and R^2 as evaluation indices which read,

$$MAE = \frac{1}{m} \sum_{i=1}^m |y_i - \hat{y}_i| \quad (1)$$

$$MSE = \frac{1}{m} \sum_{i=1}^m (y_i - \hat{y}_i)^2 \quad (2)$$

$$RMSE = \sqrt{\frac{1}{m} \sum_{i=1}^m (y_i - \hat{y}_i)^2} \quad (3)$$

$$R^2 = 1 - \frac{\sum_i (\hat{y}^{(i)} - y_i)^2}{\sum_i (\bar{y} - y_i)^2} \quad (4)$$

In the above equation, \hat{y}_i and y_i represent the predicted and real data, respectively. Lower MAE, MSE, and RMSE and larger R^2 values represent better prediction performance of the model.

We use the DM test [18–20] improved by Harvey et al. to perform a robustness test.

$$DM = \frac{\bar{D}}{\sigma_D} \quad (5)$$

$$D = e_1^2 - e_2^2 \quad (6)$$

where e_1, e_2 represents the prediction errors of Models 1 and 2. \bar{D} is the mean value of D . σ_D represents the standard deviation of D . Then, according to the DM value, we calculate the corresponding p -value in the standard normal distribution. When the p -value is greater than 0.05, Model 1 has the same effect as that of Model 2. When the p -value is less than 0.05, and the DM value is negative, Model one exhibits better performance. When the p -value is less than 0.05, and the DM value is positive, Model 2 exhibits better performance.

3.3 Characteristic screening analysis

We adopt the Pearson correlation coefficient and random forest to detect the two components. Figure 4 shows the Pearson coefficients between the closing prices of the forex data. We set 0.8 as the threshold value, that is, we preserve only the relationships with the absolute value of Pearson coefficients larger than 0.8 and filter out the others.

We select foreign exchange-related data with a cumulative percentage of 90% or more of the random forest feature importance ranking as the filtering condition. Figure 5 shows the results of the random forest algorithm for feature importance ranking.

3.4 Comparative experimental analysis

To verify the prediction effect of the proposed model, we conduct a comparative analysis between CNN [21], LSTM [22], CNN-LSTM [23], and attention-LSTM [24], which are deep learning models. Table 1 shows that the prediction effect of the LSTM model is higher than that of the CNN model. This indicates that the LSTM model with the introduction of a gating unit has better adaptability for the prediction of time-series data with a nonlinear nature. The prediction effect of the CNN-LSTM model was higher than that of the LSTM model. This indicates that the convolution operation of the CNN helps in extracting long time-series features. Compared with the other models, the proposed model achieves the best prediction results for each prediction index. This indicates that, relative to the simple model superimposed by CNN and LSTM, it is easier to mine the change rules in the time-series data.

Table 2 shows the results of the DM detection. Most p -values are less than 0.05, and the DM value is less than 0. This shows that this study's model is better than the other models in most cases. Relative to the CNN-LSTM model only on the GBP/RMB dataset, all p -values exceed 0.05. In this case, both models perform equally. Overall, the TCN model performs better than the other models.

To show the prediction effect of each model more intuitively, we visually integrate the prediction data. As shown in Figure 6 (for better visibility of the length of the graphs, we chose to plot the first 150 predictions in this study). The method proposed in this study can fit the real data better than the other comparative models. This indicates that the model has a certain degree of robustness.

4 Conclusion

We present a method for predicting the movement of the currency market based on the combined model. We also analyse the multiple characteristics of foreign exchange rates as inputs. The Pearson correlation coefficients and random forest characteristics are used as input filters. The findings show that the exchange rate has a high correlation with the target extraction features. The results of the simulated empirical data based on the EUR, RUB, AUD, and GBP show that the proposed approach for exchange rate prediction has stronger stability and accuracy than that of the traditional methods. This proposed approach can be used to provide recommendations regarding the currency market projections. This study also indicates that, when forecasting exchange rates, it is crucial to refer to the movement of exchange rate in other economies. Our future work will continue to mine features, other than the exchange rate data, to improve the robustness of the model.

Data availability statement

The original contributions presented in the study are included in the article/Supplementary Material, further inquiries can be directed to the corresponding author.

Author contributions

XL: conceptualization, methodology, formal analysis, software, writing—original draft preparation, writing—review and editing. XX: formal analysis, visualization, investigation, supervision. BG: data curation, writing—review and editing.

Funding

This work was supported by National Natural Science Foundation of China (Grants Nos. 72141304 and 71790594), Fundamental Research Funds for the Central Universities, Tianjin Development Program for Innovation and Entrepreneurship.

Conflict of interest

The authors declare that the research was conducted in the absence of any commercial or financial relationships that could be construed as a potential conflict of interest.

Publisher's note

All claims expressed in this article are solely those of the authors and do not necessarily represent those of their affiliated

organizations, or those of the publisher, the editors and the reviewers. Any product that may be evaluated in this article, or claim that may be made by its manufacturer, is not guaranteed or endorsed by the publisher.

References

1. Liu J. Impact of uncertainty on foreign exchange market stability: Based on the LT-TVP-VAR model. *China Finance Rev Int* (2020) 11:53–72. doi:10.1108/CFRI-07-2019-0112
2. Wu Y. The causes and challenges of low interest rates: Insights from basic principles and recent literature. *China Finance Rev Int* (2020) 11:145–69. doi:10.1108/CFRI-06-2020-0071
3. Mate C, Jiménez L. Forecasting exchange rates with the iMLP: New empirical insight on one multi-layer perceptron for interval time series (ITS). *Eng Appl Artif Intelligence* (2021) 104:104358. doi:10.1016/j.engappai.2021.104358
4. Cao H, Lin F, Li Y, Wu Y. Information flow network of international exchange rates and influence of currencies. *Entropy* (2021) 23:1696. doi:10.3390/e23121696
5. Antwi A, Kyei KA, Gill RS. The use of mutual information to improve value-at-risk forecasts for exchange rates. *IEEE Access* (2020) 8:179881–900. doi:10.1109/ACCESS.2020.3027631
6. Henrique BM, Sobreiro VA, Kimura H. Literature review: Machine learning techniques applied to financial market prediction. *Expert Syst Appl* (2019) 124:226–51. doi:10.1016/j.eswa.2019.01.012
7. Sezer OB, Gudelek MU, Ozbayoglu AM. Financial time series forecasting with deep learning: A systematic literature review: 2005–2019. *Appl Soft Comput J* (2020) 90:106181. doi:10.1016/j.asoc.2020.106181
8. Bai S, Kolter JZ, Koltun V. *An empirical evaluation of generic convolutional and recurrent networks for sequence modeling* (2018). *arXiv [Preprint]* arXiv:1803.01271.
9. Torres JF, Hadjout D, Sebaa A, Martinez-Alvarez F, Troncoso A. Deep learning for time series forecasting: A survey. *Big Data* (2021) 9:3–21. doi:10.1089/big.2020.0159
10. Soleymani F, Paquet E. Long-term financial predictions based on Feynman–Dirac path integrals, deep Bayesian networks and temporal generative adversarial networks. *Machine Learn Appl* (2022) 7:100255. doi:10.1016/j.mlwa.2022.100255
11. Totannanavar S. *Co-relation between the financial news articles and Stock prices and Stock Prediction*. Dublin: National College of Ireland (2019).
12. Wiese M, Knobloch R, Korn R, Kretschmer P. Quant GANs: Deep generation of financial time series. *Quantitative Finance* (2020) 20:1419–40. doi:10.1080/14697688.2020.1730426
13. Janssen P. *Attention based Temporal Convolutional Network for stock price prediction*. Utrecht: Utrecht University (2022).
14. Tan X, Zhang Z, Zhao X, Wang S. DeepPricing: Pricing convertible bonds based on financial time-series generative adversarial networks. *Financial Innovation* (2022) 8:64–38. doi:10.1186/s40854-022-00369-y
15. Lei B, Zhang B, Song Y. Volatility forecasting for high-frequency financial data based on web search index and deep learning model. *Mathematics* (2021) 9:320. doi:10.3390/math9040320
16. Dai W, An Y, Long W. Price change prediction of ultra high frequency financial data based on temporal convolutional network. *Proced Comp Sci* (2022) 199:1177–83. doi:10.1016/j.procs.2022.01.149
17. Zhang CX, Li J, Huang XF, Zhang JS, Huang HC. Forecasting stock volatility and value-at-risk based on temporal convolutional networks. *Expert Syst Appl* (2022) 207:117951. doi:10.1016/j.eswa.2022.117951
18. Dai PF, Xiong X, Zhang J, Zhou WX. The role of global economic policy uncertainty in predicting crude oil futures volatility: Evidence from a two-factor GARCH-MIDAS model. *Resour Pol* (2022) 78:102849. doi:10.1016/j.resourpol.2022.102849
19. Dai PF, Xiong X, Huynh TLD, Wang J. The impact of economic policy uncertainties on the volatility of European carbon market. *J Commodity Markets* (2022) 26:100208. doi:10.1016/j.jcomm.2021.100208
20. Harvey D, Leybourne S, Newbold P. Testing the equality of prediction mean squared errors. *Int J Forecast* (1997) 13:281–91. doi:10.1016/S0169-2070(96)00719-4
21. Panda MM, Panda SN, Pattnaik PK. Forecasting foreign currency exchange rate using convolutional neural network. *Int J Adv Comp Sci Appl* (2022) 13:607–16. doi:10.14569/IJACSA.2022.0130272
22. Adekoya AF, Nti IK, Weyori BA. Long short-term memory network for predicting exchange rate of the Ghanaian cedi. *FinTech* (2021) 1:25–43. doi:10.3390/fintech1010002
23. Sun L, Xu W, Liu J. Two-channel attention mechanism fusion model of stock price prediction based on CNN-LSTM. *Trans Asian Low-Resource Lang Inf Process* (2021) 20:1–12. doi:10.1145/3453693
24. Zhang T, Zheng XQ, Liu MX. Multiscale attention-based LSTM for ship motion prediction. *Ocean Eng* (2021) 230:109066. doi:10.1016/j.oceaneng.2021.109066



OPEN ACCESS

EDITED BY

Dun Han,
Jiangsu University, China

REVIEWED BY

Mingtao Li,
Taiyuan University of Technology, China
Xiaoguang Zhang,
Shanxi University, China
Zhang Lei,
North University of China, China

*CORRESPONDENCE

Xinghua Chang,
✉ xh_chang@126.com

SPECIALTY SECTION

This article was submitted to Social
Physics,
a section of the journal
Frontiers in Physics

RECEIVED 04 November 2022

ACCEPTED 28 December 2022

PUBLISHED 12 January 2023

CITATION

Chang X (2023), Study on an SIR rumor propagation model with an interaction mechanism on WeChat networks. *Front. Phys.* 10:1089536. doi: 10.3389/fphy.2022.1089536

COPYRIGHT

© 2023 Chang. This is an open-access article distributed under the terms of the [Creative Commons Attribution License \(CC BY\)](#). The use, distribution or reproduction in other forums is permitted, provided the original author(s) and the copyright owner(s) are credited and that the original publication in this journal is cited, in accordance with accepted academic practice. No use, distribution or reproduction is permitted which does not comply with these terms.

Study on an SIR rumor propagation model with an interaction mechanism on WeChat networks

Xinghua Chang*

Department of Mathematics, Taiyuan University, Taiyuan, China

The spread of rumors does great harm to society. It will not only disrupt the social order but also damage public interests and even cause public safety and social shock. With the development of social platforms, it has become a fertile ground for rumors to breed and spread. The WeChat group as a very popular social platform is an important medium of rumor spreading with accurate and fast characteristics. In this paper, in order to describe the dynamic characteristics of rumors spread in WeChat groups, a susceptible–infected–removed rumor propagation model with an interaction mechanism and population dynamics on WeChat groups is proposed. In order to analyze the dynamic characteristics of the system, the next-generation matrix method is used to calculate the basic reproduction number of the proposed model. Then, the stability of a disease-free equilibrium point and a positive equilibrium point of the system is analyzed in detail. Finally, the accuracy of the analysis results is verified by numerical simulation. The research results are of great significance for controlling the rumors spread in WeChat groups.

KEYWORDS

rumor propagation model, WeChat group, basic reproduction number, interactive mechanism, population dynamics

1 Introduction

With the rapid development of Internet technology, it provides a broad space for information exchange among people. However, a large number of online rumors are generated without foundation or malice at the same time. These rumors not only seriously pollute the network environment and disrupt the public order but also seriously affect social stability and endanger national security [1–3]. If the public inadvertently become the audience of online rumors, it will gradually lose the right judgment and rational discrimination. In the long run, these audiences may believe these rumors and spread them widely on social networks [4]; [5].

The earliest research on the rumor propagation model originated in the 1960s. A large number of the existing rumor propagation models are derived from the epidemic model [6,7]. The DK model, as a basic rumor propagation model, was first proposed. [8,9] established a perfect mathematical theory and MK model for the rumor propagation model. However, the topological characteristics of social networks were not considered by DK and MK and were not suitable for the description of the rumor propagation mechanism in large-scale social networks. A matching model of rumor propagation based on dynamic behavior was proposed [10]. [11,12] established a small-world network rumor propagation model and calculated a propagation threshold. The dynamic mechanism of rumor propagation based on the scale-free network model was established [13–15]. The MK model was applied to the complex network model and described by the interactive Markov chain theory [16,17]. Furthermore, a rumor-spreading model in the homogeneous network called 2SIH2R was studied, in which

there are both spreader 1 (people who spread the rumor) and spreader 2 (people who spread the truth) [18]. Considering the heterogeneity of the network, a 2SIH2R model was studied with the mechanisms of discernment and confrontation in a heterogeneous network to examine the dissemination of the rumor and the truth [19]. Taking the management and control of rumors by relevant departments in real life into account, the SIDRQ rumor-spreading model with the forgetting mechanism, immune mechanism, and suspicion mechanism and guides on a uniform network was established [20]. A novel susceptible–exposed–infected–recovered (SEIR)-delayed rumor propagation model with saturation incidence on heterogeneous networks was devoted to investigation [21].

The rumor propagation model with the forgetting mechanism on the online social blog LiveJournal was considered [22]. The results showed that there was an average threshold of influencing rumor saturation in LiveJournal. A mechanism based on the thermal theory was proposed to analyze the spread of rumors on large-scale social networks [23]. The results showed that the initial rumor maker and the probability of sending the rumor were greatly affected by the attraction of the rumor. The influence of the network structure on rumor propagation was studied [24]. The social reinforced rumor propagation model based on two-way emotion was considered [25]. A novel SIR susceptible–infected–removed (SIR) information propagation model based on the characteristics of the microblog was constructed [26]. However, in the real online social network, due to the influence of characteristics, educational background, personal legal awareness, and some other factors, some people cannot determine the authenticity of rumors when they are exposed to them. So, they will not spread immediately, which is a hesitation state. The rumor propagation model with the characteristics of the hesitation state was discussed, yet the conversion of hesitant nodes to immune nodes was not considered [27]. An SEIR rumor propagation model of heterogeneous networks was proposed and analyzed for propagation dynamics of the microblog rumor [28]. In order to study the influence of forcing silence on spreaders, a rumor propagation model with a silence-forcing function in online social networks was proposed [29]. By incorporating the dissemination of a rumor through groups in social and mobile networks and by considering the people's cognitive factor (hesitate and forget), a new model on the rumor spreading process was presented [30].

In recent years, considering the individual activity and refutation mechanism simultaneously, a new multifactor model was proposed [31]. The structure of patches (nodes) is divided by connectivity distribution on metapopulation networks. A lot of research results for the dynamics of the infectious disease model among patches were invented based on the reaction–diffusion process [32–34]. Many epidemic models with demographic characteristics (such as birth and death) were considered [35]. In addition, some research results also considered the prevention and control strategies of rumor propagation [36,37].

WeChat, as a free application, is launched by Tencent to provide instant messaging services for intelligent terminals, including public platforms, circle of friends, message push, and other functions. As an important and popular social form, WeChat groups are widely used by the public. Therefore, WeChat groups have also become the hotbed of rumor propagation, which has the characteristics of accurate infection and rapid diffusion. Therefore, in this paper, an SIR rumor propagation model with an interaction mechanism and population dynamics on WeChat networks is proposed.

TABLE 1 Description of symbols.

| Symbol | Description |
|----------------|--------------------------------------------------------------------------------------------------|
| $\rho_{Si}(t)$ | Density of ignorants with degree i in the patches at time t |
| $\rho_S(t)$ | Density of ignorants in the whole all patch network at time t , then |
| | $\rho_S(t) = \sum_{i=1} p(i) \rho_{Si}(t)$, where $p(i)$ is the probability of the patches with |
| | degree i |
| $\rho_{Ii}(t)$ | Density of spreaders with degree i in the patches at time t |
| $\rho_I(t)$ | Density of spreaders in the whole all patch network at time t , then |
| | $\rho_I(t) = \sum_{i=1} p(i) \rho_{Ii}(t)$, where $p(i)$ is the probability of the patches with |
| | degree i |
| $\rho_{Ri}(t)$ | Density of stiflers with degree i in the patches at time t |
| $\rho_R(t)$ | Density of stiflers in the whole all patch network at time t , then |
| | $\rho_R(t) = \sum_{i=1} p(i) \rho_{Ri}(t)$, where $p(i)$ is the probability of the patches with |
| | degree i |

In Section 2, an SIR rumor propagation model with an interaction mechanism and population dynamics on WeChat networks is proposed. In order to analyze the dynamic characteristics of the system, the next-generation matrix method is used to calculate the basic reproduction number of rumor propagation. Then, the stability of a disease-free equilibrium point and a positive equilibrium point of the system is analyzed in detail. In Section 3, the accuracy of the analysis results is verified by numerical simulation. In the last section, we discuss and conclude the results of this paper.

2 Main content

In this section, an SIR rumor propagation model with an interaction mechanism and population dynamics on WeChat networks will be considered. Assume that each WeChat group is regarded as a patch (node), in which the particles (group members) construct a fully coupled network. From the perspective of rumor audience, we can divide particles into three categories in the patches: ignorants (S), spreaders (I), and stiflers (R). The symbols of population classification are shown in Table 1.

In WeChat groups, people will spread rumors from one WeChat group to other WeChat groups through forwarding and sharing, which forms an interactive mechanism for rumor spreading. We use a density symbol ρ , which means the proportion of particles in a patch. Therefore, we consider the population dynamics and interaction mechanism among patches, the rumor dynamics in the i th patch is given by the following expression.

$$\begin{cases} \frac{d\rho_{Si}(t)}{dt} = B - \beta\rho_{Si}\rho_{Ii} - \mu\rho_{Si} - D_S\rho_{Si} + D_S\frac{i}{\langle k \rangle}\rho_S, \\ \frac{d\rho_{Ii}(t)}{dt} = \beta\rho_{Si}\rho_{Ii} - \mu\rho_{Ii} - \gamma\rho_{Ii}\rho_{Ri} - D_I\rho_{Ii} + D_I\frac{i}{\langle k \rangle}\rho_I, \\ \frac{d\rho_{Ri}(t)}{dt} = \gamma\rho_{Ii}\rho_{Ri} - \mu\rho_{Ri} - D_R\rho_{Ri} + D_R\frac{i}{\langle k \rangle}\rho_R, \end{cases} \quad (1)$$

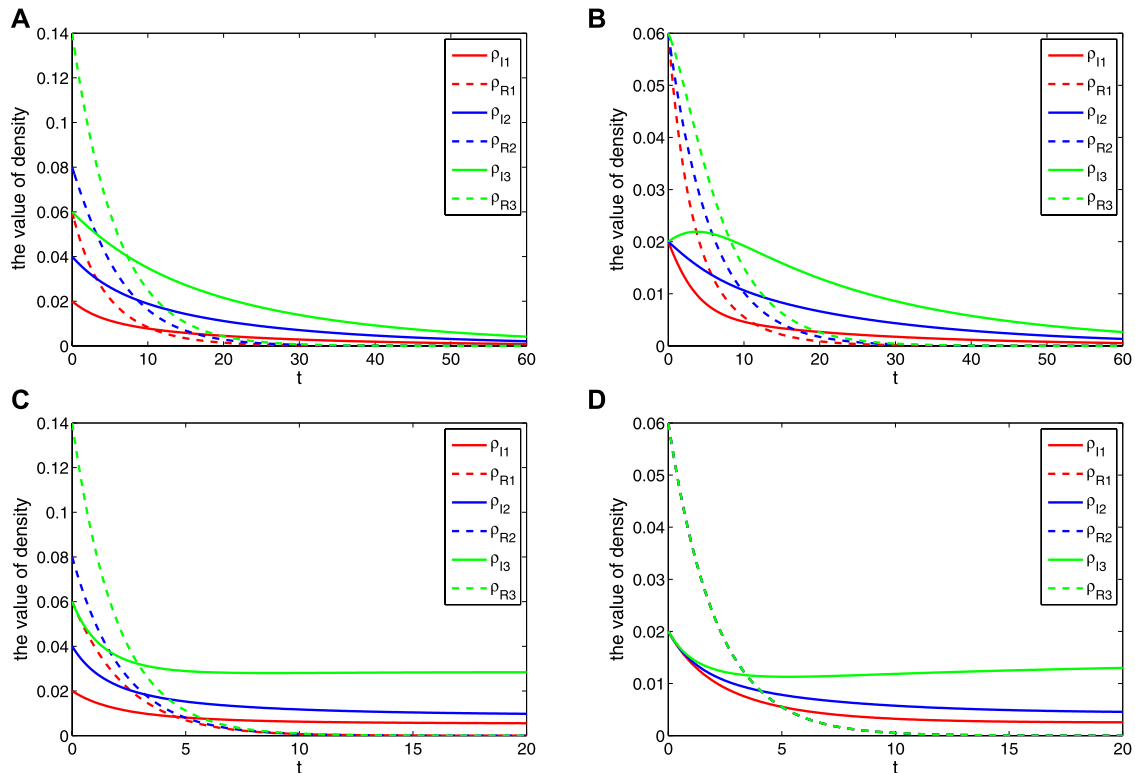


FIGURE 1
Effect of different newly added rates on the stability of rumor spreading.

where B is the rate of newly added ignorants with degree i in WeChat groups. μ is the rate of ignorants, spreaders, and stiflers who exit from WeChat group with degree i . β is the rate of conversion from ignorants to spreaders. γ is the rate of conversion from spreaders to stiflers. D_S is the positive or negative interaction rate of ignorants in one WeChat group with other WeChat groups. D_I is the positive or negative interaction rate of spreaders in one WeChat group with other WeChat groups. D_R is the positive or negative interaction rate of stiflers in one WeChat group with other WeChat groups. $\langle k \rangle$ is the average degree of the whole WeChat group networks.

Next, we analyze the dynamic behavior of system (2.1). According to system (2.1), we can obtain Eq. 2 as follows:

$$\begin{cases} B - \beta \rho_{Si}^* \rho_{Ii}^* - \mu \rho_{Si}^* - D_S \rho_{Si}^* + D_S \frac{i}{\langle k \rangle} \rho_S^* = 0, \\ \beta \rho_{Si}^* \rho_{Ii}^* - \mu \rho_{Ii}^* - \gamma \rho_{Ii}^* \rho_{Ri}^* - D_I \rho_{Ii}^* + D_I \frac{i}{\langle k \rangle} \rho_I^* = 0, \\ \gamma \rho_{Ii}^* \rho_{Ri}^* - \mu \rho_{Ri}^* - D_R \rho_{Ri}^* + D_R \frac{i}{\langle k \rangle} \rho_R^* = 0. \end{cases} \quad (2)$$

The dynamic behavior analysis of rumor spreading is closely related to the disease-free equilibrium. Let $\rho_{Ii}^* = 0$ and $\rho_{Ri}^* = 0$, then we obtain the equation as follows:

$$B - \mu \rho_{Si}^* - D_S \left(\rho_{Si}^* - \frac{i}{\langle k \rangle} \rho_S^* \right) = 0. \quad (3)$$

Therefore, the disease-free equilibrium of model (2.1) can be calculated and given by the following equation:

$$\rho_{Si}^* = \frac{B + D_S \frac{i}{\langle k \rangle} \rho^0}{\mu + D_S}, \rho_{Ii}^* = 0, \rho_{Ri}^* = 0, \quad (4)$$

where $\rho^0 = \rho_S^* + \rho_I^* + \rho_R^* = \frac{B}{\mu}$.

Linearizing Eq. 1 around the disease-free equilibrium $(\rho_{Si}^*, 0, 0)$, it follows that the Jacobian matrix of Eq. 1 is a block matrix, which is given as follows:

$$\begin{pmatrix} (\mu + D_S)(A - E) & \text{diag}(-\beta \rho_{Si}^*) & O \\ O & (\mu + D_I + \gamma)(A - E) + \text{diag}(\beta \rho_{Si}^*) & O \\ O & O & (\mu + D_R)(A - E) \end{pmatrix},$$

where each block is an $N \times N$ matrix with N being the number of degrees in the metapopulation, O is the null matrix, E is the identity matrix, $\text{diag}(a_i)$ denotes a diagonal matrix whose i th element is a_i , and A is the connectivity matrix. According to the eigenvalues of matrix A , in order to ensure the stability of the disease-free equilibrium point of system (2.1), the following inequality needs to be satisfied:

$$1 < \frac{\langle k \rangle}{i_{\max} \rho^0} \frac{(\mu + D_S)(\mu + \gamma + D_I)(\mu + D_R) - \beta B}{\beta D_S}.$$

Then, the basic reproduction number R_0 can be obtained as follows:

$$R_0 = \frac{i_{\max} \rho^0}{\langle k \rangle} \frac{\beta D_S}{(\mu + D_S)(\mu + \gamma + D_I)(\mu + D_R) - \beta B}, \quad (5)$$

where i_{\max} represents the max degree of the particles.

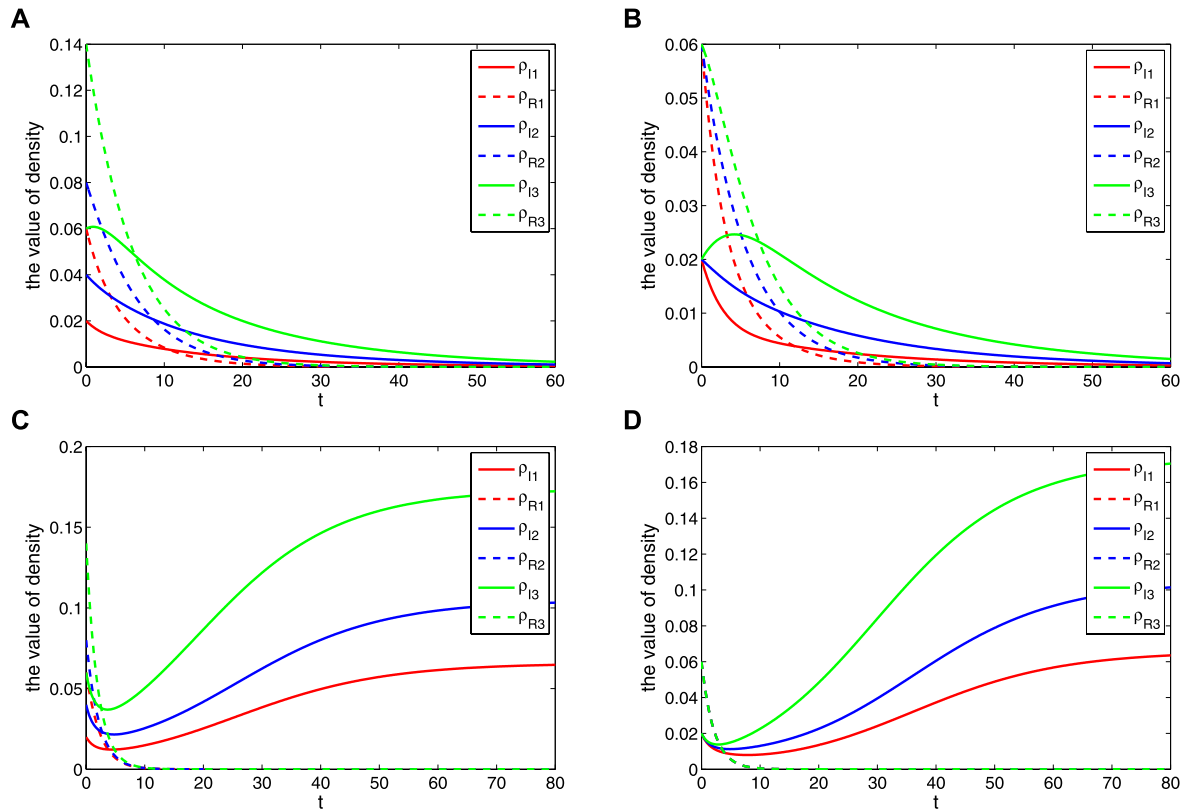


FIGURE 2
Effect of different infection rates on the stability of rumor spreading.

Theorem 2.1: If $R_0 < 1$, system (2.1) has a unique disease-free equilibrium, and it is globally asymptotically stable; if $R_0 > 1$, the disease-free equilibrium is unstable. **Proof.** In order to determine the global stability of the disease-free equilibrium point, we define the Lyapunov function $V = \frac{1}{2}\rho_{Ii}^2$ ([38]). We have

$$\begin{aligned} \frac{dV}{dt} &= \rho_{Ii} \frac{d\rho_{Ii}}{dt} \\ &= \left(\frac{i\rho^0}{\langle k \rangle} \beta D_S + \beta B - (\mu + D_S)(\mu + \gamma + D_I) \right) \rho_{Ii}^2 \\ &\leq \left(\frac{i_{\max} \rho^0}{\langle k \rangle} \beta D_S + \beta B - (\mu + D_S)^2 (\mu + \gamma + D_I) \right) \rho_{Ii}^2 \\ &= (R_0 - 1) \rho_{Ii}^2. \end{aligned}$$

If $R_0 < 1$, then $(R_0 - 1)\rho_{Ii}^2 < 0$.

Also, we have $\frac{dV}{dt} \leq 0$ and $\frac{dV}{dt} = 0$ if and only if $\rho_{Ii} = 0$. By using the principle of the LaSalle invariant set, we can see that the disease-free equilibrium point of system (2.1) is globally asymptotically stable when $R_0 < 1$. If $R_0 > 1$, the disease-free equilibrium is unstable. **Theorem 2.2:** If $R_0 > 1$, system (2.1) has a unique endemic equilibrium $E^* = \{\rho_{I1}^*, \rho_{I2}^*, \dots, \rho_{In}^*\}$, where E^* is globally asymptotically stable. **Proof.** We define a function using the second equation of system (2.1) as follows: $f: G \rightarrow G$, $G = \{\rho_{Ii}(t) | t \in R^+, \rho_{Ii}(t) \geq 0\}$ yields

$$f(\rho_{Ii}(t)) = \beta \rho_{Si} \rho_{Ii} - \mu \rho_{Ii} - \gamma \rho_{Ii} \rho_{Ri} - D_I \rho_{Ii} + D_I \frac{i}{\langle k \rangle} \rho_{Ii}. \quad (6)$$

By using Corollary 3.2 of [39], we know that $f: G \rightarrow G$ is a continuous differentiable function, and $Df(\rho_{Ii}(t))$ is irreducible for any $\rho_{Ii}(t) > 0$, $\rho_{Ii}(t) \in G$; then, for any $\theta \in (0, 1)$ and $\rho_{Ii}(t) > 0$, we have

$$\begin{aligned} f(\sigma \rho_{Ii}(t)) &= \beta \rho_{Si} \sigma \rho_{Ii} - \mu \sigma \rho_{Ii} - \gamma \sigma \rho_{Ii} \rho_{Ri} - D_I \sigma \rho_{Ii} + D_I \frac{i}{\langle k \rangle} \sigma \rho_{Ii} \\ &= \beta (\rho_{Ni} - \rho_{Ri} - \sigma \rho_{Ii}) \sigma \rho_{Ii} - \mu \sigma \rho_{Ii} - \gamma \sigma \rho_{Ii} \rho_{Ri} - D_I \sigma \rho_{Ii} + D_I \frac{i}{\langle k \rangle} \sigma \rho_{Ii} \\ &\geq \sigma \beta (\rho_{Ni} - \rho_{Ri} - \rho_{Ii}) \rho_{Ii} - \sigma \gamma \rho_{Ii} \rho_{Ri} - \sigma D_I \rho_{Ii} + \sigma D_I \frac{i}{\langle k \rangle} \rho_{Ii} \\ &= \sigma f(\rho_{Ii}). \end{aligned}$$

Hence, $f(\rho_{Ii}(t))$ is sublinear. According to Lemma 2.1 and Corollary 3.2 in (X.Q [40]), system (2.1) has a unique endemic equilibrium E^* , which is globally asymptotically stable. **Theorem 2.3:** If $R_0 > 1$, system (2.1) has a unique endemic equilibrium $E^* = \{\rho_{S1}^*, \rho_{S2}^*, \dots, \rho_{Sn}^*, \rho_{I1}^*, \rho_{I2}^*, \dots, \rho_{In}^*, \rho_{R1}^*, \rho_{R2}^*, \dots, \rho_{Rn}^*\}$, where E^* is globally asymptotically stable. **Proof.** Set $\phi(t): R^+ \rightarrow R^+$; let it be a solution semiflow of the third equation of system (2.1), and $\phi(t)$ is a finite set. Assume ω is an internal propagation chain set of $\phi(t)$ [40].

Obviously, there are only two equilibrium points for the system, if $R_0 \leq 1$, there is a disease-free equilibrium point E_0 . If $R_0 > 1$, there is a unique endemic equilibrium point E^* .

Next, we prove that ω has only one endemic equilibrium, that is, $\omega = \{E^*\}$.

If the aforementioned conclusion is not true, then $\omega = \{E_0\}$. Therefore, there is

$$\lim_{t \rightarrow \infty} \rho_{Si}(t) = \frac{B + D_S \frac{i}{\langle k \rangle} \rho^0}{\mu + D_S}, \lim_{t \rightarrow \infty} \rho_{Ii}(t) = 0, \lim_{t \rightarrow \infty} \rho_{Ri}(t) = 0. \quad (7)$$

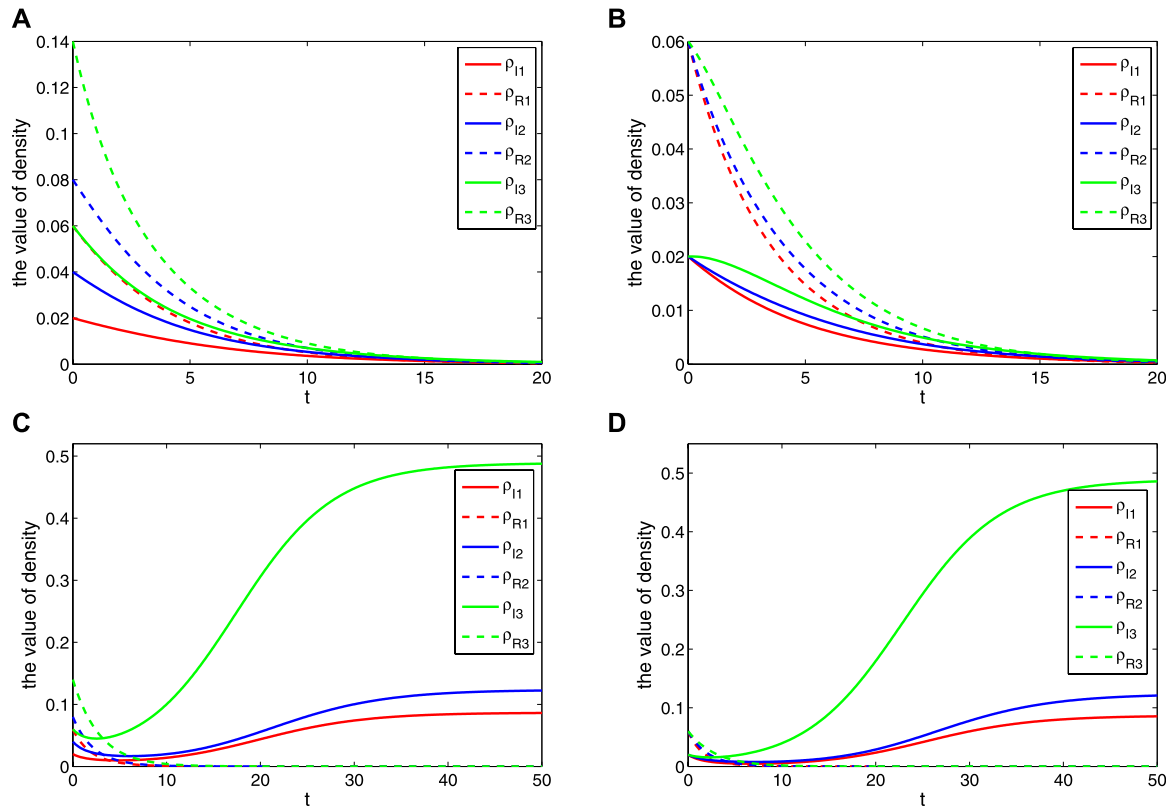


FIGURE 3
Effect of different interaction rates on the stability of rumor spreading.

If $R_0 > 1$, the spectral radius $s(M_1)$ is defined for the eigenmatrix FV^{-1} of system (2.1) at E_0 [39]. Here, the expressions of F and V are followed as

$$F = \begin{pmatrix} \beta \rho_{Si} \rho_{Ii} \\ O \\ \gamma \rho_{Ii} \rho_{Ri} \end{pmatrix}, V = \begin{pmatrix} \mu \rho_{Ii} + \gamma \rho_{Ii} \rho_{Ri} + D_I \rho_{Ii} - D_I \frac{i}{\langle k \rangle} \rho_I \\ -B + \beta \rho_{Si} \rho_{Ii} + \mu \rho_{Si} + D_S \rho_{Si} - D_S \frac{i}{\langle k \rangle} \rho_S \\ \mu \rho_{Ri} + D_R \rho_{Ri} - D_R \frac{i}{\langle k \rangle} \rho_R \end{pmatrix}.$$

Choose any one $\varepsilon > 0$ small enough to make $s(M_1 + \varepsilon M_2) > 0$, where $M_2 = \text{diag}(\sigma_1, \sigma_2, \dots, \sigma_n)$. Then, there is 1 t' , for any $t > t'$ so that

$$\beta(\rho_{Ni} - \rho_{Ri} - \rho_{Ii}) > \beta \rho_{Ni}^* - \varepsilon, \quad (8)$$

where $\rho_{Ni}^* = \frac{B + D_S \frac{i}{\langle k \rangle} \rho^0}{\mu + D_S}$. Hence, we have

$$\frac{d\rho_{Ii}(t)}{dt} > \beta(\rho_{Ni}^* - \varepsilon)\rho_{Ii}(t) - \mu \rho_{Ii} - \gamma \rho_{Ii} \rho_{Ri} - D_I \rho_{Ii} + D_I \frac{i}{\langle k \rangle} \rho_I. \quad (9)$$

Let v be a positive eigenvector of $M_1 + \varepsilon M_2$ associated with $s(M_1 + \varepsilon M_2)$, then choose an arbitrarily small number ζ satisfying $I \geq \zeta v$. According to the comparison theorem, we have

$$\rho_{Ii}(t) \geq e^{s(M_1 + \varepsilon M_2)(t-t')} v, t \geq t'. \quad (10)$$

Therefore, if $t \rightarrow \infty$, this is contrary to the hypothesis $\lim_{t \rightarrow \infty} \rho_{Ii}(t) = 0$, then the unique positive equilibrium solution E^* of the system is globally asymptotically stable.

3 Numerical simulation

In this section, we present numerical simulations to support the results obtained in previous sections. In order to simulate the solutions of the system, we consider the case that the model with three patches. Suppose that the average degree of interaction among each patch and the other two patches is 1, 2, and 3, respectively, and the average degree of the whole network is 10. First, the system with three patches is considered by the following equation:

$$\begin{cases} \frac{d\rho_{S1}(t)}{dt} = B_1 - \beta_1 \rho_{S1} \rho_{I1} - \mu_1 \rho_{S1} - D_{S1} \left(\rho_{S1} - \frac{1}{10} (\rho_{S1} + \rho_{S2} + \rho_{S3}) \right), \\ \frac{d\rho_{I1}(t)}{dt} = \beta_1 \rho_{S1} \rho_{I1} - \mu_1 \rho_{I1} - \gamma_1 \rho_{I1} \rho_{R1} - D_{I1} \left(\rho_{I1} - \frac{1}{10} (\rho_{I1} + \rho_{I2} + \rho_{I3}) \right), \\ \frac{d\rho_{R1}(t)}{dt} = \gamma_1 \rho_{I1} \rho_{R1} - \mu_1 \rho_{R1} - D_{R1} \left(\rho_{R1} - \frac{1}{10} (\rho_{R1} + \rho_{R2} + \rho_{R3}) \right), \\ \frac{d\rho_{S2}(t)}{dt} = B_2 - \beta_2 \rho_{S2} \rho_{I2} - \mu_2 \rho_{S2} - D_{S2} \left(\rho_{S2} - \frac{1}{5} (\rho_{S1} + \rho_{S2} + \rho_{S3}) \right), \\ \frac{d\rho_{I2}(t)}{dt} = \beta_2 \rho_{S2} \rho_{I2} - \mu_2 \rho_{I2} - \gamma_2 \rho_{I2} \rho_{R2} - D_{I2} \left(\rho_{I2} - \frac{1}{5} (\rho_{I1} + \rho_{I2} + \rho_{I3}) \right), \\ \frac{d\rho_{R2}(t)}{dt} = \gamma_2 \rho_{I2} \rho_{R2} - \mu_2 \rho_{R2} - D_{R2} \left(\rho_{R2} - \frac{1}{5} (\rho_{R1} + \rho_{R2} + \rho_{R3}) \right), \\ \frac{d\rho_{S3}(t)}{dt} = B_3 - \beta_3 \rho_{S3} \rho_{I3} - \mu_3 \rho_{S3} - D_{S3} \left(\rho_{S3} - \frac{3}{10} (\rho_{S1} + \rho_{S2} + \rho_{S3}) \right), \\ \frac{d\rho_{I3}(t)}{dt} = \beta_3 \rho_{S3} \rho_{I3} - \mu_3 \rho_{I3} - \gamma_3 \rho_{I3} \rho_{R3} - D_{I3} \left(\rho_{I3} - \frac{3}{10} (\rho_{I1} + \rho_{I2} + \rho_{I3}) \right), \\ \frac{d\rho_{R3}(t)}{dt} = \gamma_3 \rho_{I3} \rho_{R3} - \mu_3 \rho_{R3} - D_{R3} \left(\rho_{R3} - \frac{3}{10} (\rho_{R1} + \rho_{R2} + \rho_{R3}) \right). \end{cases} \quad (11)$$

Next, we consider the effect of different parameters on the stability of system (3.1), which is analyzed with two different cases of the initial values and is given as follows.

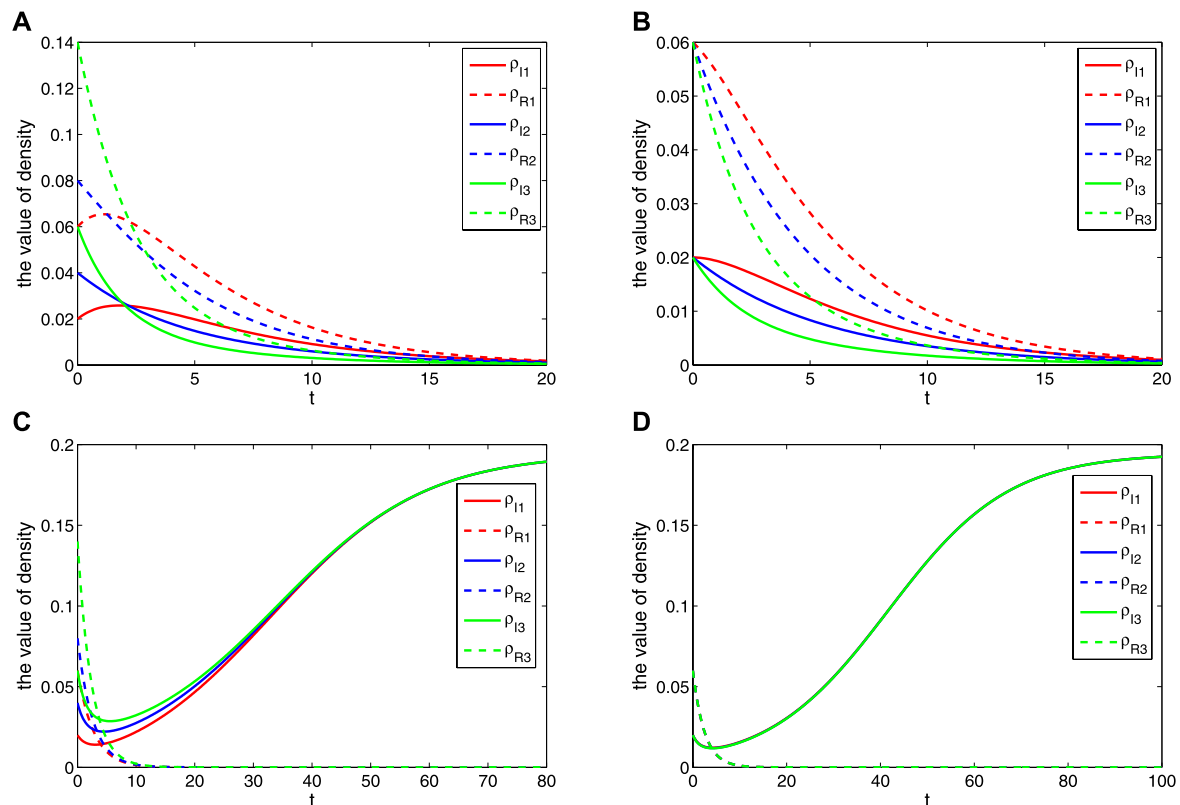


FIGURE 4
Effect of different recovery rates on the stability of rumor spreading.

Case 1: $\rho_{SI}(0)$, $\rho_{II}(0)$, $\rho_{RI}(0)$, $\rho_{SI}(0)$, $\rho_{II}(0)$, $\rho_{RI}(0)$, $\rho_{SI}(0)$, $\rho_{II}(0)$, and $\rho_{RI}(0)$ are, respectively, equal to 0.1, 0.02, 0.06, 0.2, 0.04, 0.08, 0.3, 0.06, and 0.14.

Case 2: $\rho_{SI}(0)$, $\rho_{II}(0)$, $\rho_{RI}(0)$, $\rho_{SI}(0)$, $\rho_{II}(0)$, $\rho_{RI}(0)$, $\rho_{SI}(0)$, $\rho_{II}(0)$, and $\rho_{RI}(0)$ are, respectively, equal to 0.25, 0.02, 0.06, 0.25, 0.02, 0.06, 0.25, 0.02, and 0.06.

Based on the aforementioned two cases of initial values, we consider the stability of the system with the effect of different factors, such as the newly added rate, infection rate, interaction rate, and recovery rate. Then, assume

$$D_{S1} = D_{I1} = D_{R1} = D_1, D_{S2} = D_{I2} = D_{R2} = D_2, D_{S3} = D_{I3} = D_{R3} = D_3.$$

3.1 Different newly added rates

Here, the parameters $B_1 = 0.01$, $B_2 = 0.04$, $B_3 = 0.07$, $\beta_1 = \beta_2 = \beta_3 = 0.5$, $\mu_1 = \mu_2 = \mu_3 = 0.02$, $D_1 = D_2 = D_3 = 0.4$, and $\gamma_1 = \gamma_2 = \gamma_3 = 0.2$. According to Eq. 5, it can be calculated by $R_0 = 0.9537 < 1$. It can be seen that the spread of rumors is also increasing with the growth of the newly added rate, which is shown in Figure 1A and Figure 1B. However, the rumor will eventually die out for a long time with the growth of the newly added rate. When the parameters are set with $B_1 = 0.3$, $B_2 = 0.5$, and $B_3 = 0.7$, it can be calculated by $R_0 = 1.3636 > 1$. It can be seen that the spread of rumors formed the stable state of a

local equilibrium point with the growth of the newly added rate, which is shown in Figure 1C and Figure 1D.

3.2 Different infection rates

Here, the parameters $B_1 = B_2 = B_3 = 0.03$, $\beta_1 = 0.2$, $\beta_2 = 0.5$, $\beta_3 = 0.8$, $\mu_1 = \mu_2 = \mu_3 = 0.02$, $D_1 = D_2 = D_3 = 0.4$, and $\gamma_1 = \gamma_2 = \gamma_3 = 0.2$. According to Eq. 5, it can be calculated by $R_0 = 0.9537 < 1$. It can be seen that the spread of rumors also increased with the increase of the infection rate, which is shown as Figure 2A and Figure 2B. However, because of the existence of suppressors, the rumors will eventually die out. When the parameters are set with $B_1 = B_2 = B_3 = 0.5$, $\beta_1 = 0.6$, $\beta_2 = 0.5$, and $\beta_3 = 0.4$, it can be calculated by $R_0 = 1.9474 > 1$. It can be seen that the spread of rumors formed the stable state of a local equilibrium point with the growth of the infection rate, which is shown in Figure 2C and Figure 2D.

3.3 Different interaction rates

Here, the parameters $B_1 = B_2 = B_3 = 0.03$, $\beta_1 = \beta_2 = \beta_3 = 0.5$, $\mu_1 = \mu_2 = \mu_3 = 0.02$, $D_1 = 0.4$, $D_2 = 0.6$, $D_3 = 0.8$, and $\gamma_1 = \gamma_2 = \gamma_3 = 0.2$. According to Eq. 5, it can be seen that the spread of rumors also increased with the increase of the interaction rate, which is shown in Figure 3A and Figure 3B. However, because of the existence of suppressors, the rumors will eventually die out. When the parameters are set with $B_1 =$

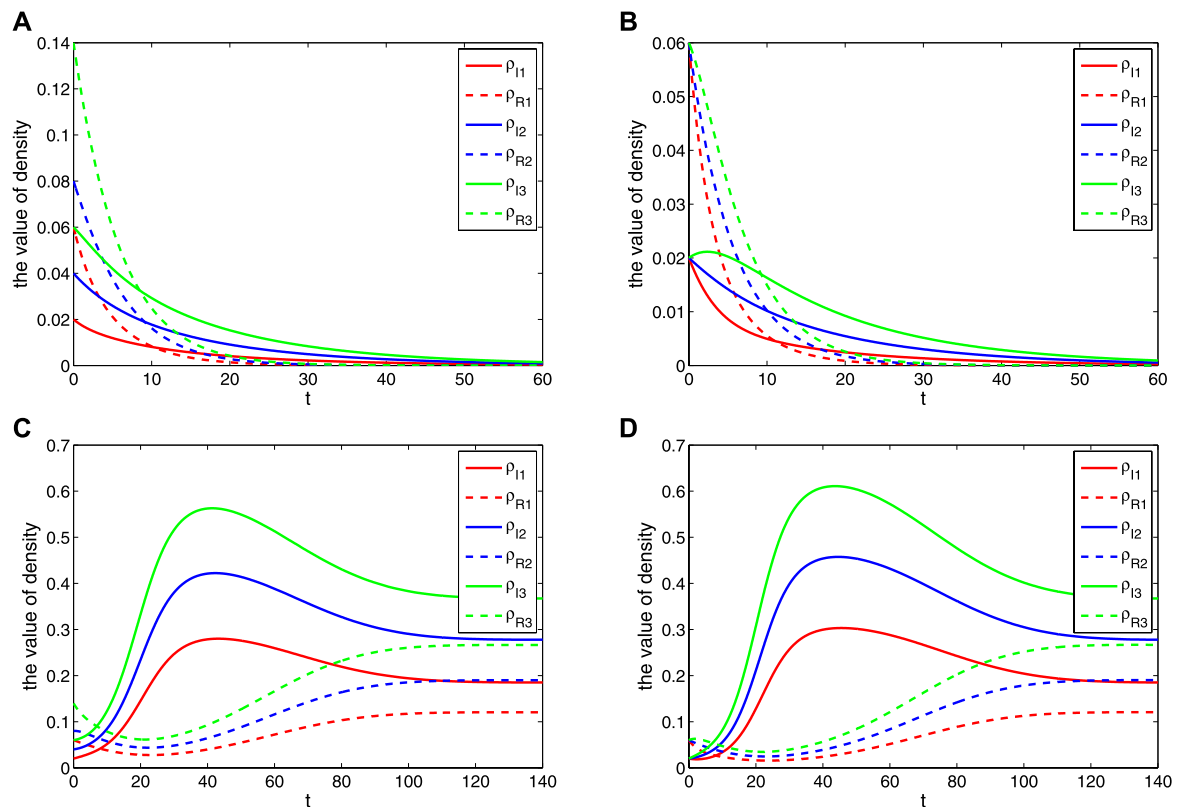


FIGURE 5
Effect of the degree of patches on the stability of rumor spreading.

$B_2 = B_3 = 0.5$, $D_1 = 0.4$, $D_2 = 0.6$, and $D_3 = 0.8$, it can be calculated by $R_0 = 1.3636 > 1$. It can be seen that the spread of rumors formed the stable state of a local equilibrium point with the growth of the interaction rate, which is shown in Figure 3C and Figure 3D.

3.4 Different recovery rates

Here, the parameters $B_1 = B_2 = B_3 = 0.03$, $\beta_1 = \beta_2 = \beta_3 = 0.5$, $\mu_1 = \mu_2 = \mu_3 = 0.02$, $D_1 = D_2 = D_3 = 0.4$, $\gamma_1 = 0.2$, $\gamma_2 = 0.5$, and $\gamma_3 = 0.8$. According to Eq. 5, it can be seen that the spread of rumors also increased with the increase of the recovery rate in a short term, which is shown in Figure 4A and Figure 4B. However, with the increasing number of suppressors, the rumors will eventually die out quickly. When the parameters are set with $B_1 = B_2 = B_3 = 0.5$, $\gamma_1 = 0.3$, $\gamma_2 = 0.5$, and $\gamma_3 = 0.7$, it can be calculated by $R_0 = 2.160 > 1$. It can be seen that the spread of rumors formed the stable state of a local equilibrium point with the growth of the recovery rate, which is shown in Figure 4C and Figure 4D.

3.5 Increase in the degree of patches

Here, the parameters $B_1 = B_2 = B_3 = 0.03$, $\beta_1 = \beta_2 = \beta_3 = 0.5$, $\mu_1 = \mu_2 = \mu_3 = 0.02$, $D_1 = D_2 = D_3 = 0.4$, and $\gamma_1 = \gamma_2 = \gamma_3 = 0.2$; it can be seen that the spread of rumors also increased with the growth of the degree of patches in a short term, which is shown in Figure 5A and

Figure 5B. However, with the increasing number of suppressors, the rumors will eventually die out quickly. When the degree of patches is increased, namely, $\frac{1}{\langle k \rangle}$ are 0.2, 0.3, and 0.4, respectively. It can be seen from Figure 5C and Figure 5D that the stability of rumor spreading changes from the disease-free equilibrium to the local equilibrium.

4 Conclusion

The WeChat group is a very popular social platform and also an important medium for spreading rumors. Based on the classic SIR epidemic model, in this paper, an SIR rumor propagation model with an interaction mechanism and population dynamics on WeChat networks was proposed. In order to analyze the dynamic characteristics of the system, the next-generation matrix method is used to calculate the basic reproduction number of the system model. When $R_0 < 1$, the disease-free equilibrium was gradually stable. When $R_0 > 1$, the disease-free equilibrium was unstable. Then, the stability of a disease-free equilibrium point and a positive equilibrium point of the system is analyzed in detail. In numerical simulation, the influence of different parameters (the newly added rate, infection rate, interaction rate, recovery rate, and the degree of patches) on the stability of the system was considered. Meanwhile the accuracy of the analysis results was verified. The results of this study had a certain reference for controlling rumor spreading in the WeChat group.

Data availability statement

The original contributions presented in the study are included in the article/supplementary material; further inquiries can be directed to the corresponding author.

Author contributions

XC, the author, is fully responsible for the research work of this manuscript, including the modeling and analysis of infectious diseases, the simulation of infectious disease models, and the writing of the manuscript.

Funding

This research is supported by the China Postdoctoral Science Foundation under Grant 2021M692400 and the Fundamental Research Program of Shanxi Province under Grant 202203021211091.

References

1. Galam S. Modelling rumors: The no plane pentagon French hoax case. *Physica A* (2003) 320:571–80. doi:10.1016/s0378-4371(02)01582-0
2. Grein TW, Kamara KB, Rodier G, Plant AJ, Bovier P, Ryan MJ, et al. Rumors of disease in the global village: Outbreak verification. *Emerging Infect Dis* (2000) 6:97–102. doi:10.3201/eid0602.000201
3. Thomas S. Lies, damn lies, and rumors: An analysis of collective efficacy, rumors, and fear in the wake of Katrina. *Sociological Spectr* (2007) 27:679–703. doi:10.1080/02732170701534200
4. Liu DC. Rumor propagation in online social networks like twitter simulation study. In: 2011 The Third International Conference on Multimedia Information Networking and Security; Nov. 4 2011 to Nov. 6 2011; Shanghai, China (2011). p. 278–82.
5. Kim JH. A study on the factors affecting the behavior of spreading online rumors: Focusing on the rumor recipient's emotions. In: PACIS 2011 Proceedings; 7–11 July 2011; Pacific Asia, Brisbane, Queensland, Australia (2011). p. 98–106.
6. Anderson RM. *Infectious diseases of humans*. Oxford, United Kingdom: Oxford University Press (1992).
7. Hethcote H. The mathematics of infectious diseases. *SIAM Rev* (2000) 42:599–653. doi:10.1137/s0036144500371907
8. Daley DJ, Kendall DG. Epidemics and rumours. *Nature* (1964) 204:1118–8. doi:10.1038/2041118a0
9. Maki D. *Mathematical models and applications*. United States: Prentice-Hall (1973).
10. Sudbury A. The proportion of the population never hearing a rumour. *J Appl Probab* (1985) 22:443–6. doi:10.1017/s0021900200037906
11. Zanette D. Critical behavior of propagation on small-world networks. *Phys Rev E* (2001) 64:050901. doi:10.1103/physreve.64.050901
12. Zanette D. Dynamics of rumor propagation on small-world networks. *Phys Rev E* (2002) 65:041908. doi:10.1103/physreve.65.041908
13. Moreno Y, A P, Nekovee M. Dynamics of rumor spreading in complex networks. *Phys Rev E* (2004) 69:066130. doi:10.1103/physreve.69.066130
14. Moreno Y, A V, Nekovee M. Efficiency and reliability of epidemic data dissemination in complex networks. *Phys Rev E* (2004) 69:055101. doi:10.1103/physreve.69.055101
15. Moreno Y, Vespignani A., Pastor-Satorras R. Epidemic outbreaks in complex heterogeneous networks. *Eur Phys J* (2002) 26:521–9. doi:10.1140/epjb/e20020122
16. Nekovee M, Bianconi G, Moreno Y, Marsili M. Theory of rumour spreading in complex social networks. *Physica A* (2007) 374:457–70. doi:10.1016/j.physa.2006.07.017
17. Isham V, M N, Harden S. Stochastic epidemics and rumours on finite random networks. *Physica A* (2010) 389:561–76. doi:10.1016/j.physa.2009.10.001
18. Wang Y, Qing F, Ni YP. Spreading dynamics of a 2s1h2r rumor spreading model in the homogeneous network. *Complexity* (2021) 2021:1–9. doi:10.1155/2021/6693334
19. Wang Y, M Y, Qing F. Dynamics of 2s1h2r rumor-spreading model in a heterogeneous network. *Wireless Commun Mobile Comput* (2022) 2022:1–13. doi:10.1155/2022/7398387
20. Zhang W, X. L HL, Deng HY, Liu H. Dynamics of the rumor-spreading model with control mechanism in complex network. *J Math* (2022) 2022:1–17. doi:10.1155/2022/5700374
21. Chen SS, Jiang HJ, Li J. Dynamical behaviors and optimal control of rumor propagation model with saturation incidence on heterogeneous networks. *Chaos Solitons Fractals* (2020) 140:110206. doi:10.1016/j.chaos.2020.110206
22. Zhao LJ, J. C YC, J. W WH, Wang Q, Chen Y, Wang J, et al. Rumor spreading model with consideration of forgetting mechanism: A case of online blogging livejournal. *Physica A* (2011) 390:2619–25. doi:10.1016/j.physa.2011.03.010
23. Han S, Q. H Z, S. X A, Zhuang FZ, Shi Z, Ao X. Energy model for rumor propagation on social networks. *Physica A* (2014) 394:99–109. doi:10.1016/j.physa.2013.10.003
24. Zhou J, Li B, Liu ZH. Influence of network structure on rumor propagation. *Phys Lett A* (2007) 368:458–63. doi:10.1016/j.physleta.2007.01.094
25. Ma J, Tian Z, Li D. Rumor spreading in online social networks by considering the bipolar social reinforcement. *Physica A* (2016) 447:108–15. doi:10.1016/j.physa.2015.12.005
26. Su Q, Zhao X, Huang J. An information propagation model considering incomplete reading behavior in microblog. *Physica A* (2015) 419:55–63. doi:10.1016/j.physa.2014.10.042
27. Xia L, B. S YS, Jiang G. Rumor spreading models considering hesitating mechanism in complex social networks. *Physica A* (2015) 437:295–303. doi:10.1016/j.physa.2015.05.113
28. Liu QM, M S, Li T. The analysis of an seir rumor propagation model on heterogeneous network. *Physica A* (2017) 469:372–80. doi:10.1016/j.physa.2016.11.067
29. Zhu LH, Wang B. Stability analysis of a sair rumor spreading model with control strategies in online social networks. *Inf Sci* (2020) 526:1–19. doi:10.1016/j.ins.2020.03.076
30. Myilsamy K, Satheesh Kumar A, Kumar MS. Optimal control of a rumor model with group propagation over complex networks. *Int J Mod Phys C* (2021) 329(3):2150035. doi:10.1142/s0129183121500352

Acknowledgments

The authors would like to thank the referees for helpful comments which resulted in much improvement of the manuscript.

Conflict of interest

The author declares that the research was conducted in the absence of any commercial or financial relationships that could be construed as a potential conflict of interest.

Publisher's note

All claims expressed in this article are solely those of the authors and do not necessarily represent those of their affiliated organizations, or those of the publisher, the editors, and the reviewers. Any product that may be evaluated in this article, or claim that may be made by its manufacturer, is not guaranteed or endorsed by the publisher.

31. Li RQ, Li YW, Song Y, Jiang G. Rumor spreading model considering individual activity and refutation mechanism simultaneously. *IEEE Access* (2020) 8:63065–76. doi:10.1109/access.2020.2983249
32. Saldana J. Continuous-time formulation of reaction-diffusion processes on heterogeneous metapopulations. *Phys Rev E* (2008) 78:012902. doi:10.1103/physreve.78.012902
33. Juher D, Saldana J, Ripoll J. Analysis and Monte Carlo simulations of a model for the spread of infectious diseases in heterogeneous metapopulations. *Phys Rev Lett* (2009) 80:041920. doi:10.1103/physreve.80.041920
34. Masuda N. Effects of diffusion rates on epidemic spreads in metapopulation networks. *New J Phys* (2010) 12:093009. doi:10.1088/1367-2630/12/9/093009
35. Zhang F, Zhao SQ. A periodic epidemic model in a patchy environment. *J Math Anal Appl* (2007) 325:496–516. doi:10.1016/j.jmaa.2006.01.085
36. Tong X, Jiang H, Yu S, Li J. Dynamic analysis and optimal control of rumor spreading model with recurrence and individual behaviors in heterogeneous networks. *Entropy* (2022) 24:464. doi:10.3390/e24040464
37. Wang Y, L W, Qing F. Rumor dynamic model considering intentional spreaders in social network. *Discrete Dyn Nat Soc* (2022) 2022:1–10. doi:10.1155/2022/6044099
38. Zuo LX, Liu M. Effect of awareness programs on the epidemic outbreaks with time delay. *Abstract Appl Anal* (2014) 2:1–8. doi:10.1155/2014/940841
39. van den Driessche P, Watmough J. Reproduction numbers and sub-threshold endemic equilibria for compartmental models of disease transmission. *Math Biosci* (2002) 180:29–48. doi:10.1016/s0025-5564(02)00108-6
40. Zhao XQ. Global asymptotic behavior in some cooperative systems of functional differential equations. *Appl Math Quart* (1996) 4:421–44.



OPEN ACCESS

EDITED BY

Jianrong Wang,
Shanxi University, China

REVIEWED BY

Jun Hu,
Rey Juan Carlos University, Spain
Manman Yuan,
University of Science and Technology
Beijing, China

*CORRESPONDENCE

Jun Chen,
✉ dellohan815@gmail.com

SPECIALTY SECTION

This article was submitted to
Social Physics, a section of the journal
Frontiers in Physics

RECEIVED 17 August 2022

ACCEPTED 30 January 2023

PUBLISHED 02 March 2023

CITATION

Chen J, Wang L and Weng W (2023),
Investigating the searching behavior of
Sino-U.S. relations in China based on
complex network.
Front. Phys. 11:1021565.
doi: 10.3389/fphy.2023.1021565

COPYRIGHT

© 2023 Chen, Wang and Weng. This is an
open-access article distributed under the
terms of the [Creative Commons
Attribution License \(CC BY\)](#). The use,
distribution or reproduction in other
forums is permitted, provided the original
author(s) and the copyright owner(s) are
credited and that the original publication
in this journal is cited, in accordance with
accepted academic practice. No use,
distribution or reproduction is permitted
which does not comply with these terms.

Investigating the searching behavior of Sino-U.S. relations in China based on complex network

Jun Chen^{1*}, Lei Wang² and Wuyan Weng³

¹School of Foreign Studies, Northwestern Polytechnical University, Xi'an, China, ²College of International Cooperation, Xi'an International University, Xi'an, China, ³School of Economics and Management, Fuzhou University, Fuzhou, China

The Sino-U.S. relationship is one of the most important bilateral relationships in the literature of global geopolitics. Not only the two countries, but also other nations in the relevant regions have been influenced by their economic, cultural, political, educational, and diplomatic relations. In this paper, we have applied Visibility Graph as the method, analyzed the data from Baidu searching index of the keyword "Sino-U.S. relations" from 2011 to 2021 into a directionless and authoritarian network, and studied its dynamic characteristics. From the time series data, it has been found that the relationship between the data is closer with more edges, greater degrees, and greater clustering coefficients. Meanwhile, the shorter the average path length, the closer the relationship between the data. The results provide a new perspective for analyzing the time series characteristics of Sino-U.S. relations.

KEYWORDS

Sino-U.S. relationship, visual graph, complex network, social behavior, geopolitics

1 Introduction

In recent years, the increasing instability of Sino-U.S. relations result in the conflicts of interest between two countries, and various neighbor countries have also introduced new policies due to the change of Sino-U.S. relations: trading policies, tariff policies, migration policies *etc.*, which have aroused widespread concern among researchers in the field of geopolitics and others. For instance [1], have studied the dynamic relationship between the political conflict and bilateral trading connections of China and the U.S., The results showed that along with the decreasing global economic, the Chinese and U.S. governments should strengthen trading cooperation and seek consensus on economic interests in order to improve bilateral relations [2]. Studied how to discuss Sino-U.S. relations in the news coverage of Sino-U.S. trading conflict. They found that Sino-U.S. relations can be divided into antagonistic relations, negotiatory relations and cooperative relations. In these relationships, China is structured as a victim of the trade conflict, a defender of the free trade, a facilitator of negotiations, and a beneficiary of cooperation. These identities and relationships are constructed through constructive, disruptive, justified, and transformative strategies. It was further found that the diversity of China's ethnic identity and Sino-U.S. relations in Chinese news reports were the result of political, social, and economic differences between the two countries [3]. Considered the impact of artificial intelligence (AI) industry on Sino-U.S. relations and argued that AI would become a more focused area of competition between China and the U.S., especially in the context of increasingly fierce and complex strategic competition between both countries in recent years, which can be used as a microcosm of changes between the two countries [4, 5]. Also believe that AI could profoundly affect Sino-U.S. relations. On the one hand, the competition between China and the

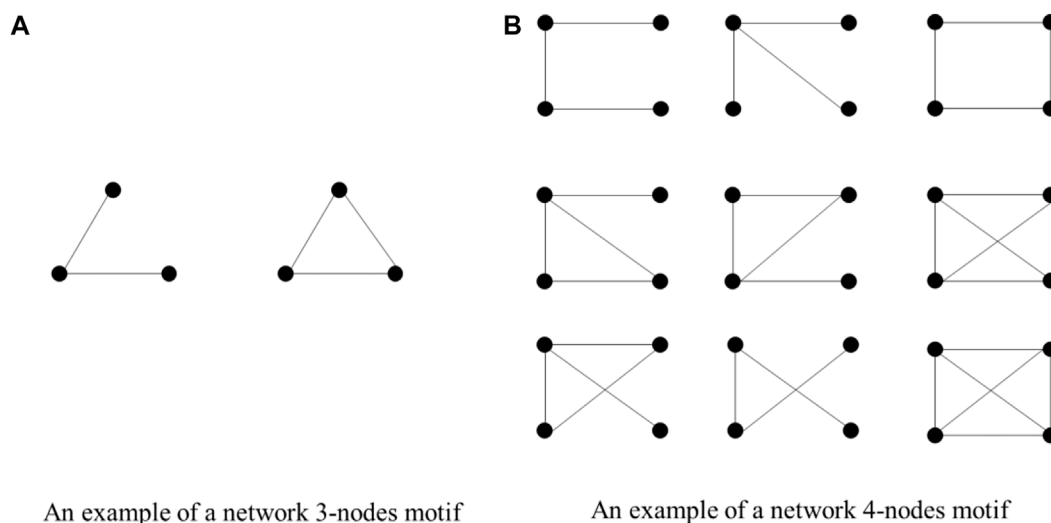


FIGURE 1
An example of a network motifs.

U.S. around AI area may exacerbate strategic suspicion, accelerate the arms race in AI industry, and undermine the strategic stability of the two countries. On the other hand, the rapid development of AI industry has the potential to open new areas of Sino-US cooperation. As AI introduces new forms of uncertainty into the international geopolitics arena, China, and the U.S., as two global powers, need to increase trust and resolve disputes [6]. Analyzed the impact of the latest shift in Chinese naval strategy on Sino-U.S. maritime relations [7]. Further studied the Sino-U.S. relationship from the year of 2008–2021. The main purpose of this research is to reveal the connections of Sino-U.S. relationship through the network. Based on previous studies from international relationship and geopolitics area, this paper introduced visibility graph theory into this topic for the first time. The results from the analysis provide a novel research methodology for scholars to analyze Sino-U.S. relationship.

The rapid development of information technology and the popularity of the Internet have changed people's lives. The Internet has become a hub for receiving and transmitting information. Moreover, searching engines provide Internet users with the most convenient way to acquire the information they need. Due to the large amount of data stored in its servers, searching engines can now demonstrate the searching trend within a time frame. Internet giants such as Google and Baidu have both released their own searching engine products. *Google Trends* and *Baidu Index*, these two searching engines often considered as the largest in English and Chinese. Moreover, these products can now show searching trends for certain keywords over time, and it can also provide a source for analysts to explore the behavior of Internet users, analyze market trends, and monitor public sentiments. Based on the complexity of Internet user relationships and their information, the entire Internet is a complex network.

Since the birth of complex networks at the end of the last century, this discipline has become an important way for scholars to reveal hidden connections between multiple systems and their components [26]. As this new research has evolved over the decades, the study of

complex networks flourished in many directions [9], and view-based network analysis is one of them. Meanwhile, network science has been used in many fields of science: epidemic spreading process in the complex network [10–12], locating multi-sources in social networks [13], the social network problems in the multiplex networks [14]. [15] proposed a simple and fast computational method called the visibility graph algorithm in 2008. This method converts the time series data into a visibility graph which explores a new direction for the development of complex network, providing a new method for characterizing time series from a new perspective. Visibility graph analysis is a method based on the principle of time series visualization; hence, various networks can be derived, such as transportation networks, world-wide networks, interpersonal networks, *etc.* thereby providing a novel method for characterizing time series from a totally different perspective. After developing rapidly for years, this technique has been widely used in various researches [10, 16–19]. Inspired by this, we adopt the visibility graph to explore a typical time series data, i.e., the Baidu searching index about the keyword “Sino-U.S. relations” (in Chinese pinyin “zhong mei guan xi”); thus, the dynamic characteristics of Sino-U.S. relations can be analyzed explicitly. From the aspect of complex network, we hope to reveal more information about time series data. Based on previous studies, this research method has been implemented into many academic backgrounds [20]. Studied time series by constructing complex networks through pseudo-periodic time series, and studied the relationship between constructed networks and primitive time series [21]. Mapped time series to the nearest neighbor network [22]. Introduced the concept of recursive networks [23]. Found out that the visibility graph algorithm preserved the characteristics of the time series [24]. Also indicated that by using visibility graph algorithm, it is possible to determine whether the studied system has the feature of definiteness and randomness based on the characteristics of complex network [25]. Also applied visibility graph algorithm to analyze the similarity and heterogeneity of price time series in seven carbon pilot markets in China. At present, time series analysis based on visibility graph

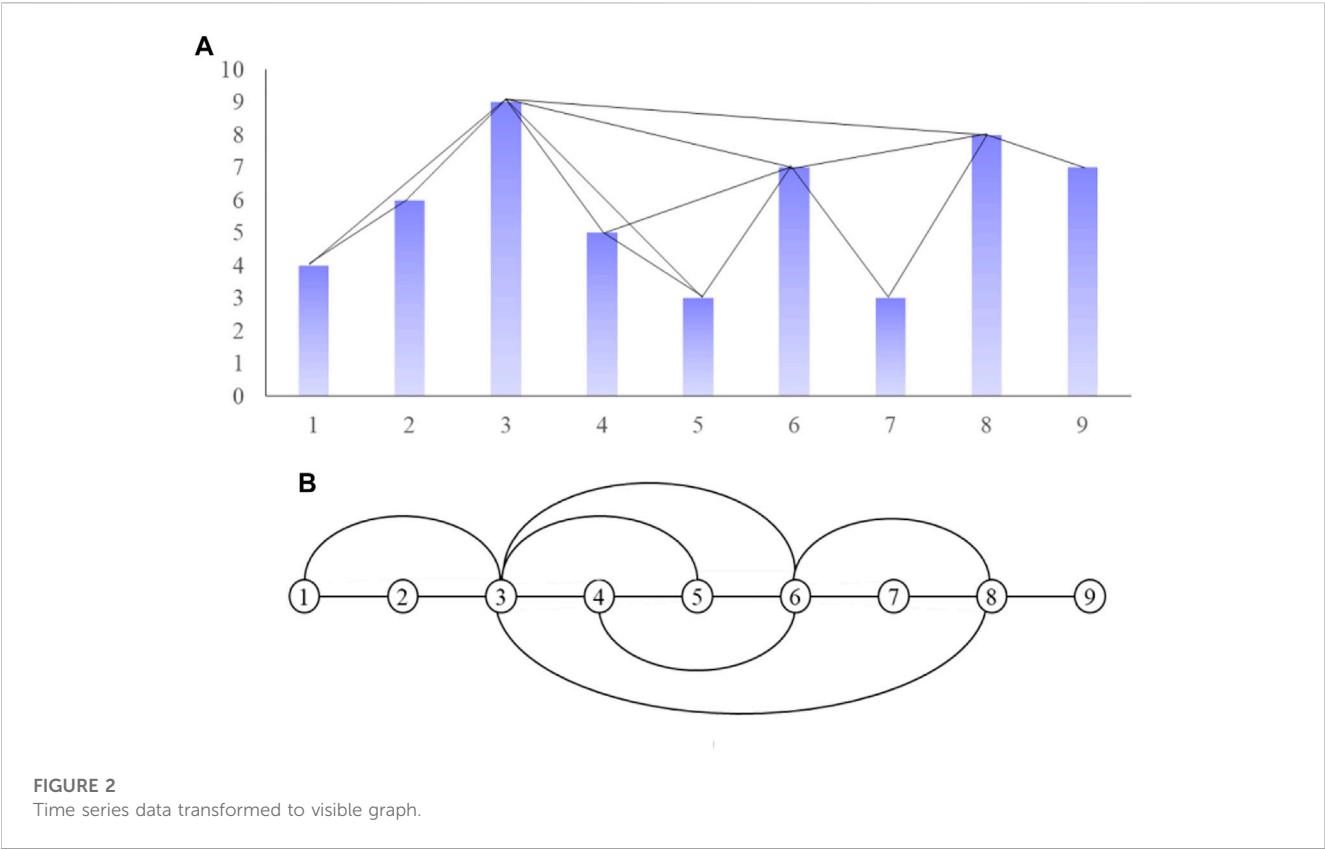


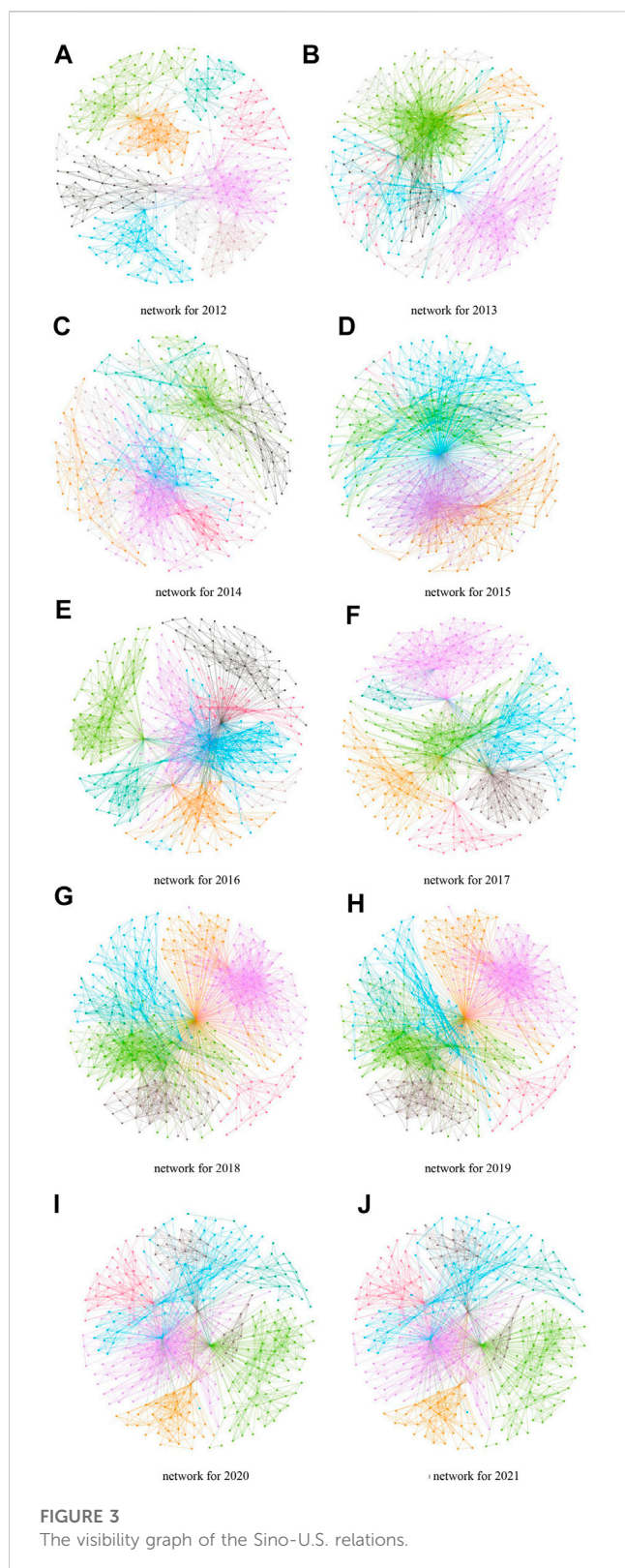
TABLE 1 Descriptive data on the keyword “Sino-U.S. relations” in Baidu index.

| year | Number of nodes | Number of edges | Average degree | Weighted average degree | Network diameter | Density | Average clustering coefficient | Average path length | Modularization |
|------|-----------------|-----------------|----------------|-------------------------|------------------|---------|--------------------------------|---------------------|----------------|
| 2011 | 365 | 3,456 | 9.468 | 9.468 | 9 | 0.026 | 0.752 | 3.979 | 0.683 |
| 2012 | 366 | 3,174 | 8.672 | 8.672 | 11 | 0.024 | 0.754 | 4.347 | 0.775 |
| 2013 | 365 | 3,766 | 10.318 | 10.318 | 10 | 0.028 | 0.719 | 3.749 | 0.61 |
| 2014 | 365 | 3,350 | 9.178 | 9.178 | 8 | 0.025 | 0.731 | 3.784 | 0.654 |
| 2015 | 365 | 4,128 | 11.31 | 11.31 | 6 | 0.031 | 0.796 | 2.445 | 0.632 |
| 2016 | 366 | 4,422 | 12.082 | 12.082 | 5 | 0.033 | 0.758 | 2.394 | 0.546 |
| 2017 | 365 | 4,336 | 11.879 | 11.879 | 7 | 0.033 | 0.723 | 3.153 | 0.629 |
| 2018 | 365 | 3,900 | 10.685 | 10.685 | 7 | 0.029 | 0.744 | 3.069 | 0.681 |
| 2019 | 365 | 4,644 | 12.723 | 12.723 | 6 | 0.035 | 0.742 | 2.441 | 0.579 |
| 2020 | 366 | 6,212 | 16.973 | 16.973 | 4 | 0.047 | 0.777 | 2.076 | 0.539 |
| 2021 | 365 | 3,682 | 10.088 | 10.088 | 7 | 0.028 | 0.759 | 3.07 | 0.685 |

algorithm has been applied in multiple fields [26]. Summarize the model of converting time series into complex network [27]. Analyzed the rate change during the past years based on the visibility graph in order to explore new features.

From the perspective of time series, this paper converts the time series data from Baidu searching index with the keyword “Sino-U.S. relations” into a complex network through the principle of visibility

graph algorithm. Then, we analyze the kinetic characteristics and influence mechanism of the time series through various evaluation metrics, including the degree distribution, cluster coefficient, network diameter and other indicators. As revealed by the obtained results, we find that Chinese searching behavior is typical social behavior, and the degree distribution of the search index is a power-law distribution, which shows that the network is a scale-free network. Chinese people



have a long-term memory of the attention of China and the United States. Furthermore, essential time nodes can also be identified through the centrality of the network.

The following sections of the paper will be listed as: [Section 2](#) will introduce the adopted model and corresponding research methods;

[Section 3](#) will list the incorporated data to be analyzed in this paper; the paper will draw the conclusions in [Section 4](#), also with some further research orientations.

2 Model and method

2.1 Research description

When we discuss relations between countries, scholars usually focus on international relations, linguistics, diplomacy, geopolitics, and other fields of study. However, the relationships of all varieties of data can construct a complex network. Therefore, we construct this network using the time series visibility graph (VG) method proposed by Lacasa et al. [15, 28]; with the help of this VG theory, we can perform sufficient analysis on the Sino-U.S. relationships. The notion of complex networks is a branch of statistical physics and network science. It describes the characteristics of complicate systems and their corresponding dynamics. In addition, time series data can be mapped into a complex network by multiple algorithms. By studying the topologies of different networks, it is possible to discover their dynamic characteristics, which in turn reveals hidden connections on the Internet. According to Lacasa et al., different time series can be converted into multiple networks. That is, periodic time series, random time series and fractal time series can be constructed as regular networks, random networks, and scale-free networks, respectively.

2.2 Complex networks

Considering that time series data will be projected into a complex network, the concept of a complex network will be briefly described. The graph consists of a node set and an edge set, usually thought of as a network, and is often described as $G = (V, E)$, where $Num = V$ represents the number of nodes and $M = E$ represents the number of edges. In addition, if a complex network is a weighted network, then edges can also be described as (u, v, w) , where u and v represent different nodes ($u \neq v$), and w represents the weight of the edge. Complex networks are an effective tool for analyzing problems, which are widely used for analysis of social problems, management science problems, computer and statistical problems, and other issues.

Aiming to discover the features of the chosen dataset, we then will apply various evaluation metrics to analyze the derived networks, including degree distribution, cluster coefficient, average cluster coefficient, network diameter and other indicators [27].

2.2.1 Degree and degree distribution

For the analysis of complex network, degree is one of the most fundamental properties. For a single node v , its degree (i.e., $d(v)$) is defined as the number of edges with node v . Moreover, for the directed graph, according to the start and end points of the edges, two types of degrees are defined, i.e., out-degree and in-degree respectively. In a complex network, we usually anticipate that the larger the degree of node, the higher importance is. Once the degrees of all the nodes are derived, the

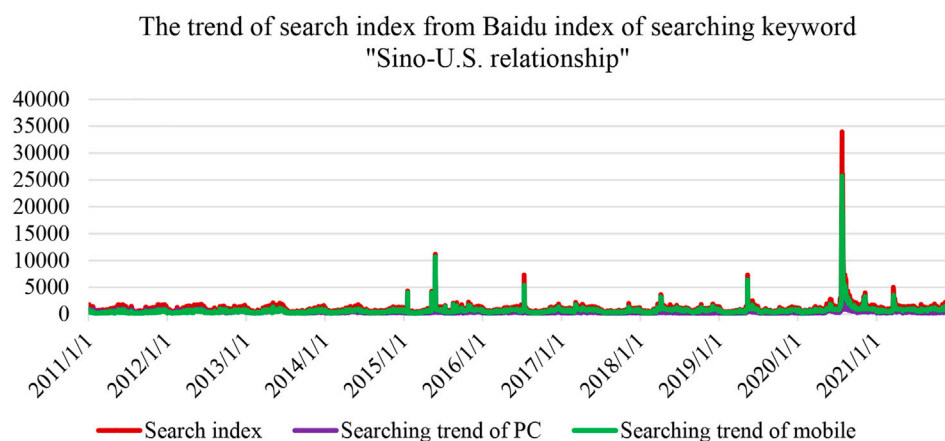


FIGURE 4

Searching trends of Baidu index keyword "Sino-U.S. relations" from the year of 2011–2021.

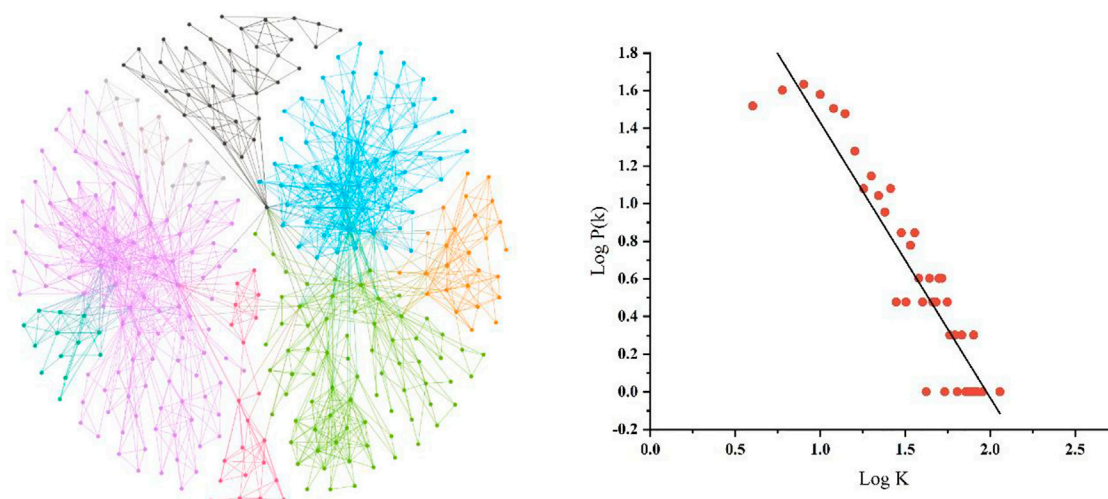


FIGURE 5

Visualization and degree distribution of the 2011 Sino-U.S. relations Search Index.

average degree of the network can be obtained accordingly which is calculated as:

$$\langle k \rangle = \frac{1}{N} \sum_{i=1}^N k_i \quad (1)$$

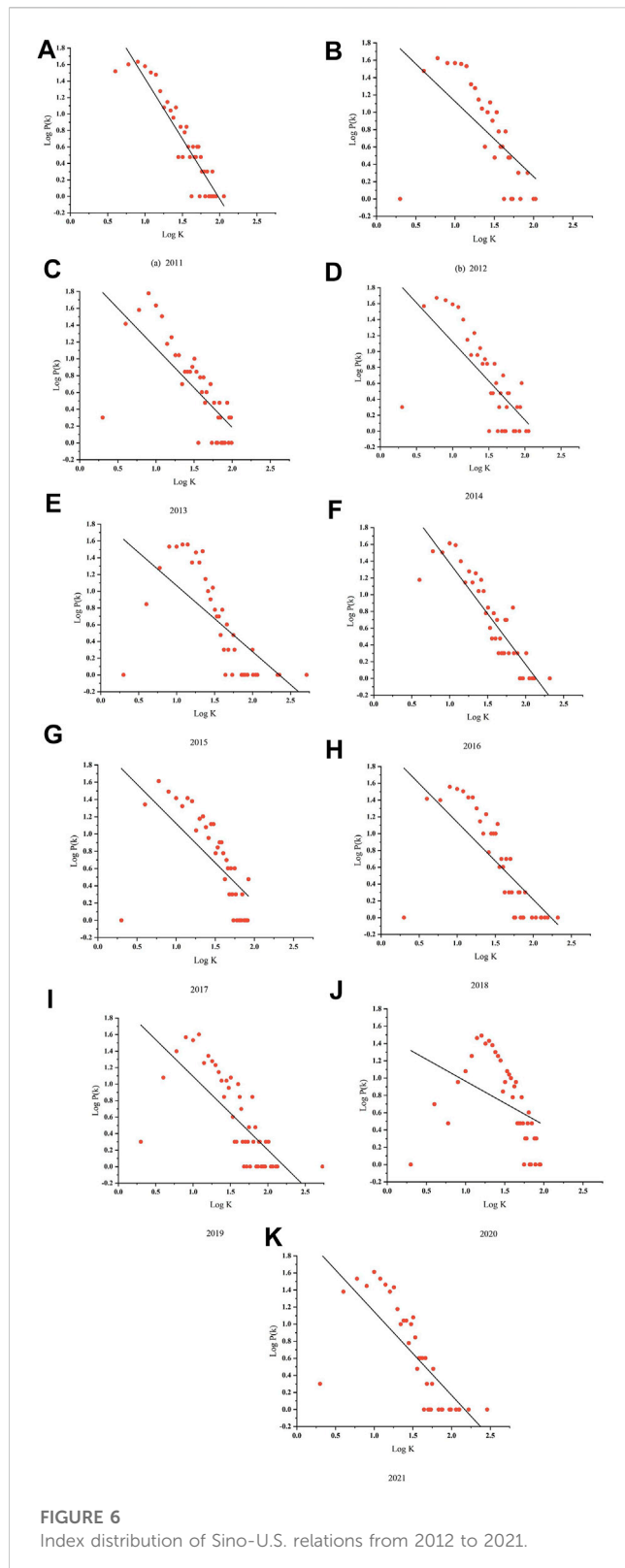
where k_i represents the degree of nodes v_i and N denotes the total number of nodes in the studied networks. The distribution of the degrees of nodes in the network can be described by the distribution function $P(k)$, which represents the proportion of nodes in the network with a moderate degree of k in the network. Common degree distributions are listed as: *Delta* distributions for regular networks, *Poisson* distributions for completely random networks, and power-law distributions for most real-world networks.

2.2.2 Cluster coefficient

For complex networks, clustering coefficient is another important static geometric feature. If a node is directly connected to v_b , then it is referred as the neighbor node of v_i . Aiming to measure the level of a node being are connected, scholars defined the clustering coefficient. For node v_i , corresponding clustering coefficient C_i is defined as the ratio between the actual number of edges E_i and the total number of possible edges for neighbors of node v_i (i.e., $C_2^{k_i}$).

$$C_i = \frac{E_i}{C_2^{k_i}} \quad (2)$$

where k_i represents the total number of neighbors for v_i . On the other hand, the average clustering factor C is the average of the



clustering coefficients for all nodes in the entire network, which is given as:

$$C = \frac{1}{N} \sum_{i=1}^N C_i \quad (3)$$

where N indicates the total number of nodes. Obviously, the value of C varies from 0 to 1. When all nodes are isolated, we can have $C = 0$; when any two nodes in the network are directly connected which in another word, globally coupled, then we have $C = 1$. When the value of N is large enough, $C = O(N^{-1})$ holds. In practice, there exist obvious clustering effects in many actual complex networks, and with the increase of the network size, the clustering coefficient C tends to be a non-zero constant, that is, when $N \rightarrow \infty$, $C = O(1)$, and similar nodes tend to be clustered together.

2.2.3 Network diameter and average path length

In the network for any two nodes i and j , we can get the shortest distance d_{ij} between these two nodes, then the network diameter D is the largest path between these shortest paths,

$$D = \max(d_{ij}) \quad (4)$$

Average path length is usually defined as L , which describes the average number of edges that are necessary to be passed from one node to another. This can also be referred to as the average of the shortest path among all node pairs in the viewable view. It is defined as:

$$L = \frac{1}{1/2N(N-1)} \sum_{i \geq j} d_{ij} \quad (5)$$

2.2.4 Graph density

For graph density, it is defined to measure the integrity of a network which also refers to the level of connection tightness among nodes in a network. Thus, the more connections exist among nodes, the larger the graph density is. We know that for any possible node pairs in a complete graph, the two nodes are connected to each other, thus, we have a graph density of 1. For the network $G = (V, E)$, corresponding graph density is calculated as:

$$d(G) = \frac{E}{C_N^2} \quad (6)$$

where N indicates the total number of nodes, and E represents the total number of edges.

2.2.5 Motif

Motif can be regarded as subgraph of a network, i.e., a “small system” in a complex system. It is a small-scale pattern that occurs rather frequently in real networks than in random networks. It belongs to one of the basic topological structures of networks. The frequency of motifs in real networks is much higher than in random networks with the same number of nodes and connections [16, 18]. For majority networks, there are some common motifs which are composed of a fixed number of four nodes. Here, we illustrate 3-motif and 4-motif as in Figures 1A, B respectively.

2.3 Visibility graph algorithm

In this paper, the VG model is employed to convert time series data into a complex network. Corresponding definition for VG theory is provided as: if any two points (t_i, y_i) and (t_j, y_j) in a time

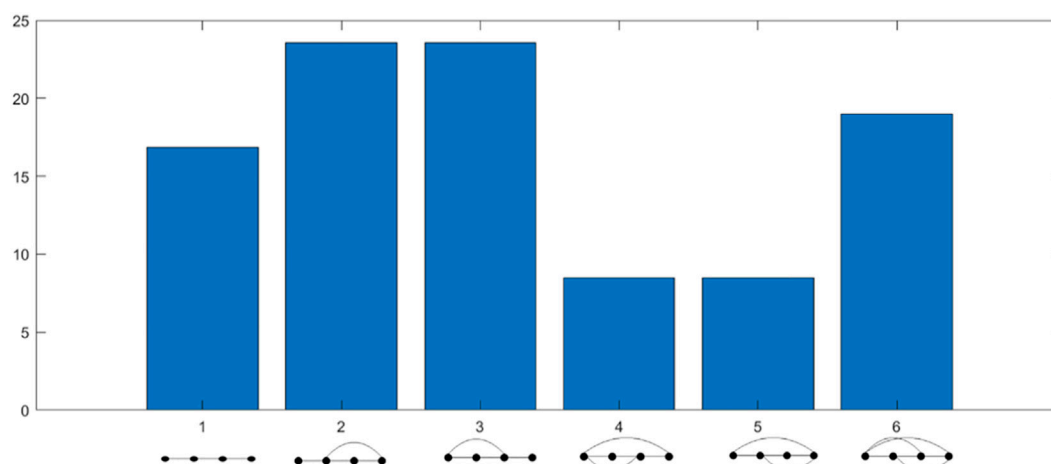


FIGURE 7
Motif-4 distribution of Sino-U.S. relations.

series $y(t)$ satisfies the following formula, then visibility in the data is satisfied:

$$y_k < y_i + (y_j - y_i) \frac{t_k - t_i}{t_j - t_i}, i < k < j \quad (7)$$

Figure 2 shows the definition in Eq. 7. In Figure 1A, the height of the straight rod represents the data value for each time step. If the tops of the two straight rods can touch each other, then we can say that the two corresponding points are connected, as shown in Figure 1B.

Specifically, Figure 2 illustrates a good illustration of the conversion of time series data into a network. As it is shown in Figure 1, the values for nodes 1, 2, and 3 are 4, 6, and 9, respectively. According to Eq. 7, it can be calculated that the values of nodes 1, 2, and 3 have a relationship $6 < 4 + (9 - 4) \frac{1 - 2}{3 - 1} = 6.5$. It can therefore be explained that Node 1 and Node 3 are connected.

3 Data

Due to the unlimited nature of time series data, the time range explored in this paper is the most recent time series data indexed by Baidu, the largest Chinese searching engine for the last 11 years. We define each day of the year as a node, so there will be a total of 365 nodes per year, in addition to 366 nodes in 2012, 2016 and 2020.

3.1 Viewable network

Based on the Baidu searching index data on “Sino-U.S. relations” for each year, we can easily obtain a complex network representing Sino-US relations through the adoption of VG theory. The characteristics of the derived networks are provided in Table 1. In this table, number of nodes are represented by days of each year, while the number of edges

reached its peak value at the year of 2020. Meanwhile, the density has also increased and reached its high at 0.047 this year with a diameter between 4 and 5, indicating that more information about Sino-US relations has been searched. Even before the year of 2020, the density has increased gradually only except the year of 2012, 2014, and 2018 with slightly decline.

Similarly, the average path length has decreased from 3.979 to 3.07, and the average clustering coefficient ranged between 0.7 and 0.8, with an overall decreasing trend. It explains that the network’s connection is becoming more intensive. Chinese citizens no longer gather in a single topic of the affairs between two countries, but gradually began developing a multi-directional circulation trend. With the interactions in multiple aspects of China and America, there are more discussions in different topics of Sino-U.S. relationships on the Internet.

As illustrated, we can find that for the year where the relationship between the data is closer with greater degrees and clustering coefficients. The path between data also obtains with shorter path length. Furthermore, the derived complex network of the U.S.-China Relations can also be visualized as in Figure 3.

Furthermore, we also present the searching trend of “Sino-U.S. relations” from the year 2011–2021. The results are provided in Figure 4, where the red line represents the total searching index consisting of PCs and mobile devices. The green line indicates that the searching index of mobile devices dominates the total searching index. In 2010, China’s GDP rise to the second in the ranking list among all the countries in the world. Then, starting from 2011, the United States introduced a series of measures to suppress the development of China, for instance, “returning to the Asia-Pacific region,” implementing “Asia-Pacific rebalancing,” and forming the TPP (Trans-Pacific Partnership) while excluding China. In 2020, the US government represented by Trump emphasized “America first”; the US government focused on promoting “decoupling” from China and vigorously suppressed Chinese technology companies such as Huawei and TikTok. As a result of the all-round suppression to China by the United States, frictions between the world’s two largest

economies in politics, economy, diplomacy, and people-to-people exchanges have been deepening, and Sino-US relations have continued to deteriorate. As the world's largest power, the economic and political measures of the United States will have a profound impact on the development of China and even the world, so Sino-US relations have also been valued by their citizens.

Figure 5 shows the visual and degree distribution of the complex network of the Sino-U.S. relations search index in 2011, while Figure 6 shows the degree distribution from the year of 2012–2022. The visual network of Sino-U.S. relations is a scale-free network. In this network, there are more time nodes with fewer consecutive edges, and a small proportion of nodes with large degree values. Meanwhile, with the increase of degrees, the number of nodes decreases. This reflects the volatility of the original time series. The degree distribution shows that the Baidu Searching Index of Sino-U.S. relations is a fractal time series with long-term correlation. On the one hand, the original time series have statistical similarities in different time ranges, such as days, weeks, months, etc.; On the other hand, due to the long-term correlation, the change in the Baidu search index of future Sino-U.S. relations may be like some past period.

Furthermore, we also try to investigate the distribution of the motifs in the derived networks for the considered Sino-U.S. relation datasets. Here, we mainly consider the 4-motif. Corresponding results are provided in Figure 7. As presented, we find that the number of the second type motif equals to that for the third type motif. Similarly, the number of fourth motif are equivalent to the fifth motif. This shows that the number of Chinese searches for Sino US relations is highly relevant in terms of time.

4 Conclusion

This paper transforms the time series data from Baidu searching index of the keyword “Sino-U.S. relations” from 2011 to 2021 into a viewable graph. After deriving the networks, we can easily study corresponding dynamic characteristics. The results provide a new perspective for analyzing the time series characteristics of Sino-U.S. relations. The network constructed by using the viewable algorithm in this paper is a directionless and authoritarian network, which lost some information of the original time series data during the conversion process, resulting in its inability to analyze the change characteristics of the time series. Therefore, other methods for analyzing the changing characteristics of the time series can be selected for optimization in the future for a better result.

For the analyzing method, we suppose the choosing of the keyword in the searching engine is quite tricky. On the one hand, this keyword cannot be too narrow and obscure, keywords

like terminologies are not appropriate; on the other hand, the keywords which are too broad do not have representativeness. Therefore, in order to fetching the most valuable data for analysis, it is important to choose the keywords more precisely. Based on the keyword of “Sino-U.S.,” we can draw the conclusion that only when China and the United States deeply understand each other's differences and promote exchanges and cooperation, both countries can avoid conflicts. This study also provides a historical diagnosis for the development of Sino-U.S. relations. The other researches related to this topic can be explored in other aspects based on more specific time series data.

Data availability statement

The raw data supporting the conclusion of this article will be made available by the authors, without undue reservation.

Author contributions

JC proposed the question and method, WW collected the data and produced all figures, LW finished the manuscript, all authors confirmed the final version of the paper.

Funding

This work was supported in part by the Research Funds for Philosophy and Social Science Disciplinary Subject under Grant 21GH031111, Northwestern Polytechnical University.

Conflict of interest

The authors declare that the research was conducted in the absence of any commercial or financial relationships that could be construed as a potential conflict of interest.

Publisher's note

All claims expressed in this article are solely those of the authors and do not necessarily represent those of their affiliated organizations, or those of the publisher, the editors and the reviewers. Any product that may be evaluated in this article, or claim that may be made by its manufacturer, is not guaranteed or endorsed by the publisher.

References

1. Su CW, Song Y, Tao R, Hao LN. Does political conflict affect bilateral trade or vice versa? Evidence from sino-US relations [J]. *Econ research-Ekonomska istraživanja* (2020) 33(1):3238–57. doi:10.1080/1331677x.2019.1694559
2. Wang H, Ge Y. Negotiating national identities in conflict situations: The discursive reproduction of the Sino-US trade war in China's news reports. *Discourse Commun* (2020) 14(1):65–83. doi:10.1177/1750481319893406
3. Wang Y, Chen D. Rising Sino-U.S. Competition in artificial intelligence. *China Q Int Strateg Stud* (2018) 4(02):241–58. doi:10.1142/s2377740018500148
4. Zhu Q, Long K. How will artificial intelligence impact sino-US relations? [J]. *China Int Strategy Rev* (2019) 1(1):139–51. doi:10.1007/s42533-019-00008-9
5. Zhu P, Wang X, Li S, Guo Y, Wang Z. Investigation of epidemic spreading process on multiplex networks by incorporating fatal properties. *Appl Math Comput* (2019) 359: 512. doi:10.1016/j.amc.2019.02.049
6. Wu Z. Towards naval normalcy: 'open seas protection' and sino-US maritime relations. *Pac Rev* (2019) 32(4):666–93. doi:10.1080/09512748.2018.1553890

7. Voloshina A. Sino-US relations: Evolution from 2008 to 2021[J]. *USA Can ekonomika, politika, kultura* (2021) 2021(8):97–107. doi:10.31857/S268667300016030-3
8. Albert R, Barabási AL. Statistical mechanics of complex networks. *Rev Mod Phys* (2002) 74(1):47–97. doi:10.1103/revmodphys.74.47
9. Wang JB, Wang L, Li X. Identifying spatial invasion of pandemics on metapopulation networks via anatomizing arrival history. *IEEE Trans Cybern* (2016) 46(12):2782–95. Epub 2015 Nov 9. PMID: 26571544; PMCID: PMC7186038. doi:10.1109/TCYB.2015.2489702
10. Qi L, Cheng L, Wang W, Li X, Li S, Zhu P. Influence maximization through exploring structural information. *Appl Math Comput* (2023) 442:127721. doi:10.1016/j.amc.2022.127721
11. Wang J -B, Li X. Uncovering spatial invasion on metapopulation networks with SIR epidemics. *IEEE Trans Netw Sci Eng* (2019) 6(4):788–800. doi:10.1109/TNSE.2018.2873609
12. Zhu P, Cheng L, Gao C, Wang Z, Li X. Locating multi-sources in social networks with a low infection rate. *IEEE Trans Netw Sci Eng* (2022) 9(3):1853–65. doi:10.1109/tNSE.2022.3153968
13. Iacovacci J, Lacasa L. Sequential motif profile of natural visibility graphs. *Phys Rev E* (2016) 94(5):052309. doi:10.1103/physreve.94.052309
14. Cheng L, Li X, Han Z, Luo T, Ma L, Zhu P. Path-based multi-sources localization in multiplex networks. *J Chaos, Solitons Fractals* (2022) 159:112139. doi:10.1016/j.chaos.2022.112139
15. Lacasa L, Luque B, Ballesteros F, Luque J, Nuno JC. From time series to complex networks: The visibility graph. *Proc Natl Acad Sci* (2008) 105(13):4972–5. doi:10.1073/pnas.0709247105
16. Hu J, Chen J, Zhu P, Wang M, Li H, Liu N. Difference and cluster analysis on the carbon dioxide emissions in China during COVID-19 lockdown via a complex network model [J]. *Front Psychol* (2022) 2022:6410. doi:10.3389/fpsyg.2021.795142
17. Hu J, Xia C, Li H, Zhu P, Xiong W. Properties and structural analyses of USA's regional electricity market: A visibility graph network approach. *Appl Math Comput* (2020) 385:125434. doi:10.1016/j.amc.2020.125434
18. Hu J, Zhang Y, Wu P, Li H. An analysis of the global fuel-trading market based on the visibility graph approach. *J Chaos, Solitons Fractals* (2022) 154:111613. doi:10.1016/j.chaos.2021.111613
19. Qiao HH, Deng ZH, Li HJ, Hu J, Song Q, Gao L. Research on historical phase division of terrorism: An analysis method by time series complex network. *Neurocomputing* (2021) 420:246–65. doi:10.1016/j.neucom.2020.07.125
20. Zhang J, Sun J, Luo X, Zhang K, Nakamura T, Small M. Characterizing pseudoperiodic time series through the complex network approach. *Physica D: Nonlinear Phenomena* (2008) 237(22):2856–65. doi:10.1016/j.physd.2008.05.008
21. Xu X, Zhang J, Small M. Superfamily phenomena and motifs of networks induced from time series. *Proc Natl Acad Sci* (2008) 105(50):19601–5. doi:10.1073/pnas.0806082105
22. Marwan N, Donges JF, Zou Y, Donner RV, Kurths J. Complex network approach for recurrence analysis of time series. *Phys Lett A* (2009) 373(46):4246–54. doi:10.1016/j.physleta.2009.09.042
23. Donner RV, Zou Y, Donges JF, Marwan N, Kurths J. Recurrence networks—A novel paradigm for nonlinear time series analysis. *New J Phys* (2010) 12(3):033025. doi:10.1088/1367-2630/12/3/033025
24. Li X, Yang D, Liu X, Wu XM. Bridging time series dynamics and complex network theory with application to electrocardiogram analysis. *IEEE circuits Syst Mag* (2012) 12(4):33–46. doi:10.1109/mcas.2012.2221521
25. Gao ZK, Cai Q, Yang YX, Dang WD, Zhang SS. Multiscale limited penetrable horizontal visibility graph for analyzing nonlinear time series[J]. *Scientific Rep* (2016) 6(1):1–7.
26. Zou Y, Donner RV, Marwan N, Donges JF, Kurths J. Complex network approaches to nonlinear time series analysis. *Phys Rep* (2019) 787:1–97. doi:10.1016/j.physrep.2018.10.005
27. Yang Y, Wang J, Yang H, Mang J. Visibility graph approach to exchange rate series. *Physica A: Stat Mech its Appl* (2009) 388:4431–7. doi:10.1016/j.physa.2009.07.016
28. Luque B, Ballesteros FJ, Robledo A, Lacasa L. Entropy and renormalization in chaotic visibility graphs. *Math Foundations Appl Graph Entropy* (2016) 6, 1–39. doi:10.1002/9783527693245.ch1



OPEN ACCESS

EDITED BY

Jianrong Wang,
Shanxi University, China

REVIEWED BY

Fuli Zhou,
Zhengzhou University of Light Industry,
China
Jinnan Wu,
Anhui University of Technology, China

*CORRESPONDENCE

Jingjing Zhang,
✉ zhjing-ujs@foxmail.com

SPECIALTY SECTION

This article was submitted
to Social Physics,
a section of the journal
Frontiers in Physics

RECEIVED 11 December 2022

ACCEPTED 09 January 2023

PUBLISHED 08 March 2023

CITATION

Zhang J, Mei Z, Zhang F and Zhou Q
(2023), An evolutionary game study on
the cooperation behavior of the
“government, banks, and guarantee
institutions” in financing guarantee for
China’s new agricultural entities.
Front. Phys. 11:1121374.
doi: 10.3389/fphy.2023.1121374

COPYRIGHT

© 2023 Zhang, Mei, Zhang and Zhou. This
is an open-access article distributed
under the terms of the [Creative
Commons Attribution License \(CC BY\)](#).
The use, distribution or reproduction in
other forums is permitted, provided the
original author(s) and the copyright
owner(s) are credited and that the original
publication in this journal is cited, in
accordance with accepted academic
practice. No use, distribution or
reproduction is permitted which does not
comply with these terms.

An evolutionary game study on the cooperation behavior of the “government, banks, and guarantee institutions” in financing guarantee for China’s new agricultural entities

Jingjing Zhang*, Zhu Mei, Fan Zhang and QiaoMei Zhou

School of Management, Jiangsu University, Zhenjiang, China

“Government, bank, and guarantee institution” cooperative financing guarantee (hereinafter referred to as the cooperation mechanism) is an important way to alleviate the financing difficulties of China’s new agricultural entities and raise the credit line of bank financing. In order to find an effective way for the improvement of low-level equilibrium in the actual operation of the cooperation mechanism, this study builds a three-party evolutionary game model using the local government, banks, and agricultural guarantee institutions, with incomplete information on all partners of the cooperation mechanism as the study object. This model focuses on the weak activeness, strong dependence, poor cooperation effect, lower credit line of guarantee, and other specific problems. Moreover, this study analyzes the equilibrium solution of this model and extracts the significant factors affecting the positive cooperation behaviors of the three parties (government, banks, and guarantee institutions) in the view of interest realization. Analog simulation is performed to explore the key conditions for truly alleviating the financing risks of new agricultural entities, thus helping improve the operation quality of the cooperation mechanism. According to the study results, the focus of “government, bank, and guarantee institution” cooperation should be shifted from post risk sharing to prior risk identification. Specifically, the government should further share high-quality information affiliated with farmland management rights and reflecting the status of risks; guide banks and agricultural guarantee institutions should share the cost of risk identification, accelerate the acquisition of higher information transformation value, and prevent the “free rider problem.” In the last part, policies are recommended in four aspects, including risk information sharing, risk identification quality improvement, risk identification cost sharing, and risk information value transformation, which have practical guiding significance for the sustainable development of “government, bank, and guarantee institution” financing guarantee for China’s new agricultural entities.

KEYWORDS

cooperation behavior, financing guarantee, China’s new agricultural entities, low-level equilibrium, evolutionary game

1 Introduction

China's new agricultural business entities (hereinafter referred to as new agricultural entities) mainly refer to large-scale business entities, such as family farms, large farmer households, farmer cooperatives, and leading agricultural industrialization enterprises, which serve as the backbone of China's rural revitalization strategy. Large farmers in Europe and the United States are privileged in terms of long-term assets and financing credits. Unlike them, most of China's new agricultural entities are experiencing an early start-up. There is a lack of guarantees and historical credit information, resulting in great financing difficulty [1]. In order to eliminate the financing difficulties, the Chinese government has arranged special funds to help upgrade the industry, hoping that new agricultural entities will achieve a stronger profitability and driving effect. Therefore, it has launched a package of construction plans for the cooperation mechanism for farmers, mainly focusing on two aspects. In the first aspect, efforts are made to improve the financing risk sharing and compensation mechanism for the cooperation mechanism. In detail, a financing guarantee cooperation system is built involving the government, banks, policy-related agricultural guarantee institutions (hereinafter referred to as agricultural guarantee institutions), and other entities, thus constituting a complete and orderly credit system characterized by revenue sharing, risk sharing, complementary advantages, mutual benefit, a win-win situation, and sustainable development among multiple entities [2]. In the second aspect, there is comprehensive exploration of the advantages of large-scale farmland management rights through "government, bank, and guarantee institution" cooperation [3]. With the support of the *Rural Land Contract Law of the People's Republic of China (Draft Amendment)*, the government took tentative action in 2019, using farmland management rights to link financing entities, land resources, and funds, and finding a new financing method for large-scale farmland management rights based on counter-guarantee. These policy constructions are regarded as important ways to solve the financing dilemma of new agricultural entities. The former focuses on the cooperation of the government, banks, and guarantee institutions to share financing risks, while the latter focuses on the cooperation of the government, banks, and guarantee institutions to tap the value of farmland. They are all concrete manifestations of the cooperation between the government, banks, and guarantee institutions. At present, "government, bank, and guarantee institution" agricultural financing guarantee cooperation, which focuses on risk sharing, has been recommended as one of the top 10 innovative agricultural support modes by China's Ministry of Agriculture and extended to different provinces and municipalities nationwide. By the end of 2021, the financing mode based on the counter-guarantee of farmland management rights had been disseminated to 232 regions of China as a pilot program, achieving a cumulative loan of RMB 96.4 billion (most of the loan receivers are new agricultural entities) [4].

However, the actual operation effect of the financing based on the cooperation mechanism deviates from expectations while experiencing large-scale promotions and is in a low-level equilibrium state [5]. Contradictions are also discovered. No matter what kind of policy, the regional implementation rate is

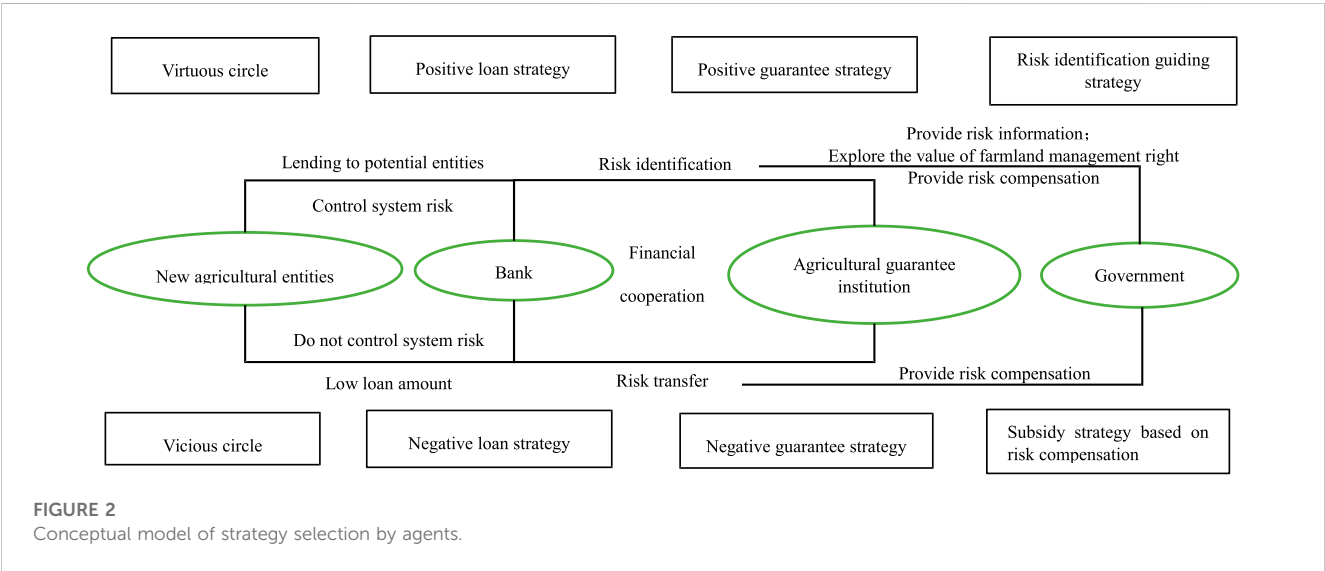
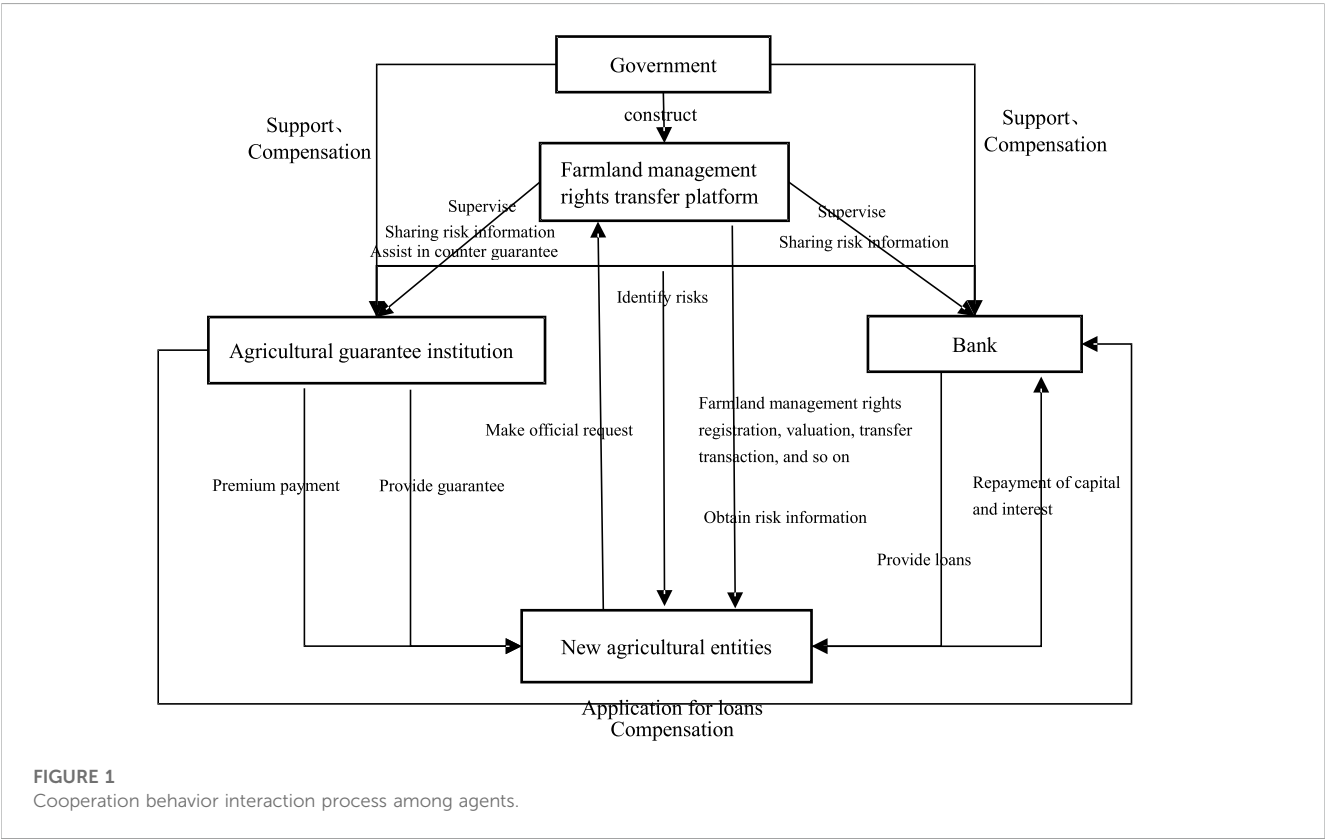
rising all the time. Nevertheless, banks and agricultural guarantee institutions are rarely passionate about actual cooperation. Specifically, some banks are reluctant to participate in the cooperation mechanism and implement the corresponding preferential interest rates. Even though banks are involved in the cooperation mechanism, they are not willing to offer funds, usually providing a conservative credit line for new agricultural entities. Agricultural guarantee institutions should spare no effort to let banks raise the credit line. However, they are not fully capable or motivated to identify the true state of customers, failing to encourage banks to reduce the credit risk of new agricultural entities and address the concern of risk control [6]. What is the cause of such contradiction? A conflict between the endowment effect of financial policies in helping those in distress and the financial attribute of seeking advantages and avoiding disadvantages is proven by the result of theoretical analysis. The main component of risk sharing lies in the cooperation among the government, banks, and agricultural guarantee institutions to share the financing risks of new agricultural entities [7]. The counter-guarantee of farmland management rights is intended for discovering the value of large-scale land management rights in guarantee and risk reduction based on the cooperation among the government, banks, and agricultural guarantee institutions. Both of them have logically given priority to post compensation and risk sharing, using beneficial financial policies to offset the financial attribute of seeking advantages and avoiding disadvantages [8]. In actual operations, we steadily find a complete dependence on the favorable policies of local governments. In the process of proportional risk sharing, for example, the active risk control behaviors of banks and agricultural guarantee institutions are seldom seen. Instead, they rely entirely on the favorable subsidies of local governments (such as tax relief) and compensations for default to transfer the financing risk of new agricultural entities [9]. Some banks even raise the credit line only after all the risks are transferred. However, the difficulty of circulating, managing, and disposing of farmland management rights and affiliated economic goods in the operation of farmland management rights based on counter-guarantee is very noticeable, resulting in a high cost. For this reason, it is necessary to rely entirely on government-supported measures and corresponding favorable compensation measures. Otherwise, banks and guarantee institutions are reluctant to accept such a counter-guarantee, thereby making it hard to implement the relevant policies [10].

Governments can increase the coverage rate of the cooperation mechanism through a series of favorable policies. However, such an increase is only a cover-up. Post-risk compensation can reduce the concern of banks, but it does not truly mitigate systemic risks [11]. If any new agricultural customer has not been identified and screened in advance, blindly raising the credit line will only lead to systemic risk and eventually tilt toward the government, which not only goes against the objective of the policy on helping those in distress but also increases the financial pressure [12]. The credit theory suggests that financial institutions should have full incentive to screen the loan risk of customers. However, both system participation and the drive of banks and agricultural guarantee institutions come from policy incentives rather than profit-seeking nature for the loans based on risk sharing and counter-guarantee of farmland management rights [13]. In addition, the seasonal fluctuations in the capital demand of agricultural business projects, the dispersion

and distance of customers, and the lack of historical credit information lead to the low profit margins and high cost of guarantees and loans in an environment with a favorable interest rate, further increasing the cost and difficulty for banks and agricultural guarantee institutions to collect and obtain risk information [14]. Therefore, even if banks and agricultural guarantee institutions are involved in cooperation, they lack the subjective motivation and ability to control the risks of new agricultural customers. In order to break through the low-level equilibrium of the “government, bank, and guarantee institution” cooperation for the financing guarantee of new agricultural entities, the mechanism should be extended on the basis of the institutional logic of “controlling the risk of financing guarantee.” Risk sharing, counter-guarantee, and mortgage of farmland management rights are classified as passive compensation of post risks, and the key to controlling the risk of financing guarantee lies in the prior identification and screening of risks.

Most current research studies focus on the financing guarantee cooperation involving government, banks, and agricultural guarantee institutions in the following aspects: (1) exploring the feasibility and plausibility of such a financing guarantee. Scholars believe that most of China’s new agricultural entities have low management standards, poor availability of historical credit information, high natural and market risks, large capital investments, long payback period, and many other high-risk factors [15]. Moreover, borrowers have more information than lenders. The information asymmetry between the two sides is more likely to cause financing risks [16]. In this sense, the original intention of the financing guarantee was for the three parties to cooperate to share the high financing risks of new agricultural entities and alleviate the credit concerns of banks [17]. In this cooperation mechanism, guarantee institutions serve as a bridge. They can bear some of the risks for banks. In the face of asymmetric information, they can work as an indirect information source to enhance banks’ ability to assess the expected return and accelerate the conclusion of loan agreements between borrowers and lenders. This serves as the basis for cooperation between banks and guarantee institutions [18]. Guarantee institutions can help reduce part of the banks’ financing risk, but their tolerance for risks is limited. If no reliable rules and regulations are available, the financing risk sharing will be unreasonable, thereby leading to a moral hazard and causing losses to banks and guarantee institutions [19]. The related scholars have further demonstrated the importance of the government accordingly. According to relevant studies, government participation is the outcome of combining government intervention theory and financing guarantee theory. It is a way for governments to assume responsibility for public financial services and also a mode for governments to fulfill the duties of public financial services [20, 21]. The cooperation mechanism reflects the complementarity and inclusiveness of China’s policy-oriented finance as inherent attributes. When the formal financial system cannot meet the financing demand of agricultural business entities, small- and medium-sized enterprises, and other financially vulnerable groups, the more authoritative credit endorsement of governments will not only increase the credit of lenders but also make up for the lack of credit for guarantee institutions, thus

helping further transfer risks [22]. Meanwhile, grassroots governmental organizations can obtain relevant information about lenders more efficiently, truthfully, and authoritatively, which is more conducive to the reasonable deployment of credit resources, and they also help guarantee institutions establish more authoritative communication channels between borrowers and banks. In addition, these efforts will facilitate the reduction of financing costs; improve economic efficiency such as the financing rate, resource allocation rate, and capital utilization rate; and further alleviate the concerns of banks [23]. (2) Exploring the behavioral dilemma of the government, banks, and guarantee institutions. First of all, in the cooperation based on proportional risk sharing, banks, as the suppliers of funds, are in an advantageous position. Faced with the higher financing risk of agricultural entities, they will choose to involve guarantee institutions when providing financing services and use their advantageous position to transfer the risks to the guarantee institution, which will further adversely influence the interests of guarantee institutions [24]. Since each party involved in financing has different credit levels, these credit levels should be balanced by guarantee institutions providing an equilibrium value [25]. However, in actual operations, the behavior of guarantee institutions has been “alienated.” For example, a large number of private capitals not accepted by the banking industry enter the guarantee industry and play the role of “shadow banking” [26]. Guarantee institutions have no advantages in information. However, a large number of risks have been transferred to them by banks. In this process, banks are arbitrary. In fact, guarantee institutions face dual moral hazards from banks and enterprises and a lack of ability to acquire risk information [27]. Moreover, profitability is lower, and guarantee institutions are not fully motivated and enabled for risk control. Extreme business behaviors in violation of relevant rules and regulations occur now and then [28]. Some studies have pointed out that whether the credit guarantee increases the amount of loans is actually difficult to measure and that the amount of guaranteed loans is not directly related to the subsequent development of credit subjects. Financing guarantee only shares the risk and does not solve the financing problem of vulnerable groups. However, if guarantees are provided to all enterprises that request financing, it will pose a systemic risk [29]. Similarly, the government behavior is also in a dilemma. On the one hand, the construction of a policy-oriented financing guarantee system by the government can indeed further facilitate guarantee institutions to increase credit and risk distribution, ease the pressure on guarantee institutions and banks, and reduce financing costs in actual operations. These benefits will help agricultural entities obtain loans [30]. On the other hand, if policy behaviors only focus on risk sharing, they will increase financial pressure and have limited effect on lowering the financing threshold [31]. In the long run, policy behaviors cannot fundamentally overcome the financing difficulties of vulnerable groups. If the policy is too inclusive, it is not helpful for systemic risk control [23]. With reference to the previous analysis, the government should guide banks and guarantee institutions to establish a grading mechanism based on the actual development level and credit level of agricultural entities, integrate the development of agricultural entities, and



judge the risk of repayment. This is the fundamental way to help banks and guarantee institutions reduce losses [32]. Second, in the cooperation of farmland management rights based on counter-guarantee, banks are not active in responding to the request of customers for loans based on the counter-guarantee of large-scale farmland management rights [33]. In this view, banks only have a slight effect on increasing the amount of financing guarantee. This situation originally arose because it is difficult to

transform the mortgage value of farmland management rights; most new agricultural entities only pay one-year land rents, and banks cannot get compensated by defaults through rents [34]. Although banks possess the land management rights and the rights to dispose of economic derivatives on the land (such as fixed assets and economic crops), disposal is accompanied by great difficulty and requires additional disposal costs [35]. Therefore, when banks get farmers with a loan request based

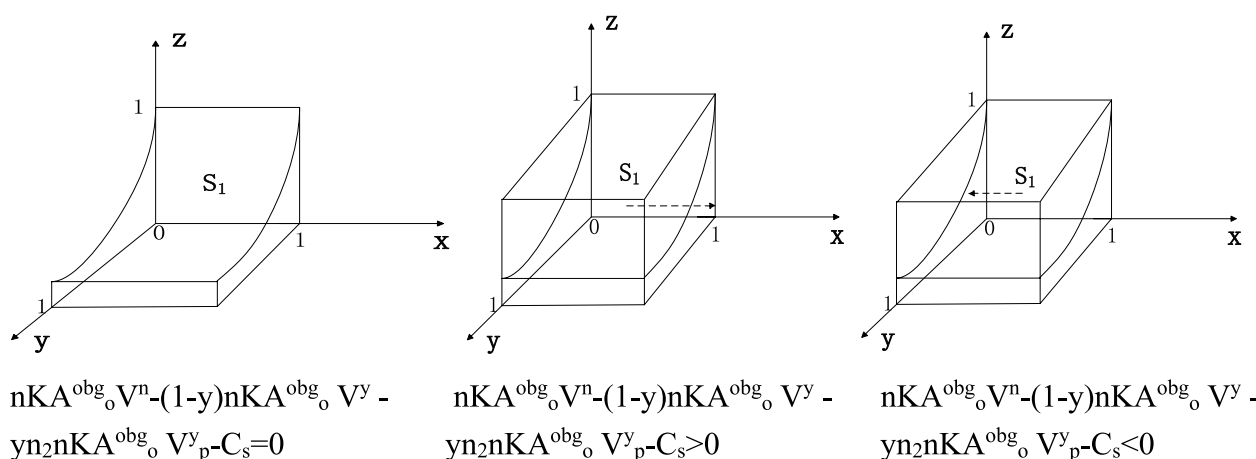


FIGURE 3

Trend of government strategy selection.

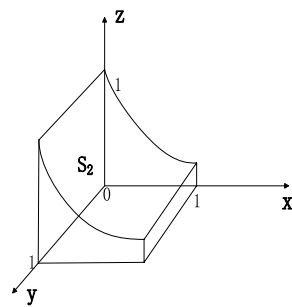
on the counter-guarantee of farmland management rights, they often require the participation of guarantee institutions. In fact, banks shift the risk of land transfer to guarantee institutions [36]. The participation of guarantee institutions can improve the financing enthusiasm of banks. However, this will increase the burden on guarantee institutions. In comparison with banks, guarantee institutions lack a grassroots network and risk control ability. It is more difficult for them to solve the problem of land management right circulation. Therefore, it is a general consensus for the government to build a land transfer platform to accelerate the land transfer rate and improve the efficiency of transforming the guarantee value of land management rights [37].

On the one hand, these studies emphasize the necessity and plausibility of the three-party cooperation model involving the government, banks, and guarantee institutions in sharing risks and discovering the mortgage value of large-scale land management rights guarantees. On the other hand, these studies reaffirm the positive effect of the cooperation model in helping new agricultural entities out of the financing dilemma. However, they fail to explain why there are still practical problems, such as low enthusiasm for cooperation and a low level of financing among the three parties in actual operation. As implied by the existing literature, the financing weakness of new agricultural entities and asymmetric information between borrowers and lenders are the significant factors leading to high financing risks and lower financing levels [38]. For those new agricultural entities with large-scale farmland management rights, the risk of bad debts will be significantly reduced if there is a large fixed asset investment in the associated agricultural land management rights or if the comprehensive asset capacity is high [39, 40]. In this view, risk reduction and financing level improvement will not only facilitate post-risk transfer but also boost prior risk screening and risk identification, thus eliminating information asymmetry. In addition to the guarantee value, farmland management rights also have the information function value of transmitting risk signals, which is of positive significance for identifying risks,

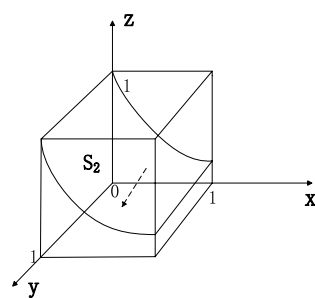
screening credit customers with development potential, and improving the operation level of the financing system [41]. However, we should not solely rely on the efforts of one party. Therefore, we should work harder to explore how to bring the respective advantages of the three parties into play and start further sustainable and positive cooperation based on the original cooperation. Based on the previous analysis, the study in this paper explores how to further mobilize the government, banks, and guarantee institutions as the principals in this model based on the current policy operation, thus identifying and reducing information asymmetry as the breakthrough point, helping the cooperation break the low-level equilibrium, and finally achieving sustainable development. This study intends to build the evolutionary game model of three-party cooperation involving the government, banks, and guarantee institutions, hoping to find the significant factors affecting the positive cooperation behaviors of these three parties. In addition, this study recommends a new approach for the sustainable cooperation to improve the operation quality of the “government, bank, and guarantee institution” cooperation mechanism. In this way, government and banks can work together to prevent the moral hazard caused by financing new agricultural entities, select new agricultural customers with development potential to offer accurate financial support, and reduce the overall risk of the financing system. With the cooperation mechanism of really sharing both risks and benefits, new agricultural entities will receive help for development, optimizing policy efficiency.

2 Conceptual model of subject behavior relationships under the “government, bank, and guarantee institution” mode

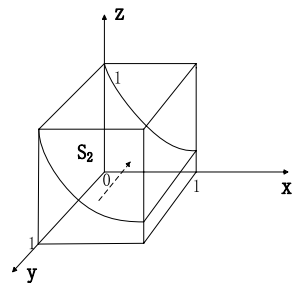
The cooperation mechanism mainly involves four types of subjects, including the government, banks, policy-oriented agricultural guarantee institutions, and new agricultural business



$$x \left[nKV^y (A_b^{obg} + R_b) - n_1 nKV_1^y (1 + R_b) - n_2 nKV_p^y (A_b^{obg} + R_b) - C_h^n \right] + xz(C_l^n + C_h^n - C_l^y) + (1 - z)x(IF - C_h^y) + (1 - z)C_h^n - zC_l^n = 0$$



$$x \left[nKV^y (A_b^{obg} + R_b) - n_1 nKV_1^y (1 + R_b) - n_2 nKV_p^y (A_b^{obg} + R_b) - C_h^n \right] + xz(C_l^n + C_h^n - C_l^y) + (1 - z)x(IF - C_h^y) + (1 - z)C_h^n - zC_l^n > 0$$



$$x \left[nKV^y (A_b^{obg} + R_b) - n_1 nKV_1^y (1 + R_b) - n_2 nKV_p^y (A_b^{obg} + R_b) - C_h^n \right] + xz(C_l^n + C_h^n - C_l^y) + (1 - z)x(IF - C_h^y) + (1 - z)C_h^n - zC_l^n < 0$$

FIGURE 4

Trend of bank strategy selection.

entities. New agricultural business entities are the object of service because they are in a weak financial position. In consideration of the aforementioned fact, whether the amount of financing guarantee can be successfully obtained is subject to the behavior decisions of the government, banks, and agricultural guarantee institutions. For this reason, this study focuses on the analysis of these three subjects.

With reference to the subject interactive process of the “government, bank, and guarantee institution” cooperative financing guarantee in a pilot area in China in 2016, we can render the interactive process of the three subjects. First, the

grassroots government builds a farmland management rights transfer platform for farmland management rights registration, valuation, large-scale farmland transfer transactions, management of guaranteed farmland management rights, and transfer of bad management rights. The government has established a special venture fund, with which discount is provided to pilot financing guarantee programs and non-performing loans are paid proportionally. Second, as a loan applicant, new agricultural entities can assess the guarantee value of farmland management rights using the platform, apply for participation in pilot financing

TABLE 1 Payment matrix.

| Strategy combination | Government | Bank | Agricultural guarantee institution |
|------------------------------------------|------------------------------------------|-------------------------------------------------------------------------------------------|------------------------------------------------------|
| (1,1,1) | $nk(Q - m) - n_2nkV_p^y A_o^{obg} - C_s$ | $nk(R_b + m_b) - n_1nkV_l^y(1 + R_b) - n_2nkV_p^y(A_b^{obg} + R_b) + IF - C_l^y - C_{bg}$ | |
| | | $n_2nk(R_g + m_g) - n_2nkV_p^y(A_g^{obg} - SW) + T + IF - C_l^y$ | (1,1,0) |
| $nk(Q - m) - n_2nkV_p^y A_o^{obg} - C_s$ | | $nk(R_b + m_b) - n_1nkV_l^y(1 + R_b) - n_2nkV_p^y(A_b^{obg} + R_b) + IF - C_l^y - C_{bg}$ | $n_2nk(R_g + m_g) - n_2nkV_p^y(A_g^{obg} - SW) + IF$ |
| (1,0,1) | $nk(Q - m) - nkV^y A_o^{obg} - C_s$ | $nk(R_b + m_b) - nkV^y(A_b^{obg} + R_b) + IF - C_{bg}$ | $nk(R_g + m_g) - nkV^y(A_g^{obg} - SW) + IF - C_h^y$ |
| (1,0,0) | $nk(Q - m) - nkV^y A_o^{obg} - C_s$ | $nk(R_b + m_b) - nkV^y(A_b^{obg} + R_b) - C_{bg}$ | $nk(R_g + m_g) - nkV^y(A_g^{obg} - SW)$ |
| (0,1,1) | $nk(Q - m) - nkV^n A_o^{obg}$ | $nk(R_b + m_b) - nkV^n(A_b^{obg} + R_b) - C_l^n - C_{bg}$ | $nk(R_g + m_g) + T - nkV^n A_g^{obg} - C_l^n$ |
| (0,1,0) | $nk(Q - m) - nkV^n A_o^{obg}$ | $nk(R_b + m_b) - nkV^n(A_b^{obg} + R_b) - C_h^n - C_{bg}$ | $nk(R_g + m_g) - nkV^n A_g^{obg}$ |
| (0,0,1) | $nk(Q - m) - nkV^n A_o^{obg}$ | $nk(R_b + m_b) - nkV^n(A_b^{obg} + R_b) - C_{bg}$ | $nk(R_g + m_g) - nkV^n A_g^{obg} - C_h^y$ |
| (0,0,0) | $nk(Q - m) - nkV^n A_o^{obg}$ | $nk(R_b + m_b) - nkV^n(A_b^{obg} + R_b) - C_{bg}$ | $nk(R_g + m_g) - nkV^n A_g^{obg}$ |

TABLE 2 Behavioral strategy combination for the government, bank, and guarantee agency.

| Space distribution | Strategy of the government, bank, and guarantee agency |
|------------------------|------------------------------------------------------------------------------------------------------|
| V_1, V_3 , and V_5 | Risk identification-guiding strategy, positive loan strategy, and positive guarantee strategy |
| V_1, V_3 , and V_6 | Risk identification-guiding strategy, positive loan strategy, and negative guarantee strategy |
| V_1, V_4 , and V_5 | Risk identification-guiding strategy, negative loan strategy, and positive guarantee strategy |
| V_1, V_4 , and V_6 | Risk identification-guiding strategy, negative loan strategy, and negative guarantee strategy |
| V_2, V_3 , and V_5 | Subsidy strategy based on risk compensation, positive loan strategy, and positive guarantee strategy |
| V_2, V_3 , and V_6 | Subsidy strategy based on risk compensation, positive loan strategy, and negative guarantee strategy |
| V_2, V_4 , and V_5 | Subsidy strategy based on risk compensation, negative loan strategy, and positive guarantee strategy |
| V_2, V_4 , and V_6 | Subsidy strategy based on risk compensation, negative loan strategy, and negative guarantee strategy |

guarantee programs, and accept the qualification examination. Third, agricultural guarantee institutions will, in accordance with relevant policies, refer to the value of farmland management rights and financial subsidies, evaluate profits and costs, make a decision on whether to provide guarantee, and apply to banks for a loan. If the application is approved, the platform will help new agricultural entities obtain the loan, thereby collecting a guarantee fee. In case of any non-performing loan, the platform will proportionally pay an amount to the bank. Then, recovery is performed by the agricultural guarantee institution for the defaulter. If the recovery fails, the platform will assist the agricultural guarantee institution in disposing of the farmland management rights as a counter-guarantee to make up for the losses. Fourth, based on the application, the bank will thoroughly evaluate the farmland management rights and financial subsidies of new agricultural

entities, assess the profits and costs, and make a decision on whether to approve the loan application. This constitutes the cooperation and interaction among the government, banks, and guarantee institutions in exploring the guarantee value of large-scale farmland management rights and in sharing risks. If the risk signal value of farmland management rights is increased, improvements should be made in the following aspects: (1) the grassroots government builds a land management rights transfer platform. Based on the original responsibilities and affairs, the platform can obtain the risk information of large-scale farmland management rights involved in counter-guarantee (such as information on the transfer value of farmland management rights, the status of investment in the assets attached to the farmland, the status of crops attached to the farmland, information on the technological innovation application value, and the management model). Meanwhile, the risk information will be shared with the cooperative bank and agricultural guarantee institution to provide an objective basis for risk identification. (2) The agricultural guarantee institution and the bank individually or jointly pay the cost of risk identification and the value of the shared risk information transformation and hereby decide whether to provide guarantee services or approve the loan application. In other words, differential guarantee loan strategies should be selected through risk identification. For those new agricultural entities with risks lower than the general credit requirements, the bank can lend directly. For those new agricultural entities with risks higher than the general credit requirements but showing a certain development potential, the bank and the agricultural guarantee institution can jointly start lending. For those entities with very high risks but no development potential, the agricultural guarantee institution should reject the guarantee, and the bank should reject the loan application. In this way, a conceptual map of the cooperation behavior interaction process among the government, banks, and guarantee institutions for financing guarantee of new agricultural entities is developed (Figure 1).

In this process, the three parties not only cooperate with each other in risk sharing and exploring the mortgage value in guarantee but also identify and use the risk information value of the farmland management rights.

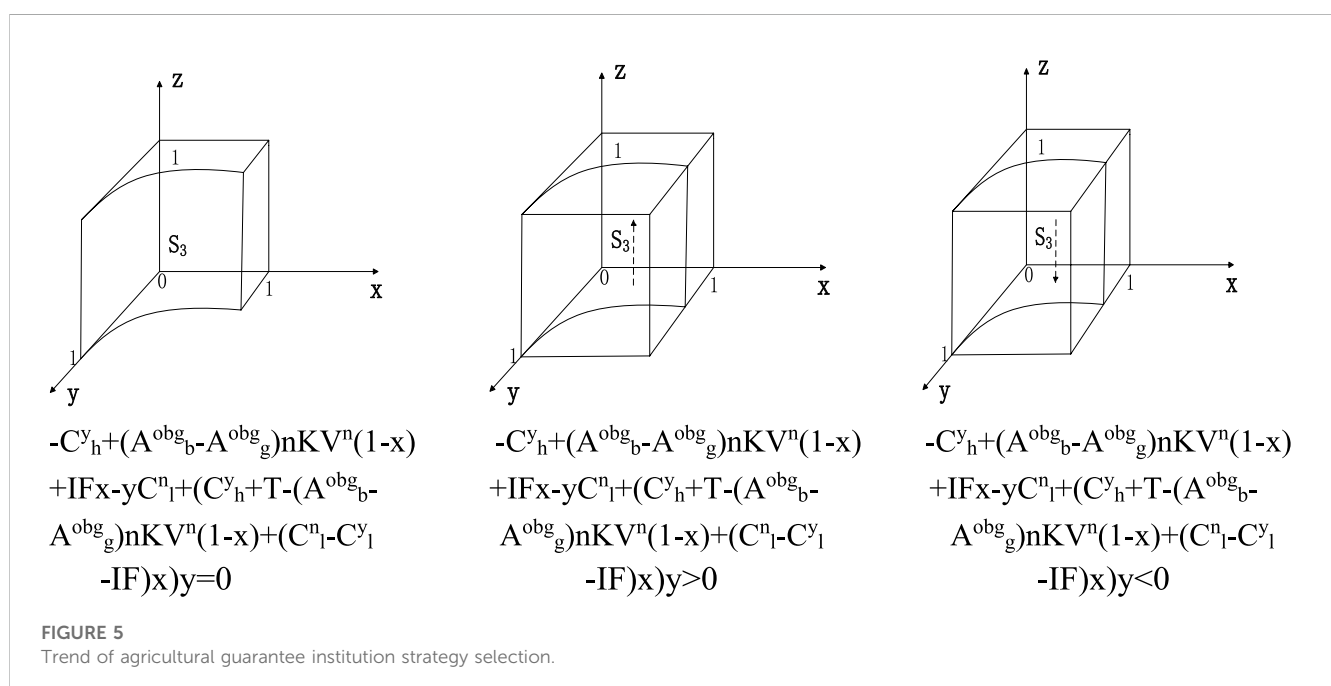
TABLE 3 Stability conditions of the equilibrium point.

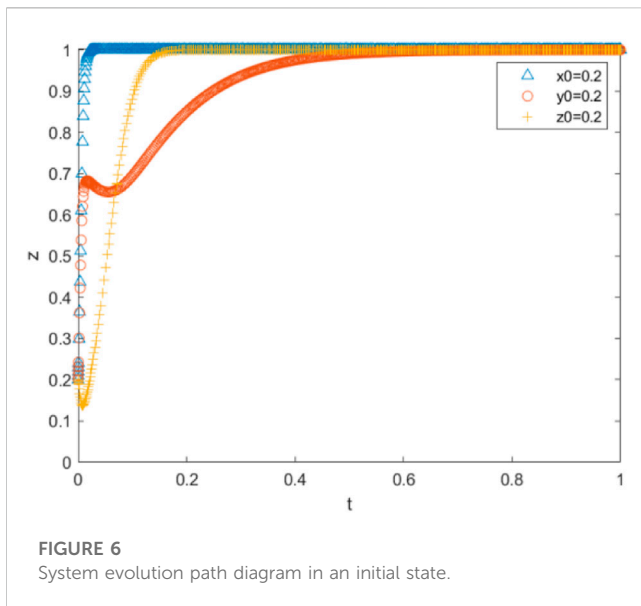
| Equilibrium point | λ_1 | λ_2 | λ_3 |
|-------------------|-------------------------------------------------------|--------------------------------------------------------------------------------------------------------|---------------|
| (1,1,1) | $C_s + n_2 n K A_o^{obg} V_p^y - n K A_o^{obg} V^n$ | $[C_l^y + n_1 n K V_l^y (1 + R_b) + n_2 n K V_p^y (A_b^{obg} + R_b)] - n K V^y (A_b^{obg} + R_b)$ | $C_l^y - T$ |
| (1,1,0) | $C_s + n_2 n K A_o^{obg} V_p^y - n K A_o^{obg} V^n$ | $[C_h^y + n_1 n K V_l^y (1 + R_b) + n_2 n K V_p^y (A_b^{obg} + R_b)] - n K V^y (A_b^{obg} + R_b) - IF$ | $-C_l^y + T$ |
| (1,0,1) | $C_s + n K A_o^{obg} V^y - n K A_o^{obg} V^n$ | $n K V^y (A_b^{obg} + R_b) - [C_l^y + n_1 n K V_l^y (1 + R_b) + n_2 n K V_p^y (A_b^{obg} + R_b)]$ | $-C_h^y - IF$ |
| (1,0,0) | $C_s + n K A_o^{obg} V^y - n K A_o^{obg} V^n$ | $n K V^y (A_b^{obg} + R_b) + IF - [C_h^y + n_1 n K V_l^y (1 + R_b) + n_2 n K V_p^y (A_b^{obg} + R_b)]$ | $-C_h^y + IF$ |
| (0,1,1) | $n K A_o^{obg} V^n - (n K A_o^{obg} n_2 V_p^y + C_s)$ | C_l^n | $C_l^n - T$ |
| (0,1,0) | $n K A_o^{obg} V^n - (n K A_o^{obg} n_2 V_p^y + C_s)$ | $-C_h^n$ | $-C_l^n + T$ |
| (0,0,1) | $n K A_o^{obg} V^n - (n K A_o^{obg} V^y + C_s)$ | $-C_l^n$ | C_h^n |
| (0,0,0) | $n K A_o^{obg} V^n - (n K A_o^{obg} V^y + C_s)$ | C_h^n | $-C_h^n$ |

During the cooperation, the government aims to maximize social and economic benefits, hoping to expand the scale of new agricultural entities and reduce overall systemic risks. The government tries to raise the credit line and reduce risk for guarantee institutions through measures such as risk sharing based on proportional compensation and counter-guarantee of farmland management rights so as to relieve the pressure of risk control on banks. Moreover, various incentive policies are formulated to strengthen the role of agricultural guarantee institutions as a bridge. Banks are encouraged to cooperate with agricultural guarantee institutions to actively perform their duties and identify and reduce systemic risks. All the aforementioned efforts are made to achieve the policy goal of extending both guarantee and loan businesses to include new agricultural entities. If the policies place particular stress on the compensation of post risks, the policy effect will be weakened accordingly. For example, banks rely too much on risk transfer.

Guarantee institutions are incapable of eliminating banks' concerns of risk control. Banks and guarantee institutions are not fully motivated to identify customer risks and expand the financing guarantee business for potential new agricultural entities. If we fail to mobilize banks and guarantee institutions' cooperation, the policy will get entangled in a negative state.

As the fund provider, banks are in a more competitive position, hoping to increase financing returns based on reduced risks. As independent economic units, they always try to maximize their own interests. The new agricultural financing is essentially inclusive finance with a lower loan interest rate and return. Most new agricultural entities lack historical credit information and collaterals, resulting not only in a high financing risk but also in high risk identification difficulty and cost. Affected by low return but high risk and cost, risk control mainly depends on government incentive policies, default compensation, counter-guarantee of farmland management rights, and the guarantee of an





agricultural guarantee institution for risk transfer. In respect of the aforementioned fact, banks are far less motivated to identify the real risks of new agricultural entities by spending additional human resources, materials, and financial costs. Therefore, in the whole process of financing, banks adopt a passive attitude. When the government offers weak incentives and little compensation that cannot cover the risk suffered by banks, banks will be reluctant to lend to new agricultural entities, or the loan scale is small. When government incentives and risk-sharing measures can greatly transfer risks, banks will increase the loan amount. Due to the asymmetry between cost and benefit, banks are passive in risk control, causing a high level of risk in the financing system. Then, banks cannot wait for sustainable development.

Agricultural guarantee institutions are in a weaker position in the whole “government, bank, and guarantee institution” financing system. They are policy- and market-oriented. With these dual attributes, they hope to maximize their own interests and should take into account the policy implementation of inclusive finance. Agricultural guarantee institutions often have a large amount of government investment, laying a more sufficient financial foundation than market-oriented guarantee institutions and a stronger immunity against risks. However, due to the policy constraints on behavioral decisions and the necessity of considering the risk of state-owned asset loss, their behavior is more conservative. Along with insufficient market competition, there are fewer policy-oriented agricultural guarantee institutions. They are small scale and lack high risk-control abilities. Therefore, policy-oriented agricultural guarantee institutions hope to expand the scope of financing credit for new agricultural entities, raise the overall credit line of banks, and become a bridge between banks and new agricultural entities based on the requirements of inclusive finance. While helping more new agricultural entities apply for more bank loans, they can obtain the expected guarantee income. Moreover, they are incapable of bearing the default risk of new agricultural entities alone and identifying these default risks. They are also afraid to bear the responsibility for the loss of state-owned

assets caused by the high default rate of new agricultural entities. In the face of the guarantee claims from new agricultural entities, their behavior is conservative, and they neither dare to significantly vouch for new agricultural entities nor alleviate the banks’ concern over risks. Therefore, they are in a dilemma.

In summary, the government, banks, and agricultural guarantee institutions are closely linked in the process of financing guarantees for new agricultural entities. The government needs the active cooperation of banks and agricultural guarantee institutions to screen new agricultural entities with development potential for financial support, reduce the risk of the financing system, increase the amount of financing, and create more social and economic benefits. In this cooperation mechanism, banks will issue loans to new agricultural entities based on risk sharing, guarantee, counter-guarantee, and policy incentives. Agricultural guarantee institutions need government support to obtain financial support and risk resistance. Moreover, they require bank loans so as to achieve their goals of inclusive finance and profitability. These subjects have different value attributes and objectives. Therefore, the effectiveness of various government measures is limited; banks are in a negative state and rely on risk transfer. Agricultural guarantee institutions are not motivated and empowered to increase the amount of financing guaranteed and alleviate the concern of banks over risk control. In this sense, they are also in a negative state. The entire financing guarantee system enters a vicious circle. By clarifying the interaction and game relationship among the government, banks, and agricultural guarantee institutions, it is of great significance to properly avoid the negative behavior of all the subjects in the process of financing new agricultural entities, thus promoting the sustainable development of the financing market. Each party has its own goals, making it difficult to meet the requirements of all parties. Under such circumstances, they will choose different strategies according to their own interests, adapting them to specific situations. The conceptual model of strategy selection by the government, banks, and agricultural guarantee institutions is shown in Figure 2.

3 Building a game model related to the cooperation behavior in the cooperation mechanism of financing guarantee for new agricultural entities

In order to more specifically analyze how the three parties carry out sustainable and active cooperation and open the black box of tripartite interests, the authors build a cooperative game model of “government, bank, and guarantee institution” financing guarantee, observe the evolution trend of the system, and verify the feasibility of the cooperation path through simulation based on practical source data.

3.1 Basic hypothesis of the model

Hypothesis 1: government, banks, and agricultural guarantee institutions are limited rational decision-makers. It is difficult for each game subject to make the best strategic choice in an event.

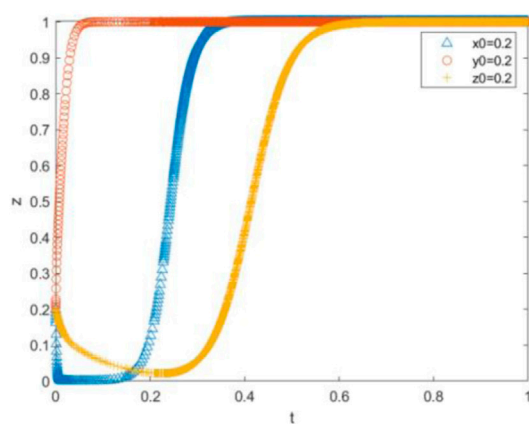
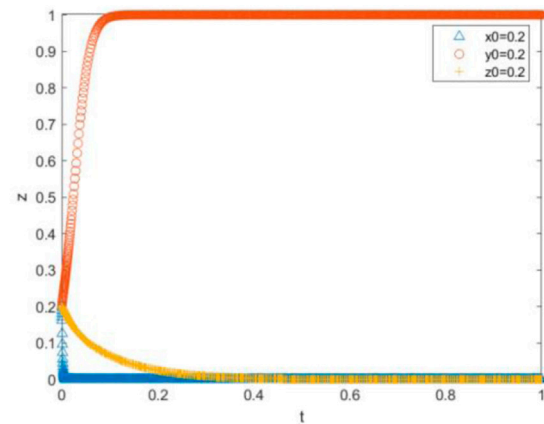
① $V^y=0.28$ turn into $V^y=0.3$ ② $V^y_p=0.03$ turn into $V^y_p=0.3$

FIGURE 7

System evolution path under the change in risk identification quality.

Therefore, they should keep simulating and learning from each other in the process of the game, thus steadily optimizing their own behaviors.

Hypothesis 2: government, banks, and agricultural guarantee institutions can choose two strategies. There are two types of government strategies [29]. The first one is the subsidy strategy based on risk compensation, in which the government only offers a certain amount of discount subsidy to guarantee loans for new agricultural entities and proportional risk compensation. The second one refers to the risk identification-guiding strategy, in which the government further shares the affiliated risk information of farmland management rights based on the previous strategy and motivates banks and guarantee institutions to cooperate for risk identification.

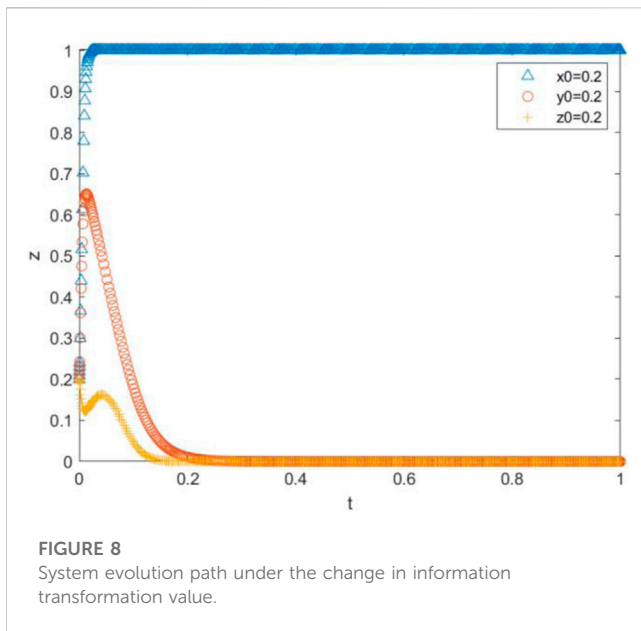
There are two bank strategies [30]. In the first strategy, banks issue loans in a negative way and approve loan applications when both guarantee and subsidy can offset specific risks. In the second strategy, banks issue loans in a positive way, play an active role in identifying the risk level of customers, and make differential loan decisions based on guarantees. Banks develop risk identification products that comply with the characteristics of new agricultural entities based on the shared risk information and expenditures. Using the product, they can find three types of new agricultural customers, including the customers that meet the existing credit criteria, the customers having development potential but failing to meet the existing credit criteria of banks, and the customers failing to meet the development potential standard. Banks selectively issue loans based on the status of guarantee.

There are two strategies for agricultural guarantee institutions [31]. In the first strategy, agricultural guarantee institutions provide guarantee services in a negative way and decide to guarantee only when the incentives and subsidies can offset the specific risks. In the second strategy, they provide guarantee services in a positive way, play an active role in developing and using the shared risk

information, and then identify the risk level of new agricultural entities. Agricultural guarantee institutions develop risk identification products based on the shared risk information and expenditures. Using the product, they can find new agricultural customers with development potential failing to meet the existing credit criteria of banks and selectively provide guarantee services. If the second strategy is chosen, it means that the agricultural guarantee institution will cooperate with the bank to jointly bear the risk identification cost. Then, both parties will cover a lower cost.

Based on the aforementioned analysis, the following strategies are recommended: the government (the subsidy strategy based on risk compensation and the risk identification-guiding strategy), banks (the strategy of issuing loans in a negative way and the strategy of issuing loans in a positive way), and agricultural guarantee institutions (the strategy of providing guarantee service in a negative way and the strategy of providing guarantee service in a positive way). Each party has two strategies. The possibilities for each of them to choose the positive strategy are x , y , and z , respectively, all of which are functions of time.

Hypothesis 3: Both government benefits and costs can be quantified [23]. The government builds a land transfer platform, which helps reduce the transfer cost of large-scale farmland management rights and improves the transfer efficiency and guarantee value of the rights. In addition, the platform can acquire risk information from the rights and share the information with banks and agricultural guarantee institutions. The benefits obtained by the government include the local agricultural development tax revenue, the increase of jobs, the improvement of social equity, and the improvement of the government's reputation due to the government's active solution to the financing problems of new agricultural entities. In theory, the governmental benefits should increase in proportion to the scale of financing and lending. In the cooperation mechanism, it is supposed that the loan amount is determined by the risk reserve and credit

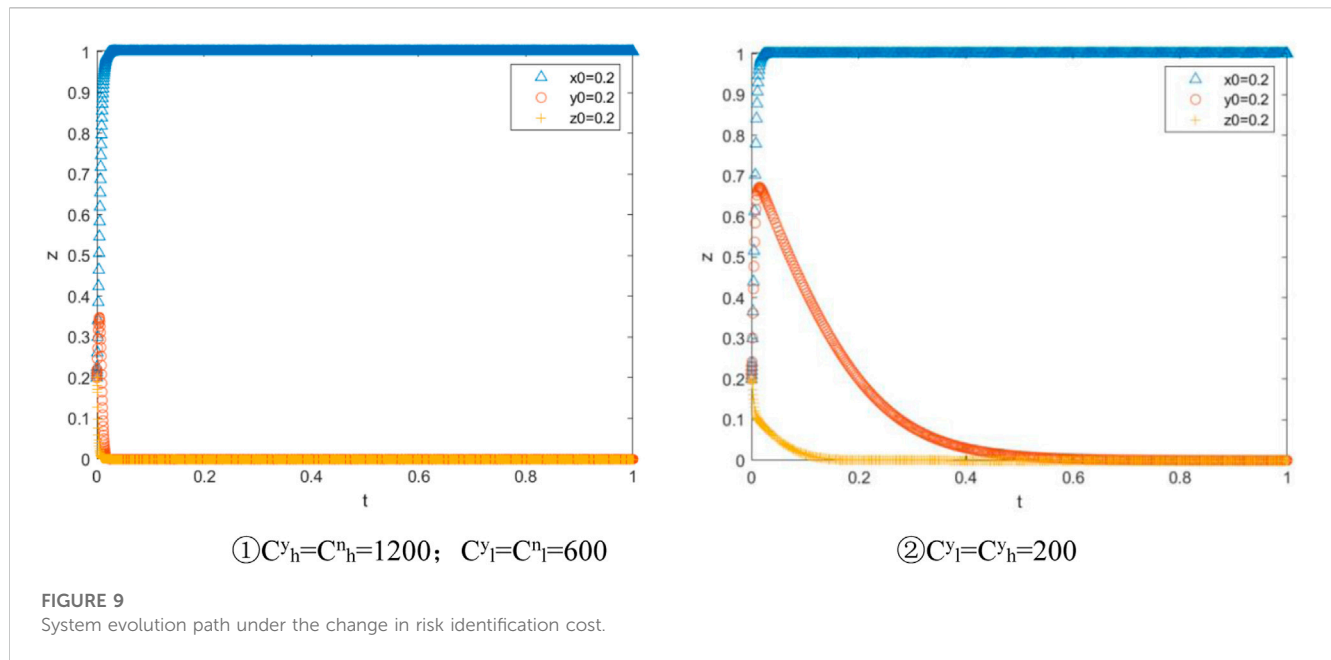


guarantee leverage jointly established by the government and agricultural guarantee institution. The yield was set as Q , the bank's basis point as k (k comes from the established risk reserve), and the guarantee leverage as n . The costs paid by the government consist of the following items. If the government shares risk information, these costs include the cost of platform construction, the cost of resource allocation, and the cost of collecting risk information for new agricultural entities based on farmland management rights, which can be quantified as C_s . Moreover, the government will give a certain subsidy to the new agricultural financing business and bear a certain proportion of the default compensation. The government's total subsidy rate was set as m . When any compensation occurs, the government's share of compensation is A_b^{obg} . Considering that the more transparent the risk information, the lower the default rate of new agricultural entities, the average default rate for new agricultural entities is V^y when it is assumed that the risk information of farmland management rights is shared. When risk information is not shared, the average default rate for new agricultural entities is V^n , which meets $V^y < V^n$.

Hypothesis 4: The bank's benefits and costs can be quantified [32]. Assuming that R_b is the benchmark interest rate for bank loans and m_b is the interest rate subsidized by the government to banks ($0 \leq m_b < 1$), the bank loan yield is $nk(R_b + m_b)$, and the yield increases in positive proportion with the increase in the amount of bank loans. Affected by different strategies of the government and agricultural guarantee institutions, different strategies chosen by banks will produce different benefits and costs. (1) When the government shares risk information, banks have to pay the cost of risk identification first if they are actively issuing loans. If banks perform only risk identification, they should bear the cost (C_h^y) separately. If it is implemented with agricultural guarantee institutions, both of them should jointly bear the cost (C_l^y). Here, the criterion $C_h^y > C_l^y$ is met. Second, banks obtain the

transformation value (IF) of risk information. In other words, one or two parties of banks and agricultural guarantee institutions will process the risk information shared by the government (for example, develop the guaranteed loan product based on risk levels), which helps banks reduce risks, expand business, and gain reputation. As a result, banks obtain a series of economic and social benefits. Third, those banks that have chosen the positive loan policy will issue loans to projects (the default rate, V_l^y) of high-quality new agricultural entities that meet the risk requirements of general loan projects, based on the credit line of n_1nk . In case of any default, the bank will bear the loss of full principal and profit with the amount of $n_1kV_l^y(1 + R_b)$. For any loan project involving suboptimal new agricultural entities with risks higher than the requirements for general loan projects but showing development potential (default rate V_p^y and $V_p^y > V_l^y$), the bank chooses to cooperate with agricultural guarantee institutions (with the project review cost C_{bg} paid by the bank) for the loan based on the credit line of n_2nk . If a default occurs, they will bear the loss of the loan principal in the proportion of A_b^{obg} and the total profits with the total loss amount of $n_2kV_p^y(A_b^{obg} + R_b)$. (2) If banks issue loans in a negative way when the government shares risk information, they will not pay the cost of processing risk information but will only choose to cooperate with agricultural guarantee institutions to guarantee the loan and rely on various government subsidies for risk transfer. In the event of a default at this time, the bank will bear the loss of principal and the total profits in the proportion of A_b^{obg} , and the amount of the loss is $nkV^y(A_b^{obg} + R_b)$. (3) Even if the bank subjectively wants to identify the risk of new agricultural customers and issues loans in a positive way when the government does not share risk information, due to the lack of necessary objective conditions, not only is the cost of risk identification extremely high but the identification is also extremely difficult and the effect is poor, making it hard to achieve the positive loan strategy. When a default occurs, the bank will bear the loss of principal and the total profits in the proportion of A_b^{obg} , and the amount of the loss is $nkV^n(A_b^{obg} + R_b)$.

Hypothesis 5: The benefits and costs of an agricultural guarantee institution can be quantified [33]. Agricultural guarantee institutions can obtain guarantee fees by providing guarantee services for new agricultural business entities. Affected by the different strategies of the government and banks, there will also be different benefits and costs if the strategies chosen by agricultural guarantee institutions are different. Here, it is assumed that the government shares information about risks associated with the farmland management rights and that agricultural guarantee institutions provide guarantee services in a positive way. First, agricultural guarantee institutions should bear the risk identification cost. If they perform risk identification with banks, both of them should bear the cost. If banks carry out risk identification solely, they should bear the cost themselves. Second, the transformation value (IF) of risk information can be obtained. Third, if both agricultural guarantee institutions and banks choose positive strategies, the former ones will be recognized by banks, and banks will achieve long-term cooperation with them, resulting in long-term benefit T . Fourth, the agricultural guarantee institutions that have adopted a positive



strategy will guarantee those loan projects of new agricultural entities that have risks higher than the requirements of general banks for separate loans but show development potential. In other words, the institution will apply to banks for the loan based on the “government, bank, and guarantee institution” cooperative guarantee. If the bank agrees, the agricultural guarantee institution will obtain the subsidy to the rate of guarantee fee and receive the government guarantee rate subsidy (assuming that R_g is the rate of guarantee rate and m_g is the government’s subsidy to the rate of guarantee fee, meeting $0 \leq m_g < 1$). Fifth, once the subject of the guaranteed loan defaults, it shall bear the principal loss of the guaranteed loan in the proportion of A_g^{obg} . There is the counter-guarantee of farmland management rights. Therefore, the agricultural guarantee institution will get the compensation from collateral. SW refers to the expected return on the average compensation from collateral. (2) It is assumed that agricultural guarantee institutions choose the negative guarantee strategy in the context where the government shares risk information. The benefit composition of agricultural guarantee institutions remains unchanged without triggering any risk identification costs. In the case of compensation, the institution should bear the principal loss of the guaranteed loan in the proportion of A_g^{obg} and also obtain the compensation from collaterals. (3) No matter which strategy is chosen by agricultural guarantee institutions when risk information is not shared, the benefit composition remains unchanged and is similar to that of banks. If the institutions subjectively intend to adopt the positive strategy and they lack objective risk information, the guarantee will suffer a very high cost, great difficulty, and poor effect. In case of compensation, the institutions must bear the principal loss of the guaranteed load in the proportion of A_g^{obg} .

The payment matrix can be established according to the assumption (Table 1).

3.2 Construction of the replicated dynamic equation

When one party’s expected value of a particular strategy is higher than the average expectation of a mixed strategy in a three-party game, the strategy is more likely to be adopted. According to the Malthusian dynamic equation, as long as the individual who adopts this strategy has a higher degree of adaptation than the average group, the strategy will grow over time, and the expected value of each subject can be calculated accordingly.

U_{11} was set as the benefits of the government when it adopts Strategy 1 (the risk identification-guiding strategy) and U_{12} as the benefits of the government when it adopts Strategy 2 (the subsidy strategy based on risk compensation). U_1 indicates the average expected return of the government. Then,

$$\begin{aligned}
 U_{11} &= yz(nk(Q-m) - n_2nkV_p^yA_o^{obg} - C_s) \\
 &\quad + y(1-z)(nk(Q-m) - n_2nkV_p^yA_o^{obg} - C_s) \\
 &\quad + (1-y)z(nk(Q-m) - nkV^yA_o^{obg} - C_s) \\
 &\quad + (1-y)(1-z)(nk(Q-m) - nkV^yA_o^{obg} - C_s), \\
 U_{12} &= yz(nk(Q-m) - nkV^nA_o^{obg}) \\
 &\quad + y(1-z)(nk(Q-m) - nkV^nA_o^{obg}) \\
 &\quad + (1-y)z(nk(Q-m) - nkV^nA_o^{obg}) \\
 &\quad + (1-y)(1-z)(nk(Q-m) - nkV^nA_o^{obg}), \\
 U_1 &= xU_{11} + (1-x)U_{12}.
 \end{aligned}$$

U_{21} indicates the return of the bank after choosing Strategy 1 (the positive loan strategy). U_{22} indicates the return after choosing Strategy 2 (the negative loan strategy). U_2 indicates the average expected return of the bank. Then,

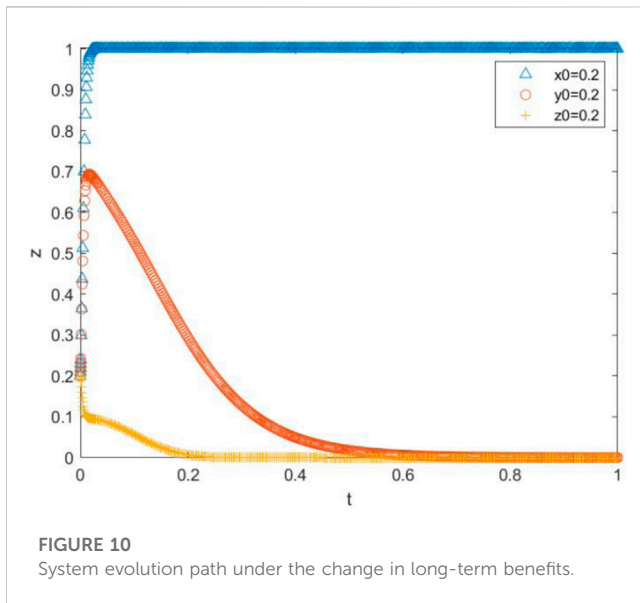


FIGURE 10
System evolution path under the change in long-term benefits.

$$\begin{aligned}
 U_{21} &= xz(nk(R_b + m_b) - n_1nKV_1^y(1 + R_b) - n_2nKV_p^y(A_b^{obg} + R_b) \\
 &\quad + IF - C_1^y - C_{bg}) + x(1 - z)(nk(R_b + m_b) - n_1nKV_1^y(1 + R_b) \\
 &\quad - n_2nKV_p^y(A_b^{obg} + R_b) + IF - C_h^y - C_{bg}) + (1 - x)z(nk(R_b + m_b) \\
 &\quad - nKV^n(A_b^{obg} + R_b) - C_1^n - C_{bg}) + (1 - x)(1 - z)(nk(R_b + m_b) \\
 &\quad - nKV^n(A_b^{obg} + R_b) - C_h^n - C_{bg}), \\
 U_{22} &= xz(nk(R_b + m_b) - nKV^y(A_b^{obg} + R_b) + IF - C_{bg}) \\
 &\quad + x(1 - z)(nk(R_b + m_b) - nKV^y(A_b^{obg} + R_b) - C_{bg}) \\
 &\quad + (1 - x)z(nk(R_b + m_b) - nKV^n(A_b^{obg} + R_b) - C_{bg}) \\
 &\quad + (1 - x)(1 - z)(nk(R_b + m_b) - nKV^n(A_b^{obg} + R_b) - C_{bg}), \\
 U_2 &= yU_{21} + (1 - y)U_{22}.
 \end{aligned}$$

U_{31} indicates the return of agricultural guarantee institutions when choosing Strategy 1 (the positive guarantee strategy). U_{32} indicates the return after choosing Strategy 2 (the negative guarantee strategy). U_3 indicates the average expected return of agricultural guarantee institutions. Then,

$$\begin{aligned}
 U_{31} &= xy(n_2nK(R_g + m_g) - n_2nKV_p^y(A_g^{obg} - SW) + T + IF - C_1^y) \\
 &\quad + x(1 - y)(nK(R_g + m_g) - nKV^y(A_g^{obg} - SW) + IF - C_h^y) \\
 &\quad + (1 - x)y(nK(R_g + m_g) + T - nKV^n(A_g^{obg} - C_1^n) \\
 &\quad + (1 - x)(1 - y)(nK(R_g + m_g) - nKV^n(A_g^{obg} - C_h^n)), \\
 U_{32} &= xy(n_2nK(R_g + m_g) - n_2nKV_p^y(A_g^{obg} - SW) + IF) \\
 &\quad + x(1 - y)(nK(R_g + m_g) - nKV^y(A_g^{obg} - SW)) \\
 &\quad + (1 - x)y(nK(R_g + m_g) - nKV^n(A_g^{obg})) \\
 &\quad + (1 - x)(1 - y)(nK(R_g + m_g) - nKV^n(A_g^{obg})), \\
 U_3 &= zU_{31} + (1 - z)U_{32}.
 \end{aligned}$$

Therefore, the replicated dynamic equation of the government, banks, and agricultural guarantee institutions is, respectively,

$$\begin{aligned}
 F(x) &= \frac{dx}{dt} = x(U_{11} - U_1) = x(1 - x)(U_{11} - U_{12}) \\
 &= x(1 - x)[nKA_o^{obg}(V^n - (1 - y)V^y - n_2yV_p^y) - C_s], \\
 F(y) &= \frac{dy}{dt} = y(U_{21} - U_2) = y(1 - y)(U_{21} - U_{22}) \\
 &= y(1 - y)[-zC_1^n + x(IF + nK(A_b^{obg}V^y + R_bV^y \\
 &\quad - n_1V_1^y - n_1R_bV_1^y - n_2(A_b^{obg} + R_b)V_p^y) - C_h^y(1 - z) + zC_1^n \\
 &\quad - z(C_1^y + IF)) + C_h^n(1 - x - z + xz)], \\
 F(z) &= \frac{dz}{dt} = z(U_{31} - U_3) = z(1 - z)(U_{31} - U_{32}) \\
 &= z(1 - z)[-C_h^y - IFx(-1 + y) + C_h^y y - (C_1^n - T - C_1^n x + C_1^y x)y].
 \end{aligned}$$

3.3 Solving the equilibrium point of the evolutionary game

In the process of a dynamic game, the probability x , y , and z of the selection strategy for the government, banks, and agricultural guarantee institutions, respectively, participating in the game are related to time t , thus knowing that the solution domain of the replicated dynamic equation set is $[0, 1] \times [0, 1] \times [0, 1]$. The equilibrium point of the three-party dynamic game can be obtained according to the three-party replicated dynamic equation. The simultaneous equation shows that there are eight special equilibrium points, including $(0, 0, 0)$, $(0, 0, 1)$, $(0, 1, 0)$, $(0, 1, 1)$, $(1, 0, 0)$, $(1, 0, 1)$, $(1, 1, 0)$, and $(1, 1, 1)$, and these eight equilibrium points constitute the solution domain of the evolutionary game $\Omega = \{(x, y, z) | 0 < x < 1, 0 < y < 1, 0 < z < 1\}$. There is also an equilibrium solution satisfied with the following equation in the solution domain Ω :

$$\begin{aligned}
 (1 - 2x)[-C_s + nKA_o^{obg}(V^n - V^y(1 - y) - n_2yV_p^y)] &= 0, \\
 (1 - 2y)[-zC_1^n + x(IF + nK(A_b^{obg}V^y + R_bV^y - n_1V_1^y - n_1R_bV_1^y \\
 &\quad - n_2(A_b^{obg} + R_b)V_p^y) - C_h^y(1 - z) + zC_1^n - z(C_1^y + IF)) \\
 &\quad + C_h^n(1 - x - z + xz)] \\
 &= 0, \\
 (1 - 2z)[-C_h^y + (A_b^{obg} - A_g^{obg})nKV^n(1 - x) + IFx - yC_1^n \\
 &\quad + (C_h^y + T - (A_b^{obg} - A_g^{obg})nKV^n(1 - x) \\
 &\quad + (C_1^n - C_1^y - IF)x)y] = 0.
 \end{aligned}$$

4 Stability analysis of the evolution of subject behaviors

According to the basic nature of the replicated dynamic equation in the game model, $F'(x)$ represents the ratio of group strategy selection over time. When $F'(x)$ is 0, group strategy selection does not change over time. When $F'(x)$ is greater than 0, the rate of change in group strategy selection increases over time, and x is an unstable point. When $F'(x)$ is less than 0, the rate of change in group strategy selection decreases over time, and x is a stable point.

(1) Analysis of government's asymptotic stability

①When $nKA_0^{obg}(V^n - V^y(1-y) - n_2yV_p^y) - C_s = 0$, the strategy selection of the government will not change over time, so the strategy selection of subjects is the curved surface S_1 in Figure 3; any point on the curved surface is an evolutionary stability point.

②When $nKA_0^{obg}(V^n - V^y(1-y) - n_2yV_p^y) - C_s > 0$, then $F'(0) > 0$ and $F'(1) < 0$, and the stability theorem of the replicated dynamic differential equation shows that $x = 1$ is the stability point, indicating that the government chooses Strategy 2 to gain more than the cost and that the government chooses the evolutionary stability strategy as its strategy.

③When $nKA_0^{obg}(V^n - V^y(1-y) - n_2yV_p^y) - C_s < 0$, then $F'(0) < 0$ and $F'(1) > 0$, and it is known from the stability theorem of the replicated dynamic differential equation that $x = 0$ is the stability point, indicating that the government's selection of Strategy 1 brings more than the cost. Therefore, Strategy 1 is an evolutionary stability strategy.

The dynamic trend and stability analysis of government strategy selection are shown in Figure 3.

(2) Analysis of bank's asymptotic stability

①When $x(IF + nk(A_b^{obg}V^y + R_bV^y - n_1V_1^y - n_1R_bV_1^y - n_2(A_b^{obg} + R_b)V_p^y) - C_h^y(1-z) + zC_1^n - z(C_1^y + IF)) + C_h^n(1-x-z+xz) - zC_1^n = 0$, the strategy selection of the bank will not change over time, so the strategy selection of subjects is the curved surface S_2 in Figure 4; any point on the curved surface is an evolutionary stability point.

②When $x(IF + nk(A_b^{obg}V^y + R_bV^y - n_1V_1^y - n_1R_bV_1^y - n_2(A_b^{obg} + R_b)V_p^y) - C_h^y(1-z) + zC_1^n - z(C_1^y + IF)) + C_h^n(1-x-z+xz) - zC_1^n > 0$, then $F'(0) > 0$ and $F'(1) < 0$, and the stability theorem of the replicated dynamic differential equation shows that $y = 1$ is the stability point, indicating that the bank chooses Strategy 2 to gain more than the cost and that the bank chooses the evolutionary stability strategy as its strategy.

③When $x(IF + nk(A_b^{obg}V^y + R_bV^y - n_1V_1^y - n_1R_bV_1^y - n_2(A_b^{obg} + R_b)V_p^y) - C_h^y(1-z) + zC_1^n - z(C_1^y + IF)) + C_h^n(1-x-z+xz) - zC_1^n < 0$, then $F'(0) < 0$ and $F'(1) > 0$, and it is known from the stability theorem of the replicated dynamic differential equation that $y = 0$ is the stability point, indicating that the bank's selection of Strategy 1 brings more than the cost. Therefore, Strategy 1 is an evolutionary stability strategy.

The dynamic trend and stability analysis of bank strategy selection are shown in Figure 4.

(3) Analysis of agricultural guarantee institution's asymptotic stability

①When $-C_h^y + (A_b^{obg} - A_g^{obg})nKV^n(1-x) + IFx - yC_1^n + (C_h^y + T - (A_b^{obg} - A_g^{obg})nKV^n(1-x) + (C_1^n - C_1^y - IF)x)y = 0$, the strategy selection of the agricultural guarantee institution will not change over time, so the strategy selection of subjects is the curved surface S_3 in Figure 5; any point on the curved surface is an evolutionary stability point.

②When $-C_h^y + (A_b^{obg} - A_g^{obg})nKV^n(1-x) + IFx - yC_1^n + (C_h^y + T - (A_b^{obg} - A_g^{obg})nKV^n(1-x) + (C_1^n - C_1^y - IF)x)y > 0$, then $F'(0) > 0$ and $F'(1) < 0$, and the stability theorem of the replicated dynamic differential equation shows that $z = 1$ is the stability point, indicating that the agricultural

guarantee institution chooses Strategy 2 to gain more than the cost and that the bank chooses the evolutionary stability strategy.

③When $-C_h^y + (A_b^{obg} - A_g^{obg})nKV^n(1-x) + IFx - yC_1^n + (C_h^y + T - (A_b^{obg} - A_g^{obg})nKV^n(1-x) + (C_1^n - C_1^y - IF)x)y < 0$, then $F'(0) < 0$ and $F'(1) > 0$, and it is known from the stability theorem of replicated dynamic differential equation that $z = 0$ is the stability point, indicating that the agricultural guarantee institution's selection of Strategy 1 brings more than the cost. Therefore, Strategy 1 is an evolutionary stability strategy.

The dynamic trend and stability analysis of agricultural guarantee institution strategy selection are shown in Figure 5.

(4) System stability analysis of a three-party game

Different equilibrium states can be obtained by analyzing the evolutionary game of three-party subjects. It is assumed that the curved surface S_1 is taken as the boundary in Figure 3, and there are two parts (V_1 and V_2). With the curved surface S_2 as a boundary in Figure 4, there are two parts (V_3 and V_4). With the curved surface S_3 as a boundary in Figure 5, there are two parts (V_5 and V_6). The spatial distribution and strategy selection of the initial state are shown in Table 2.

The stable strategy combination obtained through asymptotic stability analysis is not necessarily the stable evolutionary strategy of the game system, and the stability of the equilibrium point of eight strategy combinations requires further analysis about points (0,0,0), (1,0,0), (0,0,1), (1,0,1), (0,1,0), (1,1,0), (0,1,1), and (1,1,1). According to the replicated dynamic equation of subjects, the corresponding Jacobian matrix is obtained as follows:

$$\begin{bmatrix} (1-2x)(-C_s + A_0^{obg}nk(V^n + V^y(-1+y) - n_2V_p^y)) & x(1-x)A_0^{obg}nk(V^y - n_2V_p^y) & 0 \\ y(1-y)(IF + nk(A_b^{obg}V^y + R_bV^y - n_1V_1^y - n_1R_bV_1^y - n_2(A_b^{obg} + R_b)V_p^y) - C_h^y(1-z) + zC_1^n - z(C_1^y + IF)) - C_h^n(1-x-z+xz) - zC_1^n & (1-2y)(C_1^n(-1+x)(-1+z) - C_1^y x + x)(IF + nk(A_b^{obg}V^y + R_bV^y - n_1V_1^y - n_1R_bV_1^y - n_2(A_b^{obg} + R_b)V_p^y) - C_h^y(1-z) + zC_1^n - z(C_1^y + IF)) - C_h^n(1-x-z+xz) - zC_1^n & (-C_h^n - C_1^n + (C_1^n + C_1^y - C_h^y)(1-y))y \\ (IF(-1) + (-C_1^y + C_1^n)(-1+z)z & (C_1^n - C_1^y - T - C_1^y x + IFx)(-1+z)z & (C_1^n + IFx(-1+y) - C_1^y y + (C_1^n - T - C_1^y x + IFx)(-1+2z)) \end{bmatrix}$$

According to the Lyapunov stability theorem, the equilibrium point is stable if all characteristic values of the Jacobian matrix are negative. The results of the local stability analysis of the game system are shown in Table 3.

According to the results of the local stability analysis in the table, the characteristic value corresponding to (0,1,1), (0,0,1), and (0,0,0) already has a value determined to be a positive number, which is definitely not outside the range of a stable point. Several other equilibrium points require further discussion. According to the strategy space of the three subjects and the actual situation, the following criteria should be met if intending to make the business cooperation of subject space evolve toward the ideal direction (1,1,1):

$$\begin{aligned} C_s + n_2nKA_0^{obg}V_p^y - nKA_0^{obg}V^n &< 0, \\ [C_1^y + n_1nKV_1^y(1+R_b) + n_2nKV_p^y(A_b^{obg} + R_b)] \\ &- nKV^y(A_b^{obg} + R_b) < 0, \\ C_1^y - T &< 0. \end{aligned}$$

For the government, the sum of the cost of risk information sharing and the default loss borne by the government after the

transformation of risk information value is less than that of the loan loss borne by the government when value transformation is not performed for the information. The government tends to choose the risk identification-guiding strategy. When the sum of the costs paid in the positive loan strategy and the loan default losses is less than that of the default losses borne in the negative loan strategy, banks tend to choose the former situation. For agricultural guarantee institutions, when the cost of adopting the positive guarantee strategy is less than the long-term benefits brought by the bank's recognition, they tend to choose this strategy.

Through the analysis, the following conclusions are drawn: (1) whether the government shares high-quality information related to large-scale farmland management rights that can reflect the risks of new agricultural entities is closely related to whether banks and agricultural guarantee institutions adopt the corresponding positive strategies. (2) The following criteria will decide whether banks select the positive loan strategy. First, they make sure that default losses can be tangibly reduced. Second, agricultural guarantee institutions should choose the same strategy as banks to jointly reduce costs. If the strategy cost of banks is too high or unprofitable, banks will evolve toward the negative loan strategy. (3) If the agricultural guarantee institution adopts a positive strategy, it can indeed get the bank's affirmation and long-term benefits. When the benefits are higher than the cost paid, the agricultural guarantee institution will tend to use this strategy for a long time. Otherwise, the behavior of agricultural guarantee institutions will evolve toward the negative strategy. In summary, the stability analysis, the cost of risk information sharing, the default control rate of new agricultural entities, and the amount of the government's compensation for losses are significant factors deciding whether the government builds a platform to share risk information. The transformation value of risk information, the cost of risk identification, the default rate of new agricultural entities, and the amount of compensation for the losses of banks are significant factors deciding whether banks adopt the positive loan strategy. The transformation value of risk information, the cost of risk identification, the default rate of new agricultural entities, the amount of compensation for the losses of agricultural guarantee institutions, and the long-term cooperative benefits brought by bank recognition are significant factors deciding whether agricultural guarantee institutions adopt the positive loan strategy. Among these factors, the transformation value of risk information, the cost of risk identification, and the default control rate of new agricultural entities are related to the yield of multiple subjects. Therefore, it is necessary to explore the impact of these key factors on the strategy selection of three parties and system evolution based on the stability of a single subject to verify the theoretical hypothesis.

5 Simulation and theoretical hypothesis verification

5.1 Initial situation parameter setting

According to the constraints of the replicated dynamic equation and optimal equilibrium (1,1,1), the interactive behavior evolution of the government, banks, and agricultural guarantee institutions is numerically simulated and analyzed using MATLAB software based

on theoretical analysis. x_0 , y_0 , and z_0 , respectively, indicate the initial proportion for the government to choose the positive guiding strategy, the initial proportion for the bank to choose the positive loan strategy, and the initial proportion for the agricultural guarantee institution to choose the positive guarantee strategy. It is assumed that the initial state is (0.2,0.2,0.2), the initial time is 0, and the evolution end time is 1.

It is also assumed that in the initial ideal situation, the return will be higher than the paid cost if the government chooses the risk identification-guiding strategy. If both banks and guarantee institutions choose a positive strategy, they will share the cost of risk identification, reduce the default rate, and jointly promote an increase in the guarantee leverage. The guarantee institution will be recognized by the bank and then receive long-term benefits. The initial value of the ideal state of the model parameters is parameterized with reference to actual situations.

According to the estimation and calculation data of a regional bank in China, the average financing default rate of new agricultural entities is about 0.3% in the natural situation without risk information sharing, mortgage guarantee, and positive customer screening of banks and guarantee institutions. Assuming that under the ideal system operation state, the risk information sharing by governments can better restrain the default behavior of new agricultural entities and reduce the system default rate to 0.28. If banks issue loans in a positive way, they can effectively identify the risk of new agricultural entities, screen loan customers, and finally control the default rate at 0.015. If banks cooperate with guarantee institutions, both parties will choose the positive loan and guarantee strategy, and guarantee institutions will share the risk; therefore, banks will appropriately lower the loan threshold, increase the tolerance for default rates, and finally control the default rate at 0.03.

According to the data from a local statistical yearbook in China, the loan interest rate of China's banks for new agricultural entities is 0.04, and the guarantee leverage is about 3. The proportion of issuing loans by banks alone is 0.1, and the proportion of issuing loans through the cooperation of banks and guarantee institutions is 0.9, meeting the criterion of $n_1 + n_2 = 1$.

According to the statistical yearbook and the author's study data in the "government, bank, and guarantee institution" financing guarantee pilot area, it is assumed that the loan principal basis point is 10,000, and the cost required by the government to collect and share risk information is 1,000 based on proportional calculations. With available risk information, the cost paid by banks and agricultural guarantee institutions on risk identification with cooperation is 100, and the cost paid by banks and agricultural guarantee institutions is 200 when they have not cooperated with each other. In a situation without risk information, banks and agricultural guarantee institutions should separately collect risk information, resulting in a high risk identification cost. The cost, respectively, paid by either party is 600 when they cooperate with each other and 1,200 when they do not cooperate with each other.

According to the current system of the "government, bank, and guarantee institution" financing guarantee pilot area, the ratio of risks undertaken by them is 0.1, 0.3, and 0.6, respectively.

Then, the parameter initial values are set as follows: $V^y = 0.2$, $V_p^y = 0.03$, $V_l^y = 0.015$, $V^n = 0.3$, $n = 3$, $n_1 = 0.1$, $n_2 = 0.9$,

$K = 10000$, $A_o^{bg} = 0.1$, $A_b^{bg} = 0.3$, $C_s = 800$, $R_b = 0.04$, $IF = 50$, $C_l^y = 100$, $C_h^y = 200$, $C_l^n = 300$, $C_h^n = 600$, and $T = 120$.

The result of system simulation in an ideal situation is shown in Figure 6, indicating that the system is in the ideal state (1,1,1) and using this state as the benchmark to compare the change of all parameters.

5.2 Numerical simulation and result analysis

(1) Numerical simulation of changes in risk identification quality

In the initial ideal state, the farmland management rights transfer platform established by the government and the shared risk information are of high quality. In addition, the counter-guarantee of farmland management rights and the sharing of risk information serve as restraints on new agricultural entities, which can reduce the default rate V^y of new agricultural entities to 0.28. Furthermore, banks and agricultural guarantee institutions can accurately identify the risks of new agricultural business entities based on real and effective risk information and then control the financing guarantee default rate V_p^y at 0.03.

Other condition values are set, and it is ensured that they are not changed. If the risk information shared by governments is not significantly effective in restraining new agricultural entities and no notable decrease is seen in the initial default rate; $V^y = 0.28$ will be turned to $V^y = V^n = 0.3$ (the results are shown in Figure 7①). According to the simulation results, the three parties are still tending toward positive cooperation (Figure 7). If the risk identification performed by banks and agricultural guarantee institutions is of low quality and they cannot accurately determine the risk status of new agricultural entities and effectively reduce the system default rate, V_p^y will turn from 0.03 to 0.3 (the results are shown in Figure 7②), indicating that the three parties are not tending to cooperate with each other.

This result shows that the natural constraint of risk information sharing on the default of new agricultural entities is not a sufficient condition for system stability. Based on risk information sharing, the three parties should cooperate with each other for risk identification, thereby screening customers effectively and reducing the default rate. Only when the quality of risk identification is high can the government, banks, and agricultural guarantee institutions achieve profitability through the related positive strategies and ultimately realize sustainable cooperation among the three parties.

If it is intended to improve the quality of risk identification and substantially reduce the default rate, the high-quality risk information shared by the government is not a condition value but an essential condition, according to the findings of statistical analysis using the game model. Moreover, human resources, materials, technologies, and other costs of banks and agricultural guarantee institutions for risk identification are essential conditions. Both of the aforementioned conditions are indispensable.

(2) Numerical simulation of changes in the transformation value of risk information

One or two parties of banks and agricultural guarantee institutions will develop the risk information shared by the

government (for example, develop the guaranteed loan business based on risk levels). The outcomes will help banks and agricultural guarantee institutions reduce risks, expand business, and gain reputation. This series of economic and social values is defined by the transformation value of information. In the initial ideal state, the transformation value (IF) of risk information accessible to banks and agricultural guarantee institutions is quantified to 50.

Other condition values are set, and it is ensured that they are not changed. The transformation value (IF) of risk information is reduced from 50 to 30. According to the simulation results, banks and guarantee institutions have withdrawn from the risk identification of new agricultural entities, and the cooperation is therefore terminated (Figure 8). This result reaffirms that the high-quality risk information shared by the government is only the first step. It is very important to make good use of risk information and strive to transform risk information into more and more favorable economic and social values. It is also of great significance for banks and guarantee institutions to achieve continuous financing and guarantee. However, it is to be noted that both parties will obtain the benefit of transformation value as long as either a bank or an agricultural guarantee institution adopts the positive strategy. A “free rider” problem may occur. Each party hopes that the other party will pay more for cooperation, allowing them to gain more benefits. In order to explore whether the transformation value of information can continuously promote three-party cooperation, it is necessary to further study the strategy selection of both parties under the change in risk identification cost.

(3) Numerical simulation of changes in risk identification cost

If the government does not share risk information in the initial ideal state, cooperation will require a higher cost for banks and agricultural guarantee institutions to collect risk information and then identify risks. In the case of cooperation without shared information, the risk identification cost C_l^n (containing the information search cost and identification cost) is 600, while the cost C_h^n of separate risk identification is 1,200. If the government has set up a transfer platform and shares risk information, banks and guarantee institutions can save the cost of searching for risk information. Under such circumstances, the cost C_h^y of separate risk identification is 200. If they initiate cooperation, they can share technology, personnel, data, and other resources, which will greatly reduce costs. The cost C_l^y is 100.

While other conditions remain unchanged, the risk identification cost is set after the government has set up a platform and shared risk information equal to the cost when the risk information is not shared ($C_h^y = C_h^n = 1,200$ and $C_l^y = C_l^n = 600$). The simulation results are shown in Figure 9①. It can be seen that both banks and guarantee institutions have rejected the positive strategy. This result reaffirms the importance of risk information data shared by governments. In other words, the risk information data shared by governments should not only be true, effective, and high quality but also tangibly reduce and share the risk identification cost of banks and agricultural guarantee institutions, which lays an important foundation for sustainable cooperation among the three parties.

It also needs to be further studied whether the risk identification jointly implemented by banks and agricultural guarantee institutions will affect system stability when the government has shared true and effective information. All parameter values are restored to the initial ideal state, and the risk identification cost based on the cooperation of banks and agricultural guarantee institutions is set equal to the cost of separate risk identification (by changing $C_1^Y = 100$ into $C_1^Y = C_h^Y = 200$). The result shows that guarantee institutions and banks have successively rejected the positive strategy and interrupted cooperation (Figure 9②). According to the result, win-win situations can be achieved only when banks cooperate with guarantee institutions for risk identification and jointly bear the risk identification cost. If banks or guarantee institutions want to be a “free rider” and hope that the other party can pay more to obtain benefits, it is not a sustainable idea. The previous result also indicates that cooperation can be sustainable only when the government, banks, and agricultural guarantee institutions have adopted positive strategies.

- (4) Numerical simulation of changes in long-term benefits brought by the participation of agricultural guarantee institutions in risk identification.

Agricultural guarantee institutions will be recognized and encouraged by banks when they work hard to identify risks and provide guarantee services selectively in the initial ideal state. Banks will reach a long-term cooperation intention with agricultural guarantee institutions so as to facilitate them in further identifying risks, helping banks control those risks, saving costs, and bringing in more high-quality financing guarantee customers. Meanwhile, agricultural guarantee institutions can obtain benefits from the long-term cooperation. It is assumed that the initial value T of the long-term return is 120.

The strategy selection of three parties with the change in long-term benefit values is reviewed. It is ensured that other conditions remain unchanged. The condition is set as follows: agricultural guarantee institutions work hard to identify risks and are recognized by banks and the long-term benefit T is reduced from 120 to 50. The simulation results are shown in Figure 10, indicating that banks and agricultural guarantee institutions tend to be non-cooperative. For agricultural guarantee institutions, the recognition of banks and long-term cooperation with banks are of great importance. If the benefit exceeds the cost, agricultural guarantee institutions are willing to cooperate with banks, helping them share risk control pressures and costs. If not recognized by banks, agricultural guarantee institutions will withdraw from the cooperation. Then, banks must separately bear the risk identification cost and pressure. Therefore, banks will also gradually withdraw from the three-party cooperation, and the cooperation will come to an end.

6 Study conclusion

This study builds an evolutionary game model of “government, bank, and guarantee institution” cooperative financing guarantee for new agricultural entities. Based on the post-risk transfer for three parties, this study discusses the cooperation of positive financing

guarantee in relation to prior risk identification. According to the study findings, the cooperation mechanism should not only focus on the post-risk transfer but also take the prior risk identification as a breakthrough point to tangibly reduce the systemic risk of financing guarantee, which is feasible in eliminating the financing dilemma. According to the result of the simulation, efforts should be made in four aspects, including risk information sharing, risk identification quality, risk identification cost sharing, and risk information value transformation, to mobilize the three parties for positive cooperation, really reduce risks, and improve operation quality. First, the government is recommended to build a high-quality farmland management rights transfer platform and share the high-quality information data that are related to the farmland management rights and can reflect the risks of new agricultural entities. Second, banks and guarantee institutions should be guided to make good use of the information, improve the quality of risk identification, find out about new agricultural entities with development potentials, tangibly reduce the system default rate, and convert risk information into favorable economic and social values. Furthermore, banks and guarantee institutions should be encouraged to achieve long-term cooperation for risk identification and jointly bear the cost of risk identification. Banks should be encouraged to recognize the participation of agricultural guarantee institutions in risk identification and facilitate the transformation value to increase risk information. In this way, a new model of sustainable cooperation among the government, banks, and guarantee institutions for the financing guarantee of new agricultural entities is formed. The conclusions are specified as follows:

With reference to the strategies adopted by each party in the cooperation mechanism, whether the government builds a platform and shares high-quality information is closely related to whether banks and agricultural guarantee institutions adopt positive loan and guarantee strategies. Second, the tangible reduction of loss caused by default behaviors and the sharing of risk identification costs by agricultural guarantee institutions play a decisive role in driving banks to adopt positive loan strategies. Third, agricultural guarantee institutions will tend to choose the positive guarantee strategy if they are recognized by banks, and the long-term benefits are higher than the paid risk identification costs.

In respect of the “government, bank, and guarantee institution” financing guarantee system stability, the quality of risk identification is one of the significant factors affecting the sustainable cooperation among the three parties. High-quality risk information is one of the essential conditions to improve the quality of risk identification, accurately screen customers, and tangibly reduce the default rate. For this reason, it is necessary for the government to build a platform to protect the economic value of counter-guarantee with farmland management rights, further explore the associated risk information that can reflect the actual risk status of new agricultural entities, and finally realize the sharing of risk information.

Accurate processing of risk information by banks and agricultural guarantee institutions is another essential condition to improve the risk identification quality, accurately screen customers, and tangibly reduce the default rate. Therefore, it is necessary to mobilize banks and agricultural guarantee institutions for risk identification and drive both parties to choose differential

financing guarantee strategies for different new agricultural entities to control systemic risks on the basis of high-quality information sharing. In addition, banks and agricultural guarantee institutions need to be made aware of the benefits of adopting positive strategies in different aspects, such as risk identification cost sharing and risk information transformation value, thereby truly motivating both parties.

In order to mobilize banks and agricultural guarantee institutions for cooperation, the sharing of risk identification costs is one of the significant driving factors. If the risk identification cost is too high, the behavior of the three parties will evolve in an unfavorable trend. In order to reduce and save costs, the high-quality risk information of governments still plays a vital role, which exempts banks and agricultural guarantee institutions from additional human resources, materials, and financial resources. Second, banks and agricultural guarantee institutions can share technologies, personnel, and data through risk identification and reduce the identification cost based on cooperation, thus achieving a win-win situation. The idea that either party wants to be a “free rider” and hopes that the other party can pay more to obtain benefits is not sustainable. Since the “free rider” is not feasible, the three parties should be guided to create a favorable long-term mechanism for cost sharing.

More value transformations of risk information after banks and agricultural guarantee institutions choose positive financing guarantee strategies are identified as another significant driving factor to motivate all parties for cooperation. According to the simulation result, the series of economic and social values obtained by either or both banks and agricultural guarantee institutions through the processing of risk information, such as risk reduction, business expansion, and reputation promotion, will facilitate sustainable cooperation among the three parties. For this reason, the government is recommended to increase the transformation value of such risk information in some ways, such as social desirability and media publicity, thus promoting the sustainable development of “government, bank, and guarantee institution” positive cooperation.

References

- Saito K, Tsuruta D. Information asymmetry in small and medium enterprise credit guarantee schemes: evidence from Japan. *Appl Econ* (2018) 50(22) 1–17. doi:10.1080/00036846.2017.1400651
- Mei Q, Hong-Zhen XU The study of bank-guarantee risk sharing in Re-guarantee system—based on system dynamics. *Technoecon Manag Res* (2014) (2):78–82.
- Choe C. The political economy of SME financing and Japan's regional bank problems. *Pacific-Basin Finance J* (2007) 15:353–67. doi:10.1016/j.pacfin.2006.10.001
- Corrado G, Corrado L. Inclusive finance for inclusive growth and development. *Curr Opin Environ Sustain* (2017) 24:19–23. doi:10.1016/j.cosust.2017.01.013
- Jiang F, Jiang Z, Kim KA. Capital markets, financial institutions, and corporate finance in China. *J Corp Finance* (2020) 63:101309. doi:10.1016/j.jcorpfin.2017.12.001
- Arun T, Kamath R. Financial inclusion: Policies and practices. *IIMB Manag Rev* (2015) 27(4):267–87. doi:10.1016/j.iimb.2015.09.004
- Nguyen VS, Mai TTH, Thuan TD, Tien DV, Phuong NTM, Thai VH, et al. SME financing role in developing business environment and economic growth: Empirical evidences from technical SMEs in vietnam. *Environ Sci Pollut Res Int* (2022) 29(35):53540–52. doi:10.1007/s11356-022-19528-w
- Ghalke A, Kumar S, Nageswara Rao SVD. SME financing through public equity: Review of the Indian SME exchanges. *Indian Growth Dev Rev* (2022) 15(1):85–97. doi:10.1108/IGDR-10-2021-0138
- Rostam AM, Ahmed RA, Tisha RT, Ashikul IM. Does SME financing perform well from both demand and supply sides? The case of a developing country. *Int J Financial Eng* (2021) 08(04). doi:10.1142/S2424786321420020
- Van Klyton A, Rutabayiro-Ngoga S. SME finance and the construction of value in Rwanda. *J Small Bus Enterp Dev* (2018) 25(4):628–43. doi:10.1108/JSBED-02-2017-0046
- Li S, Yang Y, Zongfang Z. Research on impact of moral hazard on individual credit risk. *Proced Comp Sci* (2014) 31:577–86. doi:10.1016/j.procs.2014.05.304
- Lv Y, Ma G, Ding J. Breakthrough path of low-level equilibrium of China's policy-oriented financing guarantee market. *Front Psychol* (2022) 13:918481. doi:10.3389/fpsyg.2022.918481
- Xu R, Guo T, Zhao H. Research on the path of policy financing guarantee to promote SMEs' green technology innovation. *Mathematics* (2022) 10(4):642. doi:10.3390/math10040642
- Lv Y, Ma G, Lv L, Ding J. The design of incentive mechanism for policy-oriented guarantee institutions' digital transformation in China. *Discrete Dyn Nat Soc* (2022) 2022:1–10. doi:10.1155/2022/6334476
- Liu R, Sui JH, Jiang LT. Current status and possible solutions to the financing difficulties of small-and medium-sized enterprises in China. In: *Proceeding of the 2015 International Conference on Industrial Technology and Management Science*; Tianjin, China. Atlantis Press (2015). p. 1612–5. doi:10.2991/itm-15.2015.392

Data availability statement

The original contributions presented in the study are included in the article/Supplementary Material; further inquiries can be directed to the corresponding author.

Author contributions

JZ was responsible for building models and writing the paper; ZM was responsible for research and collecting data; FZ was responsible for analyzing the data and improving the model; and QZ was responsible for literature search and writing the review. All authors contributed to the article and approved the submitted version.

Funding

This work was supported by the Jiangsu Social Science Foundation [grant number 19JD012] and the Key Project of Philosophy and Social Science Research in Colleges and Universities in Jiangsu Province [grant number 2022SJZD017].

Conflict of interest

The authors declare that the research was conducted in the absence of any commercial or financial relationships that could be construed as a potential conflict of interest.

Publisher's note

All claims expressed in this article are solely those of the authors and do not necessarily represent those of their affiliated organizations, or those of the publisher, the editors, and the reviewers. Any product that may be evaluated in this article, or claim that may be made by its manufacturer, is not guaranteed or endorsed by the publisher.

16. Jianzhong Y, Jundan P. A research on the financing efficiency of small and medium-sized enterprises by fuzzy evaluation method. Proceeding of the 2015 8th International Conference on Intelligent Computation Technology and Automation (ICICTA). IEEE, June 2015, Nanchang, China, 2015: 89–93.
17. Adusei M, Adeleye N. Corporate disclosure and credit market development. *J Appl Econ* (2021) 24(1):205–30. doi:10.1080/15140326.2021.1901644
18. Umehara E, Ohta T. Using game theory to investigate risk information disclosure by government agencies and satisfying the public—the role of the guardian agent. *IEEE Trans Syst Man, Cybernetics-A: Syst Humans* (2009) 39(2):321–30. doi:10.1109/tsmca.2008.2010796
19. Yoon KS. Enhancing information sharing in the public sector: An empirical study. *Informatization Policy* (2012) 19(4):83–104.
20. Fan J, Zhang P, Yen DC. G2G information sharing among government agencies. *Inf Manag* (2014) 51(1):120–8. doi:10.1016/j.im.2013.11.001
21. Adhikary BK, Kutsuna K, Stephannie S. Does the government credit guarantee promote micro, small, and medium enterprises? Evidence from Indonesia. *J Small Business Entrepreneurship* (2021) 33(3):323–48. doi:10.1080/08276331.2019.1666338
22. Chowdhury MSA, Azam MKG, Islam S. Problems and prospects of SME financing in Bangladesh. *Asian Business Rev* (2013) 2(2):51–116. doi:10.18034/abr.v2i2.304
23. Beck T, Klapper LF, Mendoza JC. The typology of partial credit guarantee funds around the world. *J Financial Stab* (2010) 6(1):10–25. doi:10.1016/j.jfs.2008.12.003
24. D'Orazio P, Valente M. The role of finance in environmental innovation diffusion: An evolutionary modeling approach. *J Econ Behav Organ* (2019) 162:417–39. doi:10.1016/j.jebo.2018.12.015
25. Rehman K, Khan HH, Sarwar B, Muhammad N, Ahmed W, Rehman ZU. A multi-group analysis of risk management practices of public and private commercial banks. *The J Asian Finance Econ Business* (2020) 7(11):893–904. doi:10.13106/jafeb.2020.vol7.no11.893
26. Altman EI, Esentato M, Sabato G. Assessing the credit worthiness of Italian SMEs and mini-bond issuers. *Glob Finance J* (2020) 43:100450. doi:10.1016/j.gfj.2018.09.003
27. Bachas N, Kim OS, Yannelis C. Loan guarantees and credit supply. *J Financial Econ* (2021) 139(3):872–94. doi:10.1016/j.jfineco.2020.08.008
28. Berkman H, Cole RA, Fu LJ. Expropriation through loan guarantees to related parties: Evidence from China. *J Banking Finance* (2009) 33(1):141–56. doi:10.1016/j.jbankfin.2007.11.001
29. Scholtens B. Finance as a driver of corporate social responsibility. *J Business Ethics* (2006) 68(1):19–33. doi:10.1007/s10551-006-9037-1
30. Eshet A. Sustainable finance? The environmental impact of the Equator principles and the credit industry. *Int J Innovation Sust Dev* (2017) 11(2-3):106–29. doi:10.1504/ijisd.2017.083305
31. Gendron M, Son-lai V, Soumare I. Effects of maturity choices on loan-guarantee portfolios. *J Risk Finance* (2006) 7(3):237–54. doi:10.1108/15265940610664933
32. Gai L, Ielasi F, Rossolini M. Smes, public credit guarantees and mutual guarantee institutions. *J Small Business Enterprise Dev* (2016) 23(4):1208–28. doi:10.1108/jsbed-03-2016-0046
33. Soundarrajan P, Vivek N. Green finance for sustainable green economic growth in India. *Agric Econ (Zemed Ekon.)* (2016) 62(62):35–44. doi:10.17221/174/2014-agricecon
34. Zheng P, Zhang Z. Analyzing characteristics and implications of the mortgage default of agricultural land management rights in recent China based on 724 court decisions. *Land* (2021) 10(7):729. doi:10.3390/land10070729
35. Peng Y, Liu W, Tan C. Study on risks in mortgage financing of rural land management right. In: 6th International Conference on Social Science, Education and Humanities Research (SSEHR 2017). Atlantis Press (2018). p.692–701. doi:10.2991/ssehr-17.2018.151
36. Gai L, Ielasi F, Rossolini M. SMEs, public credit guarantees and mutual guarantee institutions. *J Small Bus Enterp Dev* (2016) 23:1208–88. doi:10.1108/JSBED-03-2016-0046
37. de la Fuente-Cabrero C, de Castro-Pardo M, Santero-Sánchez, Laguna-Sánchez P. The Role of mutual guarantee institutions in the financial sustainability of new family-owned small businesses. *Sustainability* (2019) 11(22):6409. doi:10.3390/su11226409
38. Qin M, Wachenheim CJ, Wang Z, Zheng S. Factors affecting Chinese farmers' microcredit participation. *Agric Finance Rev* (2019) 79(1):48–59. doi:10.1108/AFR-12-2017-0111
39. Yang W, Yan W. Analysis on function orientation and development countermeasures of new agricultural business entities. *J Northeast Agric Univ* (2016) 23(2):82–8. doi:10.1016/S1006-8104(16)30051-4
40. Valaskova K, Klietnik T, Svabova L, Adamko P. Financial risk measurement and prediction modelling for sustainable development of business entities using regression analysis. *Sustainability* (2018) 10(7):2144. doi:10.3390/su10072144
41. Zhang H, Luo J, Cheng M, Duan P. How does rural household differentiation affect the availability of farmland management right mortgages in China?. *Emerg Mark Finance Trade* (2020) 56(11):2509–28. doi:10.1080/1540496X.2019.1658073



OPEN ACCESS

EDITED BY

Jianbo Wang,
Southwest Petroleum University, China

REVIEWED BY

Shaoping Li,
Huzhou University, China
Wang Tao,
University of Southern California,
United States

*CORRESPONDENCE

Sha Zhu,
✉ zhushacufe@163.com

SPECIALTY SECTION

This article was submitted to
Social Physics,
a section of the journal
Frontiers in Physics

RECEIVED 14 December 2022

ACCEPTED 27 February 2023

PUBLISHED 10 March 2023

CITATION

Lai F, Li S, Lv L and Zhu S (2023), Do global
geopolitical risks affect connectedness of
global stock market contagion network?
Evidence from quantile-on-
quantile regression.
Front. Phys. 11:1124092.
doi: 10.3389/fphy.2023.1124092

COPYRIGHT

© 2023 Lai, Li, Lv and Zhu. This is an
open-access article distributed under the
terms of the [Creative Commons
Attribution License \(CC BY\)](#). The use,
distribution or reproduction in other
forums is permitted, provided the original
author(s) and the copyright owner(s) are
credited and that the original publication
in this journal is cited, in accordance with
accepted academic practice. No use,
distribution or reproduction is permitted
which does not comply with these terms.

Do global geopolitical risks affect connectedness of global stock market contagion network? Evidence from quantile-on-quantile regression

Fujun Lai¹, Sicheng Li¹, Liang Lv¹ and Sha Zhu^{2*}

¹School of Finance, Yunnan University of Finance and Economics, Kunming, China, ²School of Statistics
and Mathematics, Yunnan University of Finance and Economics, Kunming, China

Based on the Vector Autoregressive Model (VAR), this paper constructs a contagion complex network of global stock market returns, and uses the Quantile-on-Quantile Regression (QQR) to explore the impact of global geopolitical risks on the connectedness of global stock markets. By applying the risk contagion analysis framework, we depict risk contagion and correlation between financial markets in different countries. We also identify the risk contagion characteristics of international financial markets. This paper innovatively introduces the quantile-on-quantile regression method to the study of geopolitical risk. Through the quantile-on-quantile approach, we find that there is an asymmetric relationship between geopolitical risk and the global stock market correlation network. Our conclusions provide some suggestions for policy makers and relevant investors on how to deal with the current high global geopolitical risks. They also provide ideas on how to effectively hedge such risks during asset allocation and policy formulation.

KEYWORDS

global geopolitical risks, contagion network, connectedness, quantile-on-quantile regression, stock market

1 Introduction

Since the collapse of the Soviet Union in the early 1990s, the Cold War crisis has been lifted. The world pattern of two superpowers has been replaced by a single superpower. Nevertheless, all of this does not appear to be reducing global geopolitical risk. Peace is something of a mirage in the short-term, while disputes and conflicts remain the defining features of the world. Because of the one superpower and many powers pattern, the relationship between the major powers has become tense, and conflicts between small countries have also risen. The outbreak of the Russia-Ukraine conflict in early 2022 has further disrupted a world that is already affected by COVID-19. As the world's dramatic changes continue to accelerate, geopolitical risks will continue to grow.

Numerous scholars have provided different definitions of geopolitical risk, but until today, there is no unified understanding or definition. The earliest geopolitics originated in the late 19th century, and was proposed by Swedish political geographer Johan Rudolf Kjellén in his book *Der Staat als Lebensform* (1917). Since the 20th century, due to the development of global politics, economy and military, various geopolitical theories have emerged. American historian Mahan put forward the sea power theory, who can control the

sea, who can become a world power; the key to controlling the ocean is to control the world's critical sea lanes and straits. Mackinder put forward the land rights theory, that with the development of land transportation, the heartland of Eurasia has become the most critical strategic area. The land power theory has had a profound impact on world politics. In the 1940s, American international relations scholar Spykman emphasized the importance of rimland and carried forward continental margin theory, which was called another theory of continental power theory. In the 1950 s, American strategist Seversky put forward the theory that the Arctic region is very important for the United States to compete for air supremacy, namely air power theory. In 1973, American geographer Cohen proposed the geopolitical strategic zone model, which divided the world into two geopolitical strategic zones: maritime trade zone and Eurasian continental zone. Between the two regions there are three regions: South Asia, the Middle East and Southeast Asia. South Asia is a potential geostrategic region, and the Middle East and Southeast Asia are called fracture zones. In 1982, Cohen proposed a revision of the geopolitical strategic zone model, noting that Western European countries, Japan, and China had developed into world powers; the role and status of India, Brazil, and Nigeria had risen; and sub-Saharan South Africa had transformed into a third fracture zone.

The World Economic Forum in Davos releases the Global Risk Report every year. In the 2015 edition of the Global Risk Report, geopolitical risk is defined as a systematic, cross-regional and cross-industry global risk, covering violent conflicts between countries, civil strife in important countries, large-scale terrorist attacks, proliferation of weapons of mass destruction and failure of global governance. The 2019 edition of the Global Risks Report lists some specific manifestations of geopolitical risks, such as national collapse or crisis, national governance failure, regional or global governance failure, inter-state conflicts, and terrorist attacks.

David K. Bohl [1] defines geopolitical risks as trends in political and economic changes that are potentially destructive to human well being, arguing that geopolitical risks stem from three interrelated risks: first, political risks arising from competition for power among geopolitical actors, the most intense manifestation of which is violent conflict, but may also include other forms of destructive competition; second, economic risks caused by global or regional economic and financial turmoil; third, natural risks caused by non-human environmental changes, such as water shortage caused by climate change. Geopolitical risks arise not only within a single risk, but also from the contagion between risks. For example, water shortage (a natural risk) may lead to military tension (a political risk), resulting in trade disruption (an economic risk).

If we only focus on the geopolitical context of the text, maybe we will not be able to better incorporate it into the economic sphere. Fortunately, Caldara and Iacoviello [2] used big data and text-mining techniques to create a quantitative standard for geopolitical events and associated risks based directly on textual analysis of news papers. They define global geopolitical risk as the threat, realization and escalation risk caused by adverse events related to war, terrorism, and tensions between countries. These events affect the peace process in international relations. Furthermore, they classify global geopolitical risks into global geopolitical threat risk and global geopolitical act risks. Global geopolitical threats include war threats, peace threats, military

build-ups, nuclear threats and terrorist threats. Global geopolitical acts include the beginning of war, the escalation of war and terrorist acts. Based on this, three indexes, global geopolitical threat risk, global geopolitical act risk and global geopolitical risk are constructed. In order to quantify the magnitude of global geopolitical risks, Caldara and Iacoviello [2] retrieved 25 million articles published in major international English newspapers since 1900. And they calculated the frequency of occurrence of words related to geopolitical events and related threats every month, and then standardized them, and finally obtained the monthly global geopolitical risk (GPR) index. In summary, the definition of geopolitical risk has not been unified. However, this article draws on the global geopolitical risk index measured by Caldara and Iacoviello [2], so we use their definition of geopolitical risk.

Since the establishment of the geopolitical risk index, a large number of scholars have conducted various empirical studies [3–11]. World financial market volatility and even macroeconomic cycles are strongly influenced by geopolitical risk. Geopolitical risk shocks are always accompanied by periods of high risk on financial markets. There are two direct and indirect channels for this transmission. In the direct channel, after geopolitical risk increases, it will affect the financial market and reduce credit demand through cross-border capital flows, exchange rate fluctuations, large fluctuations in commodity prices (crude oil), and asset price adjustments (stocks and real estate). In terms of indirect channels, most people are averse to the uncertainty created by rising geopolitical risk, which will undoubtedly dampen consumer and investor enthusiasm. High geopolitical uncertainty may lead to lower employment and output. Consumers may delay consumption, and businesses may delay investment because of precautionary savings motives. As a result of the geopolitical risk shock, the decline in economic activity will inevitably be reflected in the financial markets. Especially when extreme events occur, there is a huge impact on the global capital market and economic environment. For example, during the three oil crises in 1973, 1979 and 1990, three major geopolitical conflicts broke out at the same time, namely, the fourth Middle East war between Arab countries and Israel, the Iran-Iraq war between Iran and Iraq, and Iraq's invasion of Kuwait war. The three major conflicts have greatly damaged global economic growth, with global GDP growth rates falling from 6.4%, 4.2%, and 4.6%–0.6%, 0.4%, and 1.5%, respectively.

Current research on global geopolitical risks mainly focuses on energy prices and stock market returns. However, the impact on the entire international stock market as a whole has not been involved. The global economy plays different roles across various industrial chains in the context of globalization. At the same time, because of the need for investment diversification, a large amount of money is invested in different stock markets to hedge risks. As a result, it is difficult for any stock market to be immune to world geopolitical shocks. Global stock markets are closely related. Stock market correlations have always played an influential role in the study of systemic financial risk. The 2008 subprime mortgage crisis accelerated the contagion of U. S. stock price volatility to the world capital markets, resulting in global stock market turbulence. In recent years, with the continuous development of modern econometric methods, examining the risk contagion effect

from the perspective of complex networks has become an emerging research topic in this field. Diebold and Yilmaz [12,13] developed a risk spillover network analysis method, which can more deeply reflect the price volatility spillover effect of financial markets. With the help of this risk contagion analysis framework, we can not only depict the intensity and correlation of risk contagion between different financial sectors, but also identify the core path of risk contagion.

Geopolitical risk is undoubtedly a systemic shock that has an impact on worldwide equity markets. The impact of this natural external impact on international stock market complex networks is an issue that researchers in the academic community should focus on. For example, after the Russia-Ukraine conflict, global stock markets experienced significant volatility. However, unfortunately, no scholars have conducted in-depth research and analysis on this issue. Therefore, this paper focuses on the relationship between global geopolitical risk and the connectedness (correlation) of the entire international stock market return network. According to the best of our knowledge, this is the first paper to focus on the impact of global geopolitical risk on the connectedness (correlation) of the entire international stock market. By using the quantile-on-quantile approach, this paper aims to illustrate the asymmetric relationship between different geopolitical risk shocks and different global stock market correlations.

The main contributions of this paper are as follows. First, in contrast to Li [8], although they also use complex networks to explore the relationship between stock market, crude oil market and geopolitical risks, they focused more on the Chinese stock market and use the nonlinear Granger causality test to analyze the potential nonlinear relationship between the three variables. They also identified the main risk sources and risk transfer paths and the lead-lag relationship between geopolitical risks, crude oil and the Chinese stock market. We focus more on how global geopolitical risks affect the total spillover effect (correlation) of the overall international stock market and quantitatively analyze the relationship between them. Second, we innovatively introduce the quantile-on-quantile regression approach into the study of geopolitical risk. The construction of the geopolitical risk index provides a better quantitative indicator of geopolitical risk. This enables us to investigate how different levels of geopolitical risk will affect the connectedness of the overall international stock market. Through the quantile-on-quantile method, it can further characterize the asymmetric potential links between geopolitical risks at different levels and global stock market networks with different degrees of tightness, so as to deeply explore the causal relationship in various states. Third, we not only study the impact of the global geopolitical risk index on the correlation of global stock prices, but also study their differential impact on the correlation of global stock markets by deconstructing GPR into the global geopolitical action risk index and the global geopolitical threat risk index. We find that global geopolitical threat risk and global geopolitical action risk have significantly varying effects on the correlation of global stock markets.

The rest of this article is organized as follows. Section 2 gives a brief literature review. Section 3 introduces the data source and description, and Section 4 summarizes the model and method. Sections 5, 6 provide empirical results and conclusions.

2 Literature review

In recent years, more and more scholars begin to pay attention to the impact of geopolitical risk on financial markets. On the one hand, it is because Caldara and Iacoviello [2] constructed a quantitative geopolitical risk index, which provides a solution for more specific quantitative exploration of the impact of geopolitical risks on financial markets. On the other hand, this is also because global geopolitical risks are at an elevated level, and their impact on financial markets is becoming more extensive and profound. As the core energy resource of human society, oil is financialized at the same time, making it an influential underlying asset in the financial market. Moreover, oil itself is also associated with geopolitics, since a substantial number of geopolitical conflicts often involve competition for crude oil. Therefore, a variety of academic papers attempt to clarify the relationship between oil prices and geopolitical risks [5,6,14,15]. The results indicate that the relationship may be positive or negative. Abdel-Latif and El-Gamal [16] argue that falling oil prices also raise geopolitical risks. For net oil importers, the rise in oil prices will increase their own geopolitical risks, because they cannot bear the cost of soaring oil prices [11]. The impact of oil on geopolitical risks is not always one-way. Many people have explored how geopolitical risks affect oil prices or their volatility. A large number of scholars have adopted mathematical models to predict oil returns and volatility using geopolitical risks [18–20].

Other scholars have given ways in which geopolitical risks can affect stock markets [8,21–25], that is, using nonlinear Granger causality tests and complex network models, they demonstrated that geopolitical risks can affect stock prices by affecting oil prices. The approach at least provides a way of thinking about the causal relationship between geopolitical risks and global stock markets, regardless of whether it accurately describes reality.

Meanwhile, academic communities have been exploring the impact of terrorist activities on stock markets since the 9/11 incident [26–30]. According to most studies, terrorist activity negatively impacts stock returns, and these effects are primarily evident in traditional financial markets and developing countries. There is, however, a limitation to these studies in that they only focus on terrorism. Other geopolitical risks, such as policy risks and war risks, also contribute significantly to the volatility of financial markets. Moreover, these studies only focus on developed countries and ignore emerging market economies. In fact, emerging markets are more vulnerable to geographical shocks.

For example, Balcilar et al. [3] studied the impact of geopolitical risks on stock returns and volatility in the BRICS countries (Brazil, Russia, India, China and South Africa) through the nonparametric causality quantile method. They found that geopolitical risk has a nonlinear and asymmetric effect on market returns in different emerging economies, but a consistent effect on volatility. Hoque and Zaidi [31] employed the Markov Switching Model to find that the global geopolitical risk index and the country-specific geopolitical risk index have completely different effects on the stock markets of emerging economies. The global geopolitical risk index has both positive and negative effects on the stock markets of these emerging economies, but the country-specific geopolitical risk index has a negative impact without exception. Some scholars have also tried to use the geopolitical risk index to predict some indicators of financial

TABLE 1 Statistical description.

| variable | N | mean | sd | min | p25 | p50 | p75 | max |
|----------|-----|--------|-------|--------|--------|-------|-------|-------|
| IBOVESPA | 377 | 3.858 | 13.41 | −50.34 | −3.310 | 1.920 | 8.219 | 67.93 |
| DJI | 377 | 0.642 | 4.180 | −16.41 | −1.483 | 0.993 | 3.275 | 11.19 |
| IXIC | 377 | 0.871 | 6.264 | −26.01 | −2.002 | 1.593 | 4.401 | 19.87 |
| SPX | 377 | 0.636 | 4.252 | −18.56 | −1.755 | 1.146 | 3.348 | 11.94 |
| FTSE | 377 | 0.317 | 3.991 | −14.86 | −1.851 | 0.786 | 2.814 | 11.65 |
| FCHI | 377 | 0.350 | 5.299 | −19.23 | −2.780 | 0.936 | 3.807 | 18.33 |
| GDAXI | 377 | 0.583 | 5.927 | −29.33 | −2.400 | 0.937 | 4.159 | 19.37 |
| N225 | 377 | 0.0331 | 5.779 | −27.22 | −3.484 | 0.419 | 3.940 | 14.97 |
| KS11 | 377 | 0.345 | 7.445 | −31.81 | −3.347 | 0.440 | 4.049 | 41.06 |
| HIS | 377 | 0.506 | 6.879 | −34.82 | −3.129 | 1.039 | 4.244 | 26.45 |
| SENSEX | 377 | 1.058 | 7.551 | −27.30 | −2.960 | 1.039 | 5.741 | 35.06 |
| SSEC | 377 | 0.866 | 11.79 | −37.33 | −4.736 | 0.632 | 4.921 | 102.0 |
| GPR | 328 | 98.44 | 50.67 | 39.05 | 75.65 | 88.02 | 106.5 | 512.5 |
| GPRT | 328 | 97.99 | 43.62 | 36.69 | 73.53 | 88.55 | 108.0 | 415.2 |

markets. Apergis [32] first used a k-order nonparametric causality test to analyze whether geopolitical risks can predict stock returns and volatility of global defense companies. The results show that there is no evidence that the predictability of stock returns of these defense companies comes from geopolitical risks, but it can affect the risk profile of the company for some time to come. By adjusting the frequency of using the geopolitical risk index, especially the mixed frequency, the robustness and reliability of this prediction can be effectively improved [33]. Salisu [34] used the GRACH-MIDAS method to predict stock return volatility in 23 emerging economies with geopolitical risks. The results show that the stock markets of these emerging economies have experienced sharp fluctuations under the influence of high geopolitical risks. Zhang and Hamori [35] directly explored the spillover effects of the geopolitical risk index of the BRICS countries on some macroeconomic variables in the United States by using the extended network analysis method. The results show that the geopolitical risks of China and Russia are the main sources affecting the US stock market and volatility. Sohag [10] focused his research on green energy stocks and green bonds. The results show that geopolitical risk has a positive spillover effect on green energy stocks and green bonds. He believes that this is because investors tend to invest in these environmentally friendly assets during the period of geopolitical risk, so as to achieve risk hedging. We can see that the use of geopolitical indexes to directly study the stock market is very limited, and the focus is primarily on stock return and volatility. However, before this, Baker et al. [36] constructed economic policy uncertainty similar to the geopolitical risk index based on news texts, and many scholars have also used economic policy uncertainty to carry out corresponding research, proving that economic policy uncertainty has a strong negative impact on stock returns (Arouri et al., 2016; Brogaard and Detzel, 2015; Kang et al., 2017). Some economic policies themselves, however, have some endogenous interference with the stock market. We hope to examine the impact of external shocks on it more. Das [37]'s research using the quantile regression method shows that whether it is geopolitical risk or economic policy uncertainty, the impact of the two shocks on the stock market at different quantiles is indeed heterogeneous, and this effect is more manifested in the mean of the return rather than the variance. Based on the above research content, this paper will focus on how global geopolitical risk index impact on the return connectedness between international stock markets under different quantiles of them.

3 Data and description

The stock market index is based on 12 major global stock market indices, including: IBOVESPA (Brazil), DJI (United States), IXIC (United States), SPX (United States), FTSE (United Kingdom), FCHI (France), GDAXI (Germany), N225 (Japan), KS11 (Korea), HIS (Hong Kong, China), SENSE (India), SSEC (China). The data sample interval is from January 1991 to June 2022, which is derived from the Wind database.

This paper uses the global geopolitical risk index created by Caldara and Iacoviello [2] to measure the degree of geopolitical risk. Based on Saiz and Simonsohn [38] and Baker et al. [36], the index uses the share of articles on geopolitical events affecting the peaceful development of international relations such as terrorist attacks and

TABLE 2 Global stock market return contagion matrix.

| | y_1 | y_2 | \cdots | y_p | FROM |
|----------|------------------------------------------------|------------------------------------------------|----------|------------------------------------------------|----------------------------------------------|
| y_1 | \tilde{d}_{11}^{gH} | \tilde{d}_{12}^{gH} | \cdots | \tilde{d}_{1k}^{gH} | $\sum_{j=1}^k \tilde{d}_{1j}^{gH}, j \neq 1$ |
| y_2 | \tilde{d}_{21}^{gH} | \tilde{d}_{22}^{gH} | \cdots | \tilde{d}_{2k}^{gH} | $\sum_{j=1}^k \tilde{d}_{2j}^{gH}, j \neq 2$ |
| \vdots | \vdots | \vdots | \ddots | \vdots | \vdots |
| y_p | \tilde{d}_{p1}^{gH} | \tilde{d}_{p2}^{gH} | \cdots | \tilde{d}_{pk}^{gH} | $\sum_{j=1}^k \tilde{d}_{pj}^{gH}, j \neq k$ |
| TO | $\sum_{i=1}^k \tilde{d}_{1i,t}^{gH}, i \neq 1$ | $\sum_{i=1}^k \tilde{d}_{2i,t}^{gH}, i \neq 2$ | \cdots | $\sum_{i=1}^k \tilde{d}_{ik,t}^{gH}, i \neq k$ | TSP |

wars reported by 10 newspapers published in the United States, Britain and Canada to construct the daily and monthly geopolitical risks of the world and some countries since 1900. Caldara and Iacoviello [2] also constructed two sub-components of global geopolitical threat risk (GPPT) and global geopolitical action risk (GPRA) to distinguish different global geopolitical risks. Articles in the GPRT index search include phrases related to threats and military buildups, while the GPRA index search involves phrases that implement or upgrade adverse events. The index is now widely used in academia [39–41]. The data interval is from March 1995 to June 2022.

Table 1 provides descriptive statistics for the data.

4 Methodology

4.1 Complex dynamic contagion network of global stock market returns

Using the Vector Autoregressive Model (VAR) method, Diebold and Yilmaz [12,13] constructed an information spillover network between financial institutions, and then implemented the rolling window method to build a continuous-time correlation network. We use this method to construct the risk contagion and correlation network of global stock market returns. The specific construction process is as follows.

Firstly, we consider an N-dimensional VAR p) process with stationary covariance:

$$Y_t = \sum_{i=1}^p A_i Y_{t-i} + \varepsilon_t \quad (1)$$

Where $Y_t = [y_1, \dots, y_p]$ represents the logarithmic return vector of the stock market, and y_i represents the logarithmic return of a certain stock market; and $\varepsilon_t \sim (0, \Sigma)$ represents the independent identically distributed disturbance vector. Convert Eq. 1 to its Vector Moving Average (VMA) representation:

$$Y_t = \sum_{i=0}^{\infty} \Psi_i u_{t-i} \quad (2)$$

Here, the $N \times N$ coefficient matrix Ψ_i obeys the following recursive formula:

$$\Psi_i = A_1 \Psi_{i-1} + A_2 \Psi_{i-2} + \cdots + A_p \Psi_{i-p} \quad (3)$$

Ψ_0 is an $N \times N$ identity matrix with $\Psi_i = 0$ for $i < 0$.

Diebold and Yilmaz [12,13] defined the information spillover effect as the contribution of forecast error variance, that is, in the case of $i \neq j$, after the impact of y_j on y_i , the proportion of the H -step forecast error variance of y_i can be explained by the impact of y_j . This contribution ratio reflects the degree to which the change of variable y_i is affected by other variables in the system.

The generalized forecast error variance decompositions matrix $\theta_{ij}^g(H) = [d_{ij}^{gH}]$ can be expressed by the following formula:

$$d_{ij}^{gH} = \frac{\sigma_{jj}^{-1} \sum_{h=0}^{H-1} (e_i' \Psi_h \Sigma e_j)^2}{\sum_{h=0}^{H-1} (e_i' \Psi_h \Sigma \Psi_h' e_i)} \quad (4)$$

Where e_j is the selection vector whose j th element is one and other elements are 0; Ψ_h is the coefficient matrix in vector moving average model; Σ is the variance matrix of ε_t ; σ_{jj} is the diagonal element of matrix Σ . This generalized forecast error variance decomposition method makes the variable ordering in the VAR model no longer affect the results of variance decomposition, so that we no longer have to stick to the variable ordering in the model, making it easier for us to analyze the relevant results [13] (Koop et al., 1996; Pesaran and Shin, 1998).

However, due to $\sum_{j=1}^k d_{ij,t}^{gH} \neq 1$, in order to match the traditional variance decomposition results, we add and standardize each element in the generalized forecast error variance decomposition matrix by rows.

$$\tilde{d}_{ij}^{gH} = \frac{d_{ij}^{gH}}{\sum_{j=1}^N d_{ij}^{gH}} \quad (5)$$

By constructing $\sum_{j=1}^N \tilde{d}_{ij}^{gH} = 1$ and $\sum_{i,j=1}^N \tilde{d}_{ij}^{gH} = N$, we can calculate the connectedness matrix $\tilde{\theta}_{ij}^g(H) = [\tilde{d}_{ij}^{gH}]$ of global stock market returns in H step, as follows:

$$\tilde{\theta}_{ij}^g(H) = \begin{pmatrix} \tilde{d}_{11}^{gH} & \tilde{d}_{12}^{gH} & \cdots & \tilde{d}_{1k}^{gH} \\ \tilde{d}_{21}^{gH} & \tilde{d}_{22}^{gH} & \ddots & \tilde{d}_{2k}^{gH} \\ \vdots & \vdots & \ddots & \vdots \\ \tilde{d}_{k1}^{gH} & \tilde{d}_{k2}^{gH} & \cdots & \tilde{d}_{kk}^{gH} \end{pmatrix} \quad (6)$$

The market contagion effect $C_{i \leftarrow j}^H$ from stock market j to stock market i can be defined by:

$$C_{i \leftarrow j}^H = \tilde{d}_{ij}^{gH} \quad (7)$$

Specifically, in the connectedness matrix $\tilde{\theta}_{ij}^g(H)$, the non-diagonal element row i , column j represents the market contagion effect of the return in the stock market j on the stock market i ; the j th row and i th column of $\tilde{\theta}_{ij}^g(H)$ reflect the market contagion effect of stock market i on stock market j .

At the same time, the net contagion (NC) effect from stock market j to stock market i can be expressed by the following formula:

$$NC_{i \leftarrow j}^H = C_{i \leftarrow j}^H - C_{j \leftarrow i}^H \quad (8)$$

In addition, the elements in the column of “FROM” in the matrix indicate that the variable i is subject to the risk contagion effect $C_{i \leftarrow \bullet}^H$ from all other variables, that is:

$$C_{i \leftarrow \bullet}^H = \sum_{j=1}^k \tilde{d}_{ij}^{gH}, j \neq i \quad (9)$$

At the same time, the elements in the row of “TO” in the matrix represent the risk contagion effect of variable j on all other variables $C_{\bullet \leftarrow i}^H$:

$$C_{\bullet \leftarrow i}^H = \sum_{i=1}^k \tilde{d}_{ij,t}^{gH}, i \neq j \quad (10)$$

On this basis, we can also calculate the net contagion effect of stock market i on all other stock markets C_i^{Net} :

$$C_i^{\text{Net}} = C_{\bullet \leftarrow i}^H - C_{i \leftarrow \bullet}^H \quad (11)$$

The total international stock market return contagion effect TSP between stock markets can be expressed as:

$$TSP = \frac{1}{N} \sum_{\substack{i,j=1 \\ i \neq j}}^k \tilde{d}_{ij}^{gH} \quad (12)$$

TSP is equivalent to summing and averaging the elements in the row of “FROM” or the column of “TO”. Based on the basic idea of the above network topology method and related formula definitions, the global stock market return contagion (connectedness/correlation) matrix in Table 2 is constructed.

In order to further obtain the time series of the above matrix, we use the rolling window estimation method according to Diebold and Yilmaz [12,13]. First, in order to avoid over-parameterization of the model, we set the VAR to order 1, that is, $p = 1$. Since we use monthly data, in order to balance the time window and the number of estimated results, we set the rolling window to 50 days. Then, we perform rolling window estimation according to the above method, and let $H = 10$ estimate the dynamic risk contagion network between global stock markets. Before the estimation of VAR model, this paper has carried out a stationary test on the logarithmic return of each stock market index. The results show that each sequence is a stationary sequence and can be estimated by a VAR model.

4.2 Quantile on quantile regression

4.2.1 Quantile regression model

The traditional linear regression model describes the mean influence of the independent variable on the value of the dependent variable. However, it is difficult to satisfy the assumption that the random disturbance term is identically distributed in real life. Therefore, in the late 1970s, Koenker and Bassett [42] first proposed the standard quantile regression model. They used the conditional quantile of the dependent variable to regress on the independent variable. Therefore, compared with the rough description of the linear model, quantile regression can more accurately describe the influence of the independent variable on different positions of the dependent variable. The model is as follows:

$$\hat{Q}_y(\tau) = \argmin_{\alpha} \left\{ \sum_{i: y_i \geq \alpha} \tau |y_i - \alpha| + \sum_{i: y_i < \alpha} (1 - \tau) |y_i - \alpha| \right\} \quad (13)$$

4.2.2 Quantile on quantile regression approach

However, the standard quantile regression model does not account for the effect of different distributions of the independent variables on the dependent variables. Therefore, Sim and Zhou [43] proposed the Quantile-on-Quantile Regression Approach (QQR) in their study regarding the relation between oil and stock returns.

TABLE 3 Global stock market return correlation network.

| | IBOVESPA | DJI | IXIC | SPX | FTSE | FCHI | GDAXI | N225 | KS11 | HIS | SENSEX | SSEC | FROM |
|----------|----------|-------|-------|--------|-------|-------|-------|-------|-------|-------|--------|--------|-------------|
| IBOVESPA | | 7.53 | 6.27 | 7.57 | 7.57 | 6.66 | 6.55 | 5.51 | 6.42 | 9.52 | 5.54 | 3.60 | 72.75 |
| DJI | 5.99 | | 10.16 | 15.30 | 9.08 | 8.42 | 9.09 | 5.99 | 5.17 | 7.52 | 3.72 | 2.39 | 82.82 |
| IXIC | 5.73 | 10.78 | | 14.05 | 7.98 | 7.66 | 8.62 | 6.49 | 5.86 | 7.48 | 4.54 | 2.17 | 81.36 |
| SPX | 6.02 | 14.39 | 12.24 | | 9.00 | 8.54 | 9.04 | 5.97 | 5.22 | 7.35 | 3.96 | 2.18 | 83.91 |
| FTSE | 6.10 | 9.84 | 8.01 | 10.44 | | 11.28 | 10.27 | 5.24 | 6.12 | 8.03 | 3.88 | 2.19 | 81.39 |
| FCHI | 5.46 | 8.96 | 7.80 | 9.74 | 11.39 | | 14.09 | 6.84 | 5.31 | 5.99 | 3.56 | 1.90 | 81.05 |
| GDAXI | 5.44 | 9.59 | 8.55 | 10.13 | 9.94 | 13.46 | | 6.72 | 5.69 | 6.84 | 3.91 | 1.93 | 82.21 |
| N225 | 6.18 | 7.86 | 7.95 | 8.20 | 6.27 | 8.58 | 8.47 | | 6.72 | 5.81 | 4.61 | 3.01 | 73.66 |
| KS11 | 6.33 | 6.72 | 7.55 | 7.42 | 7.93 | 6.47 | 7.08 | 6.68 | | 8.79 | 5.50 | 3.34 | 73.81 |
| HIS | 7.62 | 8.78 | 8.03 | 9.05 | 8.87 | 6.80 | 7.48 | 5.06 | 7.67 | | 5.27 | 5.08 | 79.71 |
| SENSEX | 7.23 | 6.66 | 7.95 | 7.42 | 5.95 | 5.59 | 6.22 | 5.72 | 7.48 | 7.70 | | 3.10 | 71.00 |
| SSEC | 5.52 | 4.78 | 4.38 | 4.59 | 4.15 | 3.97 | 3.95 | 4.06 | 5.37 | 8.33 | 3.94 | | 53.06 |
| TO | 67.61 | 95.87 | 88.90 | 103.91 | 88.14 | 87.43 | 90.87 | 64.27 | 67.03 | 83.37 | 48.44 | 30.90 | TSP = 76.40 |
| NET | -5.14 | 13.05 | 7.54 | 20.00 | 6.74 | 6.38 | 8.66 | -9.39 | -6.79 | 3.66 | -22.56 | -22.16 | |

This paper will focus on how global geopolitical risk index impact on the return connectedness between international stock markets under different quantiles of them. To this end, we first propose the linear regression model as follows:

$$\Delta TSP_t = \beta_1 GPR_t + \beta_2 \Delta TSP_{t-1} + \varepsilon_t \quad (14)$$

Convert this OLS model into QQ model:

$$\Delta TSP_t = \beta^\theta(GPR_t) + \alpha^\theta \Delta TSP_{t-1} + \varepsilon_t^\theta \quad (15)$$

ΔTSP_t represents the first difference of total international stock market return contagion effect at time t . This paper takes the first-order difference, as TSP is not stationary. GPR_t is the global geopolitical risk index at time t . θ is the θ quantile of distribution. ε_t^θ is the error term, and β^θ is the unknown parameter, which explains the influence of global geopolitical risk on the total connectedness between international stock markets for different θ quantile. The above standard quantile regression model can study the spillover effect of global geopolitical risk on different quantiles of ΔTSP_t , but it cannot explain the spillover effect of different states of GPR_t on ΔTSP_t . High-risk status and low-risk status may have different effects on the degree of international stock market correlation, and the degree of stock market correlation may also have different reactions to it. Therefore, it is necessary to examine the relationship between the τ quantile of geopolitical risk (GPR^τ) and the θ quantile of global stock market connectedness. Since β^θ is unknown, it can be approximated by the first-order Taylor expansion of GPR^τ as follows:

$$\beta^\theta(GPR_t) \approx \beta^\theta(GPR^\tau) + \beta^{\theta'}(GPR^\tau)(GPR_t - GPR^\tau) \quad (16)$$

To rewrite $\beta^\theta(GPR^\tau)$ and $\beta^{\theta'}(GPR^\tau)$ as $\beta_0(\theta, \tau)$ and $\beta_1(\theta, \tau)$, Eq. 16 is transformed into Eq. 17:

$$\beta^\theta(GPR_t) \approx \beta_0(\theta, \tau) + \beta_1(\theta, \tau)(GPR_t - GPR^\tau) \quad (17)$$

Substitute (17) into (15) and get the following formula:

$$\Delta TSP_t = \beta_0(\theta, \tau) + \beta_1(\theta, \tau)(GPR_t - GPR^\tau) + \alpha(\theta)\Delta TSP_{t-1} + \varepsilon_t^\theta \quad (18)$$

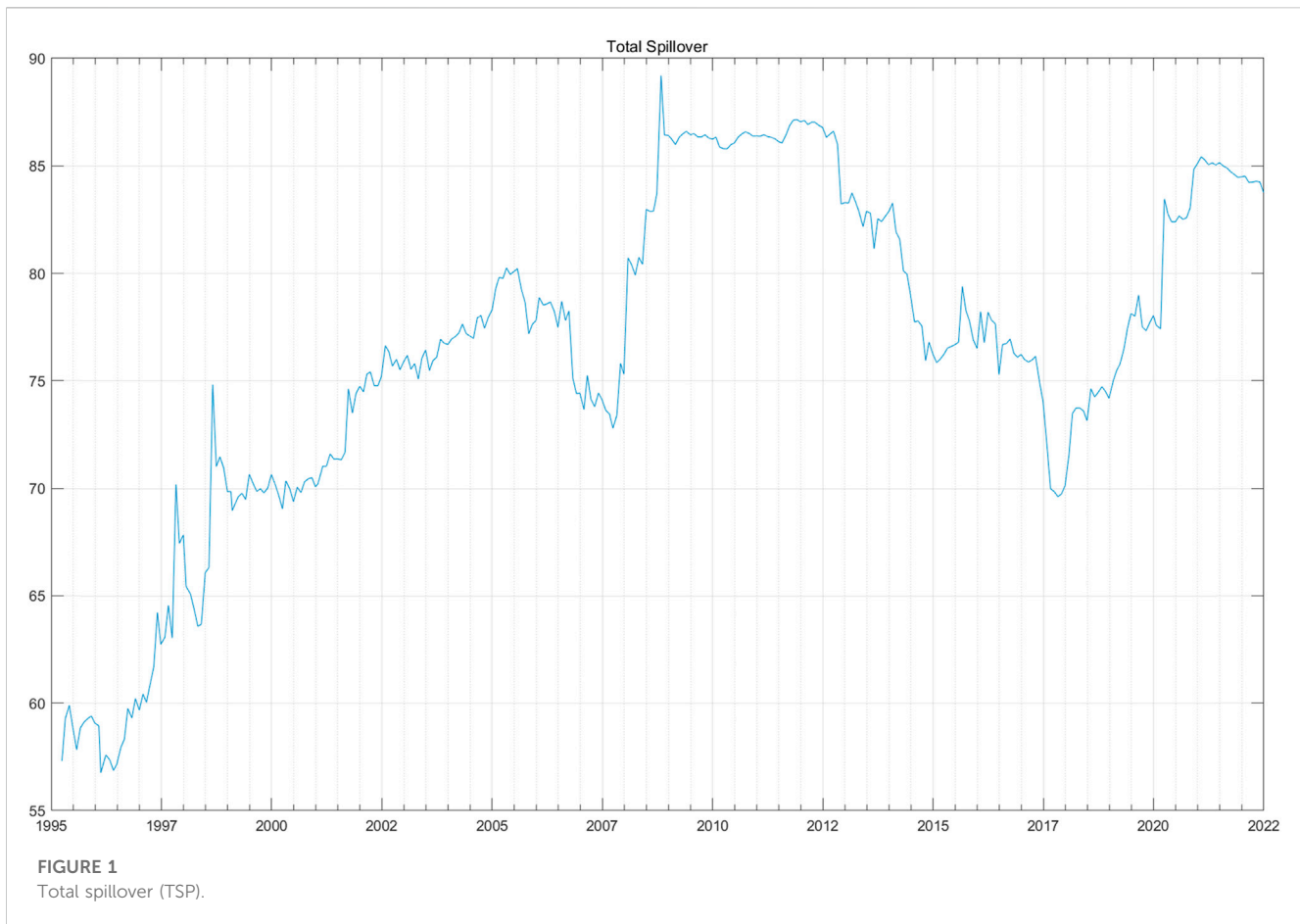
Eq. 18 represents the θ conditional quantile of ΔTSP_t , where $\alpha(\theta) = \alpha^\theta$, $\beta_0(\theta, \tau)$ is the intercept term, and $\beta_1(\theta, \tau)$ is an estimated parameter reflecting the impact of τ quantile GPR_t on θ quantile ΔTSP_t . $\beta_0(\theta, \tau)$ and $\beta_1(\theta, \tau)$ are different from the standard quantile regression, because β_0 and β_1 are associated with θ and τ . Eq. 18 can reflect the comprehensive relationship between the τ quantile global geopolitical risk and the θ conditional quantile of the first-order difference of TSP.

By minimizing Eq. 19, the local linear estimates of $b_0(\beta_0(\theta, \tau))$ and $b_1(\beta_1(\theta, \tau))$ can be obtained:

$$\min_{b_0, b_1} \sum_{i=1}^n \rho_\theta[\Delta TSP_i - b_0 - b_1(GPR_i - GPR^\tau) - \alpha(\theta)\Delta TSP_{i-1}] K\left(\frac{F_n(GPR_i) - \tau}{h}\right) \quad (19)$$

We define $\rho_\theta = u(\theta - I(u < 0))$, where ρ_θ is the loss function of the θ conditional quantile; I is the indicator function; $K(\cdot)$ is the kernel function, which is used to weight the adjacent values of GPR^τ ; and h is the bandwidth parameter of the kernel function. Because the Gaussian kernel function has the characteristics of extreme simplicity and high efficiency, this paper uses the Gaussian kernel to weight the observed values. The weight is inversely proportional to the distance between the empirical distribution of GPR_t and GPR^τ . The farther the distance from the observed value, the lower the weight, and *vice versa*, as shown in Eq. 20:

$$F_n(GPR_t) = \frac{1}{n} \sum_{k=1}^n I(GPR_k < GPR_t) \quad (20)$$



Bandwidth selection is very significant for the kernel function. If the bandwidth is too narrow, the estimation error becomes smaller but the variance increases. If the bandwidth is too large, the estimation variance becomes smaller but the error increases. This paper uses Sim and Zhou [43] bandwidth selection, and selects $h = 0.05$ in the following empirical process.

5 Empirical results

5.1 Global stock market dynamic contagion network

In this section, we give the relevant estimation results of the global stock market return contagion network.

5.1.1 Global stock price linkage network

Table 3 shows the stock market return connectedness matrix for the full sample. Since we use a rolling window to estimate the data, each window period can generate a market return connectedness matrix. Table 3 shows the mean value of the connectedness matrix $\tilde{\theta}_{ij}^g(H)$ of all window periods. The element ij represents the spillover effect of the j stock market index on the i stock market index.

Table 3 shows that the average TSP of all stock markets is 76.40 percent. This shows that on average, the world's major stock market indexes exhibit a very high correlation degree. This is a major

reason for the transmission of financial market risks to various markets.

Additionally, Table 3 indicates that the Standard & Poor's 500 Index (SPX), the Dow Jones Industrial Index (DJI), and the German Frankfurt DAX Index (GDAXI) are the three stock market indexes that have the greatest impact on the world. Their impact on global stock market returns is 20%, 13.05% and 8.66%, respectively. The results indicate that North American and European equity markets are leading the way for global equity markets, with other markets following more closely behind. The above results are not surprising. Because the United States is still the world's largest economy at this stage, its economic strength radiates around the world; and because of the special status of the dollar, the size of the United States stock market and trading volume is still the largest in the world, so the United States stock market has a huge impact on the world economy. As a powerful industry in Europe, Germany's financial strength, economic strength and political strength are second to none in Europe. The trend of the German stock market can be used as an effective indicator of European economic and financial health.

Finally, from Table 3, we can also find that India's Mumbai Sensitive 30 Index (SENSEX), Shanghai Composite Index (SSEC) and Nikkei 225 Index (N225) are the main recipients of global stock market spillover effects, with values of -22.56% , -22.16% and -9.39% , respectively. India and China are the world's two largest emerging markets, making their stock markets attractive to

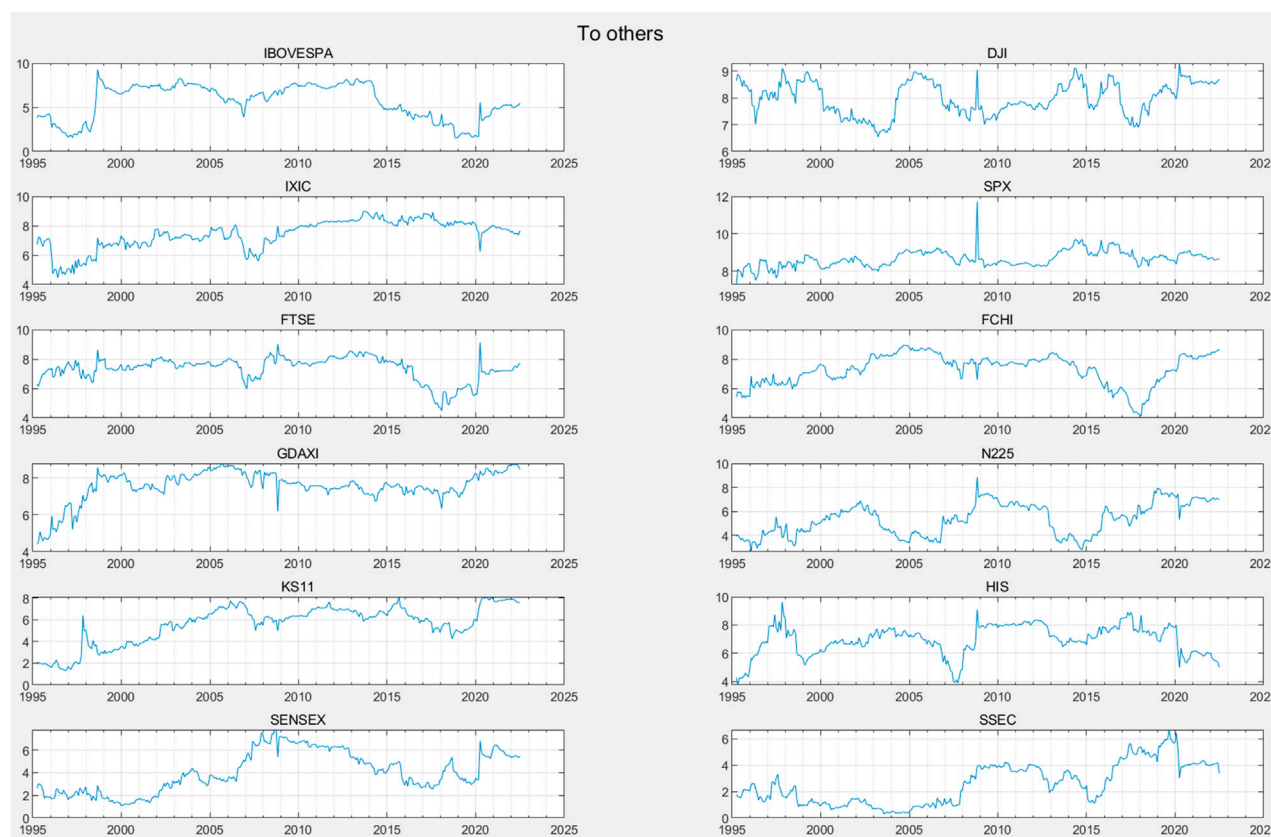


FIGURE 2
To spillover.

international investors. There is still a gap between its stock market development and scale and that of developed countries. So, it is more likely to follow the trend of the United States and European stock markets. Japan is the most sought-after haven for global investors except the United States, and the yen is also one of the most valuable reserve currencies. Investors often use the yen and the Japanese stock market for related arbitrage transactions, so Japanese stocks are very vulnerable to other markets.

5.1.2 Dynamic network in the global stock market

In Figure 1, we draw the total international stock market return contagion effect in the rolling sample window. Overall, we can observe three distinct stages. The first phase began in 1995 and ended in early 2009; the second stage lasted from early 2009 to early 2018; the third stage is from 2018 until 2022.

The first stage coincides with the process of economic globalization around the world. In the process of globalization, most countries in the world have opened up their financial markets, which has greatly increased the linkage between stock prices on various stock markets. The second phase occurred nearly 10 years after the financial crisis. In the 10 years after the financial crisis, governments and investors around the world have absorbed relevant experience. They have carried out strict supervision of capital market openings and derivatives trading. These regulatory measures have reduced the linkage between stock markets in various

countries to the level before the crisis. In the third stage, major geopolitical conflicts such as the Sino-US trade war and the Russo-Ukrainian War began to occur frequently. Major risk events not only impact a stock market, but also have a significant impact on the global economy and financial markets. Thus, the price linkage between the various stock markets has been rising in the past 5 years.

Figures 2, 3 show the time series of directional connectedness (“TO” and “FROM”) of each stock market.

From Figure 2, we can see that in the 2008 financial crisis, the “TO” spillover effect of the four stock indexes of DJI, SPX, N225 and FTSE all had an obvious peak, while the “TO” spillover effect of other stock market indexes had no obvious peak. This shows that during the financial crisis, the source of risk was mainly generated by the DJI, SPX, N225, FTSE four indexes. This result is relatively easy to understand, mainly because the US, Japan, and the UK have more active derivatives trading, similar pre-crisis financial regulatory policies, and very high financial dependence. Therefore, when the U. S. subprime mortgage crisis hit, the four indexes had the fastest response. As the crisis deepened, the impact of these four indices slowly spread to other developed and emerging markets.

Another obvious characteristic of Figure 3 is that the change of “FROM” effect is smoother than the change of “TO” effect. This result is consistent with many other studies. This difference is not difficult to explain. When a single stock market index produces an

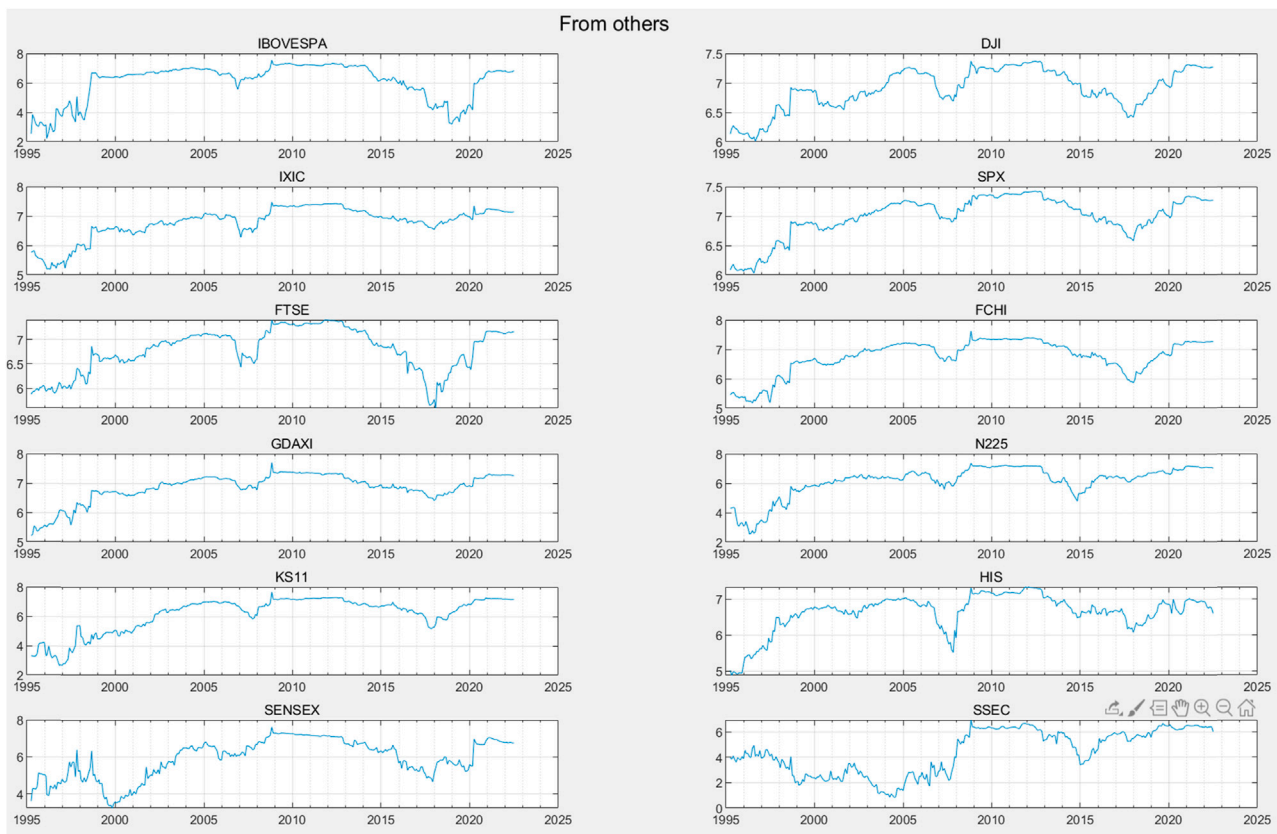


FIGURE 3
From spillover.

impact, this impact is expected to be transmitted to other stock market indexes. However, when individual stock market indexes receive total impacts from other markets, some fractions of this total impact are very small and can be ignored. Some may be quite large. At this time, the “TO” effect will obviously show more peaks. When a stock market index is hit, one can expect the impact to have a scattered spillover effect on other stock markets. Since each stock market index will be affected by the spillover effects of all other markets, these spillover effects are often smoother after being summed up.

Figure 4 shows the time series diagram of the “NET” index. From Figure 4, we can get a similar conclusion to Table 2. For the most part of the time, the “NET” indicator time series charts of the India Mumbai Sensitivity 30 Index (SENSEX) and the Shanghai Composite Index (SSEC) are below the 0 level. This shows that stock price changes in these two markets are mainly affected by changes in other stock markets. These two indicators have a limited influence on other market indexes. Additionally, the S&P 500 Index (SPX), the Dow Jones Industrial Average (DJI), and the German DAX Index (GDAXI) three “NET” indicator time series diagram is above 0 levels at most of the time, indicating that the world’s stock market index price changes are mostly driven by these three index fluctuations. These results are consistent with the conclusions of Table 2.

5.2 Global geopolitical risk (GPR) and global stock market total connectedness

Standard quantile regression can estimate the impact of global geopolitical risks on the connectedness of global stock market returns in different states. However, it cannot capture the asymmetric spillover effect of global geopolitical risks on the connectedness of global stock market returns. This ignores the possibility of different states of global geopolitical risks. For example, the impact of global geopolitical risks under high and low risk conditions on the connectedness of global stock market returns may have asymmetric heterogeneity. Therefore, standard quantile regression cannot capture the subtle economic relationship between the two.

The quantile-on-quantile regression model [43] can effectively solve this problem, which characterizes its impact on θ quantile of global stock market connectedness through the τ quantile of global geopolitical risk. Since the estimation coefficients $\beta_0(\theta, \tau)$ and $\beta_1(\theta, \tau)$ are functions of quantiles θ and τ , we can explore the spillover impact of different states of global geopolitical risk on the connectedness of global stock market returns by changing quantiles θ and τ , which can provide more useful information for regulators and market investors.

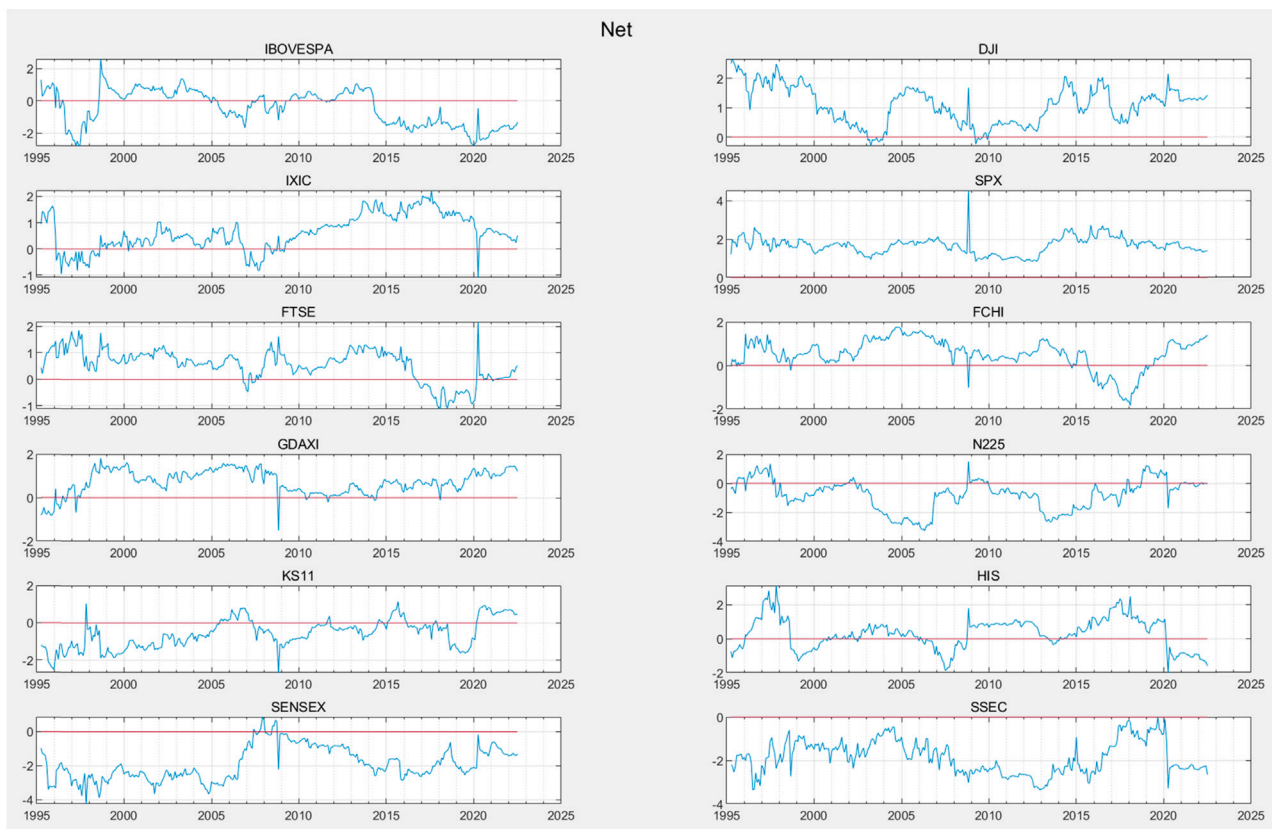


FIGURE 4
Net spillover.

In this section, we use quantile-on-quantile regression [43] to analyze the impact of global geopolitical risks on the connectedness of the global stock market at different quantiles.

5.2.1 QQR estimation results of intercept for GPR

First, we characterize the intercept influence of global geopolitical risk (GPR) on the connectedness between global stock markets through the intercept term in the formula, namely the estimate of $\beta_0(\theta, \tau)$. Because the intercept term $\beta_0(\theta, \tau)$ is determined by θ and τ , it will change at different GPR quantiles and different ΔTSP quantiles, that is, $\beta_0(\theta, \tau)$ will change at different geopolitical risk quantiles and different global stock market connectedness quantiles. The Z-axis in Figure 5 reflects an estimated value of the intercept term $\beta_0(\theta, \tau)$. The ΔTSP -axis is the θ quantile of ΔTSP , and the GPR-axis is the τ quantile of the global geopolitical risk. A low quantile of GPR indicates a low risk state, while a high quantile indicates a high risk state. The low quantile of ΔTSP implies that the global stock market is in a state of loose correlation, while the high quantile suggests that the global stock market is in a state of close correlation.

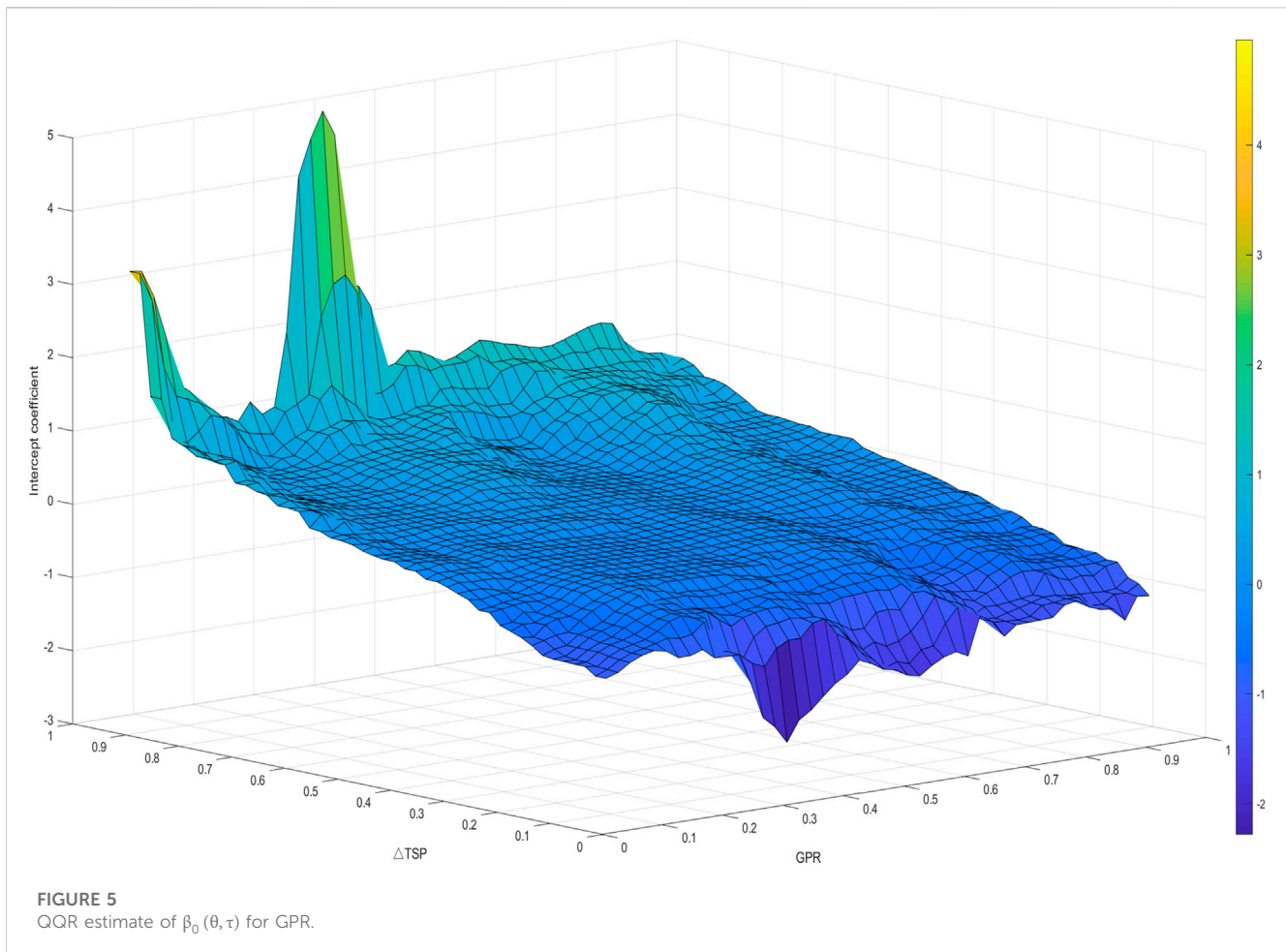
Figure 5 illustrates the estimated value of $\beta_0(\theta, \tau)$, which is influenced by geopolitical events and the tightness of global market correlation itself. Our results can be summarized as follows:

First, in general, this intercept term $\beta_0(\theta, \tau)$ increases with the rise of the connectedness degree of the global stock market. This

means that this intercept will be greater at a higher level of global market correlation. Interestingly, this change is very dramatic when the global market connectedness changes from loose to tight, that is, from the low to high of the θ quantile. When the ΔTSP is low ($\theta \in [0, 0.1]$), the increase in the global stock market correlation will cause the intercept term to rise rapidly (from negative to zero). Then, the intercept changes gently from 0.07 to 0.9 at the θ quantile and rises rapidly after 0.9.

Secondly, when ΔTSP is in the same θ quantile, the quantile change of GPR will also lead to the change of the intercept term $\beta_0(\theta, \tau)$. In particular, the intercept term $\beta_0(\theta, \tau)$ is not much different in most cases at the lower ΔTSP quantile, that is, ΔTSP is about 0.05–0.07 quantile, but at the 0.3–0.4 quantile of the GPR, it shows a sudden depression trough, where $\beta_0(\theta, \tau)$ is estimated to be an extreme negative value of -2.28. On the contrary, in the higher ΔTSP quantile (0.9–0.95), the intercept term $\beta_0(\theta, \tau)$ also has two obvious peaks, one is in the case of lower geopolitical risk, that is, GPR is near 0.05–0.07, and the other is near 0.33–0.39. This suggests that when global stock markets are closely linked and the GPR is near these two quantile values, it will further strengthen the connectedness of global stock markets. And geopolitical risk, at the 0.3–0.4 quantile, further disintegrates this correlation when global equity markets are more loosely connected.

Finally, on the whole, when ΔTSP is lower the median, no matter what the geopolitical risk is, the intercept term $\beta_0(\theta, \tau)$ is basically



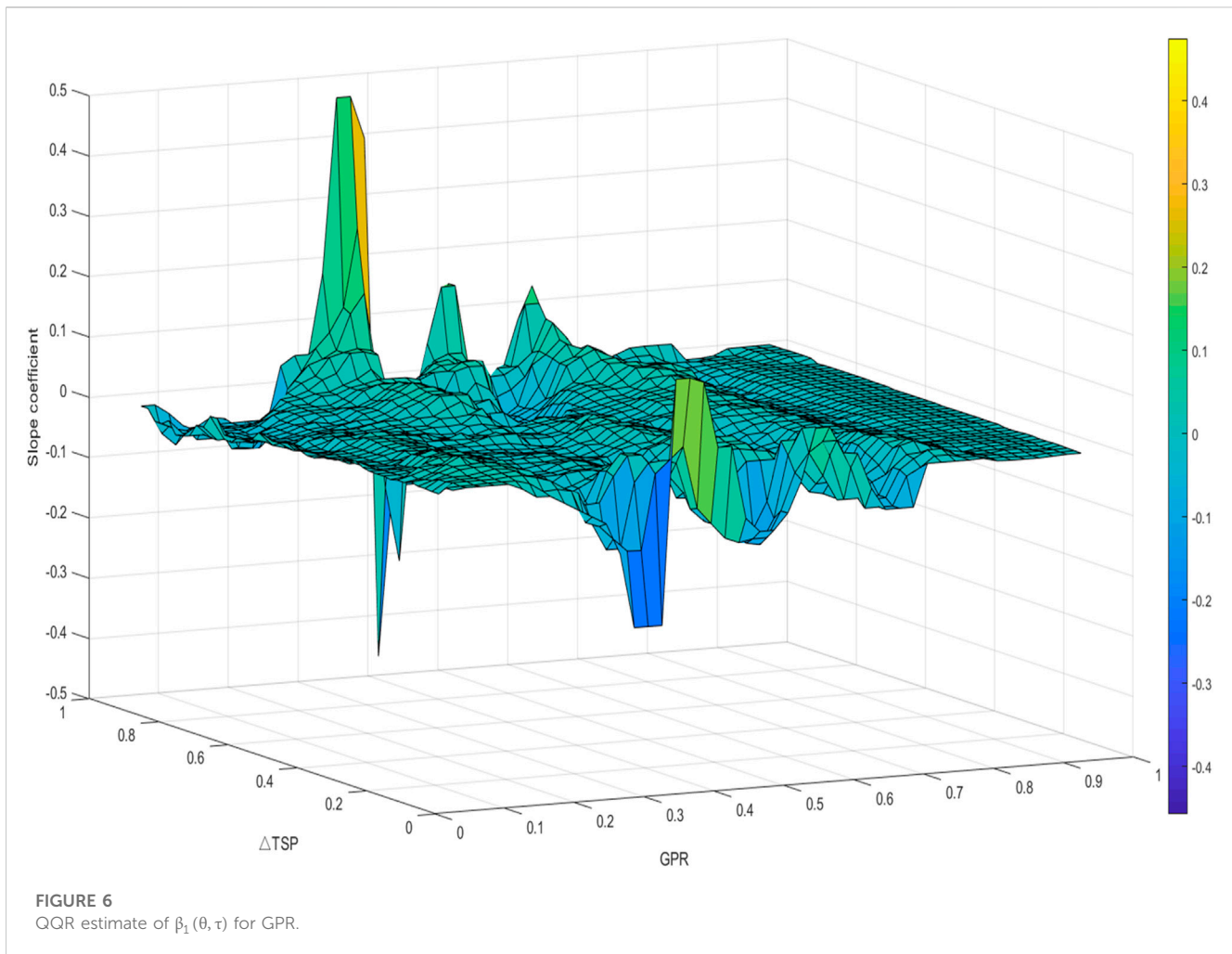
negative, and when ΔTSP is higher the median, no matter what the geopolitical risk is, the intercept term $\beta_0(\theta, \tau)$ is basically positive. This is further evidence that the same degree of geopolitical risk has heterogeneous effects on global stock markets at different levels of correlation.

5.2.2 QQR estimation results of slope for GPR

In the previous section, we discuss the estimation results of the intercept term of $\beta_0(\theta, \tau)$, and the marginal effect of the influence of geopolitical risk on the connectedness of global stock markets is represented by $\beta_1(\theta, \tau)$. Figure 6 visualizes the estimation results of $\beta_1(\theta, \tau)$. The Z-axis represents the estimated value of the slope coefficient $\beta_1(\theta, \tau)$ under different θ quantiles and τ quantiles. The ΔTSP -axis and GPR-axis have the same meaning as Figure 5.

We can see that Figure 6 is very similar to Figure 5 at the peak. When the global stock market connectedness is at a high quantile, that is, the stock markets are in a state of close interaction, about 0.9–0.95, and the global geopolitical risk is at about 0.35 quantile, $\beta_1(\theta, \tau)$ shows a significant peak, and the estimated positive value of $\beta_1(\theta, \tau)$ is 0.4748. This shows that under the condition that global stock markets are closely related, when the global geopolitical risk around the 0.35 quantile, GPR has a positive marginal effect on the connectedness of global stock markets. On the contrary, $\beta_1(\theta, \tau)$ displays a sunken trough when the global stock market connectedness is in the low quantile, about 0.05–0.07, and the

GPR is in the 0.31–0.35 quantile. And the negative value of $\beta_1(\theta, \tau)$ is estimated to be -0.2301 , which indicates that the global geopolitical risk around the 0.35 quantile will have a huge negative impact on the connectedness of global stock markets under the condition of loose interaction between international stock markets. Similarly, when the global stock market correlation is at the high quantile, about 0.91–0.95, and the GPR is at the 0.49 quantile, the estimated positive value of $\beta_1(\theta, \tau)$ is 0.1521. This shows that under the condition that the global stock market is closely related, the 0.49 quantile GPR has a positive marginal effect on the global stock market correlation. On the contrary, when the correlation degree of the global stock market is in the low quantile, about 0.09, and the GPR is in the 0.51 quantile, a negative value of $\beta_1(\theta, \tau)$ is estimated to be -0.119 , indicating that under the condition of loose correlation of the global stock market, the geopolitical risk around the 0.51 quantile has a negative marginal effect on the correlation degree of the global stock market. This “magnifying glass” effect is very significant in the extreme case of global stock market correlation, that is, global stock market connectedness is extremely close (or loose), and the positive (negative) effect of geopolitical risk on global stock market connectedness will be very obvious. The marginal effect induced by the same geopolitical risk quantile is completely different given a different closeness of global stock market correlation, which is compatible with the heterogeneous effects discussed above.



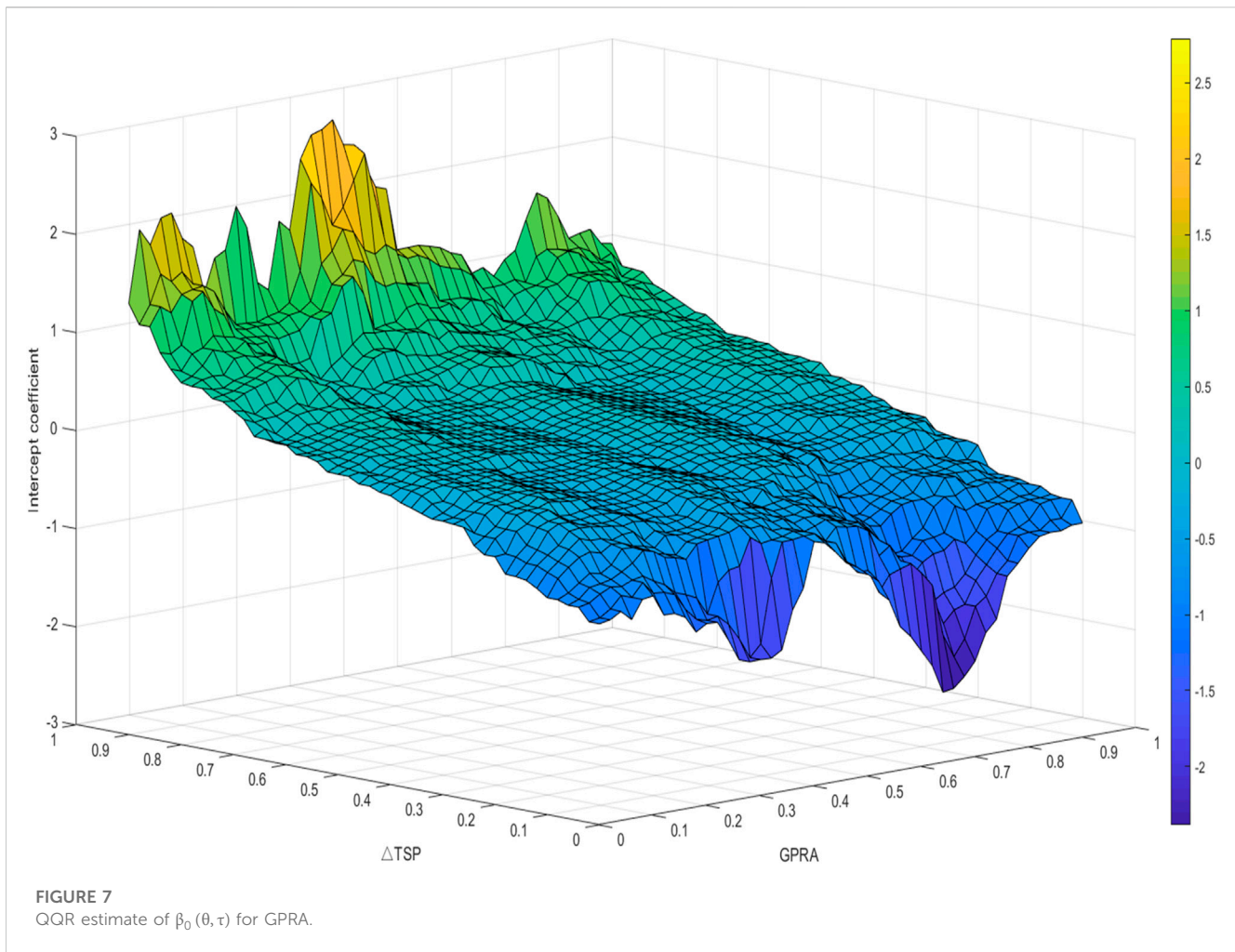
The marginal effect that is completely opposite to this “magnifying glass” effect is called the “reins” effect, which appears in the 0.37–0.40 quantile and 0.49 quantile of GPR. Specifically, when the global stock market correlation is at the low quantile, about 0.05–0.07, the GPR is at the 0.37–0.40 quantile, and the estimated positive value of $\beta_1(\theta, \tau)$ is 0.1764. This shows that under the condition of loose correlation of global stock markets, the 0.37–0.40 quantile GPR has a positive marginal effect on the correlation of global stock markets, and reduces the negative impact of GPR on the correlation of global stock markets (in Figure 5, the θ quantile of 0.05 and the τ quantile of 0.39, the estimated value of $\beta_0(\theta, \tau)$ is -1.891). On the contrary, when the correlation degree of the global stock markets is in the high quantile, about 0.91–0.95, and when the GPR is in the 0.37–0.40 quantile, a significant peak of $\beta_1(\theta, \tau)$ is estimated, which is negative -0.4571 , indicating that under the condition of close correlation of the global stock market, the GPR around the 0.37–0.40 quantile has a significant negative marginal effect on the correlation degree of the global stock markets. The positive effect of geopolitical risk on the correlation of global stock markets is reduced (in Figure 5, at the θ quantile of 0.95 and the τ quantile of 0.39, the $\beta_0(\theta, \tau)$ estimate is 4.605). In simple

terms, the “reins” effect suppresses the impact of geopolitical risk on the connectedness of global stock markets.

However, this difference appears “U-shaped” when the geopolitical risk is around 0.59–0.61, that is, in the case of high and low global market connectedness, the estimated value of $\beta_1(\theta, \tau)$ is positive, and the global geopolitical risk of this quantile has a positive marginal effect on the connectedness of global stock markets. Finally, when global geopolitical risk is at a high level, that is, 0.89–0.95 of the τ quantile, this marginal effect seems to disappear, and $\beta_1(\theta, \tau)$ exhibits an estimate close to 0, regardless of any quantile of global stock markets connectedness.

5.3 Global geopolitical action risk (GPRA) and global stock market total connectedness

In this section, we replace the variable of global geopolitical risk (GPR) with the global geopolitical action risk (GPRA). This section focuses on how geopolitical action risk (GPRA) affects the total connectedness of global stock markets.



5.3.1 QQR estimation results of intercept for GPRA

Figure 7 shows the intercept effect of global geopolitical action risks on the connectedness of global stock markets, the estimate of the intercept term $\beta_0(\theta, \tau)$. The Z-axis represents the estimated value of the intercept term $\beta_0(\theta, \tau)$, the ΔTSP -axis is still the θ quantile of the first-order difference of the global stock market correlation, and the GPRA-axis is the τ quantile of GPRA.

Figure 7 shows the intercept impact of GPRA on the connectedness of global stock markets, and the results are highly similar to Figure 5. This still represents a change in the intercept influence of GPRA on global stock market correlation from promotion to inhibition when global stock market correlation is close to loose. Based on Figure 7, it can be seen that when the global stock market connectedness is high, i.e., when the θ quantile is 0.87–0.95, regardless of GPRA, the estimated value of $\beta_0(\theta, \tau)$ is positive, meaning that any GPRA will make the global stock market more closely tied. When the global stock market interaction is at a low quantile, that is, the θ quantile is 0.05–0.11, regardless of GPRA risk, the estimated value of $\beta_0(\theta, \tau)$ is negative, indicating that any geopolitical action risk will make the global market more loosely correlated. Specifically, when the GPRA is at the 0.43 quantile, the estimated value of $\beta_0(\theta, \tau)$ reaches the maximum positive number of 2.79. Interestingly, $\beta_0(\theta, \tau)$ is estimated to have the largest negative value of -0.5367 in the case of low correlation of global stock markets

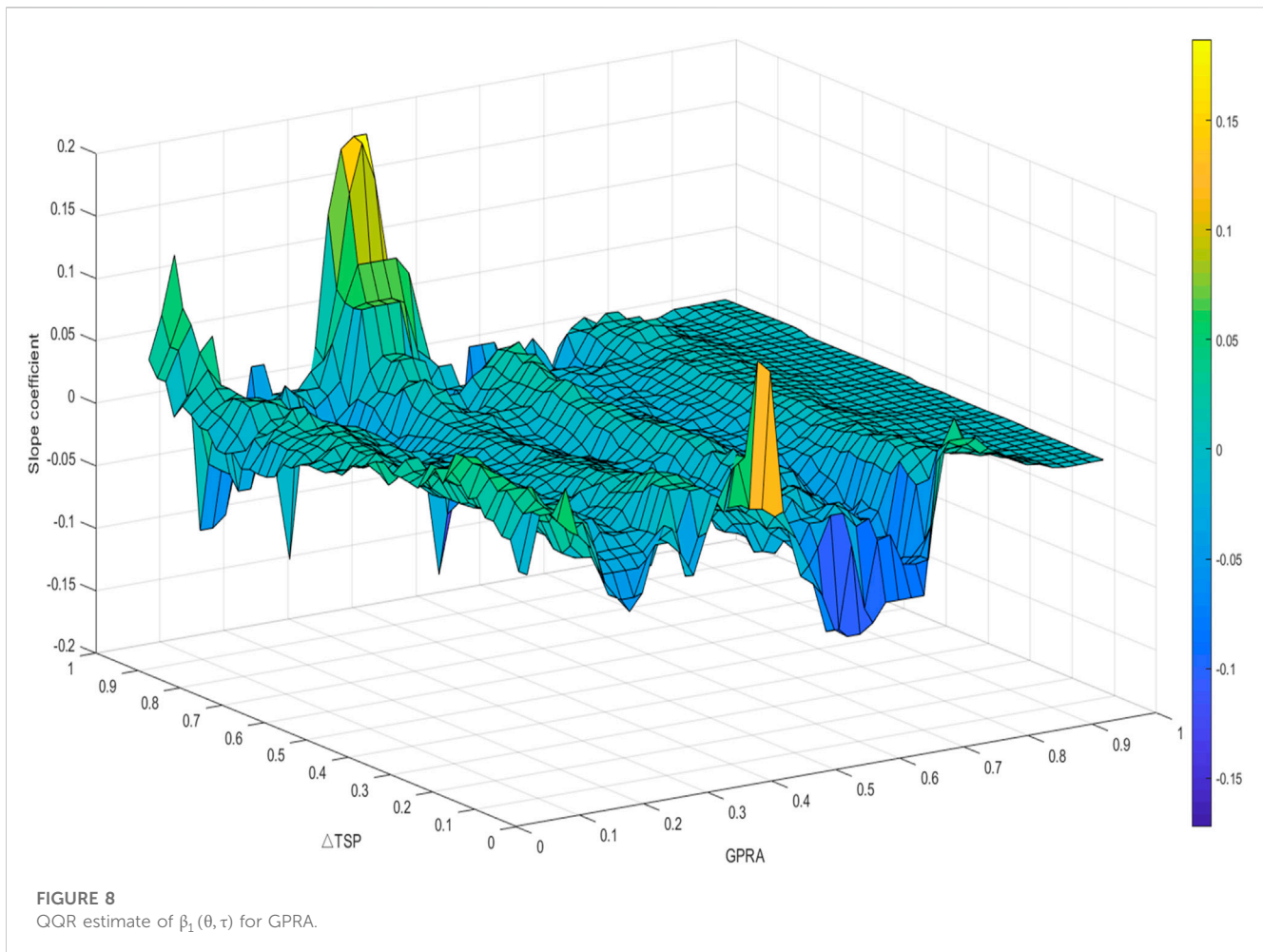
when the GPRA is in the 0.45 quantile. Similarly, when the GPRA is in the 0.69 quantile, the estimated value of $\beta_0(\theta, \tau)$ achieves a minimum negative value of -2.385 . When the quantile in the opposite direction is similar, that is, when the correlation degree of the global stock market is in the high quantile and the GPRA is in the 0.73 quantile, the estimated value of $\beta_0(\theta, \tau)$ achieves a minimum positive value of 0.8975.

In general, Figure 7 still shows a monotonous change feature, i.e., when the GPRA is at the same quantile, the impact of GPRA on the global stock market connectedness shows a trend from negative to positive.

Reflected in the estimated value of $\beta_0(\theta, \tau)$, it changes from negative to positive. Similar to Figure 5, when the connectedness degree of the global stock market is below the median, the intercept term $\beta_0(\theta, \tau)$ is basically negative regardless of GPRA. When the connectedness degree of the global stock market is above the median, the intercept term $\beta_0(\theta, \tau)$ is basically positive regardless of GPRA.

5.3.2 QQR estimation results of slope for GPRA

In Figure 8, we visualize the marginal effect of the influence of GPRA on the connectedness of global stock markets determined by different θ quantiles and different τ quantiles, that is, $\beta_1(\theta, \tau)$ in regression. The Z-axis represents the marginal effect $\beta_1(\theta, \tau)$



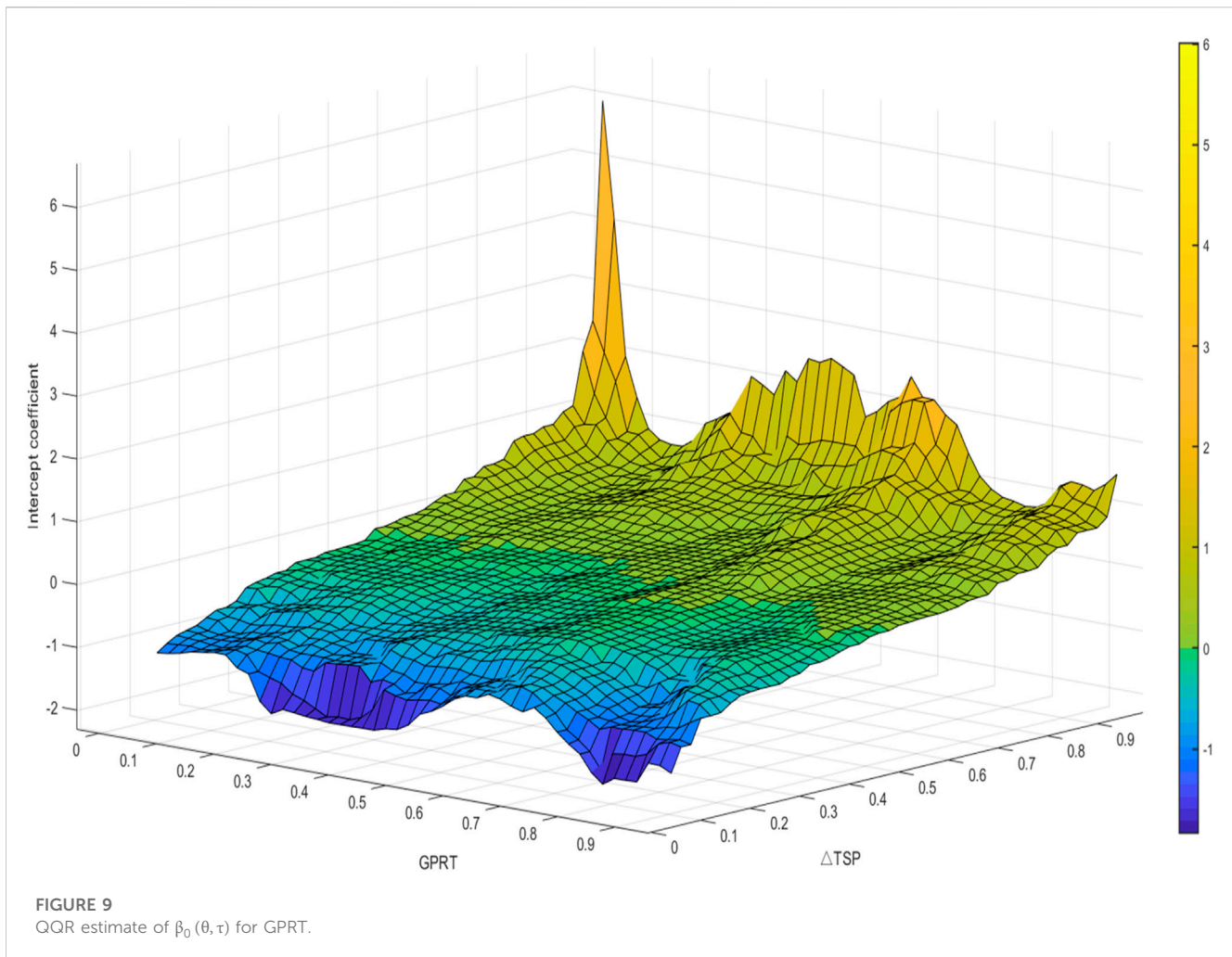
estimate. The ΔTSP -axis is still the θ quantile of the first-order difference of the global stock market correlation, and the GPRA-axis is the τ quantile of the GPRA.

When compared to the visual Figure 6 of the marginal effect, Figure 8 shows some similarities, but a closer look will reveal a lot of differences. In Figure 6, when the global stock market correlation is at a high level, about 0.91–0.95 quantile, and the GPR is at 0.39 quantile, the marginal effect of the GPR on the global stock market connectedness is estimated to be the minimum valley value. However, in Figure 8, after replacing the GPR with the GPRA, the highest peak value of 0.1869 is estimated under the same quantile conditions. That is to say, under the same quantile conditions, GPR has a negative impact on the global stock market connectedness, and this marginal effect is negative. But, the GPRA has a positive impact on the global stock market connectedness, and the marginal effect is positive. Therefore, it can be seen that after refining the types of geopolitical risks, the impact of geopolitical risks on the connectedness of global stock markets has reached very different conclusions.

Meanwhile, for Figure 8, we can observe several “U-shaped” or “inverted U-shaped” phenomena. When the GPRA is in the 0.37–0.41 quantile, if the global stock market correlation is very close or very loose, the estimated value of $\beta_1(\theta, \tau)$ shows a positive peak, and when the global stock market correlation is not in the higher

quantile or lower quantile, the estimated value of $\beta_1(\theta, \tau)$ tends to 0 or even negative. At this time, under the condition of extreme global stock market connectedness, the GPRA has a positive marginal effect on the connectedness of global stock markets, and there is a “one-way” effect, that is, whether in the case of loose connectedness of global stock market or in the case of close correlation of global stock market, the increase of GPRA shows a positive marginal effect. Under the extremely loose conditions of the global stock market, the marginal effect between the GPRA and the connectedness of global stock market is estimated to be -0.102 . So, the negative marginal effect means that under this quantile, the increase of the GPRA will aggravate the negative impact of the GPRA on the connectedness of the global stock market. When the connectedness degree of the global stock market is at a high quantile, the GPRA has a positive constant effect on the connectedness degree of the global stock market. At this time, the estimated marginal effect of the GPRA on the connectedness degree of the global stock market is -0.1722 . Therefore, the negative marginal effect means that under this quantile, the increase in the GPRA will have a negative impact on the connectedness degree of the global stock market. At this time, the “one-way” effect of the slope $\beta_1(\theta, \tau)$ becomes negative, and this “U-shaped” and “inverted U-shaped” opposite effects are very interesting.

Similar to Figure 6, the risk of local political action is at a high level, that is, 0.89–0.95 of the τ quantile. This marginal effect



disappears, and $\beta_1(\theta, \tau)$ shows an estimate close to 0 regardless of any quantile of the global stock market correlation.

5.4 Global geopolitical threat risk (GPRT) and global stock market total connectedness

In this section, we use global geopolitical threat risk (GPRT) to study how geopolitical threat risk affects the connectedness of global stock markets.

5.4.1 QQR estimation results of intercept

First, Figure 9 is a visual image of the estimated value of the intercept term $\beta_0(\theta, \tau)$ of the quantile-on-quantile regression for GPRT. Where the Z-axis characterizes the estimate of the intercept term $\beta_0(\theta, \tau)$, the Δ TSP-axis is still the θ quantile of the first-order difference of the global stock market correlation, and the GPRT-axis is the τ quantile of GPRT.

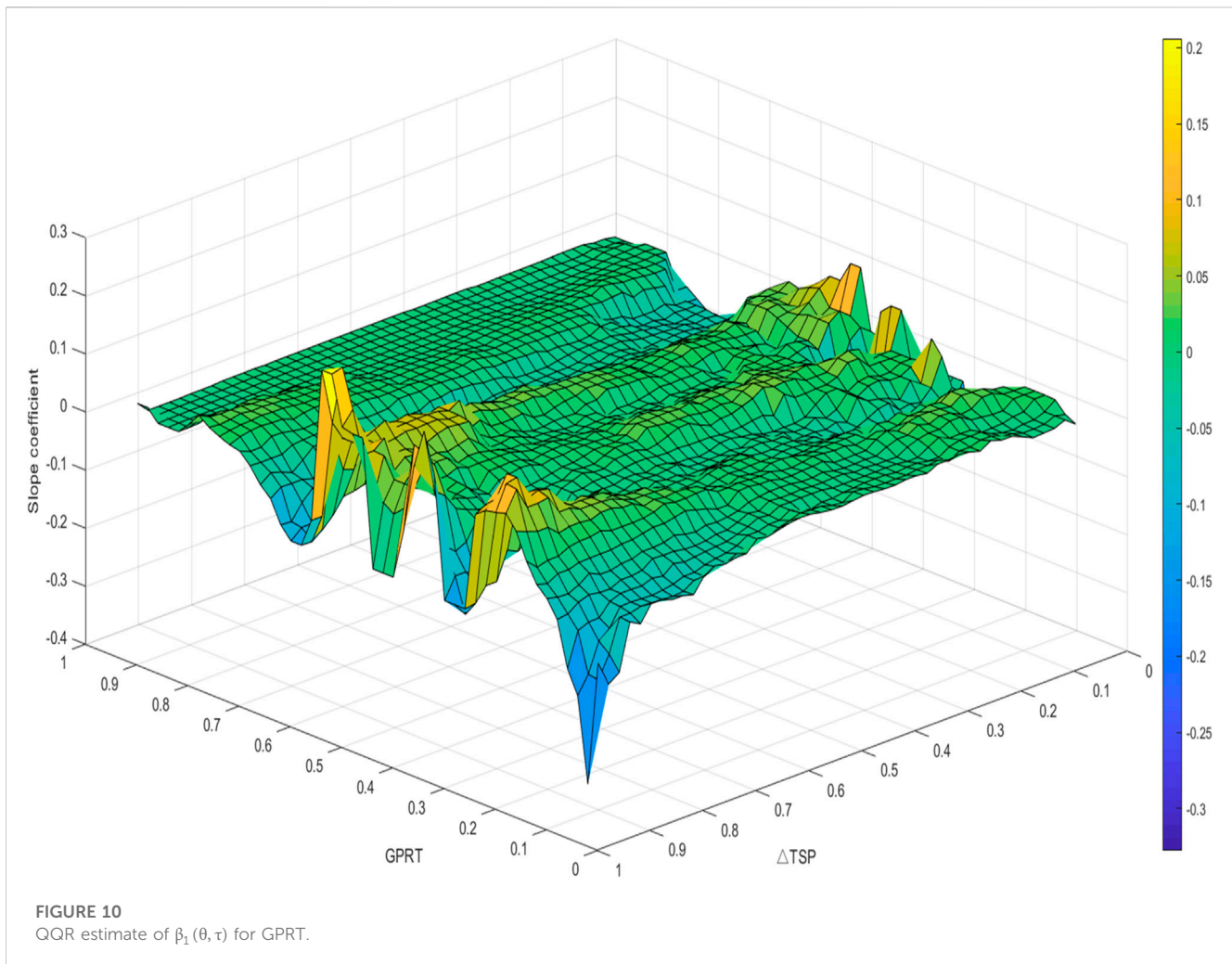
The most striking thing in Figure 9 is that when the global stock market connectedness is highly correlated (the quantile is at 0.91–0.95), while the GPRT is at a low level (the quantile is 0.05–0.09), the estimated value of marginal effect $\beta_0(\theta, \tau)$ reaches a very high peak of 6.012, indicating that the minimal GPRT at this

time will also cause a dramatic increase in the connectedness of global stock markets. In addition, when the global stock markets are highly correlated, the estimates of marginal effect $\beta_0(\theta, \tau)$ have two other lower peaks of 2.572 and 2.518 at the 0.45 and 0.59 quantiles of GPRT respectively. In contrast, the estimates of $\beta_0(\theta, \tau)$ are negative in the quantiles with low connectedness in global stock markets.

On the whole, the estimation results of Figure 9 are similar to those of Figures 5, 7. They all show the monotonic change of the estimated value of $\beta_0(\theta, \tau)$ when the connectedness degree of the global stock market is in different situations under the same quantile of GPRT. When the connectedness degree of the global stock market is low, the negative $\beta_0(\theta, \tau)$ gradually rises to 0 as the connectedness degree of the global stock market becomes closer, and then increases to positive, which means that the impact of GPRT on the connectedness of the global stock market gradually changes from negative to positive. When the global stock market connectedness is in the middle quantile part, the estimated value of $\beta_0(\theta, \tau)$ is almost zero, indicating that there seems to be no relationship between GPRT and global stock market connectedness.

5.4.2 QQR estimation results of slope

Figure 10 describes the marginal effect of GPRT on the connectedness of global stock markets. In Figure 10, the Z-axis



still represents the estimated value of the slope term $\beta_1(\theta, \tau)$ in the quantile-on-quantile regression. The ΔTSP -axis is still the θ quantile of the first-order difference of the global stock market connectedness, and the GPRT-axis depicts the τ quantile of the GPRT.

In Figure 10, when the connectedness level of the global stock market is highly related (θ is 0.95 quantile), and the GPRT is low (τ is 0.07 quantile), the estimated value of $\beta_1(\theta, \tau)$ is -0.3278 , which is the minimum estimated value of $\beta_1(\theta, \tau)$ in the quantile-on-quantile regression. This shows that when the connectedness level of the global stock market is high, the weak fluctuation in GPRT will have a significant negative impact on the connectedness level of the global stock market.

At the same time, the “magnifying glass” effect, the “reins” effect and the “unidirectional” effect in Figures 6, 8 appear in the QQR regression results of Figure 10. The “magnifying glass” effect can be clearly observed in the results of Figure 10. When the GPRT is in the 0.23 quantile, the global stock market is in a highly correlated condition, and the estimated value of $\beta_1(\theta, \tau)$ is 0.1164. The weak rise of GPRT at this τ quantile will also increase the connectedness of global stock markets when the global stock markets are closely correlated. When the GPRT is in the 0.23 quantile and the global stock market is in a very loose

condition, the estimated value of $\beta_1(\theta, \tau)$ is -0.111 . In other words, when the global stock market correlation is low, the change in GPRT will cause the global stock market correlation to decline.

The unidirectional effect in Figure 10 is also very obvious. When the GPRT is at the 0.39 quantile and the global stock market is in a highly related condition, the estimated value of $\beta_1(\theta, \tau)$ is 0.1663. When the global stock market is closely related, the rise of GPRT will further strengthen its positive effect on global stock market interconnectedness. The estimated value of $\beta_1(\theta, \tau)$ is 0.08045 when the GPRT is also at the 0.39 quantile and the global stock market is in a very loose condition. Although the estimated value is smaller, it indicates that the escalation of GPRT will still have a positive impact on the global stock market connection when the global stock market connectedness is low.

Similarly, we can also observe the “reins” effect in Figure 10. When the GPRT is at the 0.47 quantile, the estimated value of $\beta_1(\theta, \tau)$ is -0.1065 under the condition that the global stock market is highly closely linked. And when the global stock market is very loose, the estimated value of $\beta_1(\theta, \tau)$ is 0.1112. The above results show that when the GPRT is at the τ quantile of 0.47 and the global stock market connection is close, the rise of GPRT will weaken the global stock market connectedness. Under the condition that the

global stock market correlation is very loose, the increase of GPRT will increase the global stock market connectedness.

Finally, as with other slope estimates, when the GPRT is high, this marginal effect is almost 0 regardless of the global stock market correlation.

6 Conclusion

We use the vector autoregressive regression method (VAR) to construct a global stock market return contagion network, and use the quantile-to-quantile regression (QQR) to investigate the impact of global geopolitical risks on global stock market connectedness.

The main results are summarized as follows:

First, the Indian stock market and the Chinese stock market act as financial shock recipients in the global stock market. For most of the time, the net spillover effects of India's Mumbai Sensitivity 30 Index (SENSEX) and Shanghai Composite Index (SSEC) are less than 0. Generally, stock prices in these two markets follow those in other markets, and these two markets have not much influence on other market indices. The United States stock market and the German stock market are shock transmitters in the global stock market. The S&P 500 Index (SPX), the Dow Jones Industrial Average (DJI), and the Deutscher Aktien Index (GDAXI) in Germany have net spillover effects over 0. Changes in stock prices in these markets lead to fluctuation in stock prices in other markets. It is not difficult to understand that India and China, as emerging economies, are still in a relatively backward stage of capital market development. In contrast, the United States and Germany have been the world's leading economies since the economy, occupying an influential position in the global industrial chain and trade chain. At the same time, their capital markets are highly developed, so the asset prices of these two markets have played a role in the vane.

Second, in the quantile-on-quantile regression results between global geopolitical risk (GPR) and the connectedness of global stock market returns, we find that the same level of GPR has a heterogeneous impact on global stock market connectedness under different levels of connectedness. Under the high connectedness of global stock market returns, any quantile of GPR will further consolidate this connectedness; under the low connectedness of global stock market returns, any quantile of GPR will further reduce this correlation.

Third, as GPR quantiles differ, there are two opposite marginal effects: "magnifying glass" and "reins". The "magnifying glass" effect shows that an increase in GPR will intensify the connectedness of global stock market returns at high quantiles and disintegrate the connectedness of global stock market returns at low quantiles. The "rein" effect indicates that an increase in GPR will reduce the high-quantile global stock market connectedness and increase the low-quantile global stock market connectedness.

Fourth, when we further decompose the global geopolitical risk into GPRA and GPRT, we find that when the global stock market connectedness is not in extreme circumstances, different levels of GPRT will not greatly affect the global stock market's total connectedness. But when global stock markets are highly correlated and GPRT is at a very low level, any small increase in GPRT would greatly reduce that total connectedness. This phenomenon is also easy to explain. Small stones on the calm water surface will also cause very obvious ripples. In times when the GPRT level is low and global stock market total connectedness is high, any risk problem can break this quiet.

Fifth, when GPRT or GPRA is at high quantiles, their movements will not affect the total connectedness of global stock markets. This phenomenon is contrary to the previous conclusion. When GPRT or GPRA are already at a very high risk level, any further rise will no longer affect global stock market connectedness.

Sixth, we observed several 'U-shaped' or 'inverted U-shaped' phenomena when we estimated the slope between GPRA and the total connectedness of global stock markets. We call it the "one-way" effect (unidirectional effect), that is, when global stock market total connectedness is in an extreme situation (highly close or highly loose), different levels of GPRA have different marginal effects. Sometimes it increases global stock market total connectedness, and sometimes reduces global stock market total connectedness.

The findings of this study are significant for future research. This helps policymakers and relevant investors to cope with the impact of current high geopolitical risks on the global stock market contagion network. This helps them effectively manage risk in asset allocation and policy formulation. However, there are still some areas where our research can go further. For example, why do these special quantiles have different asymmetric effects? The economic logic and practical significance behind them need to be studied. In addition, research on the volatility contagion network of global stock markets and global geopolitical risks can also be discussed.

Data availability statement

The original contributions presented in the study are included in the article/supplementary materials, further inquiries can be directed to the corresponding author.

Author contributions

FL proposed the conceptualization and methodology, performed the coding and data analysis. SL performed original draft, data analysis; and gave formal writing—review and editing. LL performed the data collection and original data arrangement. SZ performed the funding acquisition, original draft preparation, data analysis and data preparation; modified final draft.

Funding

This study was supported by Yunnan Fundamental Research Projects (grant No. 202201AU070101), Scientific Research Foundation of Yunnan University of Finance and Economics (No. 2021D07), The Ministry of Education of Humanities and Social Science project (No. 22XJCZH007), Scientific Research Fund Project of Yunnan Education Department (No. 2021J0586).

Conflict of interest

The authors declare that the research was conducted in the absence of any commercial or financial relationships that could be construed as a potential conflict of interest.

Publisher's note

All claims expressed in this article are solely those of the authors and do not necessarily represent those of their affiliated

organizations, or those of the publisher, the editors and the reviewers. Any product that may be evaluated in this article, or claim that may be made by its manufacturer, is not guaranteed or endorsed by the publisher.

References

- Bohl D, Hanna T, Mapes BR, Moyer JD, Narayan K, Wasif K. Understanding and forecasting geopolitical risk and benefits. *SSRN J* (2017). doi:10.2139/ssrn.3941439
- Caldara D, Iacoviello M. Measuring geopolitical risk. *Am Econ Rev* (2022) 112: 1194–225. doi:10.1257/aer.20191823
- Balcilar M, Bonato M, Demirel R, Gupta R. Geopolitical risks and stock market dynamics of the BRICS. *Econ Syst* (2018) 42:295–306. doi:10.1016/j.ecosys.2017.05.008
- Cheng S, Han L, Cao Y, Jiang Q, Liang R. Gold-oil dynamic relationship and the asymmetric role of geopolitical risks: Evidence from Bayesian pDBEKK-GARCH with regime switching. *Resour Pol* (2022) 78:102917. doi:10.1016/j.resourpol.2022.102917
- Huang J, Ding Q, Zhang H, Guo Y, Suleman MT. Nonlinear dynamic correlation between geopolitical risk and oil prices: A study based on high-frequency data. *Res Int Business Finance* (2021) 56:101370. doi:10.1016/j.ribaf.2020.101370
- Ivanovski K, Hailemariam A. Time-varying geopolitical risk and oil prices. *Int Rev Econ Finance* (2022) 77:206–21. doi:10.1016/j.iref.2021.10.001
- Kumar S, Khalfaoui R, Tiwari AK. Does geopolitical risk improve the directional predictability from oil to stock returns? Evidence from oil-exporting and oil-importing countries. *Resour Pol* (2021) 74:102253. doi:10.1016/j.resourpol.2021.102253
- Li S, Tu D, Zeng Y, Gong C, Yuan D. Does geopolitical risk matter in crude oil and stock markets? Evidence from disaggregated data. *Energy Econ* (2022) 113:106191. doi:10.1016/j.eneco.2022.106191
- Long H, Demir E, Będowska-Sójka B, Zaremba A, Shahzad SJH. Is geopolitical risk priced in the cross-section of cryptocurrency returns? *Finance Res Lett* (2022) 49: 103131. doi:10.1016/j.frl.2022.103131
- Sohag K, Hammoudeh S, Elsayed AH, Mariev O, Safonova Y. Do geopolitical events transmit opportunity or threat to green markets? Decomposed measures of geopolitical risks. *Energy Econ* (2022) 111:106068. doi:10.1016/j.eneco.2022.106068
- Su CW, Khan K, Umar M, Zhang W. Does renewable energy redefine geopolitical risks? *Energy Policy* (2021) 158:112566. doi:10.1016/j.enpol.2021.112566
- Diebold FX, Yilmaz K. Better to give than to receive: Predictive directional measurement of volatility spillovers. *Int J Forecast* (2012) 28:57–66. doi:10.1016/j.ijforecast.2011.02.006
- Diebold FX, Yilmaz K. On the network topology of variance decompositions: Measuring the connectedness of financial firms. *J Econom* (2014) 182:119–34. doi:10.1016/j.jeconom.2014.04.012
- Cunado J, Gupta R, Lau CKM, Sheng X. Time-varying impact of geopolitical risks on oil prices. *Defence Peace Econ* (2020) 31:692–706. doi:10.1080/10242694.2018.1563854
- Mei D, Ma F, Liao Y, Wang L. Geopolitical risk uncertainty and oil future volatility: Evidence from MIDAS models. *Energy Econ* (2020) 86:104624. doi:10.1016/j.eneco.2019.104624
- Abdel-Latif H, El-Gamal M. Financial liquidity, geopolitics, and oil prices. *Energy Econ* (2020) 87:104482. doi:10.1016/j.eneco.2019.104482
- Su CW, Qin M, Tao R, Moldovan NC. Is oil political? From the perspective of geopolitical risk. *Defence Peace Econ* (2021) 32:451–67. doi:10.1080/10242694.2019.1708562
- Demirel R, Gupta R, Suleman T, Wohar ME. Time-varying rare disaster risks, oil returns and volatility. *Energy Econ* (2018) 75:239–48. doi:10.1016/j.eneco.2018.08.021
- Liu J, Ma F, Tang Y, Zhang Y. Geopolitical risk and oil volatility: A new insight. *Energy Econ* (2019) 84:104548. doi:10.1016/j.eneco.2019.104548
- Sharif A, Aloui C, Yarovaya L. COVID-19 pandemic, oil prices, stock market, geopolitical risk and policy uncertainty nexus in the US economy: Fresh evidence from the wavelet-based approach. *Int Rev Financial Anal* (2020) 70:101496. doi:10.1016/j.irfa.2020.101496
- Antonakakis N, Gupta R, Kollias C, Papadamou S. Geopolitical risks and the oil-stock nexus over 1899–2016. *Finance Res Lett* (2017) 23:165–73. doi:10.1016/j.frl.2017.07.017
- Diks C, Wolski M. Nonlinear granger causality: Guidelines for multivariate analysis: Multivariate nonlinear granger causality. *J Appl Econ* (2016) 31:1333–51. doi:10.1002/jae.2495
- Hoque ME, Soo Wah L, Zaidi MAS. Oil price shocks, global economic policy uncertainty, geopolitical risk, and stock price in Malaysia: Factor augmented VAR approach. *Econ Research-Ekonomska Istraživanja* (2019) 32:3700–32. doi:10.1080/1331677X.2019.1675078
- Smales LA. Geopolitical risk and volatility spillovers in oil and stock markets. *Q Rev Econ Finance* (2021) 80:358–66. doi:10.1016/j.qref.2021.03.008
- Su CW, Khan K, Tao R, Nicoleta-Claudia M. Does geopolitical risk strengthen or depress oil prices and financial liquidity? Evidence from Saudi Arabia. *Energy* (2019) 187:116003. doi:10.1016/j.energy.2019.116003
- Abadie B, Gardeazabal J. The economic costs of conflict: A case study of the Basque country. *Am Econ Rev* (2003) 93:113–32. doi:10.1257/00028280321455188
- Blomberg B, Hess G, Jackson JH. Terrorism and the returns to oil. *Econ Polit* (2009) 21:409–32. doi:10.1111/j.1468-0343.2009.00357.x
- Kollias C, Kyrtou C, Papadamou S. The effects of terrorism and war on the oil price–stock index relationship. *Energy Econ* (2013) 40:743–52. doi:10.1016/j.eneco.2013.09.006
- Orbaneja JRV, Iyer SR, Simkins BJ. Terrorism and oil markets: A cross-sectional evaluation. *Finance Res Lett* (2018) 24:42–8. doi:10.1016/j.frl.2017.06.016
- Toft P, Duero A, Bieliauskas A. Terrorist targeting and energy security. *Energy Policy* (2010) 38:4411–21. doi:10.1016/j.enpol.2010.03.070
- Hoque ME, Zaidi MAS. Global and country-specific geopolitical risk uncertainty and stock return of fragile emerging economies. *Borsa Istanbul Rev* (2020) 20:197–213. doi:10.1016/j.bir.2020.05.001
- Apergis N, Bonato M, Gupta R, Kyei C. Does geopolitical risks predict stock returns and volatility of leading defense companies? Evidence from a nonparametric approach. *Defence Peace Econ* (2017) 2017:1–13. doi:10.1080/10242694.2017.1292097
- Yang J, Yang C. The impact of mixed-frequency geopolitical risk on stock market returns. *Econ Anal Pol* (2021) 72:226–40. doi:10.1016/j.eap.2021.08.008
- Salisu AA, Ogbonna AE, Lasisi L, Olaniran A. Geopolitical risk and stock market volatility in emerging markets: A GARCH – MIDAS approach. *North Am J Econ Finance* (2022) 62:101755. doi:10.1016/j.najef.2022.101755
- Zhang Y, Hamori S. A connectedness analysis among BRICS's geopolitical risks and the US macroeconomy. *Econ Anal Pol* (2022) 76:182–203. doi:10.1016/j.eap.2022.08.004
- Baker SR, Bloom N, Davis SJ. Measuring economic policy uncertainty. *Q J Econ* (2016) 131:1593–636. doi:10.1093/qje/qjw024
- Das D, Kannadhasan M, Bhattacharyya M. Do the emerging stock markets react to international economic policy uncertainty, geopolitical risk and financial stress alike? *North Am J Econ Finance* (2019) 48:1–19. doi:10.1016/j.najef.2019.01.008
- Saiz A, Simonsohn U. Proxying for unobservable variables with internet document-frequency. *J Eur Econ Assoc* (2013) 11:137–65. doi:10.1111/j.1542-4774.2012.01110.x
- Kotcharin S, Maneenop S. Geopolitical risk and corporate cash holdings in the shipping industry. *Transportation Res E: Logistics Transportation Rev* (2020) 136: 101862. doi:10.1016/j.tre.2020.101862
- Le A-T, Tran TP. Does geopolitical risk matter for corporate investment? Evidence from emerging countries in Asia. *J Multinational Financial Manage* (2021) 62:100703. doi:10.1016/j.mulfin.2021.100703
- Wang KH, Xiong DP, Mirza N, Shao XF, Yue XG. Does geopolitical risk uncertainty strengthen or depress cash holdings of oil enterprises? Evidence from China. *Pacific-Basin Finance J* (2021) 66:101516. doi:10.1016/j.pacfin.2021.101516
- Koenker R, Bassett G. Regression quantiles. *Econometrica* (1978) 46:33. doi:10.2307/1913643
- Sim N, Zhou H. Oil prices, US stock return, and the dependence between their quantiles. *J Banking Finance* (2015) 55:1–8. doi:10.1016/j.jbankfin.2015.01.013



OPEN ACCESS

EDITED BY

Dun Han,
Jiangsu University, China

REVIEWED BY

Hang-Hyun Jo,
Catholic University of Korea, Republic of
Korea
Per Sebastian Skardal,
Trinity College, United States

*CORRESPONDENCE

Vaiva Vasiliauskaite,
✉ vvasiliau@ethz.ch

SPECIALTY SECTION

This article was submitted to Social
Physics, a section of the journal
Frontiers in Physics

RECEIVED 16 December 2022

ACCEPTED 20 February 2023

PUBLISHED 15 March 2023

CITATION

Vasiliauskaite V and Hausladen CI (2023),
How do circadian rhythms and neural
synchrony shape networked
cooperation?
Front. Phys. 11:1125270.
doi: 10.3389/fphy.2023.1125270

COPYRIGHT

© 2023 Vasiliauskaite and Hausladen. This
is an open-access article distributed
under the terms of the [Creative
Commons Attribution License \(CC BY\)](#).
The use, distribution or reproduction in
other forums is permitted, provided the
original author(s) and the copyright
owner(s) are credited and that the original
publication in this journal is cited, in
accordance with accepted academic
practice. No use, distribution or
reproduction is permitted which does not
comply with these terms.

How do circadian rhythms and neural synchrony shape networked cooperation?

Vaiva Vasiliauskaite^{1*} and Carina I. Hausladen^{1,2}

¹COSS, DGEES, ETHZ, Zurich, Switzerland, ²Humanities and Social Sciences, California Institute of Technology, Pasadena, CA, United States

This study investigates the effects of temporal changes at the individual and social levels and their impact on cooperation in social networks. A theoretical framework is proposed to explain the probability of cooperation as a function of endogenously driven periodic temporal variation and neural synchrony modeled as a diffusion process. Agents are simulated playing a prisoner's dilemma game, with and without evolution, in a two-player setting and on networks. Most importantly, we find that temporal variation and synchrony influence cooperation patterns in a non-trivial way and can enhance or suppress cooperation, depending on exact parameter values. Furthermore, some of our results point to promising future research on human subjects. Specifically, we find that cooperators can dramatically increase their payoff—as opposed to defectors—if neural synchrony is present. Furthermore, the more heterogeneous the synchrony between two agents, the less they cooperate. In a network setting, neural synchrony inhibits cooperation, and variation in circadian patterns counteracts this effect.

Call: Hidden Order Behind Cooperation in Social Systems.

KEYWORDS

Cooperation, neural synchrony, temporal variation, neural activity, networks, circadian rhythms

1 Introduction

The ability to cooperate on a large scale has been highlighted as the strongest competitive advantage we—the human species—have in the animal kingdom. In today's closely networked society, daily (cooperative) encounters with other individuals are a normal part of life.

Although often omitted in analyses and models, environmental and cognitive variations affect each individual's decision process, thus shaping cooperation at large. One example of such an environmental variable is the rising and setting of the sun. It profoundly impacts various physiological processes, some of which a person experiences consciously, such as sleep, drive, and appetite. For some other behaviors, such as the tendency to cooperate, a causal link to circadian or neuromodulatory variation is less evident. To make matters more complicated, the act of social interaction itself also directly impacts the brain's decision-making abilities, as individuals that engage in a social encounter experience a higher correlation in brain activity—the so-called neural synchrony or inter-brain synchrony. Knowledge of a link between these time-varying cognitive patterns and cooperation at large would be extremely powerful, enabling us to time interactions to maximize a specific outcome, such as cooperation.

It is well-known that neuronal communication is mediated by a range of neurotransmitters and neuromodulators that shape behavior during decision-making processes [1]. Studies have shown that various neurotransmitters, such as dopamine and serotonin, show rhythmic variations in concentration in many neuronal nuclei and centers of the brain [2,3]. Moreover, light, a major environmental cue, plays a central role in setting circadian cycles, which in turn impact body temperature, melatonin, cortisol, and cortical activity (as seen through EEG recordings [4–7] and biological clock neurons [8]). Additionally, the circadian system has been linked to various aspects of physiology and cognitive processes, such as learning, memory, attention, mood, and reaction time [9]. These cognitive variations resulting from circadian cycles can ultimately affect social phenomena globally.

On the other hand, social interactions also influence the dynamics of the brain. Recent developments in neuroimaging have enabled measurements of the activity of two or more brains simultaneously, a process known as “hyperscanning” [10,11]. This has allowed for the exploration of inter-brain synchrony, which has been linked to joint attention, interpersonal communication, coordination, and decision-making (for review, see [11]). Studies have revealed that higher inter-brain synchrony is associated with successful cooperation [12–17]. Intra-person variation, such as circadian variation in the expression of specific genes in the prefrontal cortex [18], is also believed to play a role in these interactions. Altogether, social dynamics are intricately linked with the dynamical system of the brain.

Classical social *network analysis*, a branch in sociology [19], typically assumes that the only essential elements that define societies are interactions—links—between individuals and their interacting units—people or animals—where the latter is modeled as internally monolithic entities. Researchers have only now begun appreciating the importance of the potentially heterogeneous internal structure of an individual in the fabric of society. These ideas are being explored in new fields of the network [20] and social [21] neuroscience and have already yielded knowledge fruits. So far, building upon the social brain hypothesis [22], these fields have mainly focused on associations between neural dynamics and structural properties of social networks, such as density [23], centrality, and homophily [24], or linking the neuroendocrine system with the structure of a social network [25]. However, the effects that neurocognitive dynamics may have on global socio-dynamic processes that take place in a network have been researched far less. Some of the examples in this direction are research on potential interventions, such as giving oxytocin to central individuals in a social network to increase their trust and enforcement of cooperation norms through peer punishment, thereby enabling cooperation [26], or linking temporal connectivity in a social network with a circadian rhythm [27]. However, the most common focus in the field is on the effects that temporal changes in interactions, such as bursty patterns [28], have on cooperation [29] rather than the temporal variability that is intrinsic to an individual, such as variation at a cognitive level.

To fill this gap, this study investigates the impact that temporal changes at the individual level may have on cooperation in a social network. We specifically concentrate on two sources of temporality, namely, the behavioral variations caused by circadian or other periodic variations in the concentration of (neuro) hormones,

and neural synchrony, namely, a transition from a less- to more-correlated inter-brain activity, as a direct consequence of social interaction itself. In Section 2, we incorporate individuality in evolutionary game theory models on graphs and allow individual preferences and tendencies to be time-varying, e.g., within a 24-h rhythm, and converging to a global mean, thereby mimicking neural synchrony. We then study the model’s predictions within the framework of a social dilemma game: the prisoner’s dilemma. At first, we introduce the game as a non-evolutionary game and then proceed with implementing evolution. Subsequently, we add another layer of complexity and consider the game to be played in a pair and then on a network. Our simulation results are discussed in Section 3. We conclude and suggest steps for future research in Section 4.

2 Methods: Theorizing cooperation as temporal variation and synchrony

We established a link between circadian rhythms, inter-person neural synchrony, and cooperation preferences in the introduction. In this section, we develop a theoretical framework that aims to quantitatively elucidate this link. Many neuromodulators posit cyclic patterns; therefore, we model decision preferences as periodic functions and dependent on neural synchrony. Subsequently, we describe the game within which we consider the cooperative action to take place. Lastly, we describe the evolutionary mechanisms introduced, the types of networks, and the metrics we will investigate after obtaining simulation results.

2.1 Periodic variability and synchrony in decision preferences

To incorporate an individual’s *periodic variability* caused by circadian rhythms and temporal changes due to *neural synchrony* into our model, we proceed as follows. First, we allow the probability associated with a random variable of cooperation to be time-varying and composed of two individual parts:

$$p_i(t) = f_i(t, \Theta_i) + g_i(t, \Omega_i), \quad (1)$$

i.e., for each individual i , the probability to cooperate at round t is composed of a time-varying part $f_i(t, \Theta_i)$ that reflects the person’s circadian rhythm or any other internal influences that affect a person without interaction with a human-populated environment and a time-varying part g_i that corresponds to that individual’s inter-person neural synchrony (interaction with a human-populated environment). Here, Θ is a set of parameters for f and similarly for g . For simplicity, we will consider $f_i = f$, $g_i = g \forall i$. It should be noted that $\langle f(t, \Theta_i) \rangle_t$ is a person’s prevalence toward cooperation in absence of influences related to other human beings.

The periodic variability part is modeled as the sum of periodic functions¹. For instance, if there is one time-varying influence,

¹ Other researchers have also described the rhythmic properties of the circadian system as sinusoidal functions [42].

$$f(t, \Theta_i) = \delta_i + a_i \sin\left(2\pi \frac{t + \theta_i}{T_i}\right), \quad (2)$$

where a_i is the amplitude of a sine wave, T_i is its period, and θ_i is the phase and δ_i is a shift. Both t and T_i are expressed in equivalent units of time. Such variability is akin to periodic changes in personal preferences that one would expect due to changes in the activity of a single neuromodulator. In the case of Q influences, f can be defined as

$$f(t, \Theta_i) = \sum_{w=1}^Q f(t, \Theta_{i,w}). \quad (3)$$

Next, we move on to a model of neural synchrony. Generally, synchronization is a temporal phenomenon whereby a system transitions from a less ordered state to a more ordered state. In cooperation dynamics, an ordered state would be a state where all individuals partake in the same decision to cooperate or to defect [10]. Therefore, a natural candidate for modeling the neural synchrony part is a simple diffusion model where individuals converge toward the same probability to cooperate over time. A diffusion model is defined as $\frac{d\mathbf{p}}{dt} = -\mathbf{K}\mathbf{L}\mathbf{p}$, where $\mathbf{K} = [K_1, K_2, \dots, K_n]$ is a vector of coupling strengths for nodes and \mathbf{L} is a graph Laplacian. All in all, we have a system of coupled non-autonomous ordinary differential equations:

$$\frac{d\mathbf{p}}{dt} = \frac{d\mathbf{f}}{dt} - \mathbf{K}\mathbf{L}\mathbf{p}. \quad (4)$$

The equilibrium solution depends on \mathbf{K} , \mathbf{f} , while the dynamics over time depend on the network structure and assortativity in δ_i . If $K_i = k \forall i$, then $\lim_{t \rightarrow \infty} p_i(t) = \langle p_i(0) \rangle_i = \langle \delta_i \rangle_i \forall i$. Note that the last equality holds since the shift terms δ_i of Eq. 1 are the initial values $p_i(0)$ with which Eq. 4 is integrated.

2.2 Non-evolutionary prisoner's dilemma

The prisoner's dilemma is a two-player game where each player has to choose one of two possible strategies (to cooperate or to defect). The payoff for each individual depends on the strategy taken by her and another player. Specifically, when both agents cooperate, they both receive a payoff R , whereas when a cooperator interacts with a defector, she receives a payoff S , and the defector gets T . Lastly, when both agents defect, they receive a payoff of value P . A matrix often represents the payoff

$$\begin{matrix} & \begin{matrix} C & D \end{matrix} \\ \begin{matrix} C \\ D \end{matrix} & \begin{pmatrix} R & S \\ T & P \end{pmatrix} \end{matrix}. \quad (5)$$

Different values of parameters R , S , T , and P bring about different dilemmas with different equilibrium points. A prisoner's dilemma is defined with values such that $T > R > P > S$. The payoff relationship $R > P$ implies that mutual cooperation is superior to mutual defection, while the payoff relationships $T > R$ and $P > S$ imply that defection is the dominant strategy for both agents. The game can be iterated, known as the iterated prisoner's dilemma. We also require that $2R > T + S$ to prevent alternating cooperation and defection, giving a greater reward than cooperation. In this study, we set the payoff matrix to values $R = 3$, $S = 0$, $T = 5$, $P = 1$.

In a pure strategy game, each agent chooses one fixed strategy. It can be changed throughout the game (evolve), and the change in strategies is typically based on a comparison of recent payoffs. In a mixed strategy game, an agent's strategy is a random variable with a probability of cooperating p . Therefore, a pure strategy game is a special (deterministic) case of a mixed (stochastic) strategy game where $p \in \{0, 1\}$ [30,31]. At each round, each player i plays an independent game with each of its k_i neighbors and accumulates a total payoff $\pi_i^t = \frac{1}{k_i} \sum_{j \in N_i} \pi_{ij}^t$, where N_i is k_i neighbors of i . In the later introduced evolutionary game setting, these strategies are subject to an evolutionary process, meaning that for every τ round, players may update their probabilities of cooperating according to a particular rule [30]. For example, p can depend on the outcomes of earlier games. If p is a function of only the most recent n encounters, the strategy is called a "memory- n " strategy.

2.3 Evolution, networks, and metrics

The evolution proceeds following the Fermi rule. Specifically, each node imitates the strategy $p_l(t)$ adopted by one of its neighbors, l , chosen at random². The node i updates its strategy with probability [32].

$$p_{i,\text{update}} = \begin{cases} \frac{1}{1 + e^{[(\pi_i^t - \pi_l^t)/K_F]}} & \text{if } t \bmod \tau = 0, \\ 0 & \text{otherwise.} \end{cases} \quad (6)$$

Here K_F is the Fermi temperature, set to 0.1 if not otherwise stated.

To explore the proposed theoretical model, we choose several different network topologies, namely, Erdős-Rényi (ER) [33], Barabási-Albert (BA) [34], and Watts-Strogatz [35] (WS) random graphs.

To analyze the impact of neural synchrony on cooperation, we consider the following two metrics:

The fraction of mutually cooperative steps f_C is the number of games in which both players adopted a cooperative strategy as a fraction of all games that were played during timesteps $[t_\tau, t_{\tau+1}, t_{\tau+2}, \dots, t_{\tau+n-1}]$ between times t_τ and $t_{\tau+n-1}$:

$$f_C(t, \tau, \Omega) = \frac{1}{n|E|} \sum_{(i,j) \in E} \sum_{k=0}^{n-1} \mathbf{1}_{\{C\}}(\{a_{ij}(t_{\tau+k})\}) \mathbf{1}_{\{C\}}(\{a_{ji}(t_{\tau+k})\}), \quad (7)$$

where $a_{ij}(t_k)$ is the decision of a node i (either to cooperate— C or to defect— D) in the game with j at time t_k , $\mathbf{1}_{\{C\}}$ is an indicator function over a set $\{C\}$, and Ω represents any other parameters of the simulations.

We will also study the standard deviation in payoffs across a network at a particular timestep of the simulation t . The second moment of the distribution is of particular importance, computed as the standard deviation in the payoffs obtained by agents in a graph, $\sigma_i[\pi_i^t]$.

² Updating in line with the Fermi rule has been found in behavioral data: payoff-based learning—not fairness preferences—best explains the rate of decline in cooperation across a large set of experimental data on social dilemma games [43].

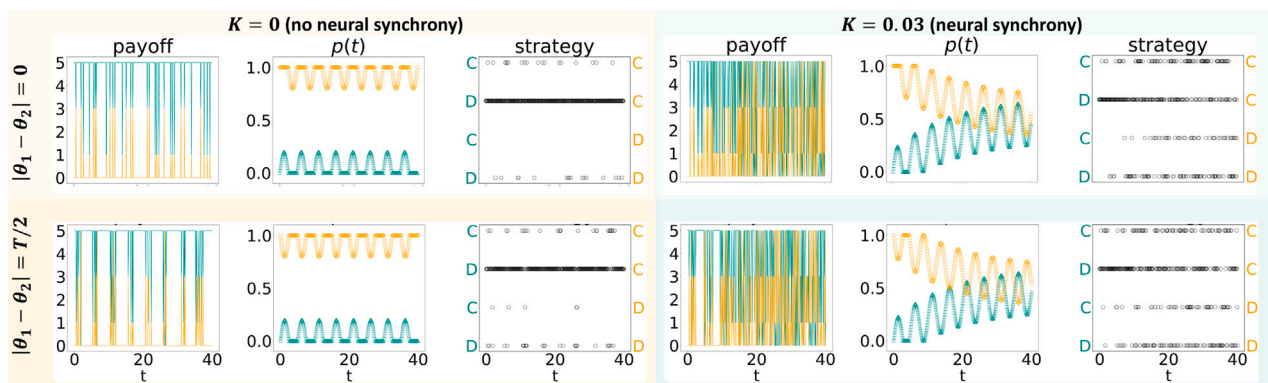


FIGURE 1

Iterated prisoner's dilemma game played by two agents, whose probability of cooperating varies in time according to Eq. 4, with \mathbf{f} defined in the main text and $K_1 = K_2$. For each agent, we show the changes over time of a payoff (left), a probability to cooperate p (middle), and a strategy (right). Depending on the phase difference, $|\theta_1 - \theta_2|$, the agents' probabilities to cooperate are either simultaneously higher/lower than their baselines or are asynchronous.

3 Simulation results

Throughout this section, we simulate a mixed-strategy of prisoner's dilemma. In all cases, we considered integration timesteps of length 0.1 units of time, and unless otherwise stated, the simulation lengths are 40 units of time (400 timesteps) and the periods of sine waves are set to 5 units of time. First, we study the results of a non-evolutionary game and then proceed with interpreting an evolutionary game, both in a 2-player scenario. We then expand the two-player game to a networked game.

3.1 Two-player game

3.1.1 Non-evolutionary game

In the simulated mixed strategy game, the first player begins as a "cooperator," signified by an initial value of $p(0) = 1$. The second player begins as a "defector" since its $p(0) = 0$ ³.

Specifically, the functional form we study is

$$\begin{aligned} \frac{dp_1}{dt} &= -\frac{a_1 T}{2\pi} \cos\left(2\pi \frac{t}{T}\right) - K_1(p_1(t) - p_2(t)) \\ \frac{dp_2}{dt} &= -\frac{a_2 T}{2\pi} \cos\left(2\pi \frac{t + \theta}{T}\right) - K_2(p_2(t) - p_1(t)), \end{aligned} \quad (8)$$

where we study the cases when $\theta = 0$ (the agents are "in-phase") or $\theta = T/2$ (the agents are "out-of-phase"). We will refer to K_1 and K_2 simply as K when $K = K_1 = K_2$.

Figure 1 illustrates the effects of variability in $p(t)$ without an evolutionary process. Here, the "cooperator's" results are shown in yellow, whereas the "defector's" results are in green. Both agents are defined as having the same amplitude, $a_1 = a_2 = 0.2$. The figure has two columns: the left column denotes the absence of neural synchrony ($K =$

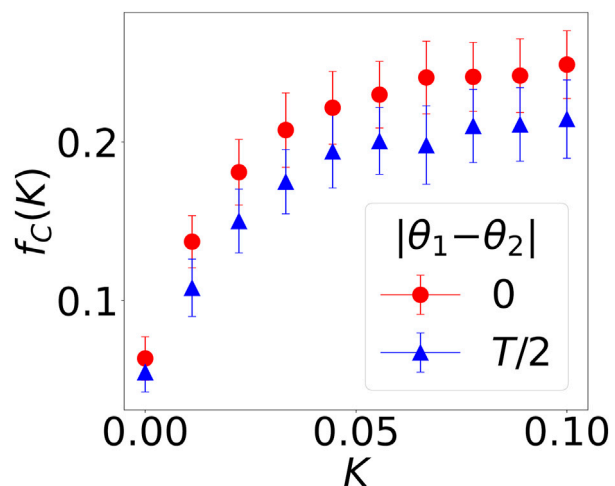


FIGURE 2

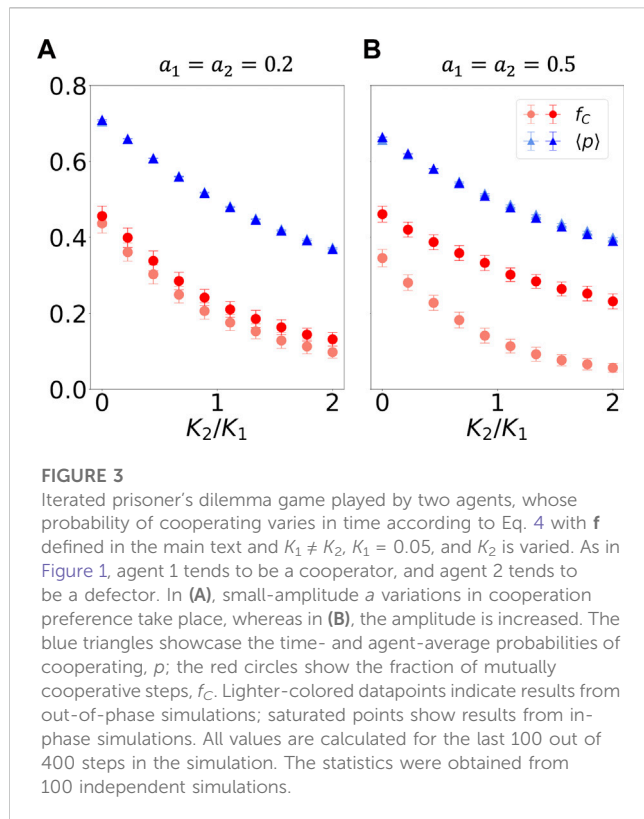
The fraction of mutually cooperative steps out of all games in the last 100 steps as a function of neural synchrony K , $f_c(K)$, in the two-player iterated prisoner's dilemma game. Out-of-phase agents are indicated by blue triangles; in-phase ones, by red dots.

0), and the right one denotes the presence of neural synchrony ($K = 0.03$). Each column has two rows, differing in in-phase neural oscillations ($|\theta_1 - \theta_2| = 0$, top row) and out-of-phase⁴ neural oscillations ($|\theta_1 - \theta_2| = T/2$, bottom row)⁵. The most prominent

³ We study the extreme cases of $p_1(0) = 0$ and $p_2(0) = 1$ to maximize the visibility of the effects being studied. The choice of these specific values for p is made to demonstrate the most prominent results possible. As the difference between $p_1(0)$ and $p_2(0)$ decreases, the differences observed are expected to decrease.

⁴ The expression "out-of-phase" refers to the state when the phases of the circadian rhythms of two individuals are shifted. As light is a key cue that helps to reset and synchronize circadian rhythms, it is possible for two individuals to become out-of-phase if they are not exposed to the same light cues at the same time [44].

⁵ We study the extreme cases of $\theta = 0$ and $\theta = T/2$ to maximize the visibility of the effects being studied. The choice of these specific values for θ was made to demonstrate the most prominent results possible. As the difference between θ_1 and θ_2 decreases, the differences observed in the study are expected to decrease.

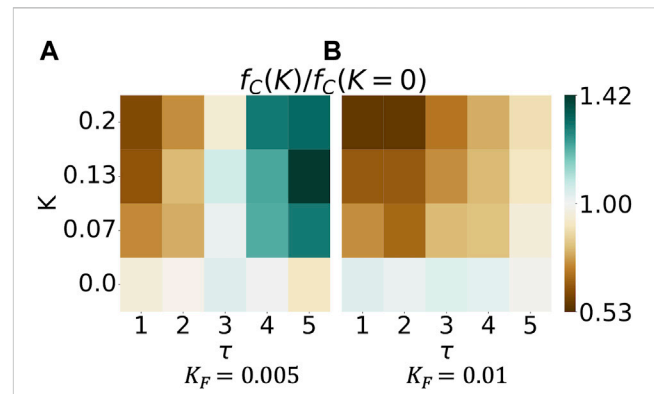


difference that a switch from $K = 0$ to $K = 0.03$ (left versus right column) introduces is observed concerning $p(t)$: neural synchrony induces agents to gravitate toward the same probability of cooperating $p(t)$. This change in $p(t)$ is followed by a change in the strategies adopted: while the cooperator only rarely defects under $K = 0$, she defects far more often under $K = 0.03$. This shift in strategies chosen, in turn, affects the payoff: while under $K = 0$, the cooperator and defector gain similar payoffs, and the cooperator is far better off under $K = 0.03$. In other words, neural synchrony leads to the redistribution of the payoffs in an unequal manner in which the cooperating entity is better off.

In Figure 1, we investigate only two values of K , while we vary K in a more fine-grained way in Figure 2. Specifically, we study the case where $K_1 = K_2$; therefore, the average probability to cooperate $\lim_{t \rightarrow \infty} \langle p_i(t) \rangle_i = \langle p_i(0) \rangle_i = \langle \delta_i \rangle_i$. Here, we consider the fraction of the mutually cooperative decisions f_C in the last 100 steps of the simulation. All other parameters are the same as in Figure 1.

Interestingly, the blue and red curves are both concave, indicating that small values of synchrony have a profound effect. The curve flattens earlier when the interacting agents are out of phase ($|\theta_1 - \theta_2| = T/2$, blue triangles); it is steeper ($|\theta_1 - \theta_2| = 0$, red circles) when the oscillations are in phase. In other words, phase alignment is not as important as achieving a small degree of synchrony. This is because when $K_1 = K_2 = a_1 = a_2 = 0$, $f_C = 0$, meaning that mutual cooperation is only possible through temporal variation (non-zero a_1, a_2). However, cooperation achieved in this way is much smaller than when K_1, K_2 are non-zero.

In Figure 1, we study the case where the value of neural synchrony is the same for both agents $K_1 = K_2$. In Figure 3, by contrast, we investigate the case where $K_1 \neq K_2$. Therefore, the $\lim_{t \rightarrow \infty} \langle p_i(t) \rangle_{i,t} \neq \langle \delta_i \rangle_i$. Figure 3 plots the ratio of synchrony levels



of the two agents, K_2/K_1 , against the fraction of mutually cooperative games, f_C , and the probability to cooperate, $\langle p \rangle$.

We see that when $K_1 > K_2$, $\lim_{t \rightarrow \infty} \langle p_i(t) \rangle_{i,t} > \langle \delta_i \rangle_i$, and the inequality is inverted when $K_1 < K_2$. Furthermore, both variables, f_C (blue triangles) and $\langle p \rangle$ (red dots), decrease with increasing inequality in synchrony K . In other words, the more incomplete the synchrony toward each other, the less cooperation occurs. Figure 3 additionally plots a third and fourth variation: lighter shades refer to out-of-phase oscillations, and panels refer to different amplitudes, a_1, a_2 of the periodic variability. The most striking difference between panels a) and b) occurs with respect to lightly shaded, red-dotted functions. For $a = 0.2$, out-of-phase results are close to in-phase results. However, for $a = 0.5$, the distance between the light and darker shaded functions is clearly visible. The distance additionally increases with increasing heterogeneity in K . These results suggest that oscillations with large amplitude aggravate the negative impact of heterogeneous synchrony levels. In other words, two agents not synchronizing equally is an increasing problem if their temporal variations have large amplitudes.

3.1.2 Evolutionary game

In Figure 4, we introduce an evolution in this two-player game. Specifically, we study the fraction of mutually cooperative games, f_C , in the evolutionary game at varied Fermi temperatures K_F . Low values of K_F can be interpreted as the agents adopting the advantageous, payoff-increasing strategy in most evolutionary steps. Large values of K_F describe an agent making mistakes more often by adopting a disadvantageous strategy at evolutionary steps. The heatmaps in Figure 4 relate the fraction of mutually cooperative games, f_C , to neural synchrony K on the y-axis and τ , the integration timesteps after which the player updates her strategy, on the x-axis. Here, we study a fraction of which the nominator refers to the fraction of cooperative games in which neural synchrony is present ($K \neq 0$ and $K_1 = K_2$). Still, there are no temporal variations ($a_1 = a_2 = 0$). In contrast, the denominator refers to the fraction of cooperative games in the absence of neural

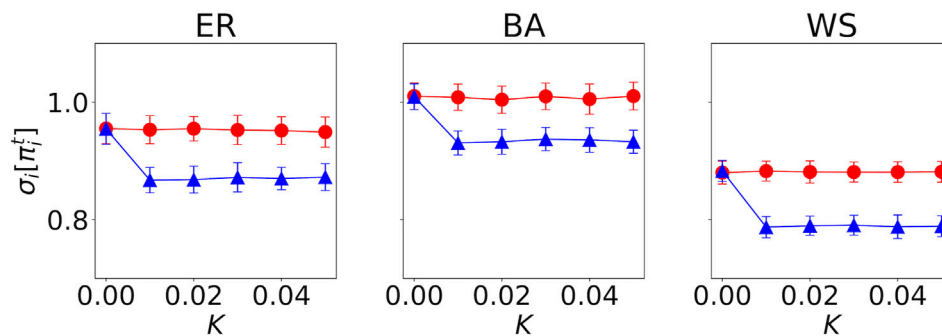


FIGURE 5

Standard deviation in the payoffs $\sigma_i[\pi_i^t]$ of agents decrease in the network over time of the simulation, if neural synchrony takes place. The three figures show results for Erdős–Rényi (ER), Barabási–Albert (BA), and Watts–Strogatz (WS) graphs with $N = 1000$ nodes and an average degree 3. For the WS graph, the rewiring probability is set to 0.05. The reported results are averages of over 100 independent simulations. Red circles show the standard deviation in the average payoff of agents at the first step of the simulation ($t = 0$), whereas blue triangles show the value at the last step of the simulation ($t = 200$).

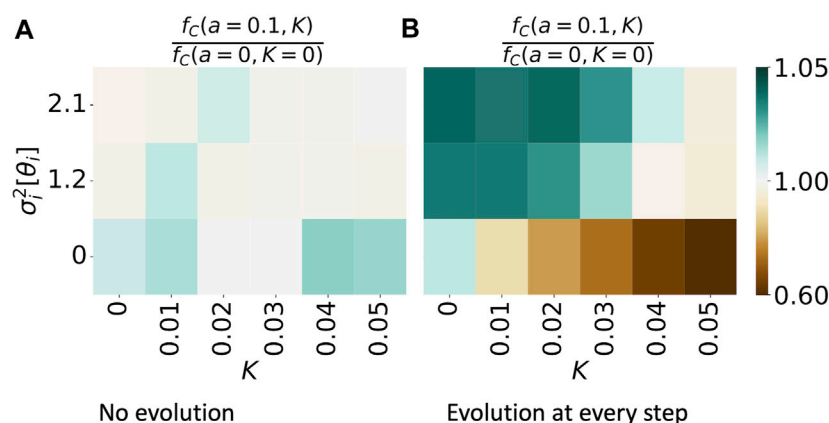


FIGURE 6

Synchronization of periodic patterns of agents' tendency to cooperate, Eq. 2, enhances cooperation in a network when cooperation has no evolutionary process (A) and suppresses cooperation if an evolutionary process exists (B). The figures show the magnitude of $f_C(a = 0.1, K)/f_C(a = 0, K = 0)$. The denominator refers to the fraction of mutually cooperative games observed in simulations without neural synchrony ($K = 0$) and without intrinsic temporal variability in cooperative preferences ($f(t) = \delta$, $a = 0$). The numerator shows the same observation in the simulations where $f(t)$ is varied; there is variance in the phase parameter θ and of strength K in the neural synchrony. The results are obtained from 100 simulations on an ER graph ensemble, with $N = 100$ and an average node degree of 3.

synchrony ($K = 0$). Consequently, $\frac{f_C(K)}{f_C(K=0)} > 1$, displayed in a green hue, denotes a game where cooperation of synced agents is more frequent than the cooperation of two non-synced agents. Brown hue, by contrast, shows more frequent cooperation by non-synced agents than synced agents $\frac{f_C(K)}{f_C(K=0)} < 1$.

We observe that the hue changes from blue to brown with increasing Fermi temperature K_F ; higher Fermi temperature K_F reduces the fraction of mutually cooperative games played by synced agents. In other words, if agents are more likely to make mistakes, it is advantageous to not have neural synchrony. Simply put, *who* cooperates depends on the likelihood of making mistakes. The left heatmap shows darker shades of green at the top right, implying that more intense neural synchrony K increases cooperation f_C the longer a specific strategy is kept

(increasing values of τ). Who cooperates, however, changes in the right heatmap: darker shades of brown are found in the top left of the figure, implying that more intense neural synchrony K increases cooperation f_C , the *shorter* a specific strategy is kept (smaller values of τ). All in all, the effect of neural synchrony depends on the likelihood of agents making irrational decisions and the frequency of evolutionary steps.

3.2 Expanding the game on a network

We now expand the game to a network scenario. More precisely, we investigate the Erdős–Rényi, Barabási–Albert, and Watts–Strogatz graphs.

We begin with a case where neural synchrony is present, but otherwise, there are no periodic variations. Namely, we study the case where $p_i(0) \sim \mathcal{U}(0, 1)$; therefore, $\langle p_i(0) \rangle_i = \frac{1}{2}$, and $a_i = 0 \forall i$. Since there is no evolution, $\lim_{t \rightarrow \infty} \langle p_i(t) \rangle_i = \langle p_i(0) \rangle_i = \frac{1}{2}$; therefore, the first moment of the distribution of, e.g., executed strategies or payoffs, is not affected by neural synchrony. However, the variance in the distribution of payoffs across nodes depends on both the network structure, specifically, degree distribution, and whether neural synchrony takes place or not.

Figure 5 shows how the standard deviation in the payoffs of agents $\sigma_i[\pi_i^t]$ is affected by the network structure and by the neural synchrony. Colors and shapes refer to two distinct points in time t . In the initial timestep, $t = 0$ (red dots), $\sigma_i[\pi_i^t]$ is constant: it does not vary with levels of synchrony K . In the last timestep $t = 200$ (blue triangles), $\sigma_i[\pi_i^t]$ varies only with the initial increase in K and stays constant afterward. The trend is similar for all networks; what differs is the intercept: $\sigma_i[\pi_i^t]$ is the highest in a BA ensemble, followed by an ER ensemble, and is the lowest for the WS ensemble. Notably, the variance in node degrees decreases in the same order. The presence of neural synchrony further leads to smaller variations in payoffs at later stages of the game. It should be noted that after a certain value of K , there is no dependence of $\sigma_i[\pi_i^t]$ on K , indicating that maximal synchrony is reached at the last simulation step for all larger values of K , and the only source of variability in payoffs is the network structure.

Next, we include the influence of temporal variations on the cooperation patterns in the network scenario. While in the two-agent case there are these two distinct cases (namely, in-phase and out-of-phase); in a network where $N > 2$, we are concerned with the variance in the distribution of the parameters of f , namely, θ_i , T_i . In the current study, we assume that $T = \text{const}$ and concentrate on heterogeneity in phases. Specifically, we considered three cases where the distribution of phases has varied amounts of variance. First, a case where $\theta_i = 0 \forall i$; second, sampled from a beta distribution $T \cdot \mathcal{B}(2, 2)$; and lastly, a uniform distribution $\theta_i \sim T \cdot \mathcal{U}(0, 1)$. These three cases have, respectively, variance $\sigma_i^2[\theta_i]$ of 0, 1.2 and 2.1.

In Figure 6, we show the effect of heterogeneity in phases for various amounts of neural synchrony K . In Figure 6A, we consider no evolutionary process, whereas in Figure 6B, we study the case where evolution takes place at every simulation step: $\tau = 1$. Similarly, as in Figure 4, we contrast the fraction of mutually cooperative games in simulations with a given variance in phases and strength of neural synchrony ($f_C(a = 0.1, K)$, emphasizing that the amplitude parameter a is set to this value for all nodes) with the values of the same measure, observed in simulations without temporal variability, namely, $f_C(a = 0, K = 0)$. We restrict the study to the case of an ER ensemble with $N = 100$ nodes and an average degree of 3, since the network structure influences the time evolution of the dynamics but not the time-averaged results.

Figure 6A shows that as variance in phases increases, mutual cooperation is suppressed. Surprisingly, the cooperation is minimal yet enhanced in cases when neural synchrony is present, and there is no phase difference, i.e., $\theta_i = \text{const} \forall i$ with respect to the fraction of mutually cooperative games observed in the baseline case.

However, as evolution is introduced, the effect of neural synchrony and variance in phases changes. Since an increase in K leads to the convergence of individual strategies to a global mean, K acts as an attractor to a suboptimal strategy for maximizing payoffs. With the presence of evolution, nodes can adopt the optimal

strategy $p_i = 1 \forall i$, and neural synchrony acts as a negative force to reach this goal. In the case where K is non-zero, variance in phases brings value by increasing the diversity of strategies at each t and allowing for the evolutionary process to override the effect of neural synchrony.

4 Conclusion

In this study, we investigate how intra-individual temporal variation impacts cooperation on a social level. To that end, we proposed a theoretical framework to explain the probability of cooperation as a function of intra-personal temporal variation due to circadian variations and neural synchrony. We simulated agents playing a prisoner's dilemma game, without and with evolution, in a two-player setting and on networks. Our simulations revealed a diverse set of insights that enrich our understanding of how temporality and individuality shape cooperation.

We find that when agents experience synchrony and gravitate toward the same probability of cooperating, there is a change in the strategies adopted, which in turn affects agents' payoffs. Interestingly, neural synchrony leads to redistribution of the payoffs in an unequal manner in which the cooperating entity is better off. This finding is highly interesting: in human subject experiments, cooperating entities are on average worse off than freeriders and defectors. Our results further allow us to comment on the *intensity* of synchrony: we find that transitioning from no synchrony to a tiny degree of synchrony profoundly and positively affects cooperation in a two-player game. Furthermore, we implemented a variation that behavioral experimentalists so far have overlooked: understanding synchrony as either a directed or an undirected phenomenon. The more heterogeneous the synchrony between two agents, the less they cooperate; large amplitudes aggravate this phenomenon. Our simulations with evolution produce further interesting results: if a pair of agents is more likely to make mistakes in choosing an advantageous strategy, not experiencing synchrony positively impacts cooperation. In other words, synchrony is not always desirable; instead, its quality is context dependent.

Lastly, we extend our simulations to networks. We find that in the later stages of the game, the agents' payoffs become more similar when they switch from no synchrony to synchrony. This can lead to enhanced cooperation if the game is non-evolutionary. However, in an evolutionary game, neural synchrony acts as a *suppressor* of cooperation, while the variance in phases of individual temporal variability counteracts the inhibitory effect of synchrony.

5 Discussion

Our aim was to extend a model of cooperation by incorporating individual- and group-level dynamics of tendencies to cooperate that are not driven solely by the goal of maximizing a payoff. In this way, we were able to compare the strength of endogenous influences and conscious decisions, such as mimicking others' strategies in order to obtain a larger individual payoff, to that of endogenous processes.

We concentrated on a case where $f(t)$ mimics circadian rhythms [36], known to impact decision-making. Regarding neural synchrony, we acknowledge that alternative mathematical models could have sufficed; e.g., models of coupled oscillators such as the Kuramoto model [37] have been used in several studies to study the emergence of synchronization and cooperation in networked populations of coupled oscillators [38]. We, by contrast, chose to use a diffusion model as it is more appropriate for our specific research question: while a coupled oscillator model would seem a natural fit, it assumes that circadian rhythms and neuromodulation are impacted by social interactions. In a context where such a coupling is desired, one would replace \mathbf{g} with Θ in the diffusion model and set $\mathbf{g} = \mathbf{0}$ in Eq. 1.

Furthermore, it should be acknowledged that the proposed model is simplistic and does not account for all aspects of brain physiology. For example, it does not capture intrinsic fluctuations at the cellular level or the need for sleep itself, which is a limitation that future research should address. Furthermore, the exact functional forms and parameter values of functions in our model should be calibrated for particular circadian and neuromodulatory causes of variability in decision-making. Social memory [39] may also be a crucial element incorporated in the future.

The results we report are a source of inspiration for investigating the phenomenon of cooperation in the real world. First, we report that cooperators can dramatically increase their payoff—as opposed to defectors—if neural synchrony is present. Experimental studies could exogenously vary synchrony levels and incentivize different groups to adopt a certain type of strategy. Furthermore, we experiment with different levels of synchrony among agents. So far, in behavioral studies, the variable of interest has been *where* in the brain(s) the neural synchrony occurs. However, our findings suggest that enormous value lies in investigating in more detail the *quality* of this synchrony. Lastly, the behavioral literature on neural synchrony almost exclusively investigates the interaction between two participants. Repeating those experiments on networks might allow for an even deeper understanding of cooperation as a temporal phenomenon. On the other hand, experimental data from a networked study would also guide a decision as to how important it is to incorporate cognitive properties into computational social science models.

Additionally, the results on networks should be studied in greater depth, e.g., by exploring how our results translate to real-world networks, temporal networks [29], simplicial complexes [32], or hypergraphs [40], and looking in greater depth at how network structure impacts the trajectory of a dynamical process in a cooperative game. Furthermore, we did not analyze the impact of assortative mixing [41], e.g., cooperation probability. The last variation left for future research to study is a redefinition of the coupling of agents, where neural synchrony affects the parameters of the functions that govern their internal periodicity patterns, as explained earlier in this section.

In conclusion, this paper advances our understanding of cooperation as a temporal phenomenon. We introduce a

mathematical framework that couples individual endogenous influences with conscious decisions in order to explain the probability of cooperation. More broadly, our work suggests that cognitive processes are linked with the social phenomenon: for cognitive science, social interactions may not be just an end goal, but an active variable; on the other hand, to understand group dynamics, neuroscientific explanations may be crucial.

Data availability statement

The data simulated during the study, together with the simulation codes are available on github at the link https://github.com/vv2246/temporal_cooperation.

Author contributions

VV: conceptualization, methodology, software, validation, formal analysis, investigation, visualization, and writing—original draft-review and editing. CH: conceptualization, writing—original draft, and writing—review and editing.

Funding

Open access funding is provided by the Swiss Federal Institute of Technology Zürich. VV acknowledges the support of the European Union—Horizon 2020 Program under the scheme “INFRAIA-01-2018-2019—Integrating Activities for Advanced Communities,” Grant Agreement no. 871042, “SoBigData++: European Integrated Infrastructure for Social Mining and Big Data Analytics” (<http://www.sobigdata.eu>).

Conflict of interest

The authors declare that the research was conducted in the absence of any commercial or financial relationships that could be construed as a potential conflict of interest.

Publisher's note

All claims expressed in this article are solely those of the authors and do not necessarily represent those of their affiliated organizations, or those of the publisher, the editors, and the reviewers. Any product that may be evaluated in this article, or claim that may be made by its manufacturer, is not guaranteed or endorsed by the publisher.

References

1. Grossman CD, Cohen JY. Neuromodulation and neurophysiology on the timescale of learning and decision-making. *Annu Rev Neurosci* (2022) 45:317–37. doi:10.1146/annurev-neuro-092021-125059
2. Lambert GW, Reid C, Kaye DM, Jennings GL, Esler MD. Effect of sunlight and season on serotonin turnover in the brain. *The Lancet* (2002) 360:1840–2. doi:10.1016/S0140-6736(02)11737-5

3. Smith A, Olson R, Justice J, Jr. Quantitative microdialysis of dopamine in the striatum: Effect of circadian variation. *J Neurosci Methods* (1992) 44:33–41. doi:10.1016/0165-0270(92)90111-p
4. Jung CM, Khalsa SBS, Scheer FA, Cajochen C, Lockley SW, Czeisler CA, et al. Acute effects of bright light exposure on cortisol levels. *J Biol rhythms* (2010) 25:208–16. doi:10.1177/0748730410368413
5. Hughes S, Jagannath A, Hankins MW, Foster RG, Peirson SN. Photoc regulation of clock systems. *Methods Enzymol* (2015) 552:125–43. doi:10.1016/B.S.MIE.2014.10.018
6. Cajochen C, Kräuchi K, Danilenko KV, Wirz-Justice A. Evening administration of melatonin and bright light: Interactions on the EEG during sleep and wakefulness. *J Sleep Res* (1998) 7:145–57. doi:10.1046/j.1365-2869.1998.00106.x
7. Badia P, Myers B, Boecker M, Culpepper J, Harsh JR. Bright light effects on body temperature, alertness, EEG and behavior. *Physiol Behav* (1991) 50:583–8. doi:10.1016/0031-9384(91)90549-4
8. Ramkisoensing A, Meijer JH. Synchronization of biological clock neurons by light and peripheral feedback systems promotes circadian rhythms and health. *Front Neurol* (2015) 6:128. doi:10.3389/FNEUR.2015.00128
9. Burke TM, Scheer FA, Ronda JM, Czeisler CA, Wright KP. Sleep inertia, sleep homeostatic and circadian influences on higher-order cognitive functions. *J Sleep Res* (2015) 24:364–71. doi:10.1111/JSR.12291
10. Dumas G, Nadel J, Soussignan R, Martinerie J, Garnerio L. Inter-brain synchronization during social interaction. *PLOS ONE* (2010) 5:e12166. doi:10.1371/JOURNAL.PONE.0012166
11. Czeszumski A, Eustergerling S, Lang A, Menrath D, Gerstenberger M, Schuberth S, et al. Hyperscanning: A valid method to study neural inter-brain underpinnings of social interaction. *Front Hum Neurosci* (2020) 14:39. doi:10.3389/fnhum.2020.00039
12. Müller V, Saarikivi K, Falcon M, Makkonen T, Martikainen S, Putkinen V, et al. Inter-brain synchronization occurs without physical co-presence during cooperative online gaming. *Neuropsychologia* (2022) 174:108316. doi:10.1016/j.neuropsychologia.2022.108316
13. Szymanski C, Pesquita A, Brennan AA, Perdakis D, Enns JT, Brick TR, et al. Teams on the same wavelength perform better: Inter-brain phase synchronization constitutes a neural substrate for social facilitation. *Neuroimage* (2017) 152:425–36. doi:10.1016/j.neuroimage.2017.03.013
14. Cui X, Bryant DM, Reiss AL. NIRS-based hyperscanning reveals increased interpersonal coherence in superior frontal cortex during cooperation. *NeuroImage* (2012) 59:2430–7. doi:10.1016/j.NEUROIMAGE.2011.09.003
15. Zhang M, Jia H, Zheng M. Interbrain synchrony in the expectation of cooperation behavior: A hyperscanning study using functional near-infrared spectroscopy. *Front Psychol* (2020) 11:542093. doi:10.3389/fpsyg.2020.542093
16. Behrens F, Snijderwint JA, Moulder RG, Prochazkova E, Sjak-Shie EE, Boker SM, et al. Physiological synchrony is associated with cooperative success in real-life interactions. *Scientific Rep* (2020) 10(1):19609–9. doi:10.1038/s41598-020-76539-8
17. Czeszumski A, Liang SHY, Dikler S, König P, Lee CP, Koole SL, et al. Cooperative behavior evokes interbrain synchrony in the prefrontal and temporoparietal cortex: A systematic review and meta-analysis of fNIRS hyperscanning studies. *eNeuro* (2022) 9:ENEURO.0268-21.2022. doi:10.1523/ENEURO.0268-21.2022
18. Chen CY, Logan RW, Ma T, Lewis DA, Tseng GC, Sibille E, et al. Effects of aging on circadian patterns of gene expression in the human prefrontal cortex. *Proc Natl Acad Sci United States America* (2016) 113:206–11. doi:10.1073/PNAS.1508249112
19. Freeman L. The development of social network analysis. *A Study Sociol Sci* (2004) 1:159–67.
20. Bassett DS, Sporns O. Network neuroscience. *Nat Neurosci* (2017) 20:353–64. doi:10.1038/nn.4502
21. Cacioppo JT, Berntson GG, Adolphs R, Carter CS, McClintock MK, Meaney MJ, et al. *Foundations in social neuroscience*. Cambridge, MA, USA: MIT press (2002).
22. Dunbar RI. The social brain hypothesis. *Evol Anthropol Issues News Rev Issues News Rev* (1998) 6:178–90. doi:10.1002/(sici)1520-6505(1998)6:5<178:aid-evan5>3.0.co;2-8
23. Schmalzle R, O'Donnell MB, Garcia JO, Cascio CN, Bayer J, Bassett DS, et al. Brain connectivity dynamics during social interaction reflect social network structure. *Proc Natl Acad Sci United States America* (2017) 114:5153–8. doi:10.1073/pnas.1616130114
24. Baek EC, Hyon R, López K, Finn ES, Porter MA, Parkinson C. In-degree centrality in a social network is linked to coordinated neural activity. *Nat Commun* (2022) 13:1118–3. doi:10.1038/s41467-022-28432-3
25. Han M, Jiang G, Luo H, Shao Y. Neurobiological bases of social networks. *Front Psychol* (2021) 12:626337. doi:10.3389/fpsyg.2021.626337
26. Li S, Ma S, Wang D, Zhang H, Li Y, Wang J, et al. Oxytocin and the punitive hub—Dynamic spread of cooperation in human social networks. *J Neurosci* (2022) 42:5930–43. doi:10.1523/jneurosci.2303-21.2022
27. Alakörkkö T, Saramäki J. Circadian rhythms in temporal-network connectivity. *Chaos* (2020) 30:093115. doi:10.1063/5.0004856
28. Karsai M, Jo HH, Kaski K. *Bursty human dynamics*. Cham: Springer (2018).
29. Li A, Zhou L, Su Q, Cornelius SP, Liu YY, Wang L, et al. Evolution of cooperation on temporal networks. *Nat Commun* (2020) 11:2259. doi:10.1038/s41467-020-16088-w
30. Beersma DG, Daan S. Generation of activity-rest patterns by dual circadian pacemaker systems: A model. *J Sleep Res* (1992) 1:84–7. doi:10.1111/j.1365-2869.1992.TB00015.X
31. Cimini G, Sánchez A. *How evolution affects network reciprocity in prisoner's dilemma* (2014). *arXiv preprint arXiv:1403.3043*.
32. Miyaji K, Tanimoto J. A co-evolutionary model combined mixed-strategy and network adaptation by severing disassortative neighbors promotes cooperation in prisoner's dilemma games. *Chaos, Solitons and Fractals* (2021) 143:110603. doi:10.1016/j.CHAOS.2020.110603
33. Burton-Chellew MN, West SA. Payoff-based learning best explains the rate of decline in cooperation across 237 public-goods games. *Nat Hum Behav* (2021) 5:1330–8. doi:10.1038/s41562-021-01107-7
34. Guo H, Jia D, Sendiña-Nadal I, Zhang M, Wang Z, Li X, et al. Evolutionary games on simplicial complexes. *Chaos, Solitons and Fractals* (2021) 150:111103. doi:10.1016/j.chaos.2021.111103
35. Erdős P, Rényi A. On the evolution of random graphs. *Publ Math Inst Hung Acad Sci* (1960) 5:17–60.
36. Barabási AL, Albert R. Emergence of scaling in random networks. *Science* (1999) 286:509–12. doi:10.1126/science.286.5439.509
37. Watts DJ, Strogatz SH. Collective dynamics of 'small-world' networks. *Nature* (1998) 393:440–2. doi:10.1038/30918
38. Davidson AJ, Menaker M. Birds of a feather clock together – sometimes: Social synchronization of circadian rhythms. *Curr Opin Neurobiol* (2003) 13:765–9. doi:10.1016/j.CONB.2003.10.011
39. Asgari-Targhi A, Klerman EB. Mathematical modeling of circadian rhythms. *Wiley Interdiscip Rev Syst Biol Med* (2019) 11:e1439. doi:10.1002/wsbm.1439
40. Kuramoto Y. International symposium on mathematical problems in theoretical physics. *Lecture Notes Phys* (1975) 30:420.
41. Antonioni A, Cardillo A. Coevolution of synchronization and cooperation in costly networked interactions. *Phys Rev Lett* (2017) 118:238301. doi:10.1103/PhysRevLett.118.238301
42. Oliva A. Neuronal ensemble dynamics in social memory. *Curr Opin Neurobiol* (2023) 78:102654. doi:10.1016/j.conb.2022.102654
43. Alvarez-Rodriguez U, Battiston F, Ferraz de Arruda G, Moreno Y, Perc M, Latora V. Collective games on hypergraphs. In: F Battiston G Petri, editors. *Higher-order systems. Understanding complex systems*. Cham: Springer (2022). p. 377–88. doi:10.1007/978-3-030-91374-8_15
44. Newman ME. Mixing patterns in networks. *Phys Rev E* (2003) 67:026126. doi:10.1103/physreve.67.026126

Frontiers in Physics

Investigates complex questions in physics to understand the nature of the physical world

Addresses the biggest questions in physics, from macro to micro, and from theoretical to experimental and applied physics.

Discover the latest Research Topics

[See more →](#)

Frontiers

Avenue du Tribunal-Fédéral 34
1005 Lausanne, Switzerland
frontiersin.org

Contact us

+41 (0)21 510 17 00
frontiersin.org/about/contact

